Katholieke Universiteit Leuven
Faculty of Sciences
Departement of Chemistry
Division of Molecular and Nanomaterials

UNRAVELLING AND GUIDING THE MOLECULAR SELF-ASSEMBLY ON SURFACES

An Ver Heyen

February 2008

Jury:
Prof. Em. Dr. F. C. De Schryver (promoter)
Prof. Dr. S. De Feyter (promoter)
Prof. Dr. W. Dehaen
Prof. Dr. S. Höger
Prof. Dr. A. M. Jonas
Prof. Dr. M. Van der Auweraer
Prof. Dr. T. Verbiest

Doctoral thesis submitted in candidacy for the degree of doctor in philosophy

Celestijnenlaan 200F, B-3001 Heverlee (Belgium)

D/2008/10.705/3
ISBN 978-90-8649-157-5

Preface

Research became part of my life several years ago when Prof. De Schryver gave me the opportunity to work in his group while I was a student. After my master studies in chemistry, I was enthusiastic and eager to initiate 'my own' research projects which started a period of challenges, including failure and success, that enabled me to develop both my personal and professional skills. As the writing of my thesis is finished, I conclude this period with satisfaction and would very much like to express my gratitude to those who helped to get me where I stand today.

First, I like to acknowledge some people for their vital contribution to the realisation of this work. I would like to thank Prof. De Schryver and Prof. De Feyter for being my promoters and scientifically motivate me with discussions and new ideas. Thank you for giving me the opportunity to visit other groups and go to scientific meetings abroad. I am also grateful to my promoters, and to the other members of the jury, for reading the preliminary version of my thesis, providing feedback and approving my thesis.

I would like to thank Prof. Müllen's group (Max-Planck Institute for Polymer Research, Germany), in particular Tianshi Qin and Roland Bauer, for our collaboration and for providing the dendrimers which they synthesised and the light scattering data of the second generation polyphenylene dendrimer. Randy de Palma (IMEC) for covering the silicon substrates with different silanes which formed the basis for further experiments in order to guide the dendrimer fibres. Cédric Buron (Université catholique de Louvain), for creating the nanotemplates, i.e. the silicon substrates covered with a pattern of silane, which made a success of the dendrimer guiding project.

I'm thankful to Prof. Höger's group (Kekulé-Institut für Organische Chemie und Biochemie, Germany) for the (synthesis of the) macrocycles used in this work. Jeroen Gielen (Radboud University Nijmegen, The Netherlands) for a fine collaboration and a successful stay in Nijmegen, for his help with the experiments in the high magnetic field lab in order to align molecular aggregates and with the light scattering experiments on the coil-ring-coil macrocycle and for finding the time to patiently answer all my questions.

I want to express my thanks to Prof. Veciana's group (Institut de Ciència de Materials de Barcelona, Spain), in particular Núria Crivillers for the nice collaboration and for the PTM derivatives she synthesised for our project and the scanning tunnelling microscopy data she obtained together with former colleague Shuhei Furukawa. Alexander Volodin from the physics department for his help with the electrostatic and magnetic force measurements.

Quite a few people contributed to my thesis either by indirect scientific input or simply through friendship. I want to thank my colleagues for the nice time I had in (and outside) the lab and their help and support: my predecessor Philippe who taught me how to perform atomic force microscopy measurements, Tom for helping me find my way in the lab and becoming one of my best friends, Atsushi, Alina, Anca, Andrey, Ania, Carine, Chuhong, Cristina, Daojun, Davey, Dominik, Eduard, Edwin, Els, Gerd, Gert, Guojie, Hiroshi, Hong, Inge, James, Jan, Jeroen, Johan, John, Jian, Jinne, Kees, Lesley, Maarten, Magda, Marino, Mark, Michel, Mikhail, Mukulesh, Peter, Renaud, Sergey, Shengbin, Shuhei, Silvia, Susana, Tibor, Toby, Virginia, Wael, Wendy, Willem, Wouter, Yasuko, Yihong, . . . I will for sure forget to mention some names because there are simply too many to write down, but thank you all!

This research was funded by the Chemistry Department and the Research Council of the KULeuven. The experiments in high magnetic field were supported by EuroMagNET under the EU contract RII3-CT-2004-506239.

Finally, I want to thank the people in my personal life: my parents, family and friends for each supporting me in their own way. A special thanks goes to my sister Wendy and her husband Roel. You kept on believing in me when I almost lost all faith and you could motivate me to carry on in difficult times. I'm very happy you brought such a loverly goddaughter like Eline into my life. To conclude I want to thank the most special person in my life: Pieter. Besides for helping me with making the movies for the DVD (very handy scripts!) and solving my LaTeX (as well as other computer) problems, I could thank you for all sorts of things which I shall not list here. Let me just say that you were a gigantic help to me and you brighten my life simply by being there.

Thank you !

Abstract

Fabrication methods with a high level of molecular precision are required to keep up with the trend of minimising devices. Therefore, the need for novel techniques to make structures from molecular building blocks is rising. This work contributes in the unravelling and guiding of molecular self-assembly processes on surfaces. Self-assembly is a phenomenon which occurs spontaneously in the nanoscale world. The use of shape-persistent organic molecules with a well-defined shape, such as dendrimers and macrocycles, was investigated in this work. The goal is to implement molecular self-assembly in existing processes and techniques to create structures at the nanometre scale with a high level of precision. Parameters which define the outcome of the organic self-assembling systems on a surface were evaluated in order to gain insight in the self-assembly process. This knowledge could be employed in a later stage to guide the self-assembly process.

The outcome of the self-assembling of organic systems was studied with a variety of techniques such as light scattering (in solution) and mainly with scanning probe microscopy (on surfaces). Second generation polyphenylene dendrimers were used to construct nanofibres on a substrate and the impact of the substrate, concentration of the dendrimer solution, sample preparation conditions, solvent, and functional groups at the molecule's periphery were studied. The 'optimised method of sample preparation' to obtain dendrimer nanofibres was found to be dropcasting a $\sim 10^{-5}$ M dendrimer solution in THF on piranha cleaned silicon in a THF saturated tank. The aggregation of another type of organic molecules, shape-persistent macrocycles, was studied to investigate the potential of these self-assembling molecules in construction methods to create nanostructures. These results reveal the importance of the intra- and extraannular substitution of the macrocycles in creating patterned surfaces and nanoscale objects.

A second aspect concerns the location and orientation of the prepared nanostructures on the substrate's surface. The self-assembly process of the second generation polyphenylene dendrimers was implemented in a number of methods to manufacture structures in the nanoscale world. Soft-lithographic approaches were carried out by using stamps and molds to successfully direct the self-assembly process towards specific locations on the surface. In contrast to this method, the templating approach using binary patterns could not only direct the location of the aggregates on the surface, but additionally was able to control the shape of the aggregated structures. Nanofibres were aligned on the surface of a silicon substrate according to the templated substrate by applying the 'optimised method of sample preparation'. Another method using a high magnetic field (up to 20 T) was employed to influence the self-assembly process of both a dendrimer and a macrocycle system. Only in case of the macrocycle, the magnetic field turned out to have an alignment effect, which is attributed to the proper (parallel) orientation of the phenyl groups in these self-assembled fibres, a situation which can not be reached in the dendrimer fibres.

The results of this study illustrate the potential and challenges of molecular self-assembly in combination with an orientation guided approach and open a path for further investigation of other systems in a combined top-down/bottom-up approach.

Samenvatting

De vraag naar vernieuwende technieken om structuren op te bouwen vanuit moleculaire bouwstenen groeit omwille van de nood aan productiemethodes met een hoge precisie op moleculair niveau om gelijke tred te kunnen houden met de schaalverkleining van bijvoorbeeld elektronica. Deze thesis draagt bij tot het ontrafelen en sturen van moleculaire zelf-assemblage op substraten. Zelf-assemblage is een fenomeen dat spontaan optreedt in de nano-wereld. Het gebruik van vormvaste organische molecules met een welgedefinieerde vorm, zoals dendrimeren en macrocycles, werd onderzocht in deze thesis met als doel het combineren van moleculaire zelf-assemblage met bestaande processen en technieken om met grote precisie structuren te creëren op nanometerschaal. De parameters die het resultaat van deze organische zelf-assemblerende systemen bepalen, werden geëvalueerd om inzicht te krijgen in het zelf-assemblage proces. Deze kennis kon in een later stadium gebruikt worden om het zelf-assemblage proces te sturen.

Het resultaat van de zelf-assemblage van organische systemen werd bestudeerd met een reeks technieken zoals lichtverstrooiing (in oplossing) en vooral rastersondemicroscopie (op substraten). Tweede generatie polyfenyleendendrimeren werden gebruikt om nanovezels te creëren op substraten. De invloed van substraat, concentratie van de dendrimeeroplossing, omgevingsfactoren tijdens staalbereiding, oplosmiddel en perifere functionele groepen van de molecules werden bestudeerd. Het

aanbrengen van een $\sim 10^{-5}$ M dendrimeer-THF-oplossing in een THF-verzadigde tank op een siliciumsubstraat dat vooraf werd gereinigd in piranha-oplossing bleek de optimale staalbereidingsmethode. Het aggregatiegedrag van vormvaste macrocyclische molecules werd eveneens onderzocht om het potentieel van zelf-assemblage van deze molecules ter vorming van nanostructuren te evalueren. De resultaten hiervan tonen het belang aan van intra- en extra-annulaire substitutie van de macrocyclische molecules in het creëren van oppervlaktepatronen en nano-objecten.

Een tweede aspect betreft de plaats en oriëntatie van de zelf-geassembleerde nanostructuren op het substraatoppervlak. Het zelf-assemblageproces van het tweede generatie polyfenyleendendrimeer werd aangewend in een aantal methodes om nanostructuren te produceren. Lithografie met stempels en mallen werd met succes gebruikt om het zelf-assemblage proces naar speficieke plaatsen op het substraat te sturen. In tegenstelling tot deze methode kon een sjabloon met binaire patronen niet enkel de plaats van de aggregaten op het substraat sturen, maar was het ook mogelijk om de vorm van de structuren te beïnvloeden. Nanovezels werden uitgelijnd volgens het sjabloon op het substraat door gebruik te maken van de optimale staalbereidingsmethode. Een andere methode, gebruik makend van een sterk magnetisch veld (tot 20 T), werd gebruikt om het zelf-assemblageproces van zowel een dendrimeersysteem als macrocyclisch systeem te beïnvloeden. Enkel in het geval van het macrocyclisch systeem bleek het magnetisch veld een uitlijnend effect te vertonen. Dit effect wordt toegeschreven aan de juiste (parallelle) oriëntatie van de fenylgroepen in deze zelf-geassembleerde vezels, wat niet mogelijk is voor de fenylgroepen in de dendrimeervezels.

Het resultaat van deze studie illustreert het potentieel en de uitdagingen van moleculaire zelf-assemblage in combinatie met een oriëntatiesturende aanpak en opent de weg voor verder onderzoek naar de combinatie tussen top-down en bottom-up methodes.

List of Abbreviations

1D one-dimensional

2D two-dimensional

AEM arylene ethynylene macrocycle

AFM atomic force microscopy/microscope

C-AFM contact mode atomic force microscopy/microscope

CUTS cyano-undecyltrichlorosilane

DLC discotic liquid crystal

DNA deoxyribonucleic acid

DOTS docosyltrichlorosilane

DPN dip-pen nanolithography

DTS decyltrichlorosilane

EBL e-beam or electron-beam lithography

ESA electrostatic self-assembly

FWHH full width at half (maximum) height

HDTS hexadecyltrichlorosilane

HOPG highly oriented pyrolytic graphite

IUPAC international union of pure and applied chemistry

LB Langmuir-Blodgett

LbL layer-by-layer

LFM lateral force microscopy/microscope

μ**CP** microcontact printing

μ**TM** microtransfer molding

MFM magnetic force microscopy/microscope

MIMIC micromolding in cappilaries

NA numerical aperture (of a lens)

NC-AFM non-contact mode atomic force microscopy/microscope

NIL nanoimprint lithography

nM nanoManipulator

NMR nuclear magnetic resonance spectroscopy

OVS optical viewing system

PAM phenylacetylene macrocycles

PDMS polydimethylsiloxane

PFM-AFM pulsed force mode atomic force microscopy/microscope

PMMA polymethylmethacrylate

PTM polychlorotriphenylmethyl

REM replica molding

RMS root mean square

S-layer surface layer

SAM self-assembled monolayer

SAMIM solvent-assisted micromolding

SEM scanning electron microscopy/microscope

SFM scanning force microscopy/microscope

SNOM scanning near-field optical microscopy/microscope

SPL scanning probe lithography

SPM scanning probe microscopy/microscope

STM scanning tunnelling microscopy/microscope

STS scanning tunnelling spectroscopy

TCB 1,2,4-trichlorobenzene

THF tetrahydrofuran

TM-AFM TappingMode^{TM} atomic force microscopy/microscope

TEM transmission electron microscopy/microscope

Contents

Chapter 1

Molecular Self-Assembly

1.1 Introduction

In order to design efficient functional devices it is important to control the structure of organic materials down to the nanometre scale. Nanofabrication methods are generally categorised into two classes: top-down and bottom-up. *Top-down approaches* such as electron-beam lithography and photolithography are used for a long time to make nanoscale devices by using larger, externally-controlled devices. The desired final structure is carved out from a larger block of matter. As conventional lithography techniques will inevitably reach their limits in terms of feature size and fabrication cost, recent years have seen considerable progress in the development of self-assembling nanostructured surfaces. Opposite to top-down methods, this *bottom-up approach* uses extremely small building blocks to make more complex structures. Molecular assembly, nanoparticle formation, monolayer self-assembly, and probe lithography lie in this latter category. Both bottom-up and top-down approaches are applied for assembling nanoscale materials and devices for technological applications, and combinations of these two strategies have proven to be very successful. See figure 1.1 for a scheme of some nanofabrication methods.

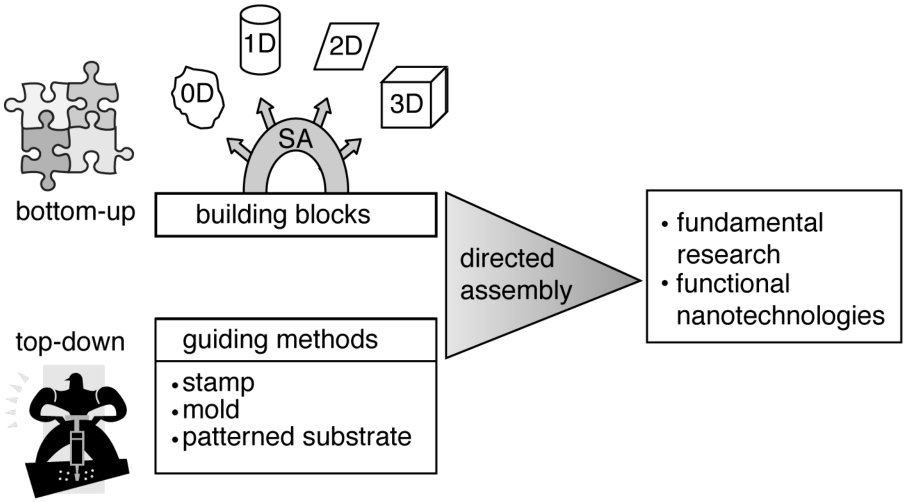

Figure 1.1: Nanofabrication methods (SA = self-assembly).

1.1.1 Definition

A self-assembled structure is spontaneously formed from building blocks that assemble without handling from the outside. This process, a prime example of the bottom-up approach, is a reversible one. A stable well-defined nanostructure can only form if it has a thermodynamic advantage in comparison with the building blocks and all the possible intermediates. The final (desired) structure is 'encoded' in the shape and properties of the individual building blocks.

Self-assembly is the fundamental principle which generates structural organisation on all scales from molecules to galaxies. It has often been taken as being synonymous to self-organisation and can be classified as either static or dynamic. Static self-assembly leads to complex structures when the system is in equilibrium and does not dissipate energy, while dynamic self-assembly requires dissipation of energy.

The best-studied sub-field of self-assembly is molecular self-assembly, used as a manufacturing method to construct things at the nanometre scale. A supramolecular assembly [Lehn, 2002], also called a supramolecular aggregate, is a molecular assembly that is beyond the scale of one molecule and is one of the most important phenomena used in supramolecular chemistry. One of the advantages of using self-assembling systems is that the quality is relatively high due to (energetically) rejection of defects.

An example of intramolecular self-assembly in nature is the folding of polypeptide chains into proteins, while the formation of a micelle results from the intermolecular self-assembly of surfactant molecules in solution. Other examples of self-assembling systems include weather patterns, solar systems, and self-assembled monolayers. Throughout this work, examples of self-assembled structures in human engineered systems will be abundantly given.

1.1.2 Interaction Forces between the Building Blocks

In contrast to molecular synthesis where molecules are formed through covalently bonding atoms, molecular assembly uses single building blocks (e.g. organic molecules) that interact with each other through weak bonds, mostly non-covalent forces. These interactions include van der Waals forces, hydrogen-bonds, hydrophobic, π-π, and electrostatic interactions (see figure 1.2 for a scheme).

1.1.2.1 Van der Waals Forces

IUPAC defines van der Waals forces as follows [McNaught and Wilkinson, 1997]. 'The attractive or repulsive forces between molecular entities (or between groups within the same molecular entity) other than those due to bond formation or to the electrostatic interaction of ions or of ionic groups with one another or with neutral molecules.' The strength of the interaction depends on the distance and relative orientation of

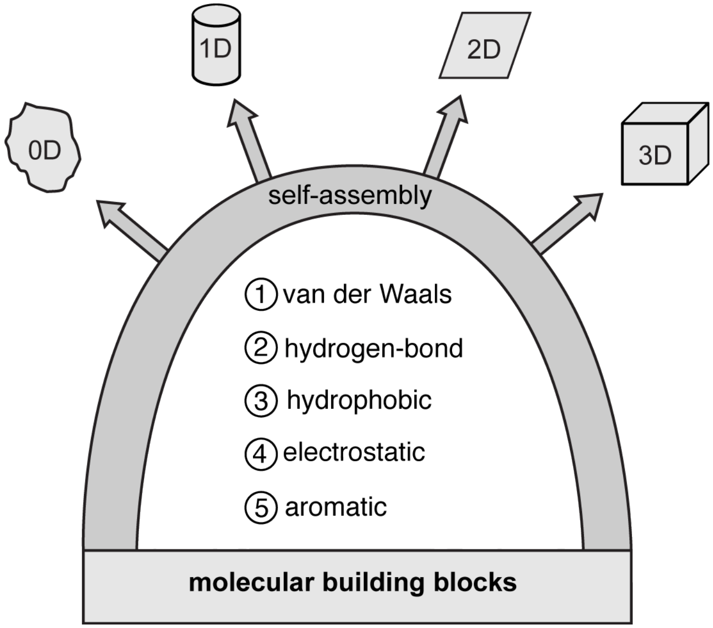

Figure 1.2: Interaction forces between the building blocks.

the dipoles. Although induction and dispersion interactions are always attractive forces, the term is sometimes used loosely for the totality of non-specific attractive or repulsive intermolecular forces.

Van der Waals forces include dipole-dipole, dipole-induced dipole and London forces. (1) *Dipole-dipole interactions* are possible between polar molecules who have a permanent electric dipole moment. (2) However, when a dipole is brought in the neighbourhood of a non-polar molecule, the latter will react to the dipole moment and can become a induced dipole itself giving rise to *dipole-induced dipole interactions*. (3) Although apolar molecules have no permanent electric dipole moment, they can interact with each other through van der Waals forces due to their mutual polarisability. These *instantaneous induced dipole-induced dipole forces* are called *dispersion* or *London forces* and arise from the movement of electrons within the electron density distribution. Moving electrons cause temporary electron imbalances leading to self-polarisation which induces polarisation in neighboring molecules. The magnitude of self-polarisation increases with increasing numbers of electrons due to their more dispersed electron density distributions. The interaction force depends on the polarisability of the interacting molecules and is inversely proportional to the sixth power of separation. The Lennard-Jones potential is often used as an approximate model for the isotropic part of a total (repulsion plus attraction) van der Waals force as a function of distance (see figure 2.9).

The ability of geckos to climb on sheer surfaces is attributed to van der Waals forces [Autumn et al., 2002]. This inspired scientists who developed materials with high adhesive properties based on van der Waals forces [Ge et al., 2007].

1.1.2.2 Hydrogen-Bond Interaction

This is a special type of dipole-dipole interaction in which the energy of the hydrogen-bond (H-bond) depends on the electronegativity of the atom the hydrogen atom is interacting with. This electronegative atom is usually fluorine, oxygen or nitrogen: $F > O > N >> Cl$. The strength of a hydrogen bond varies from a few kJ/mol (very weak) up to 40kJ/mol (strong) and is typically stronger than van der Waals forces.

Examples are interaction between molecules of water, the interaction between the base pairs in DNA, interaction between the backbone oxygens and amide hydrogens leading to 3D structures adopted by proteins which are all based on this H-bonding.

1.1.2.3 Hydrophobic Interaction

IUPAC definition [McNaught and Wilkinson, 1997]: ‘The tendency of hydrocarbons (or of lipophilic hydrocarbon-like groups in solutes) to form intermolecular aggregates in an aqueous medium, and analogous intramolecular interactions. The name arises from the attribution of the phenomenon to the apparent repulsion between water and hydrocarbons.’

Hydrophobic interactions are responsable for protein folding and formation of lipid bilayer membranes. (Note: Minimising the number of hydrophobic side chains exposed to water is generally accepted to be the main driving force for protein folding [Pace et al., 1996]. However, a recent theory was presented which reassesses the contributions made by hydrogen bonding [Rose et al., 2006].)

1.1.2.4 Electrostatic Interaction

Electrostatic forces between charged entities lead to these long-range interactions (slow power decay). Attraction results when entities with opposite charge interact, while repulsion is caused when the entities have the same charge. Electrostatic interaction changes sign upon rotation of the molecules (attractive or repulsive) depending on the mutual orientation of the multipoles. When the entities are in thermal motion, a thermal averaging effect will diminish the electrostatic forces to a large extent. For *ion-dipole interactions*, either an induced or permanent dipole around a free charge will be oriented so as to terminate some of the field lines coming from the free charge. Other interactions of this kind are *cation-π interactions* and *metal-ligand interactions*.

1.1.2.5 Interactions between Aromatic Moieties

The aromatic interaction is a non-covalent interaction between organic compounds containing aromatic moieties and is also called aromatic stacking. The electrostatic driving force of these interactions is the result of an attraction between the positively charged framework and the negatively charged electron density distribution of the neighboring units [Hunter and Sanders, 1990]. Furthermore, π-π interactions can be caused by intermolecular overlapping of p-orbitals in π-conjugated systems and hence they become stronger as the number of π-electrons increases. Examples include the self-assembly of oligothiophenes [Hoeben et al., 2005].

1.2 One-Dimensional Objects

1.2.1 Definition and Preparation Methods

One-dimensional (1D) nanostructures are materials that have a lateral size constrained to tens of nanometres or less and an unconstrained longitudinal size. 1D supramolecular objects result when interactions between the building blocks are highly directional and occur on a time scale of the self-assembling process yielding fibre or string-like objects as supramolecular polymers. These 1D structures are dynamic: they can be repeatedly assembled and disassembled in a controlled fashion based on the environment in which they are located

1.2.2 A Flavour of Self-Assembly into 1D Objects

Examples of supramolecular 1D objects from nature include deoxyribonucleic acid (DNA, figure 1.3A), actin filaments and microtubules. Microtubules (see figure 1.3B) are components of the cytoskeleton and have diameters of about 24 nm and lengths varying from several micrometres to possibly millimetres in axons of nerve cells. Microtubules serve as structural components within cells and are involved in many cellular processes including mitosis, cytokinesis, and vesicular transport.

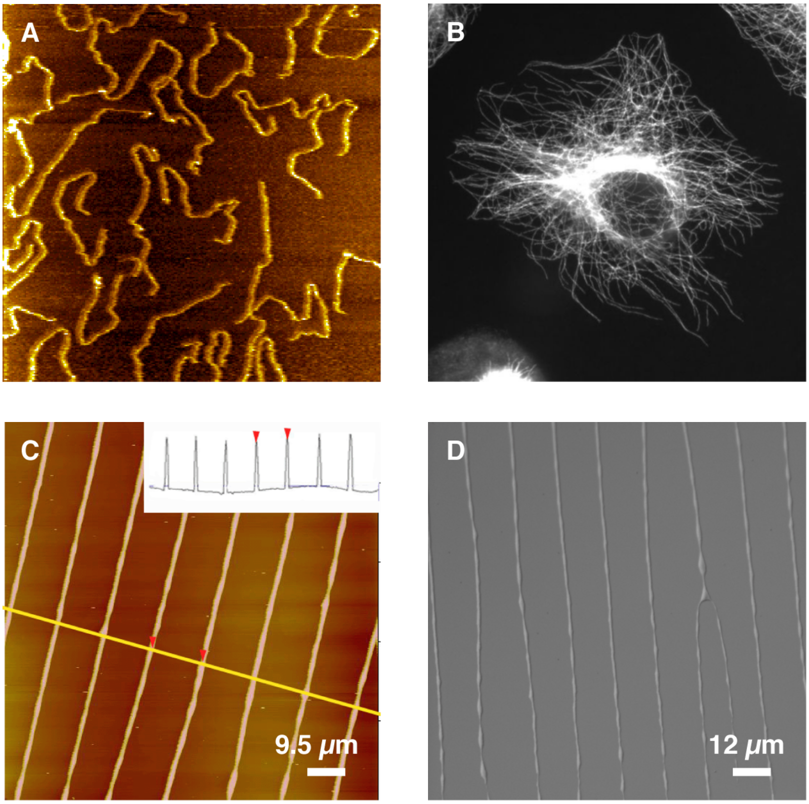

Figure 1.3: 1D objects found in nature: DNA (A) and microtubules (B). Patterns formed in the laboratory after the deposition of a disk-like porphyrin dye: AFM image (C) and optical micrograph (D) of a pattern formed on mica.

Self-assembled 1D objects made in a laboratory can be based on the π-π interactions between phthalocyanines [Shirakawa et al., 2005], [Kimura et al., 2004], or on hydrogen bonding [Barth et al., 2000], or on both for the assembly of hexasubstituted aromatics [Nguyen et al., 2004]. Striped alkanethiol structures can be used as template to direct the self-assembly of C_{60} molecules [Zeng et al., 2001]. Self-assembly of disk-like porphyrin dyes [van Hameren et al., 2006] on combination with dewetting processes can form highly periodic patterns of fibres at the macroscopic length scale which are shown in figure 1.3C and D.

1.2.3 Fundamental and Technological Interest

1D nanostructures are of both fundamental and technological interest. They are not only very interesting objects in order to study interactions and new phenomena associated with nanometre sized structures (e.g. size-dependent excitation or emission [Vosch et al., 2007]), but also represent the critical components in potential nanoscale device applications [Li et al., 2006b], important for miniaturisation in microelectronics [Luryi et al., 2002], and information storage [Ross, 2001]. A major challenge, however, remains to develop suitable chemical strategies from nanotechnology for the rational synthesis, organisation and integration of these nanoscale building blocks. Currently, inorganic nanowires are used in sensor arrays [Cui et al., 2001].

1.3 Two-Dimensional Layers

1.3.1 Definition and Preparation Methods

A two-dimensional (2D) layer, even a molecular monolayer that is only a few nanometres thick, can completely change the properties of a surface. These layers can be prepared by chemisorption or physisorption on metal and oxide surfaces, by using the Langmuir-Blodgett methodology, or by electrostatic self-assembly.

Chemisorption and physisorption can lead to spontaneous formation of self-assembled monolayers (SAMs) on substrates.

Another technique to form a monolayer is the *Langmuir-Blodgett* (LB) technique which is named after its inventors Irving Langmuir and Katharine Blodgett. The principle of this deposition technique is depicted in figure 1.4. In a first step, amphiphile molecules, which are polar molecules with a hydrophilic head and a hydrophobic tail (e.g. fatty acids), are spread over an aqueous solution (A). Moving the barriers towards each other reduces the area of the surface which results in a compression of the surface layer of amphiphilic molecules into a floating monolayer (B). This highly ordered film can be transferred to a solid surface if the latter is slowly drawn through the solution/air interface leading to the deposition of a monomolecular film (e.g. pulling the solid substrate out of the liquid, C). Multilayers with very accurate thickness can be formed by simply repeating the transfer process leading to the addition of monolayers. This is carried out by making additional immersion (D) and emersion steps.

Although this technique has proven to yield near-perfect long-range ordering of monolayers and multilayers of species that self-assemble at the liquid surface, it has its disadvantages. The technique is rather complicated, time-consuming and the required apparatus (see picture in figure 1.4E) comes at great cost and maintenance.

Multilayers can also be build using *electrostatic self-assembly* (ESA) which is based on the electrostatic interactions between nanoparticles or molecules. Oppositely charged species are held together by strong ionic bonds and thus form uniform, sturdy and stable films [Leguen et al., 2007]. The process of ESA is governed by the adsorption and desorption equilibria in cationic and anionic solutions. A clean substrate is immersed into a cationic (anionic) solution, rinsed and dried. Next, the cation (anion) coated substrate is dipped into the anionic (cationic) solution, allowing adsorption of anionic (cationic) species at the molecular level. Repeating the dipping steps in a cyclic manner allows sequential molecular build-up of thin films. A complete deposition cycle con-

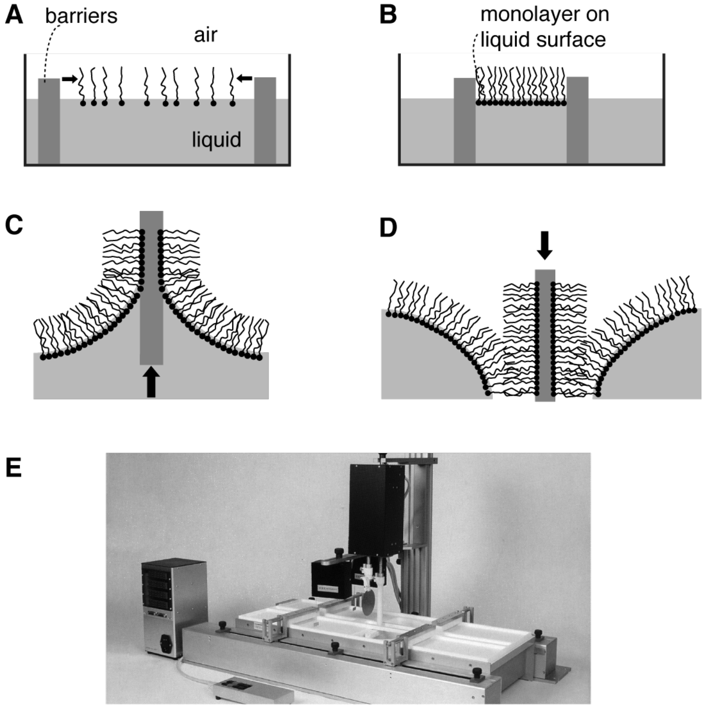

Figure 1.4: Principle of the Langmuir-Blodgett technique (A-D) and picture of such a set-up (E).

sists of a bilayer obtained from the adsorption of two oppositely charged species. This electrostatic *layer-by-layer* (LbL) self-assembly is extended to species which mutually attract each other, like molecules that form hydrogen bonding,..

1.3.2 A Flavour of Self-Assembly into 2D Objects

Surface layers (S-layers) are 2D structures that represent the outermost cell wall layer of many *Bacteria* and *Archaea*. They are built via self-assembly and enclose the whole cell surface. The constituting proteins form very regular networks as can be observed for the S-layer of *Corynebacterium glutamicum* and *Deinococcus radiodurans* which are depicted in figure 1.5A and B [Goncalves and Scheuring, 2006]. (See section 1.4.4 for an AFM image of the inner surface.)

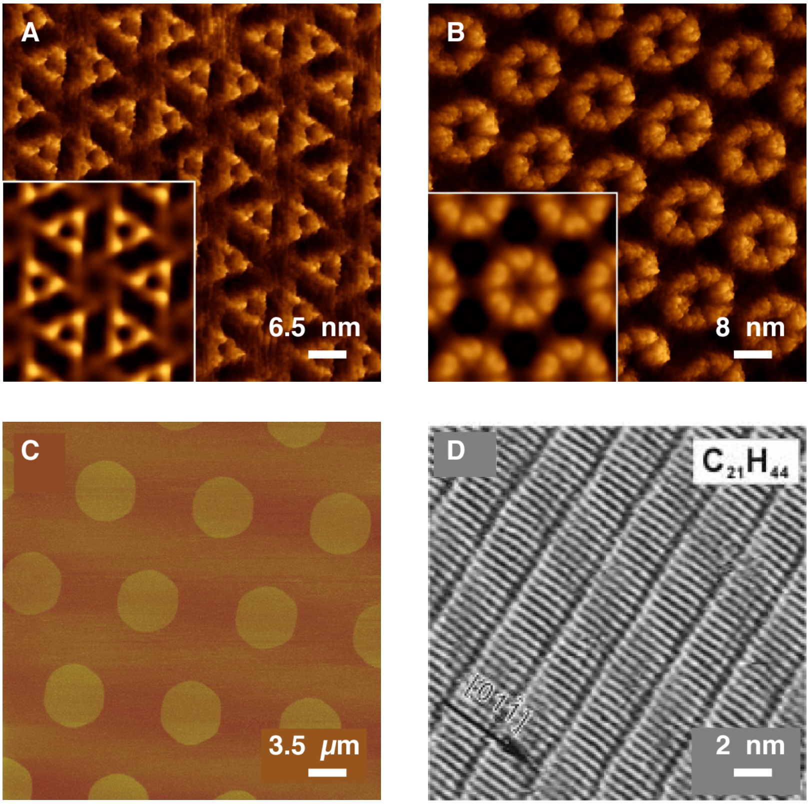

Figure 1.5: 2D objects found in nature: AFM image of the outer surface of the *Corynebacterium glutamicum* (A) and *Deinococcus radiodurans* (B) S-layer. 2D layers formed in the laboratory: AFM image of octadecanethiol dots on gold (C) and STM image from self-assembled $C_{21}H_{44}$ on gold (D).

Examples of 2D layers made in the laboratory are abundant. They can lead to crystalline structured surfaces when depositing thiols on gold and silanes on SiO_2 surfaces through chemisorption. See figure 1.5C for a contact mode AFM height image of 2D ordered dots of octadecanethiol on a gold substrate obtained by microcontact printing [Rozkiewicz et al., 2005]. Crystalline structured surfaces can also be obtained through physisorption by depositing alkane monolayers on gold [Zhang et al., 2004a], as shown for $C_{21}H_{44}$ on gold in figure 1.5D. Amorphous structures are obtained by formation of self-assembled multilayer dendrimer films made by electrostatic layer-by-layer self-assembly [Tsukruk et al., 1997].

1.3.3 Fundamental and Technological Interest

The controlled organisation of molecules and molecular assemblies on, for example, silicon oxide could have a prominent place in bottom-up nanofabrication. In recent years, SAMs on silicon oxide have reached a high level of sophistication and have been combined with various lithographic patterning methods to develop new nanofabrication protocols and biological arrays. Nanoscale control over surface properties is of paramount importance to advance from 2D patterning to 3D fabrication.

1.4 Controlling Self-Assembly Processes

A current challenge in nanotechnology is to assemble pre-synthetised nanoelements into a functional system for electronic, optoelectronic, biological, or sensing applications. To obtain useful properties, it is sometimes required to control the relative location and orientation of nanostructures on a substrate. Therefore, it is of great importance to investigate how the architecture and orientation of nanometre scale objects can be controlled. Experiments with several approaches were carried out in the past and are still being examined to acquire complete knowledge in those techniques (e.g. conventional lithography, soft lithography, nanoimprint lithography, scanning probe lithography, application of external electric or magnetic fields, using dewetting phenomena of drying droplets, molecular combing, or controlling the characteristics of the self-assembling system.)

These techniques can be used to deposit the materials of interest directly, or they can be used to make templates in order to position the materials of interest in a later step. These templating strategies allow to process a large number of organic elements at once and are often used to control organic structures at the nanometre scale.

1.4.1 Conventional Lithography

In conventional lithography an exposure source and a resist are employed to transfer the pattern of a mask to the resist and then to a substrate. These substrates need to be planar and the pattern formed on it consists of 2D structures.

Photolithography uses a light sensitive polymer, also called a photoresist, which completely covers the substrate (figure 1.6, step A). In order to create a pattern in the photoresist, a rigid photomask is put between the light source and the resist (B).

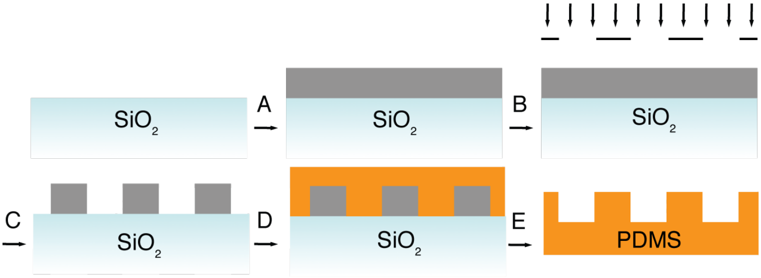

Figure 1.6: Scheme photolithography.

Different types of photoresists can be applied to form different patterns with the same mask. When a positive photoresist is subjected to light, it becomes more soluble in the developer solution and can be washed away.

The transferred pattern on the substrate will be the same as the pattern of the mask. On the other hand, if a negative photoresist is applied, it hardens and adheres to the substrate and the unexposed photoresist is washed away (step C), forming a negative image of the mask. Either way, after exposure to light the resist is developed leading to a binary resist pattern after washing. Parts of the substrate are covered with resist while other parts are completely uncovered.

This strategy can be followed to create PDMS devices as is depicted in step D and E in order to use them in a later step as stamps or molds. The remaining resist protects the parts of the substrate underneath it from etching, ion implantation, or other pattern transfer mechanism. When this strategy is applied to deposit material on the unprotected regions, the remaining resist is removed after selective deposition. Current state-of-the-art photolithography tools use deep ultraviolet (DUV) light with wavelengths of 248 and 193 nm, which allow minimum feature sizes down to 50 nm.

Electron-beam lithography (e-beam lithography or EBL) and *X-ray lithography* are important alternatives to optical lithography. Instead of light, respectively electrons and X-rays are employed to create the pattern. In contrast to photolithography, EBL is not a parallel but a serial technique. Although EBL is slower, it is regarded as complementary to optical lithography which depends on e-beam lithography to generate the masks because of its intrinsic high resolution.

EBL can be used to create a master for PDMS devices or can be applied in combination with gas-phase silanisation to form binary nanopatterned surfaces on Si [Pallandre et al., 2004] or with gas and liquid phase thiolisation on gold surfaces [Baralia et al., 2006]. This kind of patterned substrates can then be used to guide self-assembly processes as will be shown in chapter 7 were a scheme is provided in figure 7.9.

1.4.2 Soft Lithography

In soft lithography [Xia and Whitesides, 1998], a soft (elastomeric) stamp or mold transfers 2D and 3D structures on both planar as on non-planar surfaces. First, a desired pattern is etched onto a substrate (usually silicon) with photolithography or EBL. On top of this etched substrate a degassed resin, mostly PDMS or fluorosilicone, is poured. Upon removing the cured resin from the substrate, a stamp/mold contoured to the etched substrate is acquired which can be used in several techniques: microcontact printing, replica molding, microtransfer molding, micromolding in capillaries and solvent-assisted micromolding.

Microcontact printing (μCP) uses the relief pattern on the surface of a PDMS stamp to form patterns on a surface by making physical contact. A recent example is the patterning of self-assembled nanorods and nanowires [Yip et al., 2006]. A scheme of this technique is provided in chapter 7, figure 7.2.

Replica molding (REM) is an efficient method for the duplication of a stamp/mold with complementary features and yields a stamp/mold with very similar features as the original master in a simple, reliable, and inexpensive way.

In *microtransfer molding* (μTM), a thin layer of liquid prepolymer is applied to the patterned surface of a PDMS mold followed by scraping with a flat PDMS block or by blowing off with a stream of inert gas in order to remove the excess liquid. The mold filled with the prepolymer is then placed in contact with the surface of a substrate. By illuminating the mold with UV light or by heating it, the prepolymer is cured to a solid. In the last step, the mold is peeled away carefully, leaving a patterned microstructure on the substrate.

In *micromolding in capillaries* (MIMIC) a PDMS mold is placed on the surface of a substrate forming a network of empty channels between them. At the open ends of the channels, a low-viscosity prepolymer is placed which fills the channels by capillary forces. The PDMS mold is removed after curing the prepolymer into a solid, leaving the patterned microstructures of the polymer on the substrate.

Solvent-assisted micromolding (SAMIM) requires a good solvent that can dissolve (or soften) the material without affecting the PDMS mold. The PDMS mold is wet with the solvent and brought into contact with the surface of the substrate (typically an organic polymer). The solvent dissolves (or swells) a thin layer of the substrate, and the resulting fluid or gel is molded against the relief structures in the mold. The fluid solidifies when the solvent dissipates and evaporates, forming a patterned relief structure complementary to that in the surface of the mold.

SAMIM shares an operational principle similar to that of embossing, but differs from this technique in that SAMIM uses a solvent instead of temperature to soften the material and uses an elastomeric PDMS mold rather than a rigid master to imprint patterns into the surface of the substrate.

1.4.3 Nanoimprint Lithography

Nanoimprint lithography (NIL) is a novel method of fabricating nanometre scale patterns which is also referred to as embossing [Chou et al., 1996]. Patterns are formed by mechanical deformation of imprint resist and subsequent processes. The imprint resist is typically a monomer or polymer formulation that is cured by heat or UV light during the imprinting. Advantages of NIL are its simplicity, low cost, high throughput, and high resolution. A nanofabrication scheme incorporating nanoimprint lithography and layer-by-layer assembly is depicted in figure 1.7 (taken from [Crespo-Biel et al., 2006]). This approach can be used for the fabrication of high-resolution 3D nanostructures consisting of adamantyl-functionalised dendrimers and cyclodextrin-functionalised nanoparticles [Maury et al., 2007].

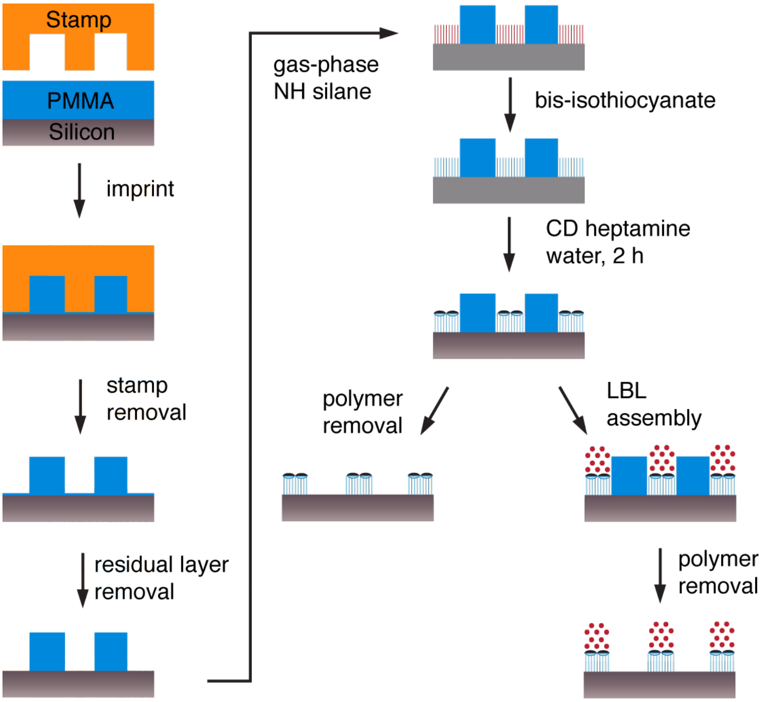

Figure 1.7: Scheme incorporating nanoimprint lithography and layer-by-layer assembly.

1.4.4 Scanning Probe Lithography

Scanning probe lithography (SPL) is a promising tool for patterning at the deep nanometre scale. Several techniques based on atomic force microscopy (AFM, see chapter 2) were developed with the aim to create molecular patterns on surfaces with nanometre scale resolution.

Dip-pen nanolithography (DPN) [Piner et al., 1999] uses the AFM-tip to deliver molecules (also called the 'ink') to a surface via a solvent meniscus, which naturally forms in ambient atmosphere, as shown in figure 1.8A.

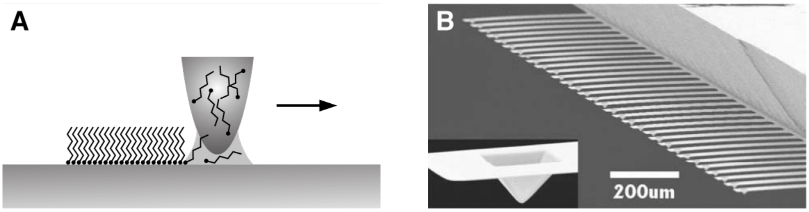

Figure 1.8: Scheme of DPN (A) and a SEM image of a DPN probe array (B). The insert shows an enlarged view of a single tip.

DPN is used throughout the world and experienced a rapid growth leading to several applications over the past several years [Salaita et al., 2007]. This scanning probe nanopatterning technique offers high-resolution patterning capabilities for a number of molecular and biomolecular inks on a variety of substrate types such as metals, semiconductors, and monolayer functionalised surfaces. Any molecule that chemically interact with the surface can potentially be used as 'ink': proteins , DNA, organic molecules, anorganic molecules, nanoparticles, sol-gel materials, or conducting polymers.

For this approach, it is required that the transported molecules anchor themselves to the substrate via chemisorption in order to create stable nanostructures. Ultra-high resolution features as small as 15 nm linewidths and 5 nm spatial resolution can be achieved with DPN. This single step process does not require the use of resists.

In addition to the initial DPN experiments that only used a single AFM probe to form nanostructures on a substrate in a serial fashion, a large and dense array of DPN pens was used (a.k.a. the multipen plotter [Hong et al., 1999]) to create features in a parallel fashion which significantly increased the throughput of DPN patterning. A scanning electron microscope (SEM, see chapter 2) image of such a DPN probe array consisting of 32 DPN-probes is depicted in figure 1.8B [Zhang et al., 2002b]. The insert shows an enlarged view of a single tip. However, since this requires that the cantilevers have the same distance to the surface and therefore, this parallel technique can only be used for flat substrates.

Arrays of proteins with 100 to 350 nm features were constructed by using DPN, exhibiting almost no detectable non-specific binding of proteins to their passivated portions even in complex mixtures of proteins [Lee et al., 2002]. This provides the opportunity to study a variety of surface-mediated biological recognition processes.

The AFM-tip can also be used to modify the surface by applying additional loading forces. This led to the development of the nanoManipulator (nM, see section 2.3.5).

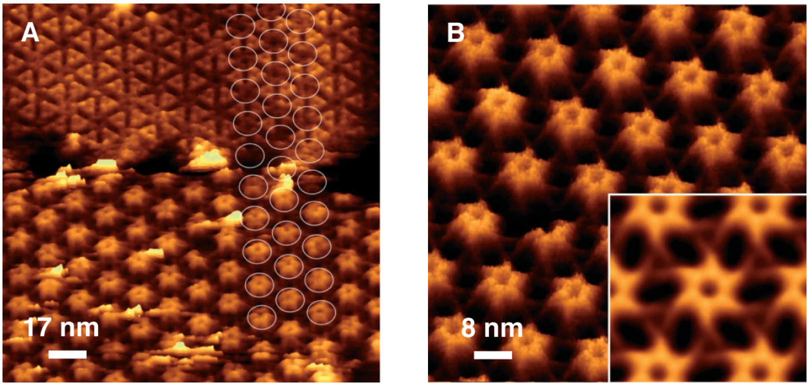

Figure 1.9: AFM images of the S-layer of *Corynebacterium glutamicum* during (A) and after (B) nanomanipulation revealing the inner surface of the S-layer.

An example of such a nanomanipulation was carried out to dissect the membrane layer shown in figure 1.5A [Goncalves and Scheuring, 2006]. The stacked membranes of the S-layer were mechanically separated during image acquisition by increasing the loading force to the tip which is depicted in figure 1.9. This resulted in access to the underlying membrane layers of an S-layer which made visualisation of the inner surface of the S-layer feasible.

Other techniques that include the use of an AFM-tip include *nanoshaving* and *nanografting*. A scheme of these techniques is depicted in figure 1.10. Hereby, the tip is used to remove material on the surface by applying a higher force during scanning. In the case of nanografting, other molecules present in solution (close to the tip) self-assemble on the surface where the tip just removed molecules, following the track of the tip.

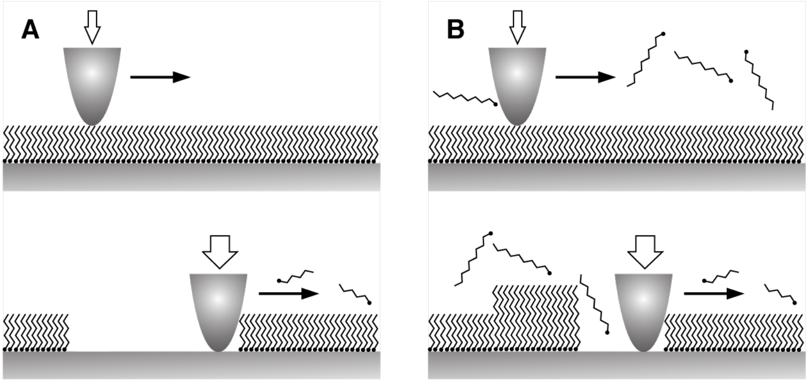

Figure 1.10: Scheme of nanoshaving (A) and nanografting (B).

One of the first examples of nanografting include the pattern formation of CH_3-$(CH_2)_{17}S$ molecules in a monolayer of CH_3-$(CH_2)_9S$ on gold [Xu and Liu, 1997]. Therefore, a monolayer of CH_3-$(CH_2)_9S$ was made on gold and the AFM-tip was used to selectively remove CH_3-$(CH_2)_9S$ from the surface. The CH_3-$(CH_2)_{17}S$ molecules present in solution occupy the spots that become vacant as the tip moves along.

1.4.5 External Electric or Magnetic Fields

Application of a magnetic field has some advantages over the techniques in previous sections, since it leads to a bulk, contact free, non-destructive force, which is homogeneous throughout the sample and thus can be used for producing highly oriented bulk samples as well as thin films. This is because high magnetic fields can be applied to align molecules exhibiting anisotropic diamagnetism, provided the magnetic anisotropy and/or the size of the molecules is sufficiently large.

In a magnetic field (B), a diamagnetic molecule acquires an extra energy (E) as expressed in equation 1.1, where χ is the molecular diamagnetic susceptibility.

$$E = -\chi B^2 \tag{1.1}$$

The diamagnetic susceptibility is closely related to the molecular structure and therefore generally anisotropic since many molecules are anisotropic. The difference in magnetic energy for different molecular orientations is expressed by equation 1.2, where $\chi_{(\|)}$ ($\chi_{(\perp)}$) is the diamagnetic susceptibility along (or perpendicular to) the molecular axis.

$$\Delta E = -\Delta\chi B^2 = -(\chi_{(\|)} - \chi_{(\perp)})B^2 \tag{1.2}$$

The molecular orientation with respect to the field direction determines the amount of extra energy in the field. This leads to a force that drives the orientation of the molecule in this way that the axis of smallest χ is along the field direction in order to minimise the magnetic energy.

For individual molecules the change in energy is small compared to the thermal energy (see equation 1.3). Therefore it is not yet possible to magnetically align single molecules due to the Brownian motion which prevents a high degree of alignment of the molecules.

$$\Delta\chi B^2 << kT \tag{1.3}$$

However, for materials that contain a sufficient amount of coupled or correlated molecules (N) the magnetic field alignment is applicable if the magnetic energy is sufficiently high to overcome the randomising thermal motion and induce orientational order (see equation 1.4). Thus by increasing the size of aggregates (with increasing concentration or decreasing temperature) the degree of alignment will increase at a given field.

$$N\Delta\chi B^2 > kT \tag{1.4}$$

Examples include the magnetic alignment of self-assembled anthracene organogel fibres due to their elongated aromatic core (see figure 1.11) [Shklyarevskiy et al., 2005], of liquid crystalline pentathiophene [Shklyarevskiy et al., 2004], and of cyanine dye J-aggregates which align with the long molecular axes of the monomers parallel to the field due to the aromatic rings present in their structure [Shklyarevskiy et al., 2002].

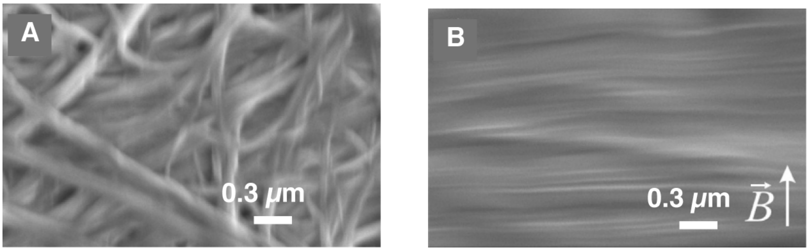

Figure 1.11: SEM images of a gel obtained at 0 T (A) and 20 T (B). The fibres are oriented perpendicular to the magnetic field direction.

1.4.6 Dewetting Phenomena of Drying Droplets

An every day example of a dewetting effect in the macroscale world is the coffee ring phenomenon (see figure 1.12). This is an illustration of ring formation in an evaporating sessile drop caused by the hydrodynamic process in which solids dispersed in the drop are advected to the contact line[1]. Indeed, after evaporation of the liquid in the coffee drop, a ring-shaped deposit containing almost all the solute (the coffee particles) is left on the substrate (figure 1.12A).

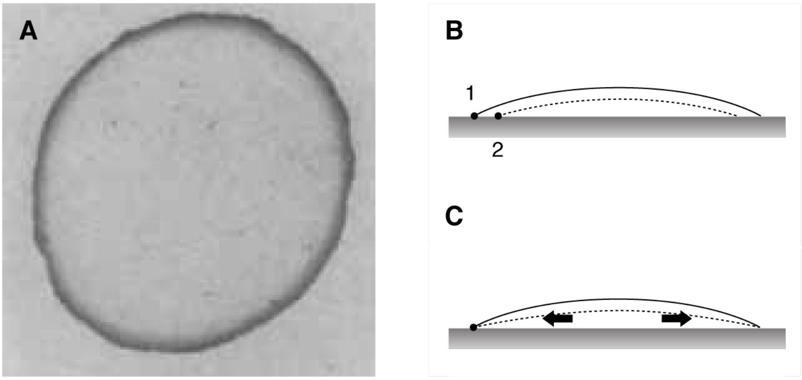

Figure 1.12: Coffee ring phenomenon. A photograph of a dried coffee drop (A) revealing a dark perimeter produced by a dense accumulation of coffee particles. Schematic illustration of the origin of the advective current (B, C).

If the contact line were not pinned as in figure 1.12B, uniform evaporation would remove the layer and the interface would move from the solid line to the dashed line. Therefore, the contact line would move from point 1 to point 2. However, the contact line can become pinned due to solute within the liquid that corrupts the substrate. If the contact line is pinned, as depicted in figure 1.12C, the retreat from point 1 to point 2 is not possible and there must be a flow that replaces the lost

---

[1] The contact line is defined as the line beyond which the solid is wet.

fluid. This compensating current keeps the substrate wet when evaporation removes liquid from around the contact line and drags the solute in the drop to the contact line where it accumulates into. The pinning of the contact line is maintained by this accumulation of solid components. This process is referred to as 'self-pinning': some preexisting conditions on the substrate temporarily anchor the contact line which permits the start of ring formation, and the additional growth increases the energy barrier the contact line must surmount to move.

Another example where contact line pinning is observed in the macroscale world is the presence of droplets on a window defying gravity after a rainstorm. The force that holds them in place arises from pinning of the contact line by irregularities, such as roughness or chemical heterogeneity, on the surface of the glass. In the microscale world, dewetting effects take place when using methods such as dropcasting, spincoating, dipcoating,...

The pinning force on the contact line is exerted by deposited solute. During the early stage of the drop's excistance the pinning force is so large that it is solely responsible for the contact line behaviour. Uncomplicated constraints produce simple structures: a ring. However, the contact line can separate from the ring. Dewetting and pinning forces are of comparable strength during this stage and the competition between these two forces can lead to an array of patterns.

Physical dewetting phenomena can be combined with self-assembly to form highly periodic patterns at macroscopic scales as shown in figure 1.3C and D [van Hameren et al., 2006]. Ordered gold and silver nanoparticle stripe patterns were obtained by the dewetting proces of a dilute monolayer formed with the LB-technique (dipcoating fashion). The stripe pattern has an uniform thickness and inter-stripe distance over the entire substrate with orientation of the stripes normal to the retreating solvent front [Huang et al., 2005]. Other examples include the liquid templating for nanoparticle organisation into complex patterns [Rezende et al., 2007].

Capillary flows in an evaporating thin film create line patterns, with widths ranging from a few micrometres to less than 100 nm. Deliberate patterning of such lines requires contact-line pinning and the presence of foaming surfactants. Large-scale photolithography can guide and control these structures by creating pinning points and steering evaporation as demonstrated by making self-assembling lines of colloidal quantum dots and microspheres [Vyawahare et al., 2006].

1.4.7 Molecular Combing

Molecular combing is a mechanical nanomanipulation technique used to stretch macromolecules in a parallel fashion, by anchoring them specifically by their extremities. It is analogue to the receding sea, which aligns algae on the beach. This technique was used to make artificial patterns of DNA [Hu et al., 2002].

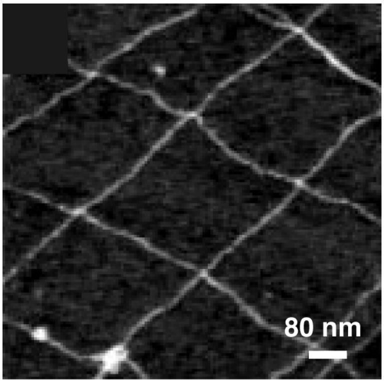

Figure 1.13: AFM image of a network consistent of aligned DNA molecules using 2D molecular combing technique.

In figure 1.13 an AFM image is shown of a network consistent of aligned DNA molecules using 2D molecular combing technique. First the DNA strands were aligned along one direction and subsequently along a second direction with a selected angle to the first one.

1.4.8 The Self-Assembling System

Besides these techniques that control the self-assembly process in an external fashion, it is also possible to control the self-assembly process in internal ways. Every self-assembling system consists of several elements or characteristics which determine both the emergence and topological features of the self-assembled structures. Despite the fact that the characteristics listed here (see also scheme in figure 1.14) are more or less artificial as many of the aspects will be closely interconnected, they are very useful to highlight the different aspects treated in this research. Two type of systems will be studied: systems in solution (figure 1.14A), and their transfer to systems on a substrate (figure 1.14B).

1.4.8.1 Building Blocks

In the self-assembling systems studied here, the building blocks are molecules in solution. It is required that the components in the system are mobile to be able to interact with one another. In solution, thermal motion (Brownian motion) provides the major part of the mobility of molecules which ensures the mass transport. Several interactions (see section 1.1.2) will take place between the molecules leading to a balance of attractive and repulsive interactions. These interactions are generally weak compared to thermal energies and are mostly non-covalent. The chemical structure of the building blocks is of great importance as varying the functional groups of a molecule can lead to different forces between molecules and thereby change the self-assembly properties dramatically. As is often used in supramolecular chemistry,

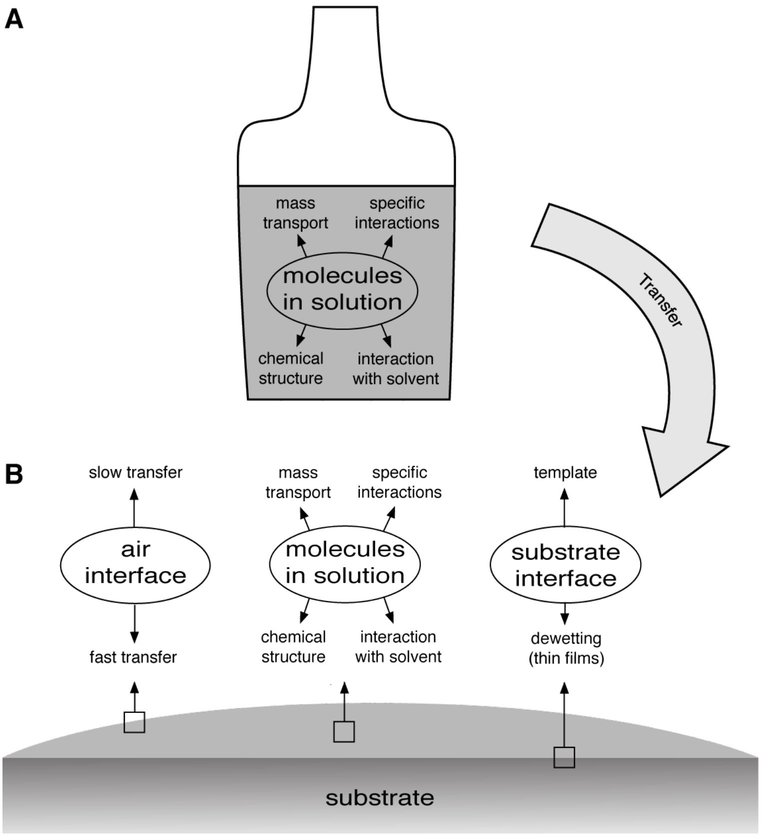

Figure 1.14: Self-assembling system in solution (A) and its transfer to a system on a substrate (B).

directly programming of these molecular units can lead to specific desired nanoscale objects. In order to investigate specific interactions between the molecules, an additional solvent can be added to block specific interactions.

For transfer of a self-assembling system in solution into a system on a substrate, the interface of the solution with the substrate and with the air can exhibit a great influence on the outcome of the self-assembly system.

1.4.8.2 Liquid/Substrate Interface

Template-based chemistry takes advantage of the influence of the surface of a substrate to guide self-assembly behaviour. When considering systems on substrates dewetting effects (see section 1.4.6) can take place upon solvent evaporation as the solution film gets thinner and thinner.

1.4.8.3 Liquid/Air Interface

If the system is transferred from solution to a substrate, the speed of transfer can be very important in certain systems. Therefore the liquid/air interface can determine the outcome of the self-assembly process. If the air is saturated with solvent molecules or a non-volatile solvent is used the transfer will be slow; however, in ambient conditions the transfer can be fast for systems with volatile solvents. The association of the components must be reversible or must at least allow the components to adjust their positions within an aggregate once it has formed. Therefore the strength of the forces tending to disrupt the aggregates, mostly thermal motion, must be comparable to the interactions forces between components. Fast transfer can lead to systems where the forces that disrupt the aggregates are not in balance with the forces that form them. In this case, components cannot adjust their position within the aggregates and corrections to the self-assembled structures are impossible leading to less ordered structures.

1.5 Objectives

The global goal of this thesis is to gather information on the self-assembly of organic molecules on a surface, to control this self-assembly, and to examine the structures formed. Phenomena such as self-assembly and dewetting will be employed to create surface structures on the submicron scale. It is expected that this low-cost approach will contribute to a new generation of surfaces with novel physical and chemical properties.

Several aspects will be studied for a number of systems in order to obtain more information on the self-assembly process of these systems leading to insight on how to control the self-assembly of the systems: the effect of the building blocks, the air/solution interface and the solution/substrate interface. Throughout this thesis, it will be illustrated that a favourable outcome of molecular self-assembly can be acquired by fine-tuning (a selection of) the characteristics of the system.

Three types of molecules will be studied: dendrimers, macrocycles, and polychlorotriphenylmethyl molecules. These molecules have in common that they are well-defined in shape and size, and that they can be modified with different functional groups, which makes them promising building blocks for creating nanostructures.

The self-assembly behaviour of a second generation polyphenylene dendrimer is presented which was taken to illustrate the ability to fine-tune self-assembly processes by playing with the characteristics of the system. To ensure the mass transport, a solvent will be used to dissolve the dendrimer molecules leading to mobile building blocks in the system. Dynamic light scattering experiments will be carried out to investigate the aggregation of the dendrimer in solution and AFM measurements will be conducted to study the aggregation between the dendrimer molecules under dry conditions when dropcast from solution onto a flat substrate. The influence of the substrate on which the self-assembled structures are deposited as well as the liquid/air interface during the sample preparation will be examined to study if the velocity of solvent evaporation (dependent on temperature as well as the presence of a saturated atmosphere) has an impact on the type of aggregated structures which will be formed. Inherent to self-assembly is the reversibility or adjustability of the system, which will be probed for this dendrimer system. In order to investigate the nature of the (solvent-mediated) dendrimer-dendrimer interactions, solvent mixtures will be applied by adding a second solvent to solutions of the dendrimer which is expected to block specific interactions by shielding the functional groups. The aggregation behaviour of dendrimers with different functional groups will be investigated with respect to the stabilisation of their assembled structures.

Different strategies to externally influence the outcome of the self-assembly process will be followed in order to obtain controlled deposition of dendrimers on a substrate and thereby aligning the nanostructures which are formed upon self-assembly of the second generation polyphenylene dendrimer. Approaches such as soft lithography, the use of patterned substrates, and the use of extremely high magnetic fields will be employed in order to influence the location and the orientation of emerged nanostructures.

A second type of building blocks are the macrocycles for which this study will be focussed on the nature of substituents on the macrocycle and the effect of the solvent in which the macrocycles are dissolved. The aggregation behaviour of oligo-alkyl-substituted macrocycles with and without a biphenyl bridge at the solution/substrate interface, as well as on the air/substrate interface will be studied. Light scattering experiments will be performed on the solution of an oligo-alkyl-substituted macrocycle with two large flexible polystyrene chains, also called the coil-ring-coil macrocycle, to investigate if aggregates are formed in solution. In addition, samples will be made on a substrate from different concentrated solutions. The effect of bulky triisopropyl- and oligo-alkyl-substituents upon the self-assembly of dibenzonaphthacene rings will be examined at the solution/substrate interface, as well as at several air/substrate interfaces.

Analogue as for the dendrimers, a macrocycle will be selected and extremely high magnetic fields will be applied to solution as well as during sample preparation on a substrate in order to control the outcome of the self-assembly process.

Polychlorotriphenylmethyl molecules make up the third type of building blocks and their assembly behaviour will be studied at the solution/substrate interface, as well as on the air/substrate interface.

Chapter 2

Scanning Probe Microscopy

2.1 Introduction

In the past, several microscopic techniques were developed to gain information about morphology and other surface properties of samples. *Far field optical microscopy* uses light and lenses to illuminate the sample and collect the light which comes from the sample with a detector to make up an image presenting the surface property of the sample. Microscopic techniques are often compared by their resolution, which is the minimal distance between two objects which can still be detected as two different objects in the recorded image. Two parameters determine in principle the resolution in far field optical microscopy: the wavelength of the excitation light (λ) and the numerical aperture (NA) of the lens which focusses the light. This is the diffraction limit as is expressed in equation 2.1.

$$Maximum\ resolution = 0,61\lambda/NA \tag{2.1}$$

To obtain the highest possible resolution with these microscopes, lenses with a high numerical aperture (NA≈1,4) are being used, leading to a resolution of about half of the wavelength of the excitation light. Since commonly visible light is used, this results in a resolution of a few hundred nm. In figure 2.1 a simplified scheme of a confocal microscope is depicted. This type of microscope has a higher resolution than conventional optical microscopy due to the use of pinholes in the set-up.

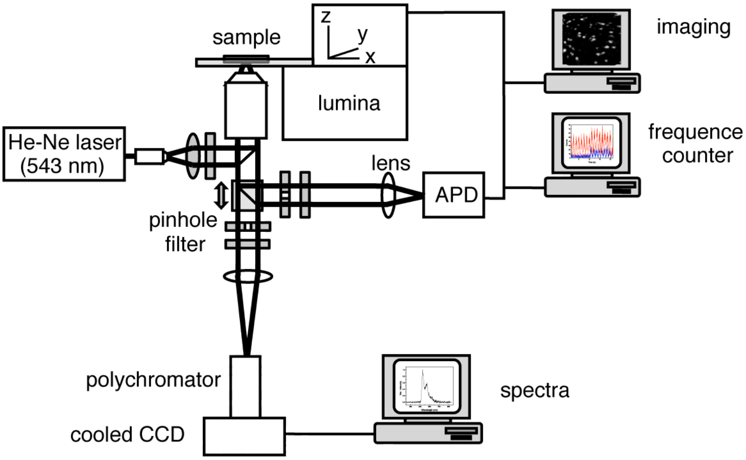

Figure 2.1: Simplified scheme of a confocal optical microscope.

In order to increase the resolution, another type of microscope was invented which was no longer based on light. In *electron microscopy* the surface of the sample is being scanned with high energetic electrons to obtain a signal representing the electron density. There are two classes of microscopes in this family: the scanning electron microscope (SEM) and the transmission electron microscope (TEM). In the case of TEM the transmitted electrons are detected, while in SEM, the scattered electrons are detected. The maximum resolution of a SEM is typically a few nanometre, while it is possible to obtain atomic resolution with a TEM.

In the early 1980's other microscopes were developed with a resolution in nm to Å scale. The common feature (see figure 2.2) of these *scanning probe microscopes* (SPM) is an ultra-sharp probe or tip. This probe scans very close (nanometre region) to the surface of a sample while some probe-sample interaction or interactions are recorded which relate to local (ultimate atomic resolution) properties such as current, force, etc...

Several SPM's were invented, each detecting some specific properties of the sample surface. Piezoelectric materials are used to move the tip or sample with extreme precision on a very small scale. The piezoelectric effect (discovered by Curie in 1880) is created by squeezing the sides of certain crystals, resulting in the creation of opposite charges on the sides. The effect can be reversed by applying a voltage across a piezoelectric crystal which will than elongate or compress. A typical piezoelectric material used in STMs is lead zirconium titanate.

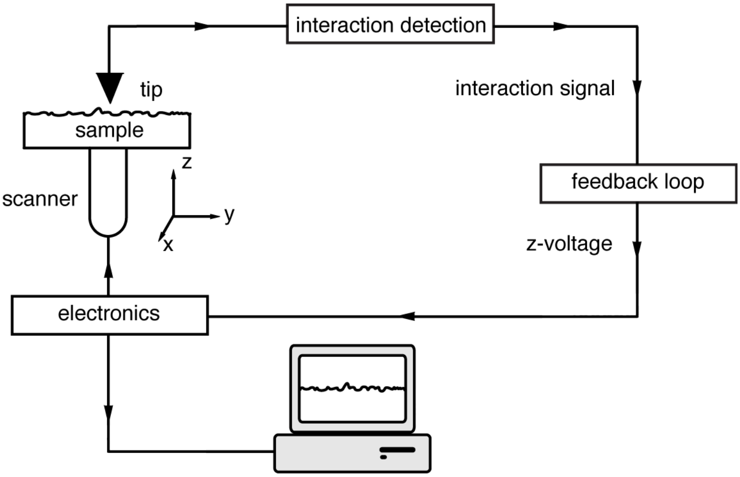

Figure 2.2: General scheme of an SPM.

The main advantage of these microscopes compared to SEM and TEM is the fact that samples can not only be investigated in UHV, but also in ambient conditions and they have a very good resolution in the z-direction of the sample (perpendicular to the surface), in the order of an Å (1Å=10^{-10}m) or even better. This is feasible thanks to the extremely small interaction area between tip and sample which is dependent on the dimension of the tip and the roughness of the sample surface.

2.2 Scanning Tunnelling Microscopy

The first SPM, which was a scanning tunnelling microscope (STM), was developed last century in the early 80's by Binnig, Rohrer, Gerber, and Weibel at IBM in Zurich, Switzerland. In 1986 Binnig and Rohrer (see picture in figure 2.3) were rewarded for this invention with the Nobel Prize in Physics.

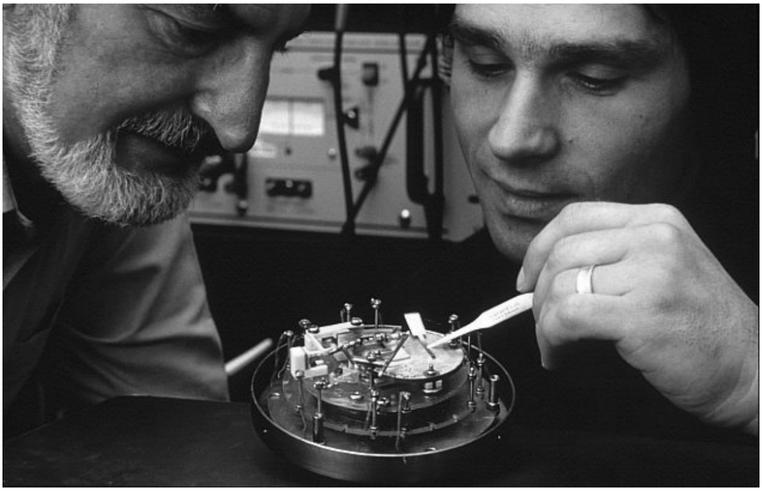

Figure 2.3: Rohrer (left) and Binnig (right) got the Nobel Prize in Physics (1986) for the invention of the STM.

2.2.1 Tunnelling Current

The interaction between an STM-tip (a very sharp metal wire) and the sample is based on the tunnelling effect of electrons which is a quantum mechanical phenomenon that occurs when two conductive objects are brought in close vicinity of each other without making physical contact (see scheme in figure 2.4). When the extremely sharp conductive tip is brought into the vicinity (few Å) of the (semi-)conductive sample surface, electron density distributions of tip and sample partially overlap each other. This gives rise to the tunnelling effect: although this is classically impossible, electrons acquire a certain probability to jump from the tip to the sample, and vice versa. Electrons tunnel through the potential barrier instead of travelling 'over' it. Since the chance of an electron to jump from tip to the sample is equal to the chance of an electron to jump from sample to tip, no net current will be observed. However, if a different potential is applied to the tip as to the sample, a net current can be observed which is typically a few pico- to nanoampères. The direction of this current is dependent on the polarity of the applied potential.

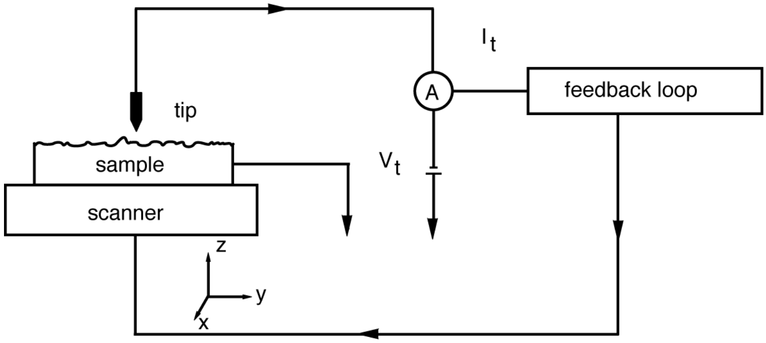

Figure 2.4: Scheme of an STM.

The observed tunnelling current (I) between tip and sample is exponentially dependent on the separation (d) as expressed in equation 2.2. Where V represents the bias voltage between tip and sample and c is a constant value.

$$I \sim Ve^{-cd} \tag{2.2}$$

2.2.2 Tunnelling Current Probability

It should be pointed out that STM images are never 100% pure topographical images but always combine electronic and topographic information. Indeed, it is not a real physical surface that is reconstructed in an STM image but a surface with constant tunnelling current probability. However, this apparent disadvantage can be transferred in an advantage for scanning tunnelling spectroscopy (STS) which can be used to study electronic properties with atomic resolution at very small scales.

2.2.3 Feedback and Modes

A piezoelectric scanner moves the sample or tip with extremely high precision to scan the sample surface with the tip. As features of different heights are encountered, the different tip-sample separation leads to a change in tunnelling current. There are two modes (see figure 2.5) in which an STM can operate: the constant current mode and the constant height mode.

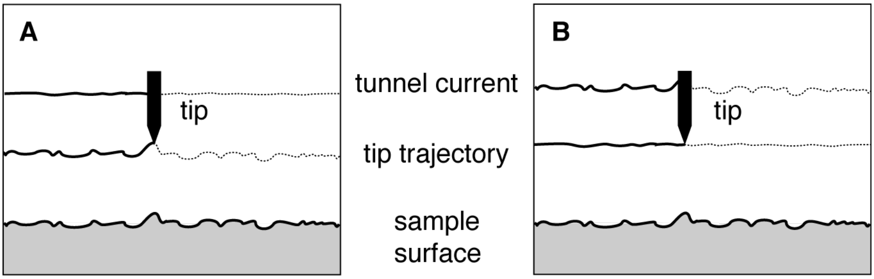

Figure 2.5: Different modes of an STM: constant current mode (A) and constant height mode (B).

2.2.3.1 Constant Current Mode

In order not do damage the sample or tip a constant tip-sample separation distance is kept by using a feedback system. The feedback loop maintains a constant tunnelling current during scanning by vertically moving the scanner at each (x,y) data point until a ‘setpoint’ current is reached. This movement pattern of the tip (vertical position of the scanner at each (x,y) data point) is magnified and displayed in the STM image.

2.2.3.2 Constant Height Mode

In this mode, the tip keeps a same absolute height, varying the distance between tip and sample when features on the surface are encountered. The tunnel current will differ for each (x,y) data point revealing information about the height or electronic properties of the features. Measurements in this mode can be carried out faster because the scanner does not need to adjust the z-position of the tip for each (x,y) data point. Measurements suffer less from thermal drift and it is possible to examine dynamic processes. However, the sample must be (atomically) flat to prevent touching the sample surface.

2.2.4 Limitations and Resolution

As this technique is based on a tunnelling effect, it is limited to semiconducting and conducting surfaces. To get around this restriction, one can put a nanometre-thin film of the material of interest on top of a conductive substrate. Due to the exponential dependence of the tunnelling current, the interaction between sample and tip is limited to the atoms at the very end of the tip, also called the tip's apex, resulting in an extremely high sensitivity for small changes in distance (see scheme in figure 2.6). An STM can image down to the atomic level due to this exponential dependence. STM has the best spatial resolution of all SPMs, better than 1 Å in all directions (x, y, and z), and is thereby capable of detecting defects on the atomic scale.

The STM measurements shown in this thesis are all carried out at the liquid/solid interface as many molecules adsorb easy at this interface, making it feasible to image them. One of the substrates is highly oriented

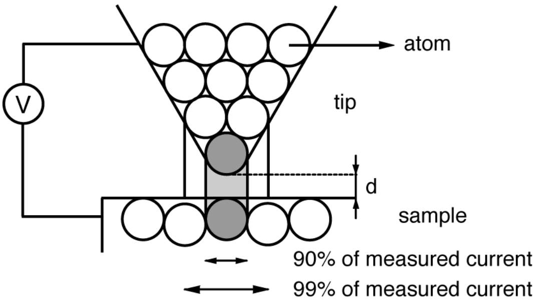

Figure 2.6: Scheme of tip-sample interaction.

pyrolytic graphite (HOPG) which is frequently used for STM since it is atomically flat due to its layered structure and it has good conductive properties.

2.3 Atomic Force Microscopy

The atomic force microscope (AFM) was developed in the mid 80's last century by Binnig, Quate, and Gerber as a collaboration between IBM and Stanford University and is also known as the scanning force microscope (SFM). Other related microscopy techniques include lateral force microscopy (LFM) and magnetic force microscopy (MFM).

2.3.1 Forces and Detection of Interaction

The interaction between an AFM-tip and the sample (see scheme in figure 2.7) is based on the forces between them which are mainly van der Waals forces (see 1.1.2.1). The ultra-sharp AFM-tip is attached to the free end of a flexible cantilever and when it approaches the surface of the sample, this cantilever will be bend due to local force interactions.

Depending on the magnitude of the force interaction between tip and sample, the magnitude of the cantilever deflection will be different. AFM

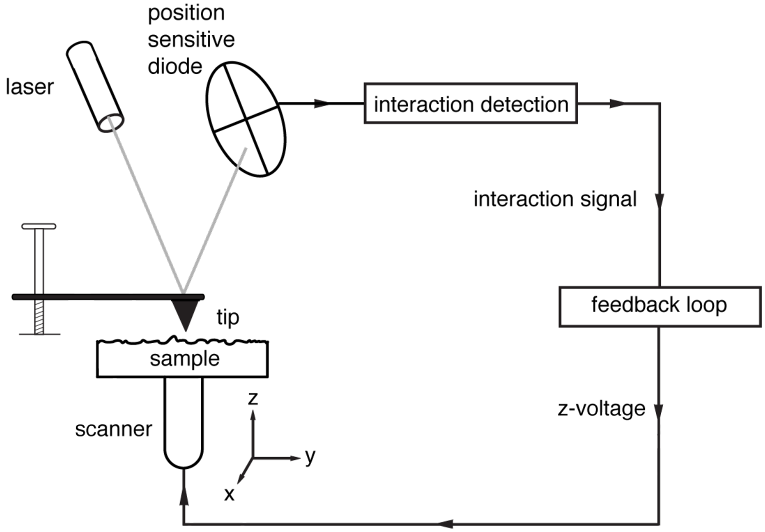

Figure 2.7: Scheme of an AFM.

operates by scanning the tip across the sample surface while monitoring the change in cantilever deflection. The amount of deflection of the probe can be detected in several ways. Detection of the cantilever's vertical movement of the first AFMs was done with a second tip - an STM placed above the cantilever. Today, most AFMs use the optical beam deflection method (see scheme in figure 2.8). A laser beam (1) is focussed on a reflective cantilever via a mirror (2) and reflected from the back of the cantilever (3). This reflected light beam is guided via a second mirror (4) onto a position sensitive detector (5). This split photodiode detector is mostly divided in four equal parts. In this way, the bending and torsion of the cantilever can be correlated with the vertical and lateral force interactions, respectively. As the cantilever is bent, the difference in signal of the upper and lower part of the photodiode will change, while if the cantilever is twisted, the difference in signal of the left and right part of the photodiode will change.

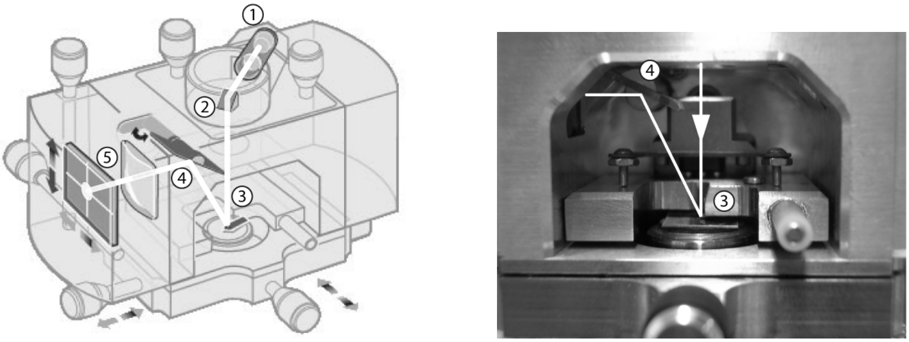

Figure 2.8: Detection of the interaction.

2.3.2 Feedback and Modes

Similar to STM, there are different modes in which an AFM can operate: the constant height mode and the constant force mode.

2.3.2.1 Constant Height Mode

In this mode, which is also called the variable-deflection mode, the AFM-tip is kept at a constant absolute height. When features on the surface are encountered, the distance between tip and sample varies. The interaction forces will therefore differ for each (x,y) data point revealing information about the height of the features. The force signal which is detected via the photodiode is directly used to construct the AFM image. This mode is however barely used for AFM, since measuring with a fluctuating force is difficult.

2.3.2.2 Constant Force Mode

In order not do damage the sample or tip a constant tip-sample separation distance is kept by using a feedback system. The force signal detected with the photodiode at each (x,y) data point can be used in a feedback loop to maintain a constant force between the tip and the sample. This is done by vertically moving the scanner at each data point until a ‘setpoint’ value is reached. This movement pattern of the tip (vertical position of the scanner at each (x,y) data point) is magnified and displayed in the AFM image.

Because this mode relies on keeping constant forces between the tip and sample, knowing these forces is important for proper imaging. The force (F) is not measured directly, but calculated from Hooke’s Law (see equation 2.3) by knowing the spring constant or the stiffness of the cantilever (k) and measuring the distance the cantilever is bent (x).

$$F = -kx \tag{2.3}$$

Force constants usually range from 0.01 to 1.0 N/m, resulting in forces ranging from nN to μN in an ambient atmosphere. Operation can take place in ambient and liquid environments.

There are three primary modes of AFM, dependent on the type of interaction: contact mode, non-contact mode, and intermittant mode AFM. When tip and sample approach each other (see scheme in figure 2.9), a weak attraction force will be induced due to the opposite polarisation of the electron density distributions. When approaching even further, the density distributions will start to overlap each other, which will result in a strong electrostatic repulsion causing the general interaction force to increase dramatically. This decrease will occur when the distance between tip and sample is typically a few Å. At the moment that the total interaction force becomes positive, and thus repulsive, it is said that the tip and sample are in contact.

The type of interaction in *contact mode AFM* (C-AFM, figure 2.10A) is mainly repulsive since the tip contacts the surface through the adsorbed fluid layer on the sample surface. The main advantage of this

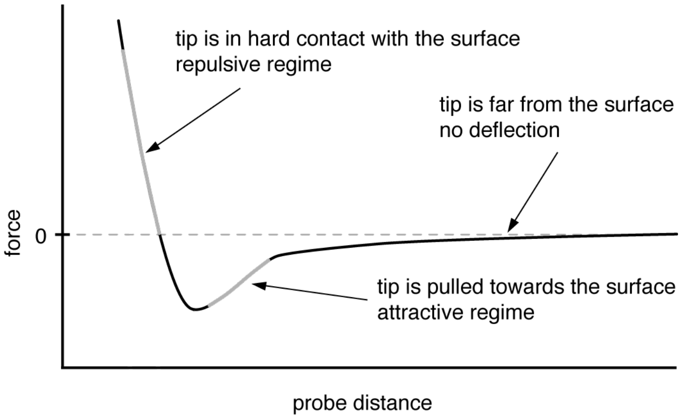

Figure 2.9: Interaction forces in function of tip-sample distance.

mode is high scan speeds. However, the lateral (shear) forces can distort features in the image due to the contact between tip and sample. The combination of lateral forces with high normal forces which are due to capillary forces from the adsorbed fluid layer on the sample surface in air can result in reduced spatial resolution. Additionally, this may damage soft samples due to scraping between the tip and sample. Because the tip is in hard contact with the surface, the stiffness of the cantilever needs to be less that the effective spring constant holding atoms together, which is on the order of 1-10 N/m. Most contact mode cantilevers have a spring constant of $<$ 1N/m.

In order to reduce the forces exerted on the sample surface, *non-contact AFM* (NC-AFM, figure 2.10B) was developed which is mainly attractive. In this mode the tip does not contact the sample surface, but oscillates (AC-mode) above the adsorbed fluid layer on the surface during scanning. The oscillation of the stiff cantilever at a frequency which is slightly above the cantilever's resonance frequency has typically an amplitude of a few nanometres (<10 nm). When approaching the tip to the surface of the sample, interaction forces will decrease the cantilever's

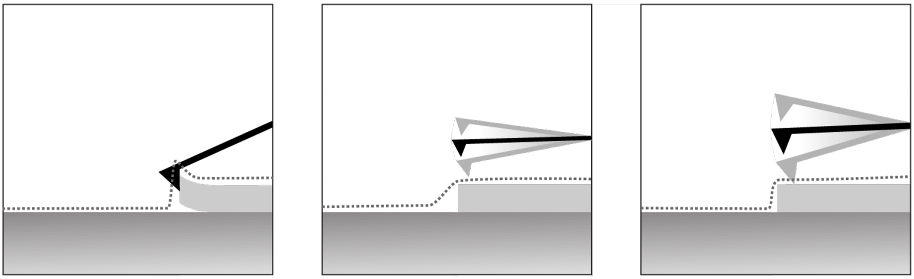

Figure 2.10: Different modes of an AFM: contact mode (A), non-contact mode (B), and intermittant contact mode (C).

resonant frequency. These forces can be van der Waals forces which extend from 1 nm to 10 nm above the adsorbed fluid layer, and other long-range forces which extend above the surface. The decrease in resonant frequency will result in a decrease of the amplitude of oscillation. Similar to C-AFM, a feedback loop maintains a constant (oscillation amplitude or frequency and thus) force between tip and sample by vertically moving the scanner at each (x,y) data point until a 'setpoint' amplitude or frequency is reached. Due to the tip-sample separation, the lateral resolution is lower than for C-AFM. The scan speed is slower than in C-AFM or TM-AFM (vide infra) to avoid contacting the adsorbed fluid layer. Non-contact usually only works on hydrophobic samples, where the adsorbed fluid layer is at a minimum. If the fluid layer is too thick, the tip becomes trapped in the adsorbed fluid layer causing unstable feedback and scraping of the sample. Due to these disadvantages, applications for non-contact mode AFM imaging have been limited.

The type of interaction in *dynamic force AFM* (DFM-AFM, figure 2.10C), also called *intermittant contact AFM* or *TappingMode*^{TM} *AFM* (TM-AFM) is both attractive and repulsive. In this AC-mode, the stiff cantilever is oscillated closer to the sample than in NC-AFM, at or near its resonance frequency with an amplitude ranging typically from 20 to 100 nm. To reduce forces exerted on the sample surface, the tip lightly 'taps' on the surface during scanning, contacting the surface at the bottom of its swing (repulsive regime). The feedback loop maintains a constant oscillation amplitude by maintaining a constant RMS of the oscillation signal acquired by the split photodiode detector. Operation can take place in ambient and liquid environments. In liquid, the oscillation does not need to be at the cantilever resonance. When imaging in air, the typical amplitude of the oscillation allows the tip to contact the surface through the adsorbed fluid layer without getting stuck. Advantages of this technique are the higher lateral resolution on most samples (1 nm to 5 nm) and lower forces leading to less damage to soft samples imaged in air. The lateral forces are virtually eliminated, so there is no scraping. A disadvantage is the scanning speed, which is slower than for C-AFM. A state-of-the-art resolution was obtained recently by imaging the surface of an alloy system and identifying the constituent atomic species at room temperature under UHV conditions [Sugimoto et al., 2007].

While using TM-AFM one can turn on phase imaging (see scheme in figure 2.11) which is a powerful tool for mapping variations in sample properties at very high resolution. Although there is currently no simple correlation between phase contrast and a single material property, a phase image can reveal variations in composition, adhesion, friction, viscoelasticity, and numerous other properties.

Phase imaging measures the phase lag of the cantilever oscillation relative to the piezo drive. Therefore it highlights edges and is not affected by large-scale height differences. However, at small-scale height differences the phase imaging can be affected by the topography of the sample, which explains different contrast for particles with similar composition but different dimensions. In addition to phase images, amplitude images can be recorded in a similar way by detecting the amplitude ratio of the

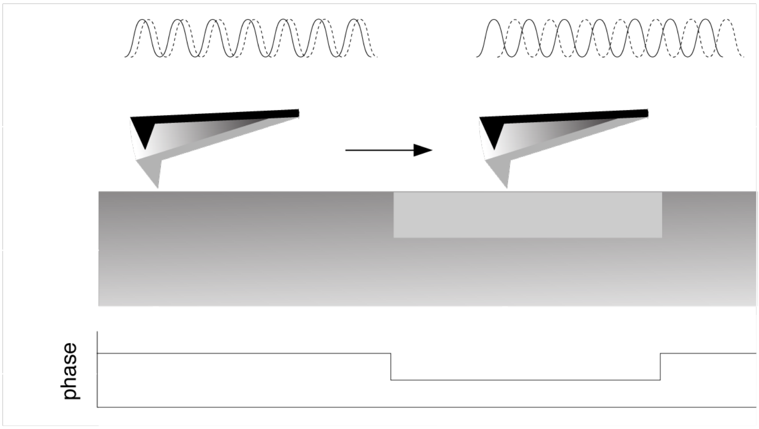

Figure 2.11: Phase imaging in TM-AFM.

cantilever oscillation relative to the piezo drive.

2.3.3 Limitations and Resolution

Although the resolution of an AFM (lateral: 1 to 10 nm and vertical: 0.1 nm) is lower than for STM, it overcomes the basic drawback with STM, which is that it can only image semi-conducting or conducting surfaces. Indeed, AFM can image almost any type of surface, including polymers, ceramics, composites, glass, and biological samples. It is possible to measure not only topography, but also friction and elasticity on the nanometre scale.

The AFM measurements shown in this thesis are all carried out at the air/solid interface on substrates such as highly oriented pyrolytic graphite (HOPG), mica, and silicon that are all extremely flat (figure 2.12). In contrast to HOPG, mica and silicon have hydrophilic surfaces. Mica has a layered structure like HOPG, and consists of aluminum silicate sheets which are not strongly bonded, but held together by K^+ ions. Therefore, both mica as HOPG can easily be cleaved with tape to

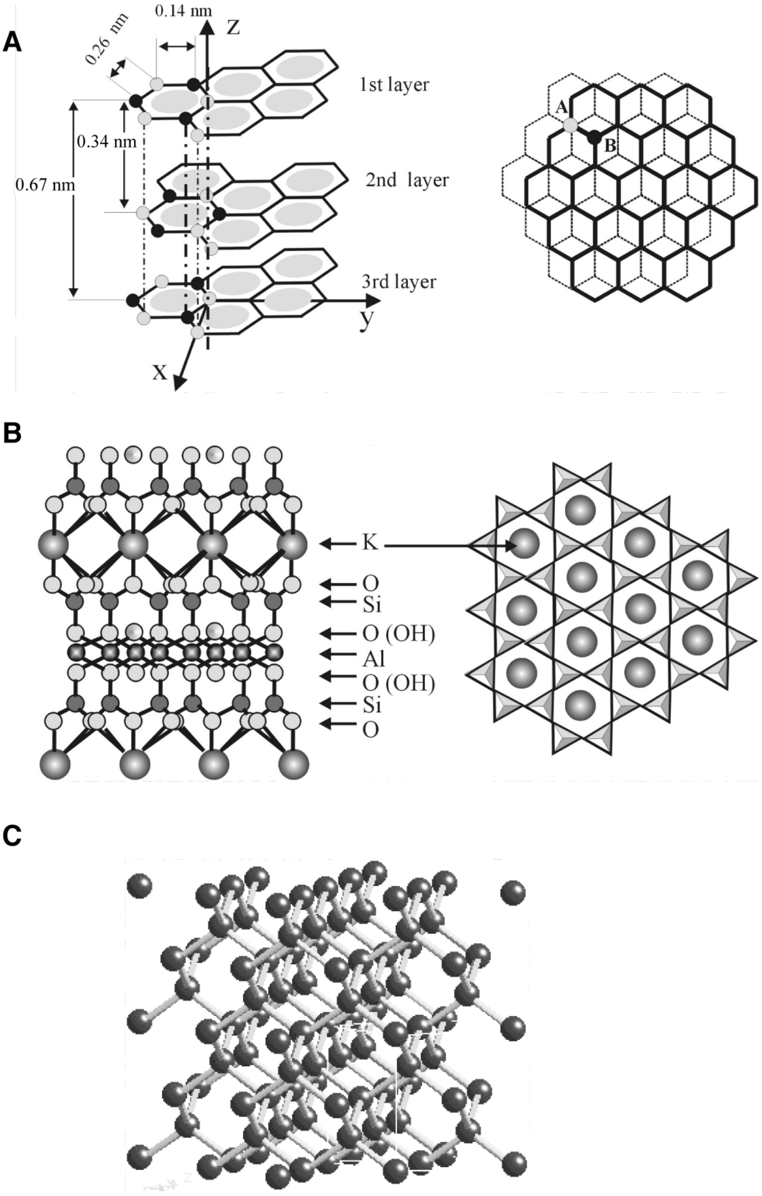

Figure 2.12: Commonly used substrates: highly oriented pyrolytic graphite (A), mica (B), and silicon (C).

remove their upper layer, leading to a clean surface. In order to clean silicon surfaces, a piranha solution is used.

2.3.4 Optical Viewing System

The optical viewing system (OVS) consists of an analog camera, which is mounted vertically over the head of the AFM to view both sample surface and tip and is therefore used to align the laser beam on the cantilever.

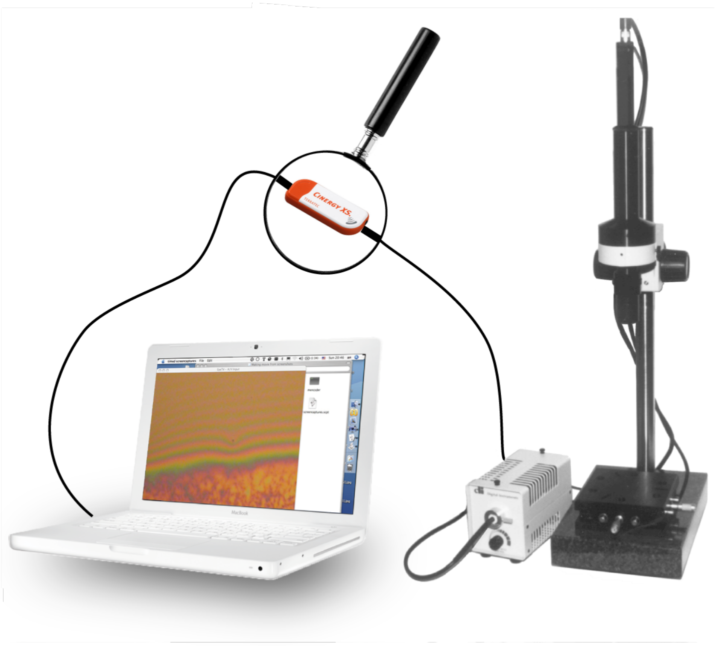

Figure 2.13: Optical viewing system with computer and frame grabber.

The camera has an image resolution of 768×576 pixels and is mounted on an objective which creates images of an area in the order of magnitude of 0.6×0.4 mm^2 giving an optical resolution of approximately 750 nm. The granite base weights twenty pounds and is supported on four isolation pads to dampen vibration for general scanning. This OVS can also be used to build a set-up, including a computer with an analog frame grabber device, to record optical images as well as to make real time optical movies. A scheme of this set-up (without AFM) is shown in figure 2.13.

2.3.5 NanoManipulator

SPMs are perfect tools to image matter at the nanometre scale, but they can also be applied to manipulate matter on this small scale. In order to avoid damage to the sample, the force applied to an AFM-tip is normally as small as possible. However, if larger forces are applied to the tip which is moved in a specific way, the tip can be employed to conduct manipulations. A schematic set-up of the nanoManipulator is depicted in figure 2.14. Three main parts are connected through a local network: an AFM (A), an advanced display and control unit (B) and an haptic interface (C).

The movement of the operator is detected via the haptic interface, which is a commercially available device called the robot arm (PHANToM ®). The function of this arm is twofold: the operator can control the movement of the tip by moving this robot arm (translating macro movements into micro movements), but can also provide the operator with information of the sample and forces from the micro world which are translated into macro movements, making it possible to 'feel' the surface of the samples of interest. It is very easy to switch between imaging (scanning of surface with minimal force interactions), haptic (feeling in real time, the tip follows the movements of the operator, a minimal force interaction is maintained) and manipulation (increasing the force interaction) mode making is possible to manipulate objects with a resolution comparable to an AFM.

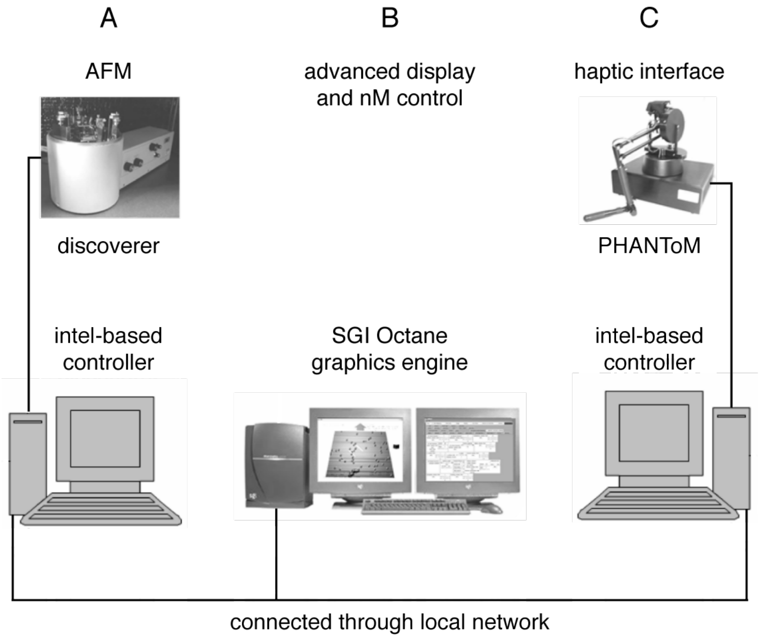

Figure 2.14: Schematic set-up of the nanoManipulator consisting of an AFM (A), an advanced display and control unit (B) and an haptic interface (C) connected with each other through a local network.

Chapter 3

'Globular' Shaped Molecules: Dendrimers

3.1 Introduction

Dendrimers are well-defined three dimensional globular shaped molecules [Tomalia et al., 1985; Newkome et al., 1985] that consist of a core surrounded by repeated branch units, which are all enclosed by a terminal group 'shell' (core-shell structures). The name comes from the Greek dendron, meaning 'tree' because it resembles a tree structure. Since extra groups can be attached at the periphery of the dendrimer, they can have a functionalised exterior. The voids between the 'arms' of the dendrimer form the interior of a dendrimer. Due to their highly controllable size which is dependent on the core type, the extent of branching and the nature of the end groups, dendrimers are essentially monodisperse (exact number of monomers). Their diameter ranges from one nanometre up to several tens of nanometres. The generation of a dendrimer indicates the extent of branching in the dendrimer. For instance, a second generation dendrimers consists of a core with two surrounding shells, a fifth generation dendrimer has five shells. In figure 3.1 a schematic presentation of a second generation dendrimer is depicted by a central core (a) with a first shell (b) around it which is included by a second shell (c) with optional functional groups (d) at the periphery.

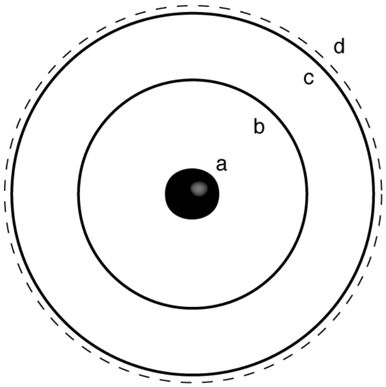

Figure 3.1: Schematic presentation of a second generation dendrimer.

The synthesis of dendrimers can be distinguished into two methods of preparation: the divergent and the convergent synthesis. The former assembles the molecule from the core to the periphery and the latter from the outside towards the core.

Divergent synthesis starts from a molecule as a central core from which successive generations of building blocks are added and in each generation new monomers react to the growing surface of the sphere. An example is Tomalia’s synthesis of starburst poly(amidoamide) (PAMAM) dendrimers [Tomalia et al., 1985]. This synthesis consist of a Michael addition reaction in which excess of ethylenediamine or methylacrelate reacts with the central core. However, when making higher generation dendrimers, some complications arise. The yield of the reactions is limited by steric hindering, intermolecular cyclisation occurs and other problems appear. Most of these problems can be avoided by choosing the right conditions (temperature, solvent, concentrations). This method is best suited for large dendrimers.

In the *convergent* approach branches (with the number of generations preset) are made first and attached in a later step to a central core. An example is Fréchet's synthesis of dendritic polyethers [Leon et al., 1996]. The synthesis starts at the periphery of the dendrimer and goes towards the middle to end with the core. In each step the amount of reactive groups per molecule is limited in contrast to the divergent method where reactive groups increase dramatically towards the end of the synthesis. Therefore, dendrimers that are synthesised in the convergent way are generally more pure. A disadvantage is that it is very sensitive to steric hindering which limits this methods to the synthesis of relatively small dendrimers (up to about generation six).

Dendrimers can also be classified according to their structure: rigid dendrimers [Bauer et al., 2005], flexible dendrimers[Tully and Fréchet, 2001], metallodendrimers [Yang et al., 2007], conjugated dendrimers [Halim et al., 1999]. Although the majority of the dendrimers prepared to-date have been built of covalent bonds, supramolecular dendrimers can be made by selecting carefully the suitable assembling units [Franz et al., 2005; Zimmerman et al., 1996]. In this thesis, all dendrimers consist of units which are connected through covalent bonds.

3.2 Properties and Applications

Because of their fascinating structure and unique chemical and physical properties, dendrimers have been studied since decades, including at surfaces and interfaces [Tully and Fréchet, 2001]. They are appropriate building blocks [Fréchet, 2002] for nanofabrication due to their exquisitely control of size in the nanometre region, shape and geometry and chemical functionality which is controllable on a molecular scale. Their interior makes them useful as molecular nanocontainers for drug delivery systems. For all these reasons, dendrimers have a wide range of applications [Dykes, 2001; Zeng and Zimmerman, 1997].

3.2.1 Individual Dendrimers

A dendrimer molecule can be highly flexible or rigid depending on its chemical structure and can be individually observed when applying the right experimental conditions. PAMAM dendrimers are roughy spherical in solution, but are known to 'collapse' when they adsorb onto a substrate surface [Hierlemann et al., 1998]. Their height (thickness) of both isolated molecules and monolayers are typically less than half the diameter in solution. The carbosilane dendrimers Jung et al. [2005] synthesised, were also found to be substantially more oblate after deposition on a substrate than would be expected from their spherical shapes in solution. Individual dendrimers containing 16 groups of terpyridine-platinum-pyridine complex with S-H end group were characterised on a gold substrate revealing their dome-shaped structures [Jung et al., 2004]. Polyphenylene dendrimers, on the contrary, are rigid nanostructures and do 'not' collapse when they adsorb onto a substrate surface [Zhang et al., 2000]. In this case spincoating was used as preparation method and the stiffness and adhesion properties of individual dendrimers were studied.

3.2.2 One-Dimensional Objects

Loi et al. [2000] reported the formation of nanorods by self-assembly of alkyl-substituted polyphenylene dendrimers on graphite which determines their orientation with its hexagonal structure.

Aggregation of a dendrimer can be induced by adding salt to aqueous solutions of polycationic phosphorus dendrimers as illustrated by El Ghzaouit et al. [2004]. If a syringe containing the dendrimer solution is moving horizontally while dendrimer solution is injected into the flocculating bath, the salt-induced self-assembly can lead to the formation of fibres. In figure 3.2A a scheme of such an experimental set-up is depicted. Fibres can be removed and dried in open air in order to investigate them. Optical and scanning electron micrographs of the resulting fibres are shown in figure 3.2B, C and D.

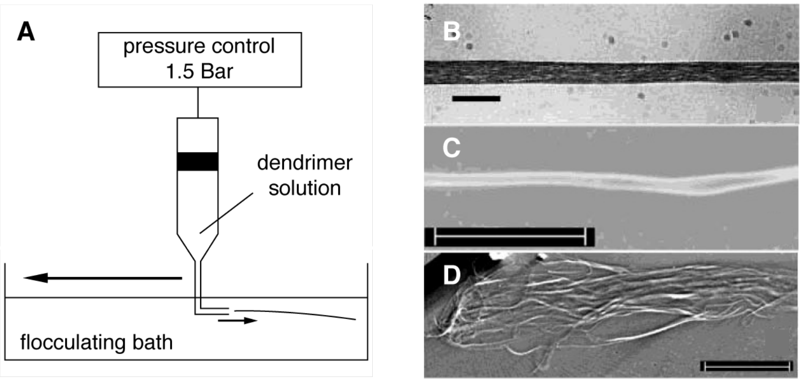

Figure 3.2: Scheme of the experimental setup for the processing of dendrimer fibres (A). Optical (B) and scanning electron micrographs (C, D) of the dendrimer fibres.

3.2.3 Two-Dimensional Layers

Structurally controlled and well-defined films can be made with standard cleaning, dipping, and rinsing procedures to deposited dendrimers on a substrate, using electrostatic or non-electrostatic interactions between the dendrimers.

A layer-by-layer approach was used by Blasini et al. [2006] to deposit PAMAM dendrimers which are interfacially coordinated with cobalt from aqueous solution leading to single dendrimer/Co^{2+} multilayers. Huo et al. [2003] used hydrogen-bonding to direct layer-by-layer assemblies by self-deposition of a carboxyl-terminated poly-ether dendrimer. The carboxyl groups on its periphery act as hydrogen bonding donor as well as hydrogen bonding acceptor. Wang et al. [2000] described the preparation of multilayer films constructed from PAMAM dendrimers and nitro-containing diazoresin via a layer-by-layer technique followed by the conversion of linkage bonds under UV irradiation. Tsukruk et al. [1997] fabricated multilayer films by self-assembly of dendritic macromolecules of two adjacent generations using electrostatic layer-by-layer deposition.

Multivalent supramolecular host-guest interactions between dendritic guest molecules and host-modified molecules and nanoparticles give rise to novel kind of self-assembled multilayers. These guest molecules can be adamantyl-terminated dendrimers [Crespo-Biel et al., 2005] or ferrocene-terminated dendrimers [Nijhuis et al., 2004], binding to cyclodextrin-modified gold nanoparticles and SAMs, respectively.

3.2.4 Patterns

Not only 2D structures, but also patterns can be formed with dendrimer molecules. Li et al. [2006a] created ring structures by using the competition effect between contact line pinning and dewetting events in evaporating drops containing PAMAM dendrimers.

Kim et al. [2006] designed a novel dendrimer combining the buffering capacity of poly(ethylenimine) (PEI) and the biocompatibility of PAMAM dendrimers. This poly(amido ethylenimine) (PAMEIM) dendrimer self-assembles with plasmid DNA illustrating its potential as a gene delivery carrier.

Microcontact printing was used by Kohli et al. [2004] to deposit stable, nanostructured, amphiphilic and crosslinkable patterns of poly(amidoamine organosilicon)-dimethoxymethylsilyl (PAMAMOS-DMOMS) dendrimer multilayers onto silicon wafers, glass (see figure 3.3), and polyelectrolyte multilayers.

Huskens et al. [2002] made adamantyl-functionalised poly(propylene imine) dendrimers water-soluble by assembling these dendrimers with β-cyclodextrin, making it possible to absorb them onto a β-cyclodextrin

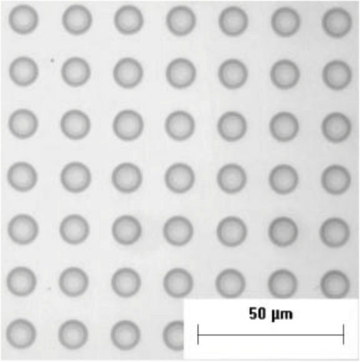

Figure 3.3: Optical micrograph of a circular pattern, obtained from a 0.5% PAMAMOS dendrimer solution, on a glass substrate.

SAM on gold, which can be seen as a molecular printboard[1]. The combination of microcontact printing and the ability to use dendrimers as hosts for the encapsulation of molecules was explored by Onclin et al. [2005] to create patterns of dyes (see figure 3.4). First, line patterns which consist of dendrimer molecules were made on a molecular printboard by using μCP followed by rinsing to obtain a monolayer of dendrimers. In a second step, the encapsulation of fluorescent anionic guests was carried out by dipping the printboard in an aqueous dye solution. Additional experiments demonstrate that, in addition to complexation from solution, immobilised dendrimers can also be filled by μCP of anionic dyes.

Other examples in literature of covalent coupling between dendrimers and an activated monolayer include the work of Degenhart et al. [2004] in which amino terminated PAMAM dendrimers were immobilised via amide linkage formation to a SAM on a gold surface. Patterning of these dendrimers was achieved by μCP and DPN.

Highly functional Si and glass surfaces for protein immobilisation have

---

[1] A molecular printboard is a monolayer of molecules that can bind suitable guest molecules by specific interactions.

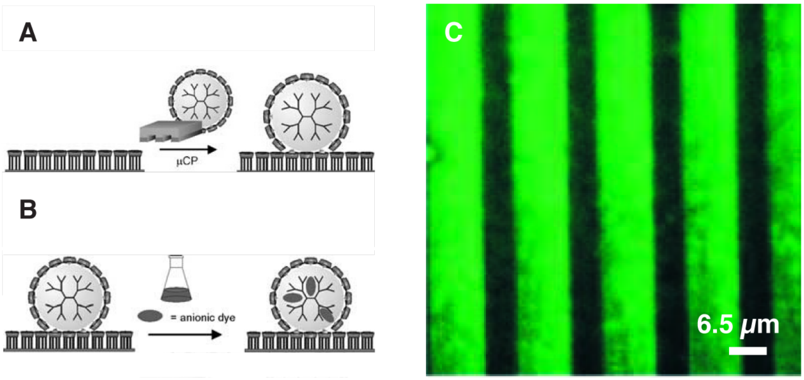

Figure 3.4: Schematic representation of μCP of the dendrimer on a molecular printboard (A) and the filling of immobilised dendrimer patterns with anionic dyes (B). Confocal microscopy image after these steps with fluorescein as dye (C).

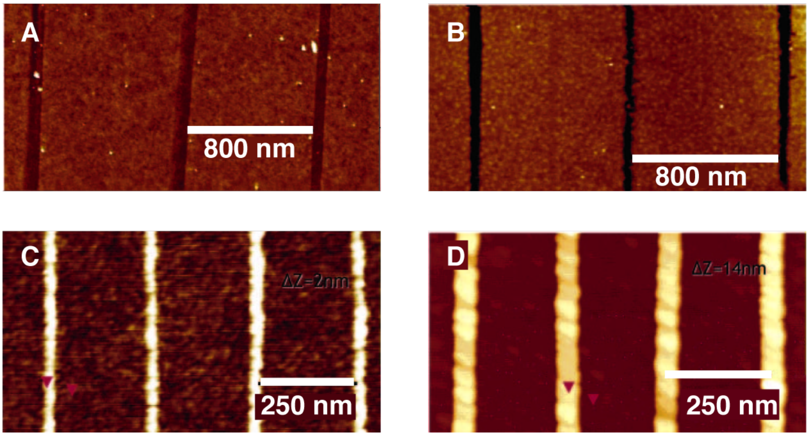

Figure 3.5: AFM images of 40 nm wide lines scribed into a dendrimer monolayer (A) and corresponding 50 nm wide trenches after etching the deprotected Ti (B). AFM images of 20 nm wide raised features produced via field-enhanced oxidation (C) and same lines after etching the film (D).

been prepared with a similar strategy [Pathak et al., 2004]. Poly(propyleneimine) dendrimers were immobilised onto the surface using a facile room-temperature coupling procedure leading to dendrimer-coated surfaces which were used to immobilise proteins.

Functionalised poly(benzylether) dendrimers were used by Rolandi et al. [2004] to form monolayers which can be employed as resists for scanning probe lithography on thin Ti films on Si. The functionalised dendrimer molecules function as etch resists by forming a densely packed self-assembled protective monolayer on the Ti film. Patterning of the Ti surface is accomplished using an AFM-tip either as an ultra sharp scribe (see figure 3.5A and B) or as an electrical field point source (see figure 3.5C and D) to modify the monolayer. In the first case, dendrimer molecules are locally removed from the SAM, while in the latter case, local oxidation of the dendrimer-SAM covered Ti surface was obtained. In this approach the use of the dendrimer monolayers as both negative and positive tone resists is possible by carefully selecting the etching conditions.

3.3 Dendritic Structures evaluated in this Study

The dendrimers used in this work were kindly provided by Prof. Müllen's group in Mainz (Germany).

Figure 3.6 shows the chemical structure of dendrimer D1 which is a second generation polyphenylene dendrimer with a sp^3-hybridised carbon core. Although the structure is presented in 2D in (A), its structure is far from being flat which is illustrated by the geometrically optimised molecular model in (B). For simplicity reasons molecule structures will be drawn in 2D further in this thesis, but one should always keep in mind that this is just to obtain some idea about the functional groups and a structure like the one shown in (B) is far more realistic than a 2D representation.

Due to the polyphenylene backbone and the high number of twisted, interlocked benzene rings, these dendrimers show a high shape-persistence.

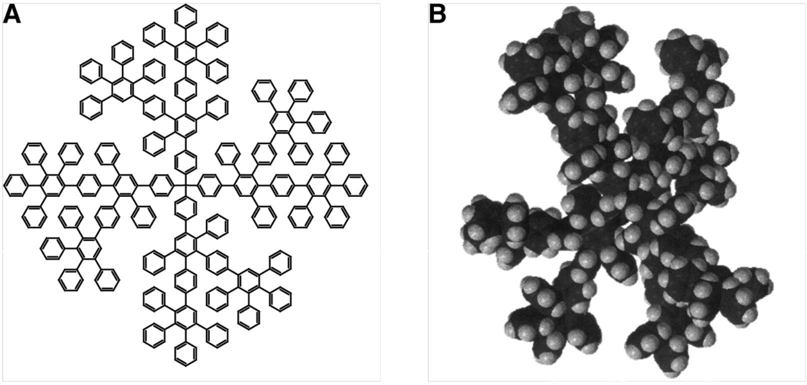

Figure 3.6: Chemical structure of dendrimer D1 drawn in 2D (A) and the geometrically optimised molecular model (B).

The synthesis and characterisation of dendrimer D1 were reported previously [Wiesler and Müllen, 1999; Wiesler et al., 2001]. A convergent approach was followed to synthesise these polyphenylene dendrimers. The Diels-Alder cycloaddition of tetraphenylcyclopentadienones to phenylene-substituted ethynyls, and the Knoevenagel condensation of benzils with 1,3-diphenylacetones to give cyclopentadienones led to the dendrons. These dendrons were then attached to a tetrakis(ethynylphenyl)-methane core via a cycloaddition step resulting in the second generation polyphenylene dendrimer.

This approach not only allows the symmetric functionalisation of the dendrimer surface as in the divergent approach, but also the controlled functionalisation of the dendrimer by adding differently functionalised dendrimer arms to selectively protected cores. Dendrimers similar to dendrimer D1 were also studied to investigate the influence of chemical structure on its assembling properties (see chapter 6).

3.4 Objectives

In this thesis the self-assembling properties of polyphenylene dendrimers into nanofibres on surfaces will be examined (see chapter 6) by analysing the important parameters in this system: functional groups attached to the periphery, interactions between the dendrimers, the reversibility of the aggregation formation, the environment,... to obtain insight on the fibre formation process. The stability of the nanofibres will be investigated and attempts will be made to increase the mechanical stability. In a later step, the acquired knowledge will be applied in several approaches (see chapter 7) in order to guide the fibre formation.

Chapter 4

'Torus' Shaped Molecules: Macrocycles

4.1 Introduction

Macrocycles are well-defined torus shaped[1] molecules that consist of cyclic oligomeric analogues of polymers forming a backbone structure. These unconventional polymers lack end groups and therefore have an interior, also called the lumen, with dimensions typically in the nanometre region. Since the backbone must be non-collapsible in order to retain the lumen, it must be made of rigid components in order to obtain shape-persistent macrocycles. Usually macromolecule segments with a large persistence length are built in the backbone to accomplish this. The ethynylene functional group is an attractive building block for shape-persistent macrocycles due to its potential for extended conjugation, its simple linear geometry, and its pure carbon composition [Zhang and Moore, 2006]. The rigidity of thiophene can be exploited to build macrocyclic oligothiophenes [Nakao et al., 2006]. Anchor groups can be introduced by using terpyridine [Grave et al., 2003] or thiophene [Mena-Osteritz and Bauerle, 2001] units in the backbone structure of

---

[1] A torus is a geometric figure formed by rotating a closed curve around a line that lies in the same plane but does not intersect it (e.g. like a ring-shaped doughnut).

the macrocycle. Shape-persistent macrocycles have an interior and an exterior at which site-specific substitution with functional groups can be accomplished. Most of these nanosized ring compounds have an aromatic backbone because the starting materials are easily available, with as additional advantage of this class the wide variety of functional groups which can be introduced on their backbone. Due to their highly controllable size, macrocycles are essentially monodisperse (exact number of monomers). Although some types of macrocycles are conformationally flexible [Finocchiaro et al., 2005], these will not be discussed here.

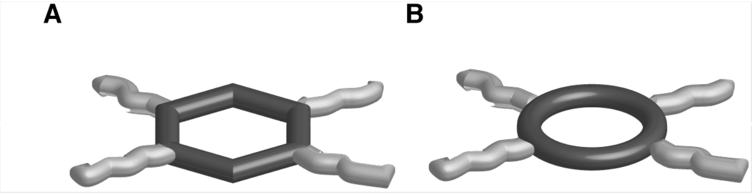

Figure 4.1: Schematic presentation of a macrocycle consisting of a polygonic shape with six vertices and four exocyclic oriented side groups (A) and its corresponding torus presentation (B).

Most macrocycles have a polygonic shape[2] with vertices introducing kinks in the structures necessary to form the typical ring structure. In figure 4.1 a schematic presentation of a macrocycle consisting of such a polygonic shape with six vertices and four exocyclic oriented side groups is depicted (A) as well as its corresponding torus presentation (B). Although these macrocycles are grouped as 'torus' shaped molecules, it should be pointed out that their actual structure is often not completely flat due to physical contraints in the molecule (comparable to the boat and chair conformations of cyclohexane). However, structures drawn in

---

[2] A polygon is a geometric figure consisting of an ordered set of three or more (but a finite number of) points called vertices which are each connected to two other vertices by line segments that are called the sides of the polygon.

2D give a relatively good idea of the actual structures because macrocycles are more or less two-dimensional.

Within the past two decades there has been a substantial improvement in the synthesis of shape-persistent macrocycles [Zhang and Moore, 2007, 2006; Yamaguchi and Yoshida, 2003; Zhao and Moore, 2003; Grave and Schlüter, 2002; Höger, 1999; Moore, 1997]. Versatile and efficient synthetic routes were developed which can be distinguished into two different approaches: the kinetic approach and the thermodynamic approach. The former includes macrocycle synthesis by cross-coupling and the latter includes dynamic covalent chemistry.

The *kinetic approach* includes a variety of coupling methods which can be divided into four major classes as depicted in the schematic presentation in figure 4.2: cyclooligomerisation (A), intramolecular ring closure of bisfunctionalised oligomers (B), intermolecular coupling between two or more oligomeric fragments followed by unimolecular cyclisation (C), and templated cyclisation (D).

The irreversible *cyclooligomerisation* reactions are one-step oligomerisation/cyclisation reactions and have as advantages the readily accessibility of the starting materials and the fact that the target molecule is generated in a single step. However, yields of macrocycles obtained by this method are usually limited by the additional formation of higher oligomers. This is because a significant portion of oligomers grow beyond the length of the target macrocycle ('overshooting'). Consequently, this coupling method has as important disadvantage the kinetically determined product distribution. To overcome this problem of 'overshooting', another method was developed which first prepares oligomers with discrete lengths. In this first step of the *intramolecular ring closure* method, functional groups can be introduced at defined positions of the oligomeric sequence and controlled incorporation of fragments into the sequence provides access to macrocycles with different geometrical

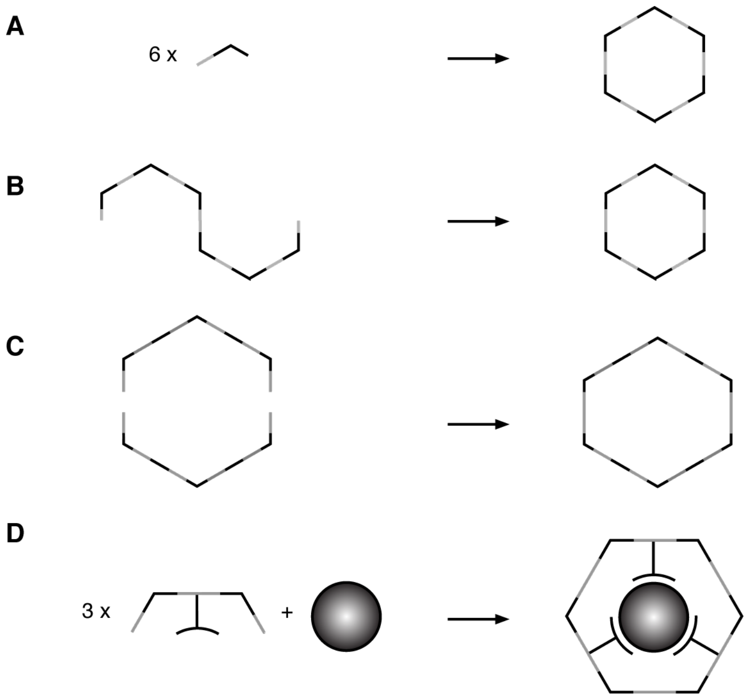

Figure 4.2: Schematic representation of cyclisation strategies: cyclooligomerisation (A), intramolecular cyclisation (B), bimolecular coupling/unimolecular cyclisation (C) and templated cyclisation (D).

shapes. In the second step of this precursor method, cyclisation was carried out, leading to a significant yield improvement. The main drawback of this method is the large number of synthetic steps which are labor-intensive and time-consuming. An alternative strategy to achieve higher yields is the *intermolecular coupling of oligomers* (also called the statistical coupling method). Two precursors are made which can undergo intermolecular coupling followed by an intramolecular cyclisation in one pot. Therefore, these precursors must be of appropriate length and carry suitable terminal functionality. Although this combined step gives in general lower yields than the oligomer macrocyclisation, fewer steps are necessary to make the precursors. Therefore, the overal yield is often higher and this method is more time-efficient. These last two approaches are the most commonly used in macrocycle synthesis by cross-coupling reactions. Examples of the intermolecular coupling include the work of Fischer and Höger [2003a] to create shape-persistent macrocycles with intraannular carboxylic acid groups. Although the macrocycle yield is greatly improved by these methods, in some cases yields are still modest. The *templated cyclisation* method was created to promote the intramolecular couling more efficiently, and thereby increasing the ratio of cyclic to linear products. This synthetic approach usually requires fewer steps in the syntheses and leads to a higher overall yield. Höger and Meckenstock [1999] used this approach to obtain shape-persistent macrocyclic amphiphiles. In some cases, the template can even have an additional function as protective group during the macrocycle formation and non-symmetrical macrocycles can be made by simply using a non-symmetrical template [Fischer and Höger, 2003b].

Despite the availability of a variety of cross-coupling synthetic approaches, the efficient preparation of macrocycles is challenged by drawbacks inherent to kinetically controlled reactions. Due to the irreversibility of the reaction, undesired bond formations can not be corrected. As an attempt to circumvent these constraints, a *thermodynamic approach* was developed.

Dynamic covalent chemistry involves reversible reactions conducted under equilibrium conditions, providing macrocycles in one step. The reversibility provides a self-healing effect of chemical 'defects' that are introduced in kinetically controlled processes. In this approach the thermodynamic stability of the target macrocycle is of extreme importance since, as for any thermodynamically controlled process, the successful generation of a unique species from a range of possible products depends on the relative free energies of all the species involved. If the energy gap between the target macrocycle and other possible products is sufficiently large, this method is able to produce the target macrocycle in high yields, even when kinetic preferences initially give undesirable products. Inherent to this approach is the difficulty to synthesise strained molecular structures which are enthalpically strongly disfavoured and to carry out site-specific functionalisation due to the fact that the energy gap between macrocycles with different site-functionalisation is most probably not large enough. Another drawback of this approach is the requirement of solubility for growing oligomers. Dynamic covalent chemistry has been successfully utilised by Zhang et al. [2004b] and Ge et al. [2000] for alkyne metathesis, circumventing the drawbacks of conventional cross-coupling reactions for cyclooligomerisation.

Although the synthesis of macrocycles discussed here are all based on covalent bonds, macrocycles can be made by carefully selecting the suitable assembling units, using for example metal-ligand interactions [Gimeno and Vilar, 2006]. In this thesis, all macrocycles used consist of units which are connected through covalent bonds.

4.2 Properties and Applications

Shape-persistent ring structures show interesting features different from their open-chain analogues. Since the solubility of macrocycles is dramatically reduced compared with their linear analogues of the same size, aliphatic, aromatic, or functionalised side groups are in general necessary to keep them in solution. They are potential molecular building blocks for constructing complex superstructures due to their exquisitely control of size in the nanometre region, shape and geometry and chemical functionality which is controllable on a molecular scale. Side groups on the ring can introduce different (aggregation) behaviour of macrocycles depending on the orientation they have with respect to the ring (extraannular, intraannular or adaptable) and their chemical composition. Zhao and Moore [2003] investigated the influence of substitution, as well as the temperature and solvent on the self-association behaviour. Instead of using functional groups to obtain specific superstructures, another approach can be followed in which the assembly into superstructures can be employed to organise functional groups. In this case, the functional groups remain free and are able to interact with other species after being assembled into the specific superstructures. This opens perspectives for macrocycles to serve as hosts since selected guest-host interactions can take place. Also the interior of macrocycles can be employed in this host-guest approach.

4.2.1 Individual Macrocycles

STM is a well-established technique to image individual macrocycles adsorbed at the liquid/solid interface since the aromatic rings in their backbone structure provide a clear contrast in the detected tunnelling current (see chapter 8 for images).

Höger [2004] combined X-ray analysis with host-guest chemistry to prove that adaptable substituents can rotate freely and therefore point to the inside or to the outside of the ring. The experiments were carried out with a macrocycle which contains OH-groups attached to a phenyl group in a line segment of the polygonic backbone. When recrystallising the macrocycle from a polar solvent, X-ray experiments revealed that the polar phenol-OH groups pointed to the outside of the molecule, while host-guest chemistry showed its ability to ‘capture’ tetraamine in the interior, indicating that the phenol-OH groups pointed to the inside of the macrocycle. Due to this adaptable behaviour depending on the environment, this type of macrocycles was named ‘molecular reversible coat’. By carefully selecting an appropriate solvent the desired conformational state of such a molecular reversible coat can be triggered [Höger et al., 2002].

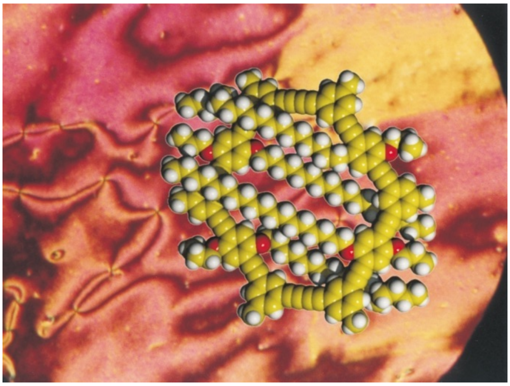

Figure 4.3: Chemical structure of the macrocycle in the crystal with as background its texture at 200 ° viewed between crossed polarisers.

4.2.2 Liquid Crystals

Disc shaped molecules can have the ability to self-assemble and thereby leading to the formation of discotic liquid crystals[3]. Generally discotic liquid crystals (DLCs) consist of flat, rigid aromatic cores surrounded by flexible chains [Kumar, 2006], but liquid crystalline macrocycles with an inverted topology have also been reported in the past. The macrocycle shown in figure 4.3 forms DLCs and has less flexible side chains that point to the inside of the ring, filling the internal cavity of the macrocycle [Höger et al., 2000]. Analogue macrocycles with the same backbone but different location of the long alkyl groups attached to the ring were also studied. DLC behaviour was observed for the macrocycles with the flexible side chains at the adaptable or intraannular positions, but the macrocycle with the long alkyl groups at the extraannular position did

---

[3] The liquid crystal state is the fourth state of matter, being an intermediate state between the solid and the liquid.

not exhibit DLC behaviour. This result illustrates the fact that groups connected to the ring can introduce different (aggregation) behaviour depending on the orientation they have with respect to the ring.

Although these macrocycles have orientational correlation in the nematic DLC phase, to obtain positional correlation it is required that they organise themselves into 1D objects or 2D layers.

4.2.3 One-Dimensional Objects

Two different stacking motifs are observed by interacting aromatic molecules: edge-to-face and offset face-to-face. Macrocycles with a rigid, non-collapsible backbone and a large aromatic surface, tend to stack face-to-face in solution in order to maximise their area of contact and thus van der Waals and π-π stacking interactions. This aromatic stacking can be proven by chemical shift changes in NMR spectroscopy. Zhang and Moore [1992] were the first to report the concentration dependent chemical shift indicating intermolecular aromatic stacking at higher concentrations. The large surface of the macrocycle provides a cooperative amplification of the interactions that are strongly solvent dependent due to the solvophobic nature of the association, while the side chains that are normally present to improve solubility also disfavour edge-to-face association. Höger et al. [2001] studied the aggregation behaviour while changing the polarity of the solvent mixture. NMR spectroscopy revealed that decreasing the solvent polarity induces aggregation of the rings by non-specific interactions and that the magnitude of aggregation can be varied by using solvent mixtures of different apolar solvent content, supporting the model of a solvophobic effect.

Assembled structures can be transferred to a substrate for further investigation with other tools like SPM, SEM,... The structure of a macrocycle and a SEM image of the gel obtained from a solution of this macrocycle in CH_2Cl_2 is shown in figure 4.4 [Lin and Tour, 2002]. The gelation is thermally reversible. The network formation is directed by the cooperative interaction of hydrogen bonds and π-stacking between macrocycles.

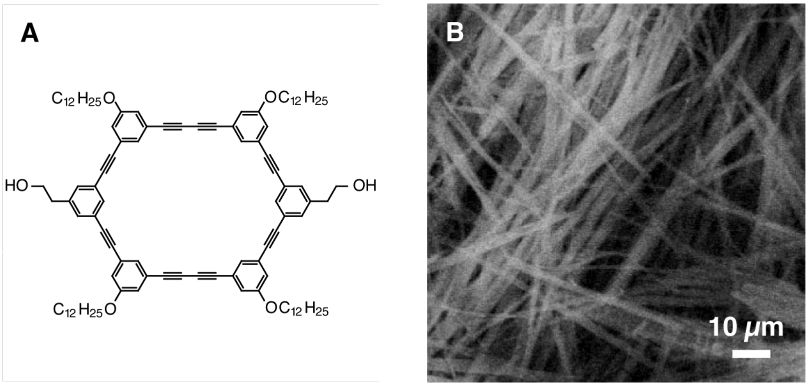

Figure 4.4: Structure of the macrocycle (A) and a SEM image of the gel it forms (B).

More recently Balakrishnan et al. [2006] fabricated nanofibrils of an arylene ethynylene macrocycle by sol-gel processing, i.e. slow cooling of a warm, homogeneous solution in cyclohexane, followed by gel spincast on a glass substrate and drying in air. AFM images of these nanofibrils are shown in figure 4.5.

The stacking of macrocycles (which have an engineerable functionality in the interior) into 1D objects is very interesting since this leads to structures containing channels which could possibly be filled with appropriate guest molecules.

4.2.4 Two-Dimensional Layers

Monolayers formed at the air/water interface can be transferred on various substrates to fabricate monolayer films. Shetty et al. [1996] studied

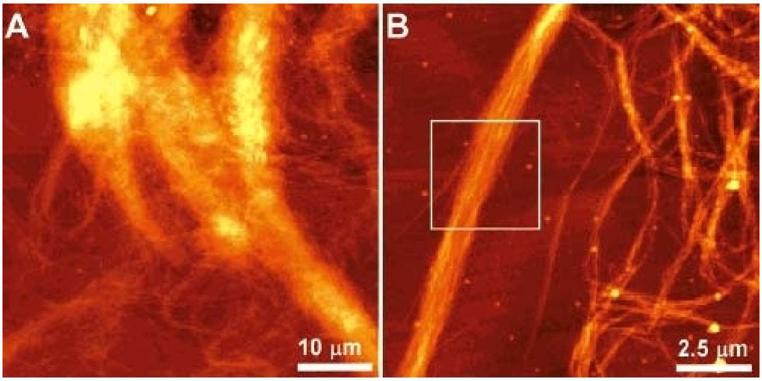

Figure 4.5: AFM images of nanofibrils formed from arylene ethynylene macrocycle by sol-gel processing.

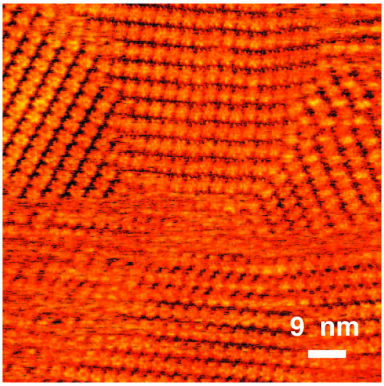

Figure 4.6: STM image of a monolayer domain structure of a macrocycle adsorbed from solution onto HOPG.

the assembly of amphiphilic phenylacetylene macrocycles (PAM) on a Langmuir-Blodgett trough and transfered the layer onto solid substrates. The disk-like PAMs can, in principle, adopt orientations in which the plane of the macrocycle can range from perpendicular (edge-on) to parallel (face-on) at the interface depending on the functional groups attached to the backbone. Dicarboxylate PAMs form a well-ordered and stable 2D array and adopt the edge-on configuration with near-vertical orientation of the macrocycle plane.

2D layers can also be formed by simple dropcasting a solution onto an appropriate substrate (mostly HOPG) onto which macrocycles can adsorb. The interaction of the macrocycles with the substrate can lead to highly ordered layers in which individual molecules are ‘visible’. Indeed, oligo-alkyl substituted macrocycles can be adsorbed at the solution/HOPG interface forming a highly-ordered and stable monolayer on the surface [Höger et al., 2001]. High-resolution STM images show clearly 2D structures of the macrocycles (see figure 4.6).

Ordered monolayer films are of interest as 2D host matrices and shape selective membranes. This valuable method for surface patterning in the nanometre regime can transform 2D layers into functionalised patterned surfaces. Ultimately, these patterned templates may provide a tool for epitaxially induced supramolecular 3D structures in a bottom-up approach.

4.3 Macrocyclic Structures evaluated in this Study

The shape-persistent macrocycles used in this work were kindly provided by Prof. Höger’s group in Bonn (Germany).

The macrocycles are based on a phenyl-ethynyl backbone resulting in a rigid structure and can be classified in different groups depending on the structure of their backbone (depicted in figure 4.7). On these backbones, a variety of side groups can be attached which have different orientations depending on the position of the ring it is attached to. Groups attached to the vertices of the polygonic backbones can either be pointing to the inside of the ring (intraannular, I) or to the outside of the ring (extraannular, E), while groups attached at the line segments are free to change their orientation towards the centre of the ring or away from it (adaptable, A).

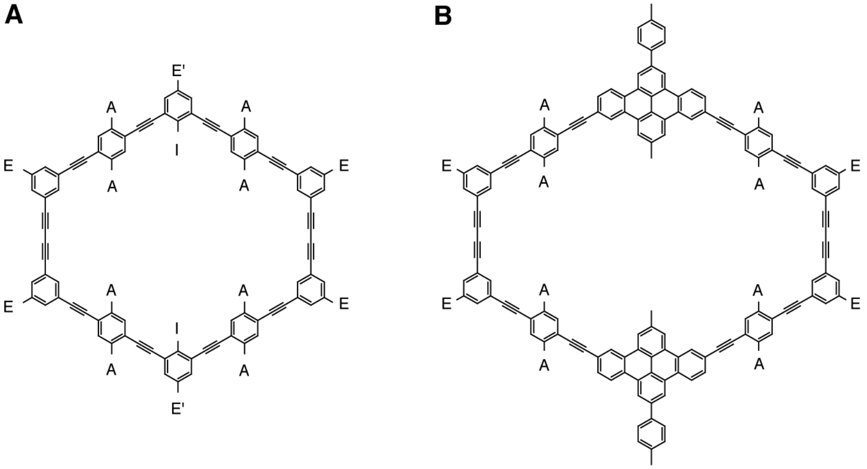

Figure 4.7: Basic chemical structure of the macrocycles evaluated in this study with extraannular (E, E'), intraannular (I) and adaptable (A) groups attached to the cyclic backbone.

4.4 Objectives

Although basic principles for the aggregation of macrocycles are known, several aspects are not fully understood (e.g. the formation of discrete 1D aggregates from shape-persistent macrocycles without competing lateral aggregation is still challenging).

Several macrocycles will be studied in this thesis in order to investigate their behaviour at the liquid/solid interface in solution as well as at the air/solid interface after dropcasting (see chapter 8). The important parameters for each system will be analysed: functional groups attached to the ring, influence of the substrate or the solvent... to obtain insight in the self-assembly process of macrocycles. In chapter 9, a macrocycle which forms discrete 1D aggregates will be selected in order to guide its fibre formation with a magnetic field.

Chapter 5

Polychlorotriphenylmethyl Derivatives

5.1 Introduction

A polychlorotriphenylmethyl (PTM) radical is a shape-persistent structure which consists of a carbon core with three phenyl groups attached to it that are fully substituted with chlorine atoms.

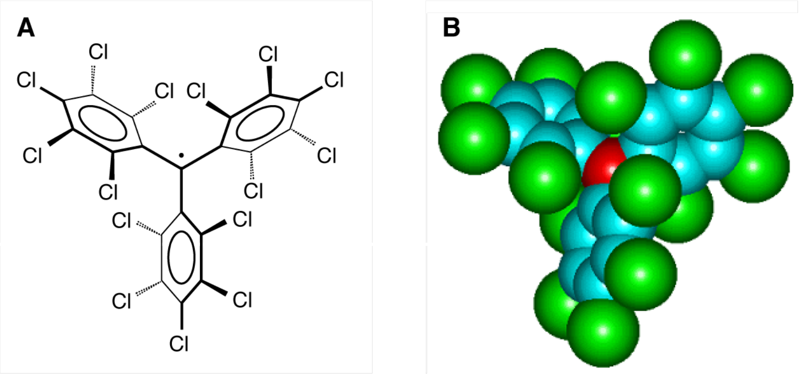

Figure 5.1: Chemical structure of the PTM radical (A) and the geometrically optimised molecular model (B).

The bulky chlorine atoms give high chemical and thermal stability to the radical [Ballester, 1985], and also promote a helicoidal structure (figure 5.1).

Radical molecules are obtained from the protonated precursor PTM-αH by deprotonation, followed by oxidation of the intermediate species. The three species, depicted in figure 5.2, can be isolated.

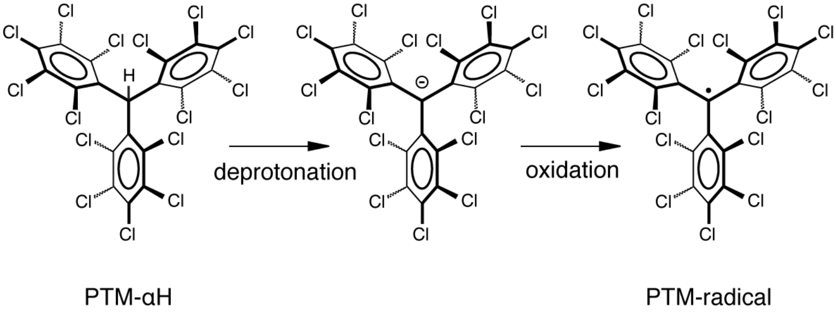

Figure 5.2: Structure of the species obtained by deprotonation and oxidation of PTM-αH.

5.2 Properties and Applications

As the interest in designing purely organic magnetic materials is increasing [Maspoch et al., 2007], one of the major requirements to obtain magnetic properties is the control of the structural arrangement of the organic spin-bearing units in the solid state. Supramolecular chemistry can be applied by using non-covalent interactions to engineer highly ordered crystals. PTM radicals are interesting building blocks [Roques et al., 2005] since they exhibit a high thermal and chemical stability, their trigonal symmetry provides a typical template and the molecular bulkiness and rigidity is expected to prevent close packing of molecular units. PTM radicals functionalised by carboxylic groups [Roques et al., 2007] give access to purely organic/molecular magnetic materials. Maspoch et al. [2004] have created supramolecular, nanoporous purely organic materials with magnetic properties from PTM radicals. Nanoporous materials exhibit a wide range of applications, such as molecular sieves, catalysis, and sensors.

By treating PTM molecules with a base followed by oxidising the resulting anions, stable radicals can be obtained which exhibit fluorescence in the red region of the spectra (600 nm) and have paramagnetic properties. PTM radicals can be easily and reversibly reduced (or oxidised) to their anionic (or cationic) species which show different absorption spectra than the radical. They are non-fluorescent and have non-magnetic properties. Sporer et al. [2004] used the PTM radical shown in figure 5.3 to render a molecular switch with three states which are also shown in the same figure.

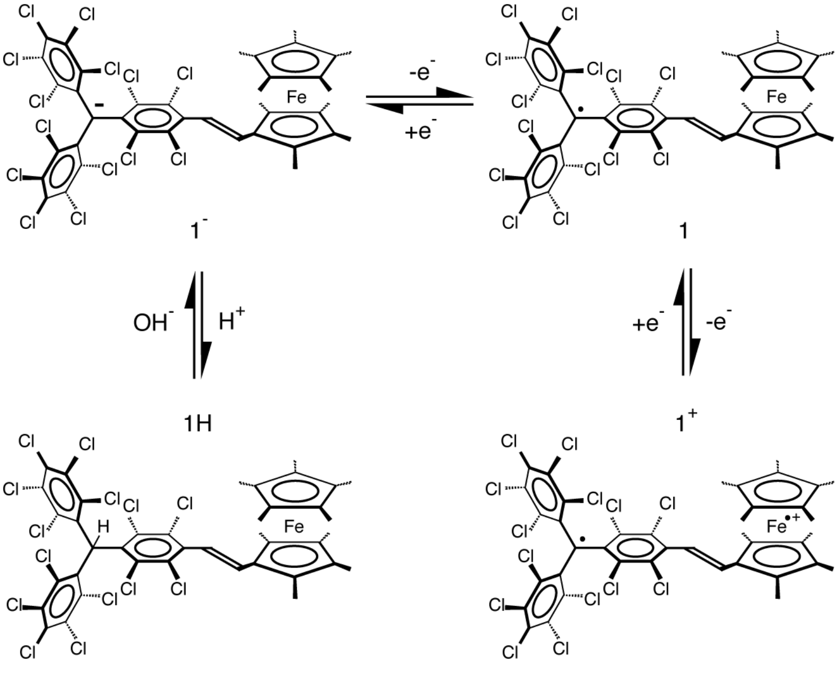

Figure 5.3: The three states of a molecular switch: 1^-, 1, and 1^+.

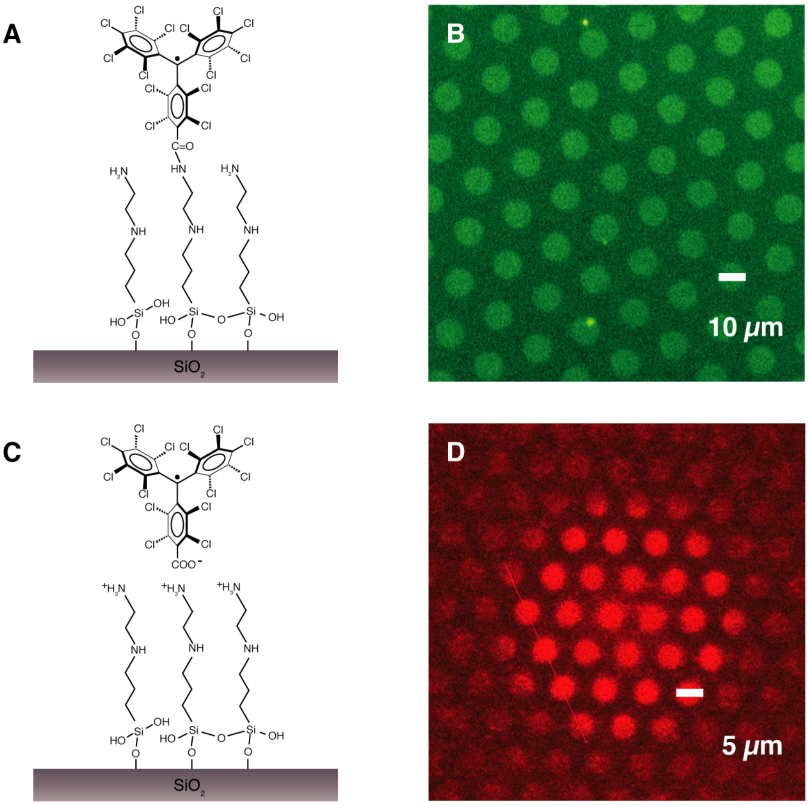

Figure 5.4: Scheme of the functionalised PTM radical on an adhesive SAM (A, C) and corresponding fluorescence image of a pattern made by microcontact printing the radical (respectively B and D) on the adhesive SAM.

Crivillers et al. [2007] used organic radicals to render multifunctional surfaces with electrochemical, optical, and magnetic activities. Both SAMs and patterns (see figure 5.4) of a functionalised PTM molecule were prepared. In both cases, the strategy involved the use of a monolayer of silane molecules with a terminal chemical group that acts as a recognition site to interact with the PTM molecules. Two different PTM radical derivatives were immobilised on the substrate either by covalent (figure 5.4A and B) or non-covalent (figure 5.4C, D) interactions. For the non-covalent interactions a 4-carboxytetradecachlorotriphenylmethyl radical was employed and for the covalent interactions a tetradecachloro-4-(chlorocarbonyl)triphenylmethyl radical was used.

As a consequence of the fully reversible redox process, these multifunctional radical SAMs and patterned structures behave as chemical switches that combine electronic absorption, fluorescence emission, and magnetic responses. The chemical flexibility and versatility of these molecules demonstrates the potential of preparing self-assembled multifunctional molecular devices on surfaces.

5.3 Polychlorotriphenylmethyl Derivatives evaluated in this Study

The polychlorotriphenylmethyl derivatives used in this work were kindly provided by Prof. Veciana's group in Barcelona (Spain).

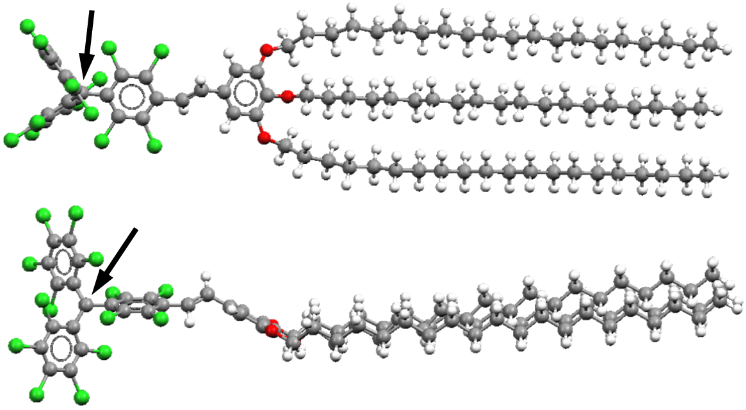

Figure 5.5: Two different views of the structure of PTM-C20 radical. The arrows indicate the central carbon atom containing the free electron.

The PTM derivative studied in this thesis, also called PTM-C20, has an additional benzene group attached via a vinylene bond in para position on one of the three benzene groups. The additional benzene group has three large alkane chains ($C_{20}H_{41}$) connected to it via an oxygen atom as depicted in figure 5.5 where the structure of the organic radical (PTM-C20-rad) is shown.

5.4 Objectives

The self-assembly behaviour of PTM-C20 will be studied upon drop-casting this compound on a (HOPG) substrate (see chapter 10). A first attempt will be carried out to measure the magnetic properties of the assembled structures with magnetic force microscopy (MFM) in order to try to distinguish the radical compound from the αH compound.

Chapter 6

Self-Assembly of Dendrimers

In a first section of this chapter, the self-assembly behaviour of the second generation polyphenylene dendrimer is investigated in solution by means of light scattering experiments. In a second section, the self-assembly of this type of dendrimers is considered at the air/solid interface with AFM and the optical viewing system as examining tools.

As explained in section 1.4.8, the outcome of molecular self-assembly can be regulated by varying the elements or characteristics constituting the self-assembling system. In this chapter these characteristics are investigated for several systems with the second generation polyphenylene dendrimers as building blocks in order to obtain insight into its fibre formation process. The stability of the nanofibres was investigated and attempts were made to increase the mechanical stability.

6.1 Aggregation in Solution

For a system in solution the most important characteristics which determine the outcome of the self-assembly include the building blocks or molecules and the solvent. The chemical structure of the second generation polyphenylene dendrimer D1 consists of a sp^3-hybridised carbon core and 64 phenyl groups and is shown in figure 6.1. Tetrahydrofuran

(THF) was chosen as solvent.

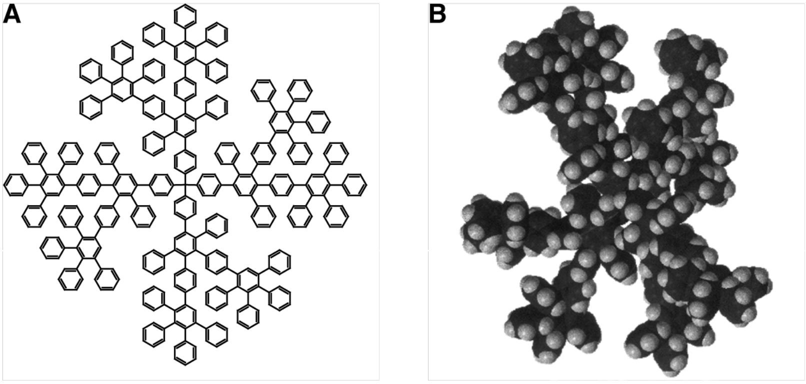

Figure 6.1: Chemical structure of dendrimer D1 drawn in 2D (A) and the geometrically optimised molecular model (B). The length of one dendrimer arm is approximately 2.1 nm, while the distance between two apexes of any two branches is approximately 3.5 nm.

Investigation of the solution phase behaviour of D1 was assessed via a series of dynamic light scattering experiments[1] (method and experimental details are described in chapter 11) in THF at different concentrations of D1.

6.1.1 Discussion and Conclusions

The hydrodynamic radius of species present in samples within a concentration range between 6×10^{-5} M and 2×10^{-4} M was determined and is plotted in figure 6.2. The results indicate that within the concentration range probed two processes were observed, resulting in two different hydrodynamic radii: 1-2 nm (symbol: hollow triangles) and ranging between 33 and 206 nm (symbol: filled triangles). This probably means that beside the monomolecular species, poorly defined dendrimer ag-

---

[1] The dynamic light scattering experiments were carried out in Prof. Müllen's group (by Tianshi Qin).

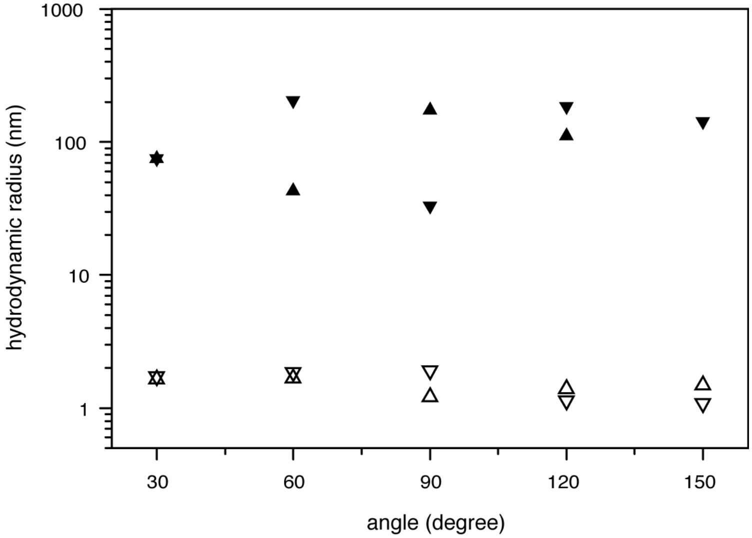

Figure 6.2: Hydrodynamic radii of the aggregates as a function of the angle at which the detector is located with respect to the sample cell by dynamic light scattering experiments of D1 at 2×10^{-4} M ('triangles pointing up') and 6×10^{-5} M ('triangles pointing down') in THF.

gregates are present in solution. Light scattering experiments disclose aggregates of strongly varying magnitude present in THF solutions. It is however not straightforward to draw conclusions about the morphology of these aggregates and hence it is not sure that these aggregates are fibres.

6.2 Aggregation on a Substrate

AFM and optical measurements were carried out to investigate the aggregation behaviour of D1 under dry conditions when dropcast from THF onto a flat substrate. Upon transferring a solution onto a substrate, the liquid/air interface and the liquid/substrate interface must be taken into account.

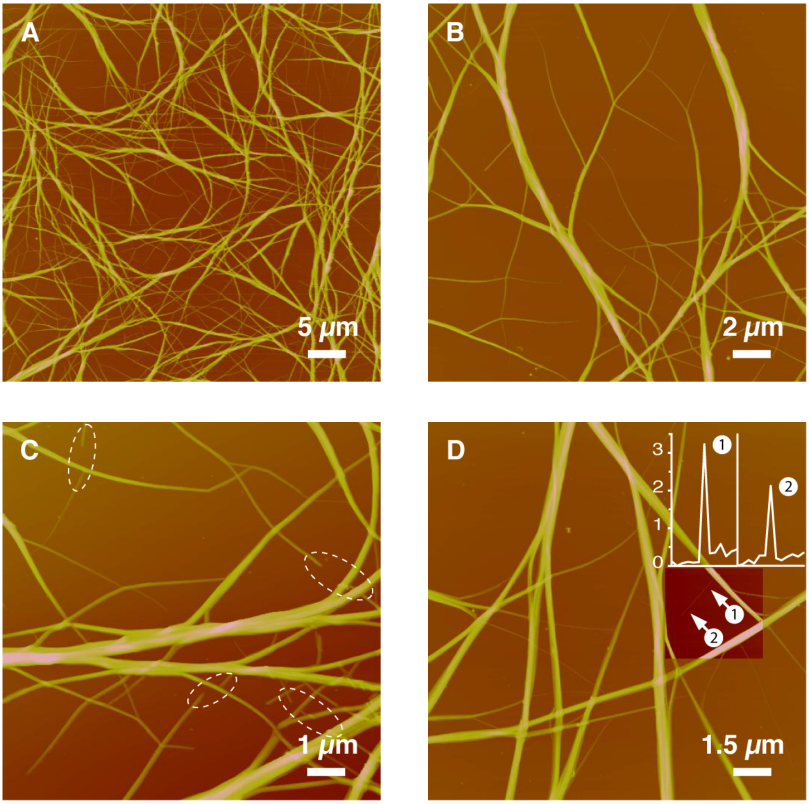

Figure 6.3: AFM topography images from samples made by dropcasting 50 μL of a $\sim 2\times10^{-5}$ M D1 solution on mica. Dashed lines indicate broken fibres. The insert on D has a lower z-scale where a small fibre is located: height at position (1) = 3.1 nm and at position (2) = 1.8 nm (end of fibre).

6.2.1 Liquid/Substrate Interface

Interactions of the dendrimer solution with the surface of the substrate can change the outcome of the self-assembly process by solvent-mediated molecule-substrate interactions and (possibly) dewetting effects. Several flat substrates were investigated: mica, HOPG, silicon, and silicon covered with a silane. Mica and HOPG substrates were cleaved with scotch tape in order to remove the upper layers. Silicon substrates were cut from a Si(100) wafer and pre-treated in aceton before cleaning in a piranha solution. Silicon substrates were also coated with several silane molecules to obtain chemical modified surfaces. Different D1 solutions in THF were dropcast on a substrate in a THF saturated environment (unless mentioned otherwise).

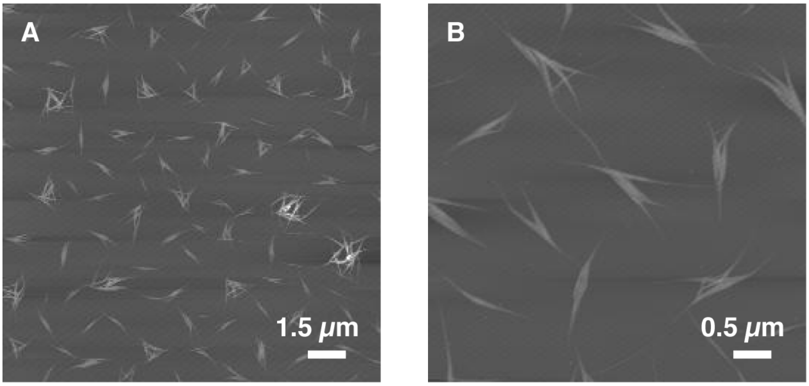

Figure 6.4: AFM topography images from samples made by casting two drops of a ~1×10^{-5} M D1 solution on mica.

6.2.1.1 Mica

On mica (figure 6.3), fibres are formed with heights ranging from a few nm up to a few tens of nm and with widths at half height ranging from a few tens of nm up to a few hundreds of nm. The smallest fibre ranges from 3.1 nm in height (measured in the middle) to 1.8 nm in height (measured at its fibre end), see insert on figure 6.3D for the two line profiles.

Fibres lie on top of each other and it is clear from the AFM images that the big fibres consist of a large amount of small fibres which interact laterally with each other. Bundles of fibres can reach heights up to

130 nm and can be several μm long. The fibres are entangled to a significant extent. The dashed lines in figure 6.3C indicate broken fibres.

At lower D1 concentrations, small whisker structures with heights of a few nm up to around 10 nm are observed (figure 6.4). Visually it can be seen that the fibres are oriented along three directions. However, this could not be illustrated with the Fourier transform of the AFM images. This is likely because the fibres are short and there is some periodic background noise present in the AFM images which influences the Fourier transformation strongly.

6.2.1.2 HOPG

Upon dropcasting D1 solution on HOPG (figure 6.5), the dendrimer assembles into fibres with similar heights as on mica. This ranges from a few nm up to a few tens of nm. The widths at half height ranges from a few tens of nm up to a few hundreds of nm and the length of the fibres can be several μm. The dashed lines in figure 6.5A indicate broken fibres. Large fibres are composed of smaller ones and fibres lie on top of each other. This is illustrated with a line profile (figure 6.5C) along the fibre in figure 6.5A as indicated with the white line. In the profile, three peaks can be distinguished which correspond with crossing points of other fibres. It is clear in the phase image that the fibre lies on top at point (1), but at both point (2) and (3) another fibre lies on top. Figure 6.5D reveals some clusters which are aligned according to the graphite terraces.

When investigating large areas, it is obvious that the fibres are oriented. The insert on figure 6.6A shows the Fourier transform of the AFM image highlighting three axes along which the fibres are aligned. Although images shown in figure 6.6 disclose fibres with preferred orientation that lie on top of each other and which laterally interact as in previous images, there is one remarkable difference. At the cross points

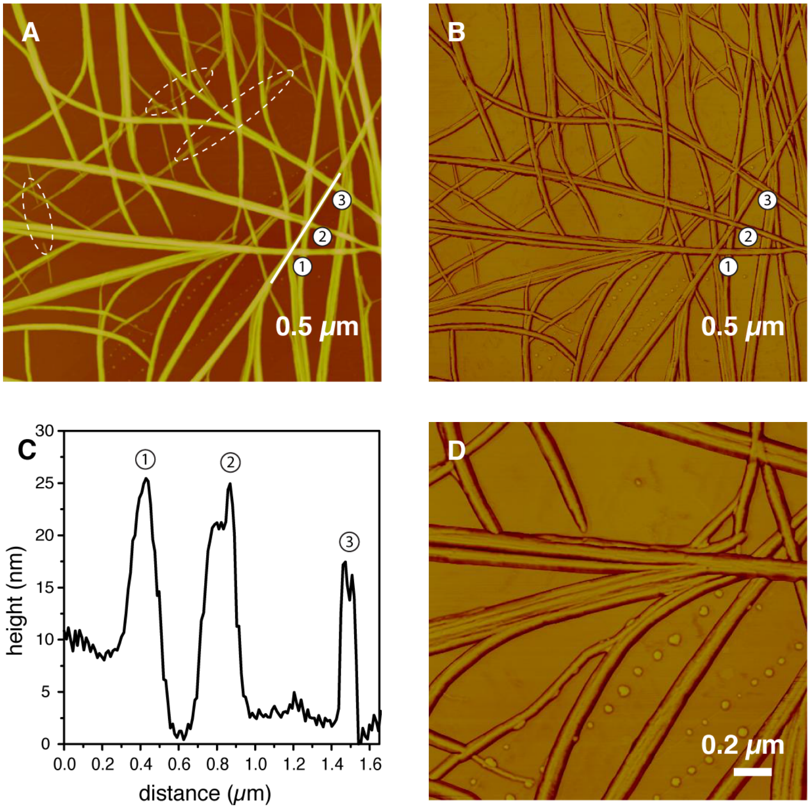

Figure 6.5: AFM topography (A) and phase (B, D) images from samples made by dropcasting 50 μL of a $\sim 2\times10^{-5}$ M D1 solution on HOPG. Dashed lines indicate broken fibres. Line profile along fibre as indicated in image A with the white line (C).

of the fibres, a thin film of amorphous material is present with heights ranging from 3 to 13 nm. This illustrates that small variations in the system can alter the self-assembled structures, since both samples were made in the same way. However, the temperature and humidity in the sample preparation room can vary slightly.

At lower D1 concentrations, fibres are still present with a preferred orientation along three axes (figure 6.7) and heights of a few nm up to

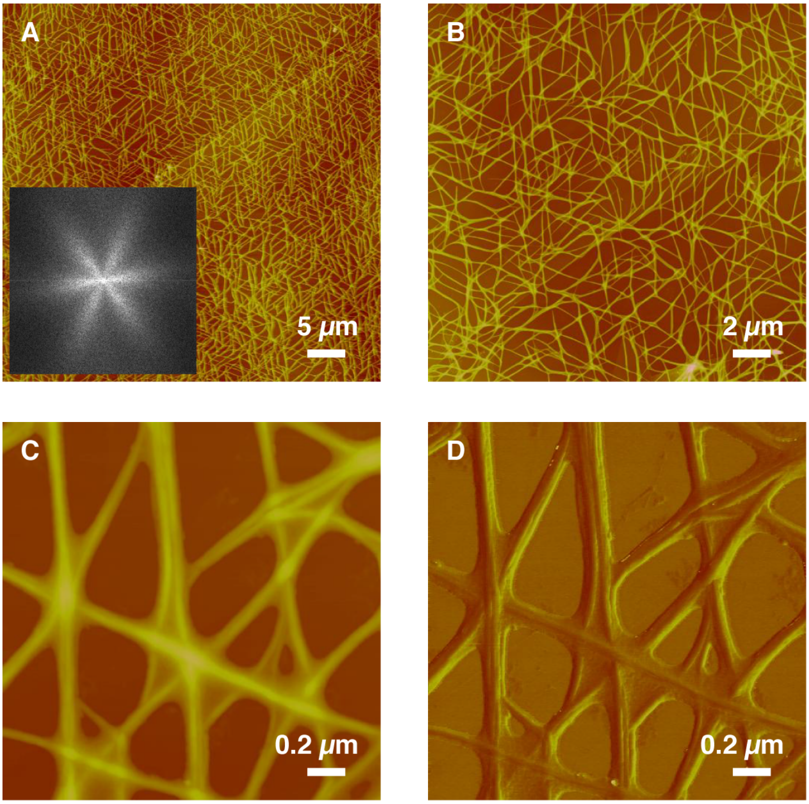

Figure 6.6: AFM topography (A, B, C) and phase (D) images from samples made by dropcasting 50 μL of a $\sim 2\times10^{-5}$ M D1 solution on HOPG. The insert on A is the Fourier transform of the image.

around 10 nm are observed. The white arrows display the edge of a graphite terrace and two fibres aligned parallel to the edges.

6.2.1.3 Silicon

Similar self-assembled fibres were observed on silicon with heights ranging from a few nm up to a few tens of nm. Their widths at half height range from a few tens of nm up to a few hundreds of nm, while the length of the fibres is several μm. Again, large fibres arise from the lat-

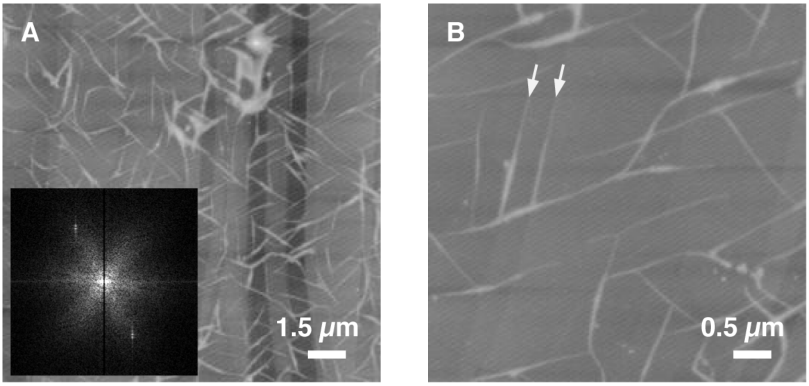

Figure 6.7: AFM topography images from samples made by casting two drops of a ~1×10^{-5} M D1 solution on HOPG. The insert on A shows the Fourier transform of the image. The white arrows on B display a graphite terrace which is followed by two fibres in the image.

eral aggregation of smaller ones and fibres lie on top of each other with random orientation.

Although the samples from which AFM images are shown in figure 6.8 were prepared using the same procedure, beside fibres additional aggregates with less order are visible in figure 6.8B, D, and F. These aggregates have the same morphology as the clusters which were observed when the samples are made in ambient conditions (see section 6.2.2). Therefore it is probable that the clusters arose from the fact that the solvent evaporation was too fast. In contrast to mica and HOPG, deposition of lower concentrated solutions on silicon (figure 6.9) leads to fibres that are several μm long.

The silicon substrates were treated with piranha solution before using them as substrates to deposit the dendrimers. Since it is known that the surface changes in time (the hydrophilic character decreases) a series of experiments were carried out to study this effect. Samples were made by dropcasting 50 μL of a ~2×10^{-5} M D1 solution on silicon immediately,

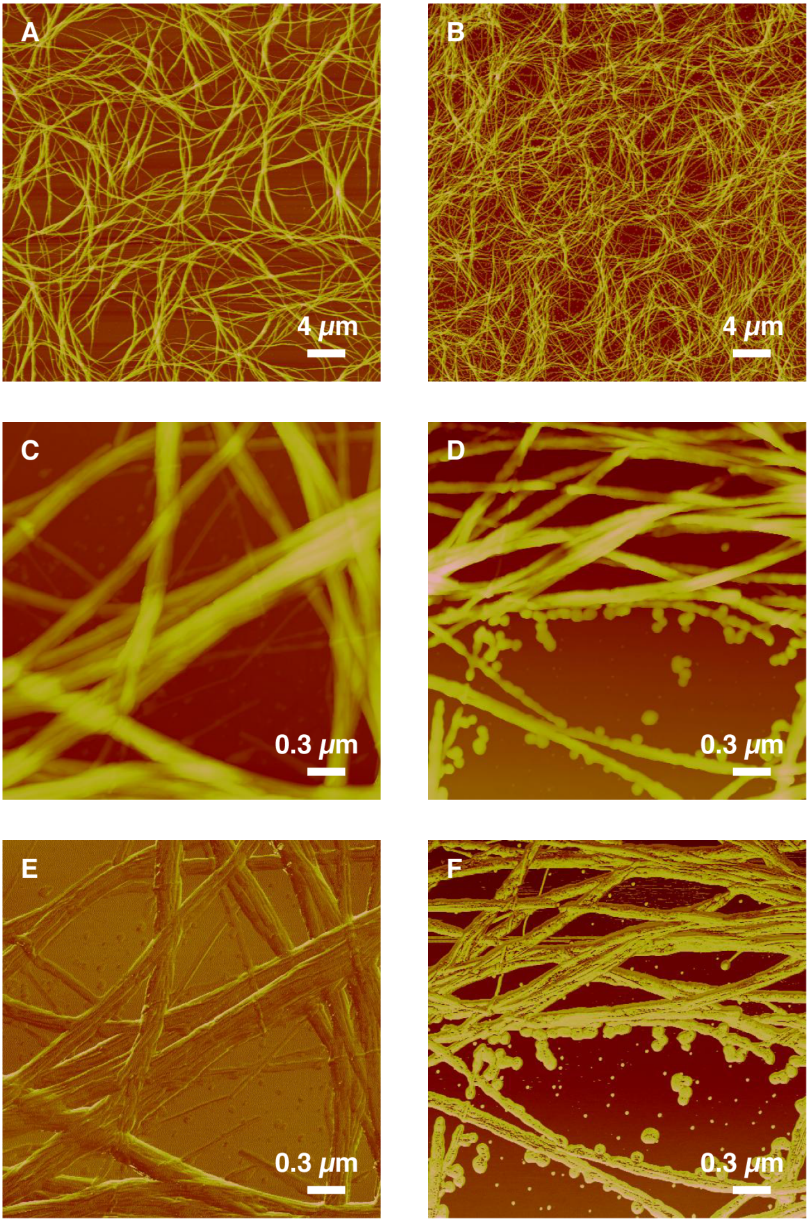

Figure 6.8: AFM topography (A-D) and phase (E, F) images from samples made by dropcasting 20 μL of a $\sim 2\times10^{-5}$ M D1 solution on silicon.

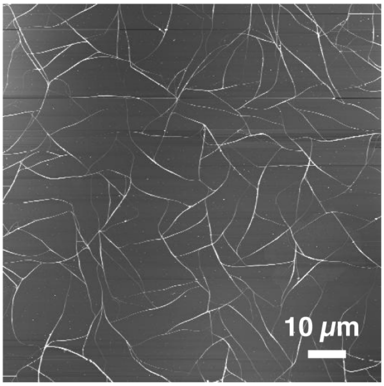

Figure 6.9: AFM topography image from a sample made by casting one drop of a ~1×10^{-5} M D1 solution on silicon.

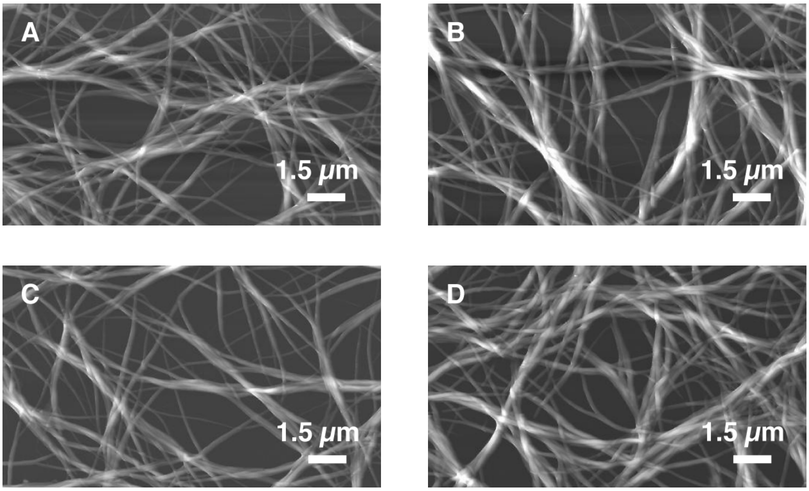

Figure 6.10: AFM topography images from samples made by dropcasting 50 μL of a ~2×10^{-5} M D1 solution on silicon immediately (A), three hours (B), one day (C), and two days (D) after treatment of the substrate with piranha solution.

three hours, one day, and two days after treatment of the substrate with piranha solution. The AFM images depicted in figure 6.10 show no dependence of the fibre formation on the time between the cleaning and the deposition step in the sample preparation.

It is not crucial to perform the dropcasting immediately after the cleaning step if silicon substrates are stored in a clean environment. Hence, it can be concluded that it is not important for the silicon surface to be perfectly hydrophilic.

6.2.1.4 Optical Images

Not only AFM images, but also optical images (figure 6.11) were recorded to investigate the self-assembled structures of D1 on mica, HOPG, and silicon. Fibres could be optically visualised on mica and silicon displaying a fibre network. Although fibres are not so easy visible on HOPG, larger aggregated structures at the edges of HOPG terraces can be seen which are in all likelihood the result of drying effects.

Figure 6.11E shows the AFM image corresponding with the area indicated by the white squares on figure 6.11C and D. In figure 6.11C, the optical unit is focussed on the top of the fibres, while in figure 6.11D, the focus is a bit closer to the surface revealing the dense fibre network.

The optical viewing system can also be used to make movies during sample preparation. This was done for the preparation of D1 fibres on silicon[2]. The optical viewing system was focussed in the middle of the substrate and pictures were taken as 50 μL of a $\sim 2\times 10^{-5}$ M D1 solution was dropcast, followed by slow evaporation of the solvent. As the film becomes thinner and thinner, fibres appear about 30 minutes after dropcasting of the dendrimer solution and the film dries out 10 to 20 minutes later. In this case, the evaporation process was homogeneous

---

[2] Movie called ‘middle’ on DVD.

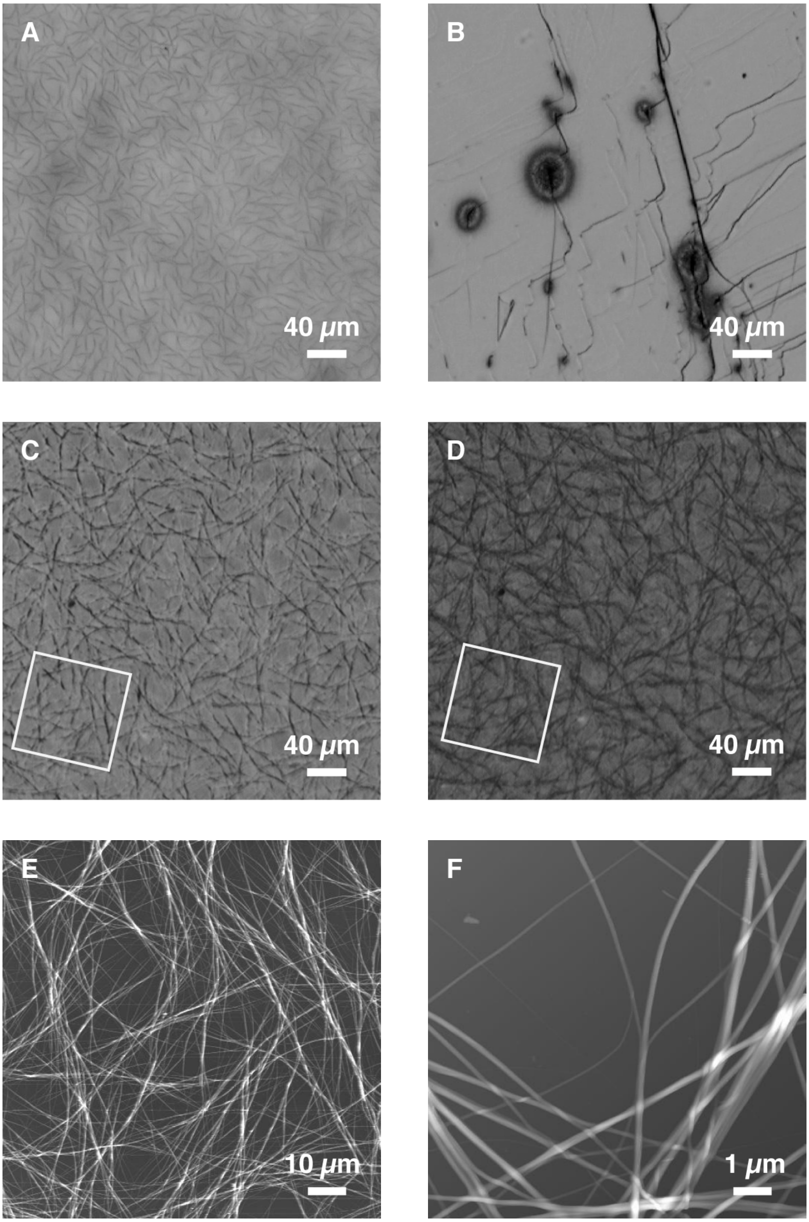

Figure 6.11: Optical (A-D) and AFM (E, F) images from samples made by dropcasting 50 μL of a $\sim 2\times10^{-5}$ M D1 solution on mica (A), HOPG (B) and silicon (C: focus on top of fibre network, D: focus on fibres close to the surface). The white squares indicate the area of the AFM image shown in E. A smaller-scale AFM image of these fibres is depicted in F.

(continuous drying of solvent) as far as the optical viewing system could resolve.

In a second experiment, the optical system was focussed near the edge of the silicon substrate. In this case a gradient effect (figure 6.12A) could be observed which is most probably caused by the fact that the solvent front was moving from top to bottom of the observed area[3]. An optical image of the edge of the drying droplet on silicon was used to calculate the contact angle during solvent evaporation of the dendrimer solution on silicon. The detailed derivation is given in chapter 11 and an estimated contact angle of 0.4 degree was found, indicating the negligible influence of dewetting effects on the fibre formation process on silicon.

Sometimes areas like in figure 6.12B were observed. This is resulting from the discontinuous evaporation of the solvent with a pinning effect which leads to accumulation of material at the pinning lines.

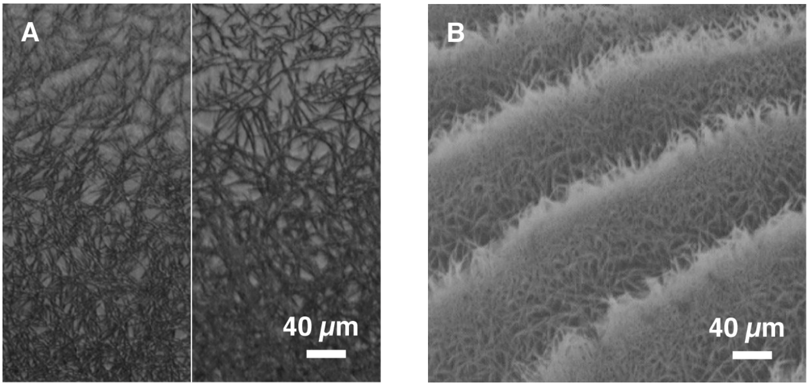

Figure 6.12: Optical images made near the edge of the silicon substrate illustrating a contineous solvent evaporation (A) or a discontinuous solvent evaporation with a pinning effect (B). The left side of image A is focussed on the high features (bottom of imaged area), while the right side is focussed on the lower features (top of the image). The sample was made by dropcasting 50 μL of a $\sim 2\times10^{-5}$ M D1 solution.

---

[3] Movie called 'near edge' on DVD.

6.2.1.5 Silicon Covered with SAMs of Silane

This section describes the preliminary experiments that were performed in order to investigate the feasibility of guiding self-assembled D1 fibres using templates. Since fibres are formed on silicon, it could be possible to direct the assembly with a template made of silicon patterned with a suitable silane that is expected to inhibit the fibre formation on silane covered regions.

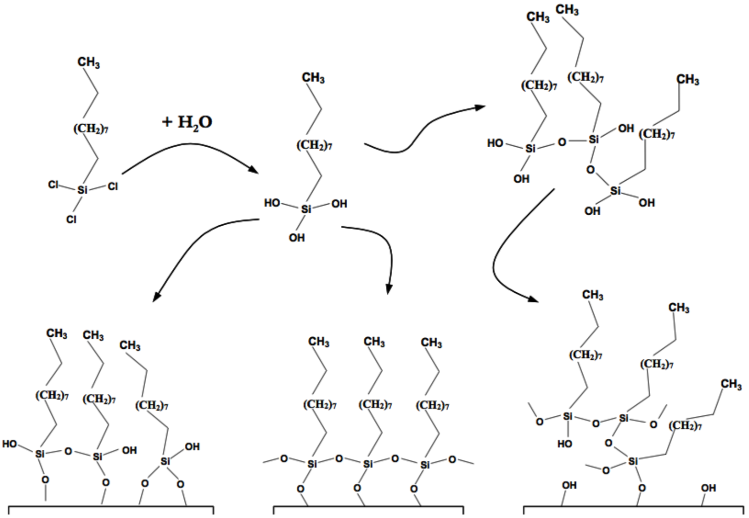

Figure 6.13: Scheme (taken from Laureyn [2002]) illustrating possible reactions and resulting products of the reaction of n-decyltrichlorosilane (DTS) in solution and with the oxide surface of the silicon substrate.

In order to completely cover the silicon substrates with silane, SAMs were formed in solution. In scheme 6.13 possible reactions and their resulting products of a trichlorosilane in solution and in the presence of a SiO_2 substrate are depicted. The upper part represents the hydrolysis of the trichlorosilane into a hydroxysilane and the possible formation of 3D siloxane-bound silane networks in solution. The lower part of the figure depicts the formation of predominantly covalently attached, self-

Table 6.1: Silane ($SiCl_3$-$(CH_2)_n$-X) information with X and n the end group and the chain length of the silane, respectively and WCA the water contact angle. CUTS = cyano-undecyltrichlorosilane, DOTS = docosyltrichlorosilane, HDTS = hexadecyltrichlorosilane and DTS = decyltrichlorosilane.

surface	-X	n	WCA	hydrophilic or -phobic	fibre formation
SiO_2	—	—	~0	hydrophilic	yes
CUTS	-CN	11	~73 °	in between	yes
DOTS	$-CH_3$	21	~109 °	hydrophobic	little
HDTS	$-CH_3$	15	~109 °	hydrophobic	no
DTS	$-CH_3$	9	~115 °	hydrophobic	no

assembled and 3D polycondensated silane layers. To obtain a SAM like depicted in the middle of the lower part, the conditions during its formation should be carefully controlled and water contact angles (WCA) of the silane covered substrates were measured as an indication of quality of the assembled layer[4].

A series of trichlorosilanes was tested by making a SAM of each silane on silicon: cyano-undecyltrichlorosilane (CUTS), docosyltrichlorosilane (DOTS), hexadecyltrichlorosilane (HDTS) and decyltrichlorosilane (DTS). Table 6.1 provides an overview of the silanes and the corresponding WCA of the resulting surface. Measuring the WCA was done by placing a water droplet on the substrate in the laboratory atmosphere and contact angles (i.e. angle formed with the surface of the substrate) were read on both sides of the droplet.

The WCA of (freshly cleaned) silicon is extremely low due to the H-bonds between the terminal OH-groups of the SiO_2 and the water molecules and therefore the WCA is negligible (~0, hydrophilic). The WCA of DOTS (~109 °), HDTS (~109 °) and DTS (~115 °) is much

---

[4] The formation of the SAMs and their characterisation with water contact angle measurements were carried out at IMEC with Randy De Palma.

higher since the interaction with water is absent on these SAMs, leading to hydrophobic surfaces. CUTS has an intermediate WCA (~73 °) and hence is significantly less hydrophobic.

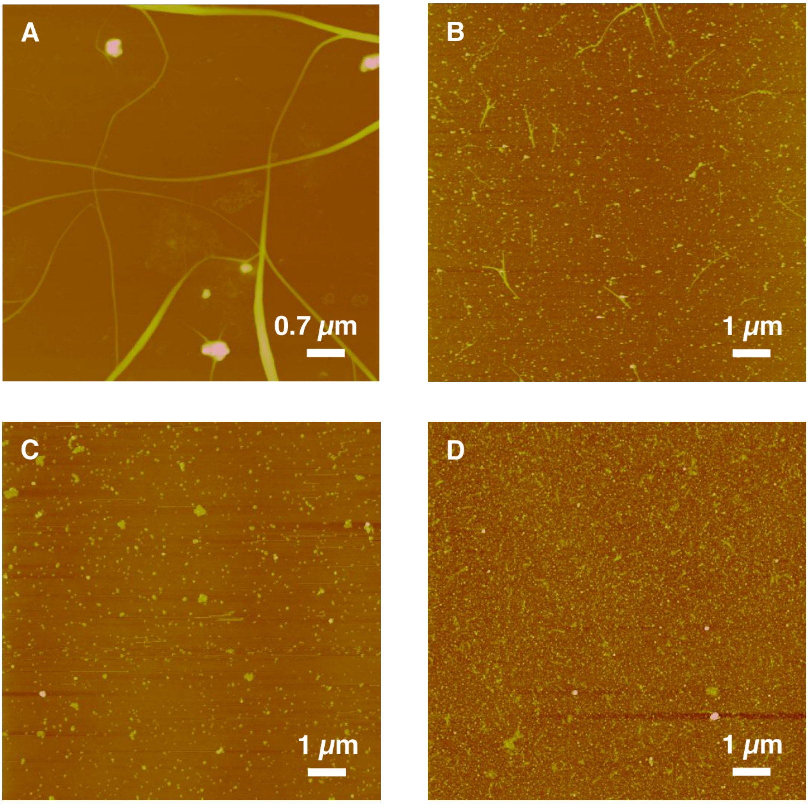

Figure 6.14: AFM topography images from samples made by dropcasting D1 solution on silicon covered completely with silane: CUTS (A), DOTS (B), HDTS (C), and DTS (D).

A D1 solution (~1×10^{-5} M) was dropcast on each of the silane modified silicon substrates under favourable conditions to form fibres and the dendrimer deposits were examined with AFM to investigate which silane would be appropriate to use for the pattern formation.

In figure 6.14 AFM topography images are shown. Although on sur-

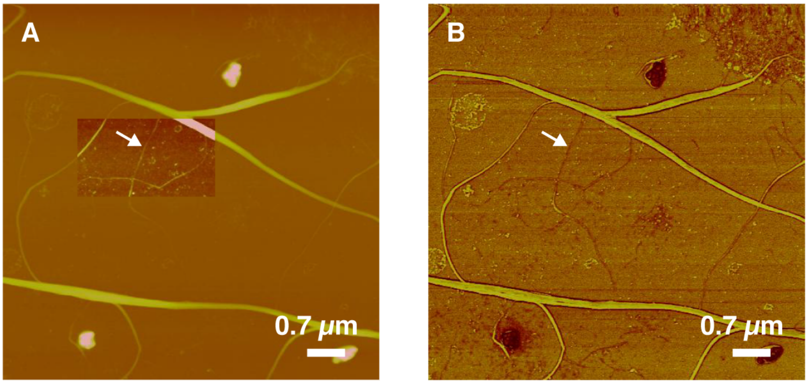

Figure 6.15: AFM topography (A) and phase (B) images from samples made by dropcasting D1 solution on silicon covered completely with CUTS. For clarity, the insert in A has a lower z-scale, revealing the small fibres. The arrow indicates a nanofibre with molecular dimensions.

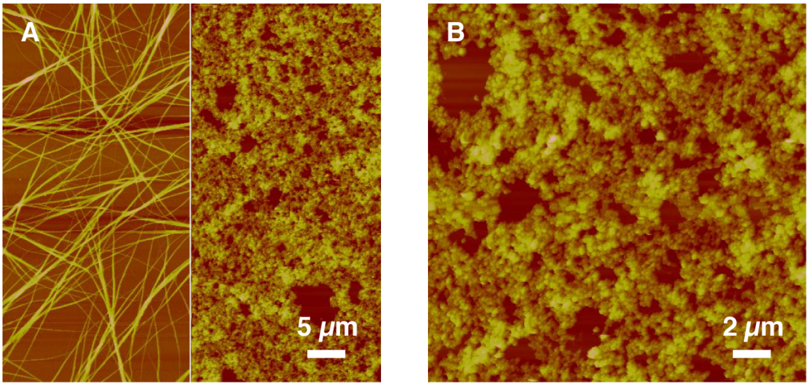

Figure 6.16: AFM topography images from samples made by dropcasting 50 μL of a $\sim 2\times10^{-5}$ M D1 solution on silicon under saturated (left half of A) and ambient conditions (right half of A, B) leading to fibres and clusters, respectively.

faces with moderate hydrophobicity (CUTS) fibres are observed over the entire surface of the sample, on surfaces that are more hydrophobic (DOTS) the fibre formation is strongly inhibited and clusters are abundantly present on the sample. For surfaces covered with HDTS or DTS, exclusively clusters were observed. In all likelihood, these clusters result from the dewetting of the dendrimer/THF film into small droplets upon evaporation of the THF since the fluid film becomes metastable in air below a critical thickness [de Gennes et al., 2004].

An additional topography image and a phase image of the sample made with CUTS is shown in figure 6.15. The dendrimer forms fibres with heights from around 1 nm up to about 30 nm and with widths at half height ranging from about 40 nm up to about 200 nm and they can be several μm long.

6.2.2 Liquid/Air Interface

The other interface which needs to be considered upon transferring a self-assembling system in solution into one on a substrate is the interface between the dropcast solution and the environment. Therefore, sample preparation on freshly cleaned silicon was carried out with and without a THF saturated environment, both at room temperature (~22 °C) and at low temperature (~4 °C).

6.2.2.1 Preparation at Room Temperature (~22 °C)

Figure 6.16 shows AFM images of samples prepared at room temperature. Since THF is a low boiling, highly volatile organic solvent it evaporates rather fast under ambient conditions. The aggregates formed in the self-assembling system become kinetically trapped during transfer to the silicon surface leading to cluster formation.

However, if the same procedure is followed in a THF saturated environment, the solvent evaporates significantly slower leading to the formation of thermodynamically more favourable aggregates (nanofibre formation). The solvent evaporation can take several hours depending on the slit of the saturated tank that allows solvent to 'escape'.

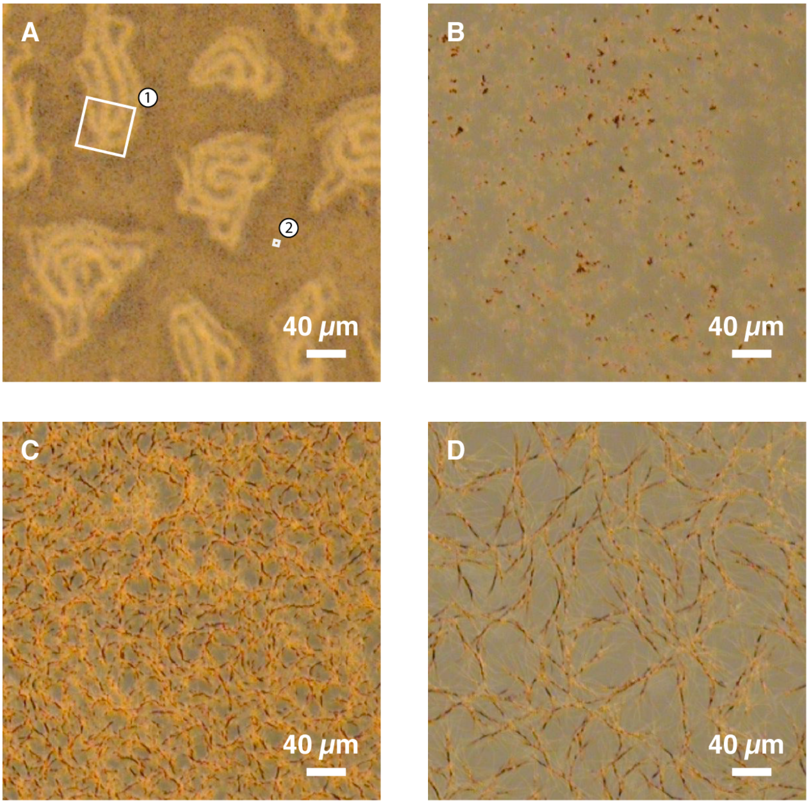

Figure 6.17: Optical images from samples made by dropcasting 50 μL D1 solution on silicon at low temperature under ambient (A, B) and THF saturated conditions (C, D) with a concentration of $\sim 2\times10^{-5}$ M for A and C, and of $\sim 2\times10^{-6}$ M for B and D. The numbers indicate the areas of which AFM images are shown in following figures.

6.2.2.2 Preparations at Low Temperature (∼4 °C)

Optical images of samples made at low temperature with and without saturated conditions are shown in figure 6.17. Similar as at room temperature, fibres are formed upon dropcasting under THF saturated environment (figure 6.17C and D).

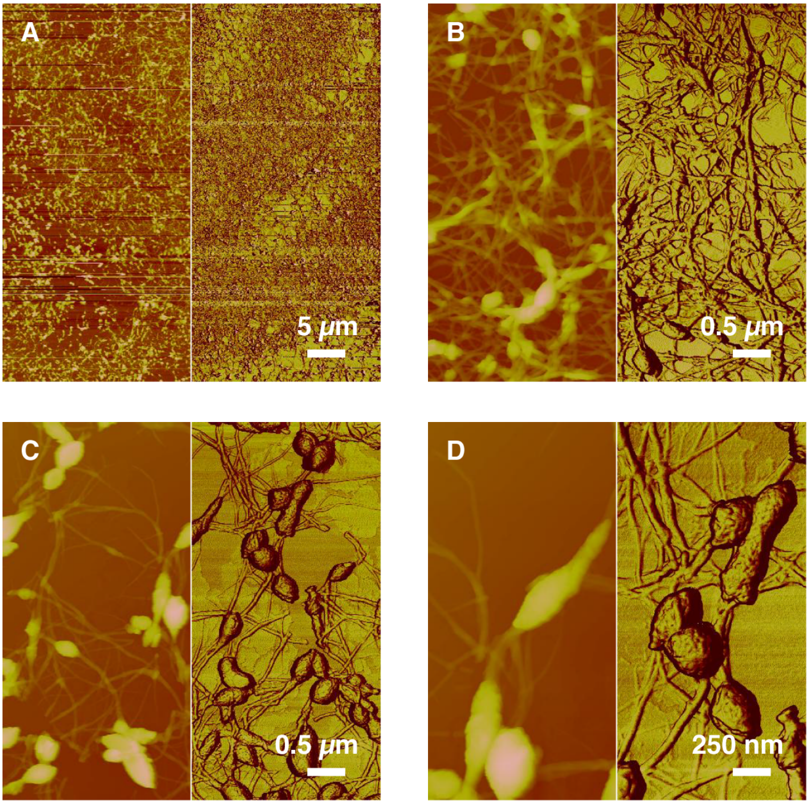

Figure 6.18: AFM topography (left half) and phase (right half) images after dropcasting a ∼2×10^{-5} M solution of D1 on silicon at low temperature under ambient conditions. A and B correspond with area (1) indicated in figure 6.17A, while C and D correspond with area (2).

In contrast to the cluster formation at room temperature, peculiar features are observed when the same sample preparation procedure (i.e.

without saturated conditions) is followed at low temperature (figure 6.17A and B). It is most likely that the features in figure 6.17A are the result of a complex drying process. In figure 6.18 AFM images are depicted of the areas indicated on the optical image, between and on top of the bright features. Area (1) corresponds with figure 6.18A and B, while area (2) corresponds with figure 6.18C and D. On both areas aggregates were observed with similar morphology, but different in concentration. This supports the idea that the large features arose from drying effects (accumulation of material). As the very last step of solvent evaporation takes place at those areas, it is easy to understand why the ratio of fibres to clusters is higher at those locations (longer evaporation time leads to thermodynamically more favourable aggregates).

The AFM images reveal that it is possible to obtain fibres at low temperature without a saturated THF atmosphere. This is probably related to the slowing down of solvent evaporation upon temperature decrease. However, additional cluster-like features arise which seem to lie on top of the fibres. This is likely related to the fact that molecules at low temperature possess less kinetic energy to move and consequently are less likely to be able to vary their orientation in the last step of the solvent evaporation, which is critical for fibres formation. From the phase images it is clear that most aggregates are positioned on top of a nm-heigh layer of dendrimer material.

6.2.2.3 Reversibility

As stated above, it is crucial that the assembly of the components is reversible or at least allows the components to adjust their positions within an aggregate once it has formed to avoid 'errors' in the aggregates. Therefore the strength of the forces tending to disrupt the aggregates, mostly thermal motion, must be comparable to the interaction forces between components.

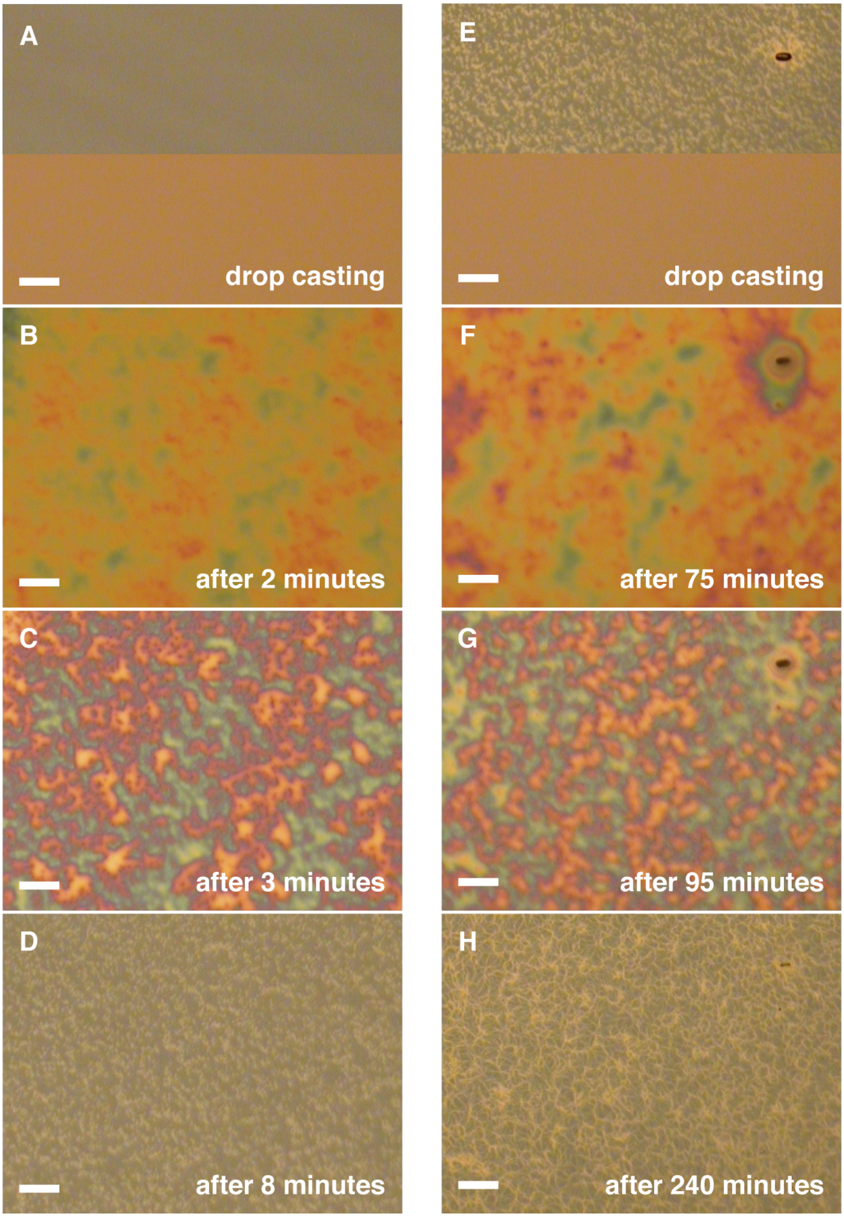

Figure 6.19: Series of optical images illustrating the reversibility of the dendrimer D1 self-assembly: cluster formation upon fast evaporation of the solvent (A-D) is followed by fibre formation (E-H) upon adding solvent and ensuring slow evaporation in a THF saturated tank. The upper half of A and E are optical images just before dropcasting, while their lower part are images just after the dropcasting. The scale bar is 50 μm.

Table 6.2: Different solvent mixtures with gradually increasing amount of C_6F_6 in THF.

mixture	C_6F_6	D1 concentration after mixing	
mix 1	5%	2.06×10^{-5} M	$\sim2\times10^{-5}$ M
mix 2	10%	1.95×10^{-5} M	
mix 3	20%	1.74×10^{-5} M	
mix 4	40%	1.30×10^{-5} M	

To prove that the dendrimers are mobile within the aggregate once it has formed, the following experiment was set up[5]. 50 μL of a D1 solution in THF was dropcast on a freshly cleaned silicon surface under ambient conditions and optical images were taken every 3 seconds during the solvent evaporation. A few images were selected and are shown in figure 6.19A-D. Cluster formation was observed during this fast evaporation of the solvent. In a second part of the experiment, the sample with clusters was put in a THF saturated environment and 50 μL of THF was dropcast on top of it. As can be seen on the optical images in figure 6.19E-H, the clusters were transformed into nanofibres during the slow solvent evaporation.

6.2.3 Solvent Mixtures

The solvent in which the dendrimer is dissolved not only provides the mobility that is necessary for molecules to ‘find each other’, but also mediates the molecule-molecule interactions. In this section, interaction of D1 with the solvent molecules is employed to influence the interactions between the dendrimer molecules.

Therefore, a solvent that was expected to interact with D1 was gradually added to the THF solution (see table 6.2 for the composition of the solvent mixtures). Hexafluorobenzene (C_6F_6) was chosen since it

---

[5] Movie called ‘reversibility’ on DVD.

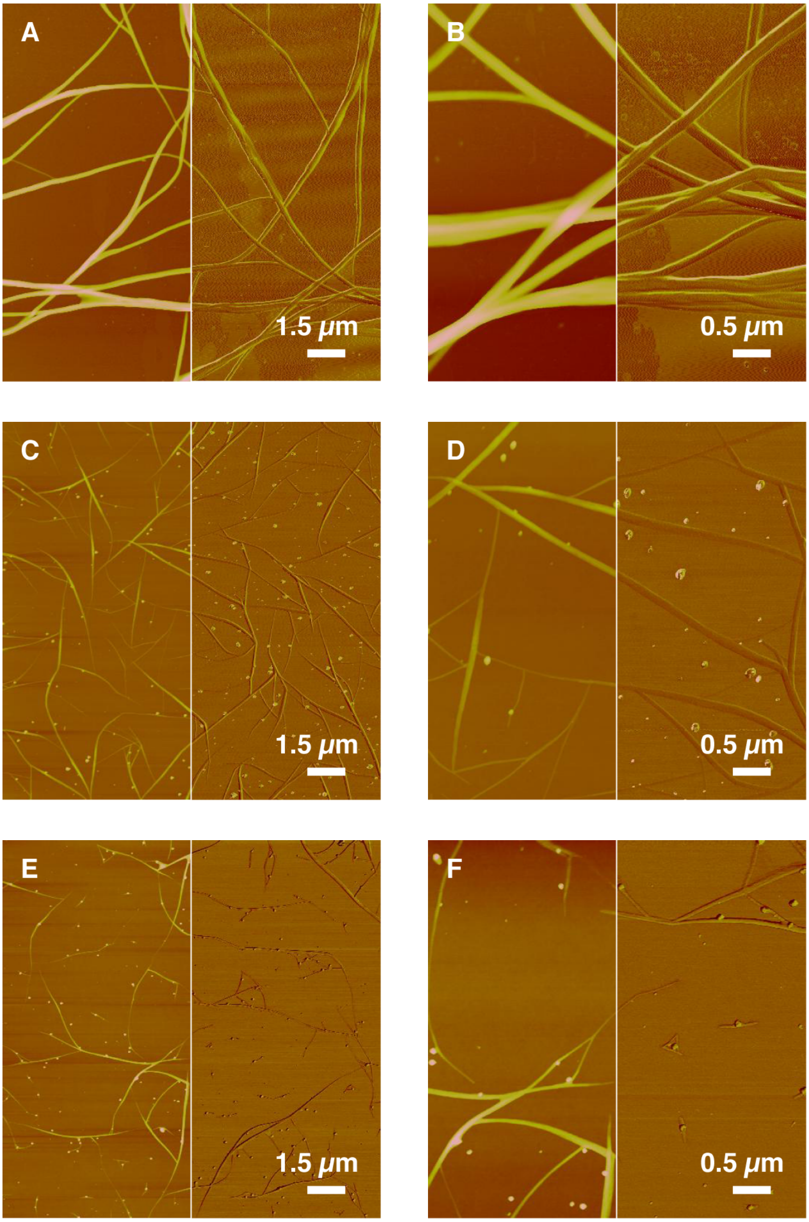

Figure 6.20: AFM topography (left half) and phase (right half) images after dropcasting a solution of D1 dissolved in THF/C_6F_6 on silicon, with 5% (A, B), 10% (C, D) and 20% (E, F) C_6F_6 in the solvent mixtures.

is expected that aromatic interactions between the two aromatic rings (phenyl groups of D1 and C_6F_6) would result [Zhu et al., 2005]. The uptake of such aromatics into the nanoporous polyphenylenic scaffold of polyphenylene dendrimers is well established [Schlupp et al., 2001]. Most likely the D1 dendrimers are gradually saturated with C_6F_6 prior to self-assembly on the substrate leading to a D1-host/C_6F_6-guest system formed in these solvent mixtures.

A series of experiments was carried out by dropcasting a D1 solution containing a variable amount of C_6F_6 onto HOPG and silicon under favourable conditions to form fibres and the resulting dendrimer deposits were examined with AFM.

Figure 6.20 reveals AFM images from samples made with low (5%) to intermediate (20%) concentrations of C_6F_6 in the solvent mixture. Fibres can clearly be observed on silicon, but an increasing amount of clusters appears with increasing amount of C_6F_6. A similar trend was observed on HOPG, as presented in figure 6.21, however the fibres formed on HOPG have smaller dimensions than those formed on silicon. Probably the saturation of the D1 dendrimers with C_6F_6 occurs randomly within the dendritic structure leading to host-guest assemblies with different intermolecular and surface affinity. This could explain the observation of a larger number of unstructured aggregates or clusters coexisting with self-assembled dendrimer fibres on both substrates.

When using solvent mixtures with 40% C_6F_6, the aggregates formed upon deposition are to a large extent dependent on the type of substrate as can be seen in figure 6.22. In the case of HOPG (figure 6.22A), no fibres are formed and in addition to many small clusters, a few very large ones were visualised with AFM. In contrast to cluster formation on HOPG, samples on silicon (figure 6.22B-D) revealed additional structures: formation of fibres with a completely different morphology compared to the D1 fibres formed from pure THF. Another important issue

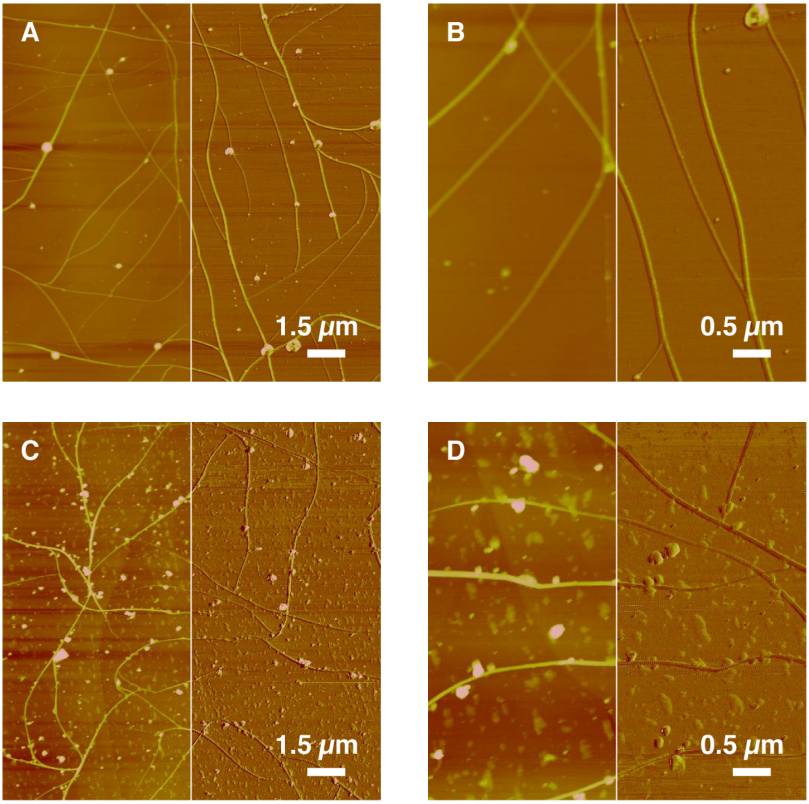

Figure 6.21: AFM topography (left half) and phase (right half) images after dropcasting a solution of D1 dissolved in THF/C_6F_6 on HOPG, with 5% (A, B) and 20% (C, D) C_6F_6 in the solvent mixtures.

is the location of most clusters which seem to be repelled from the fibres upon formation. Some clusters seem to lie on top or in between the fibres, but they are never observed on the substrate in close proximity to the fibres and have roughly all the same dimensions.

A possible explanation could be the stability of the mixtures on the substrates, since the mixtures seem to evaporate faster on HOPG than on silicon. There may be a phase separation of the THF and C_6F_6 in the mixture upon the slow evaporation on silicon. Although the origin

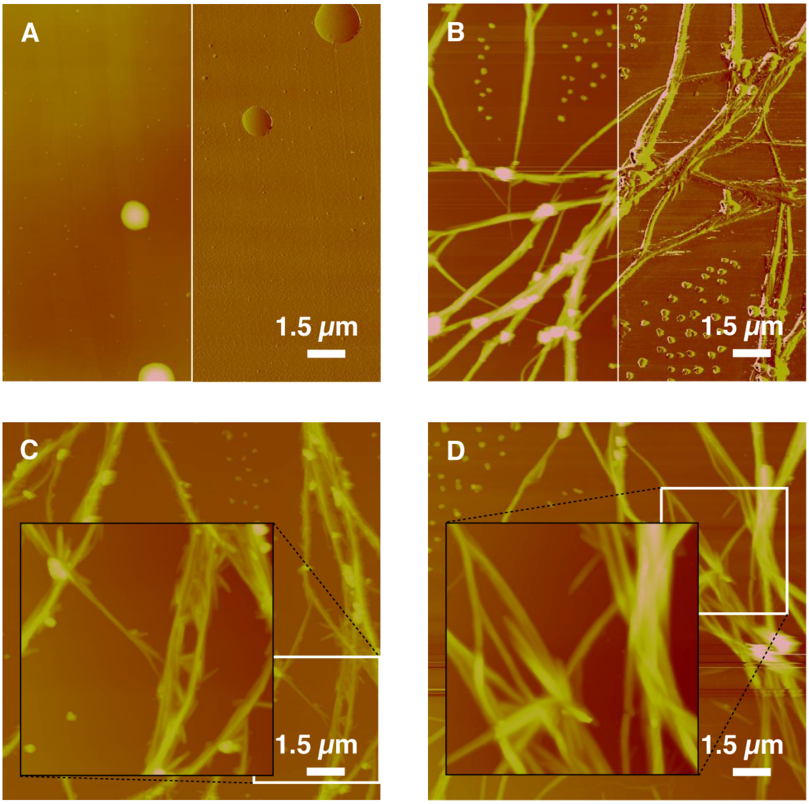

Figure 6.22: AFM topography (left half of A and B; C and D) and phase (right half of A and B) images after dropcasting a solution of D1 dissolved in THF/C_6F_6 on HOPG (A) and silicon (B, C, D), with 40% C_6F_6 in the solvent mixture. The inserts provide a zoom in of 2x.

of fibres with a different morphology remains unclear, this could explain the emergence of the different domains (clusters versus fibres).

6.2.4 Stability of the Nanofibres

6.2.4.1 Temporal Stability

AFM measurements were carried out on samples with the D1 dendrimer fibres, both immediately after formation and three months later (the

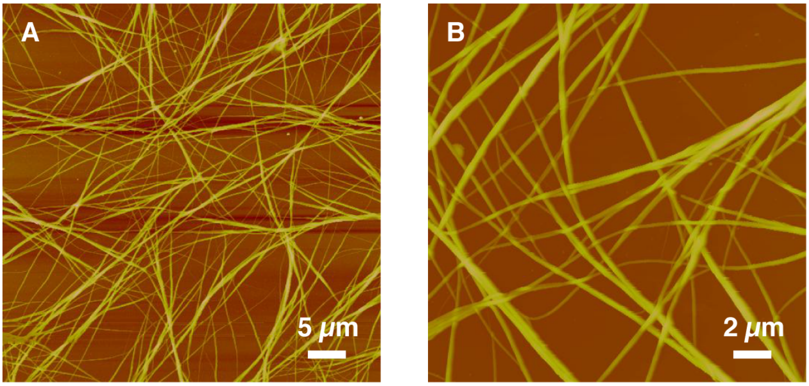

Figure 6.23: AFM images of D1 fibres immediately (A) and three months (B) after their preparation on silicon.

sample was kept under ambient conditions). As can be seen in figure 6.23B, the fibres are still present and intact after all this time, illustrating their stability in time.

6.2.4.2 Chemical and Mechanical Stability

Both milli-Q-water and THF were employed to rinse a fibre-containing sample in order to study their chemical and mechanical stability. The effect of the solvent on the fibres was investigated with AFM before and after rinsing with the solvents (figure 6.24 and 6.25). It is clear that in both cases, the fibres were destroyed or severely damaged although it was expected that milli-Q-water would not have a large influence due to the low solubility of D1 in water. The damage to the fibres is probable not caused by the chemical nature of the solvent, but is due to the 'mechanical' effect of the flow during rinsing.

After (partially) removing fibres by rinsing with water, a layer of material that is covering the substrate's surface becomes apparent (figure 6.24C and D). Although this layer was not observed before the

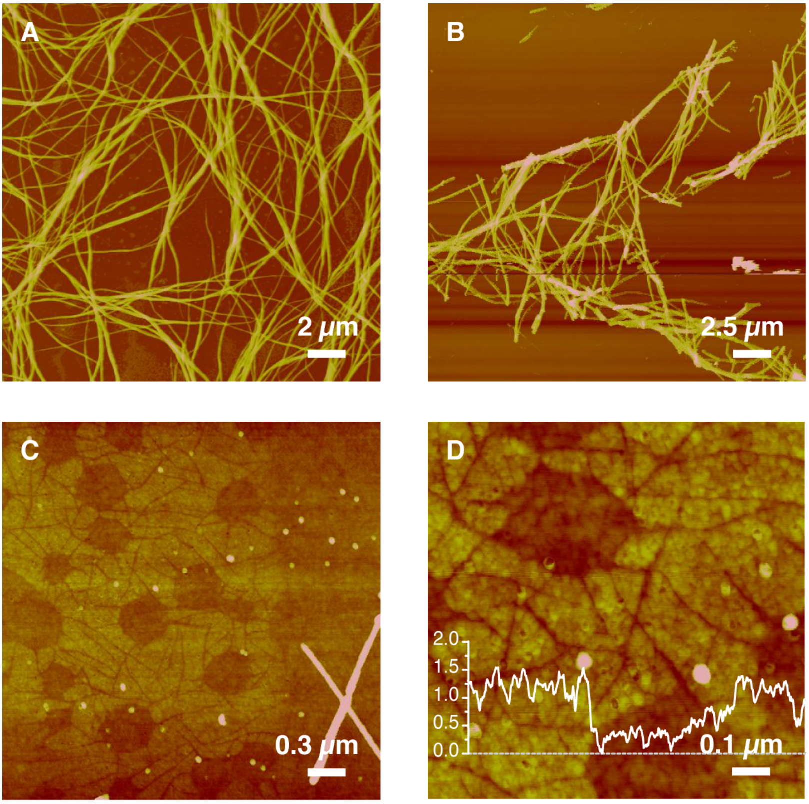

Figure 6.24: AFM images of D1 fibres on silicon before (A) and after (B, C, D) rinsing with H_2O. A cross section profile through the back ground layer is depicted on image D (height unit: nm).

rinsing step, it was most probably formed during the preparation of the fibre-containing sample and it consists of dendrimer molecules. It is very unlikely that dendrimer molecules were dissolved during rinsing and formed the layer upon drying of the sample since water is a poor solvent and the sample was tilted during rinsing enabling removal of dendrimer-containing water. The large difference in dimension of the fibres and the layer (resulting in a large z-scale of the AFM image) probably hinders the detection of the layer on the fibre-containing sample before rinsing.

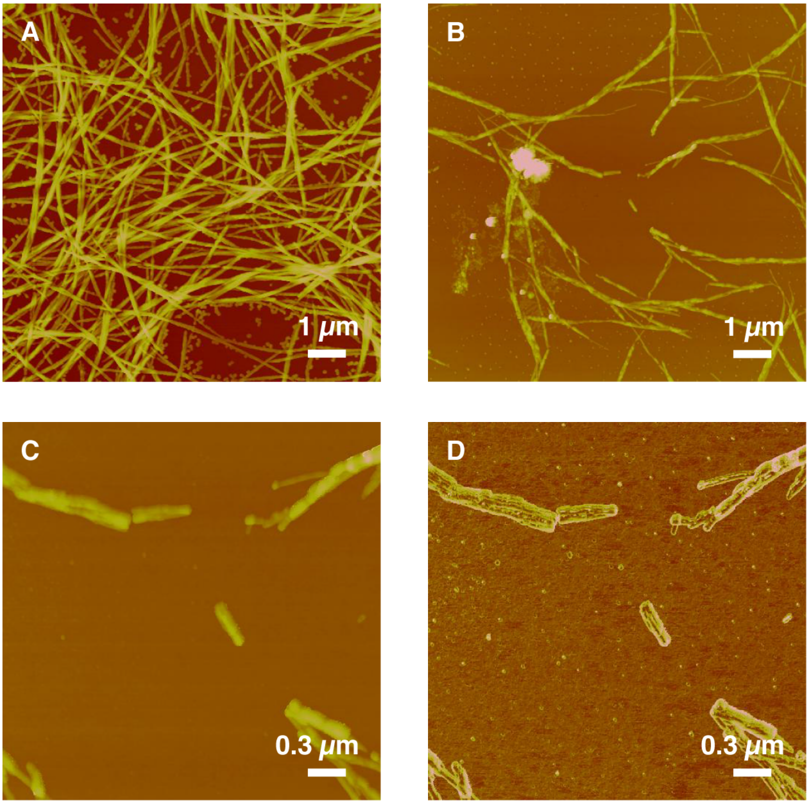

Figure 6.25: AFM images of D1 fibres on silicon before (A) and after (B, C, D) rinsing with THF.

Attempts were made to measure the fibres in liquid in order to investigate the effect of the solvent. A droplet of milli-Q-water was put on a fibre-containing sample and AFM images were recorded. A representative image is shown in figure 6.26A illustrating the disruption of the fibres during scanning the sample in water. Since water is a very poor solvent for the dendrimer molecules, measuring the fibres in THF (which is a good solvent) would also result in disruption of the fibres and hence it can be concluded that the fibres have an extreme low stability in solvents.

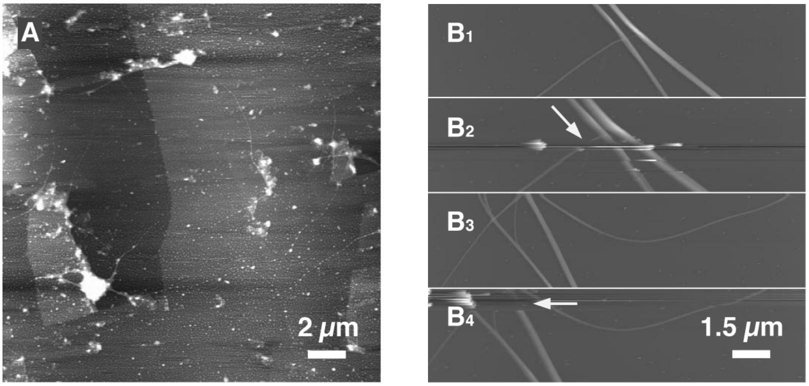

Figure 6.26: AFM images of D1 fibres on HOPG obtained through liquid AFM measurement in milli-Q-water (A) and fibres on mica (B) before (B_1, B_3) and after (B_2, B_4) repeatedly scanning a specific area. The arrows indicate 'broken' fibres.

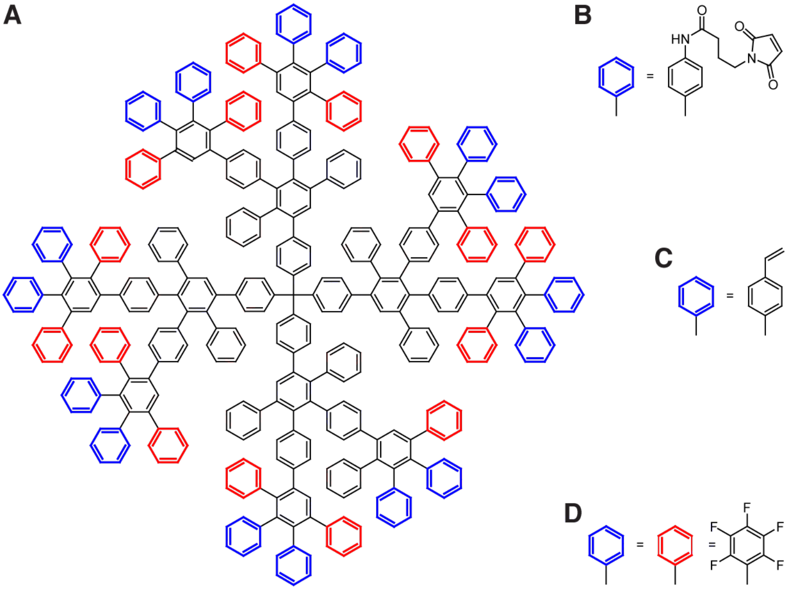

Figure 6.27: Molecular structure of the second generation polyphenylene dendrimer (A) and the different functional groups attached to its periphery (B, C, D).

Previously [Ver Heyen, 2003] the nanoManipulator was employed to investigate the mechanical stability of the fibres in the absence of solvent (ambient conditions). A slightly higher force was used while pushing against the fibres with the AFM-tip. This resulted in cutting the fibres as material was removed where the tip crossed the fibre and the cut edges did not move upon manipulation. Similar to these experiments, the mechanical stability can be investigated without using the nanoManipulator. While the nanoManipulator can be used for manipulations in all directions and in several modes, an AFM without haptic interface is limited to manipulations according to the scan direction of the tip. In figure 6.26B, images of two experiments are depicted before and after scanning a certain area (indicated with arrows) for a longer time. This results in damaging the fibres (figure 6.26B_2 and B_4).

6.2.4.3 Functional Groups at the Periphery of Dendrimers

In order to create mechanically stable nanofibres, similar dendrimers were investigated with functional groups attached to their periphery (structure shown in figure 6.27). In the past, dyes were used as the polyphenylene dendrimer core [Liu et al., 2003a] or dyes were attached to their periphery [Liu et al., 2003b] in order to investigate their optical properties. Polyphenylene dendrimers with carboxylic acid groups attached were used to build self-assembled monolayers [Zhang et al., 2002a]. In this study, functional groups were carefully selected on the basis of their possibility to introduce covalent links between the dendrimers after their assembly into nanofibres, providing additional insight in the self-assembly process of polyphenylene dendrimers.

Previously [Ver Heyen, 2003], dendrimers with a maleimide function at the periphery were studied (figure 6.27B). Maleimides are known to photoreact to form maleimide cyclobutane dimers through the formation of radicals [von Sonntag et al., 2002]. Although the maleimide dendrimers do not form fibres, dendrimer mixtures were prepared including second generation polyphenylene dendrimers with and without the maleimide functions attached. However, experiments with the nanoManipulator showed that the fibres formed from these mixtures were not mechanical stable after UV-illumination. It should also be emphasised that the use of dendrimer mixture makes it very difficult to determine which type of dendrimers are included in the fibres and to what extent.

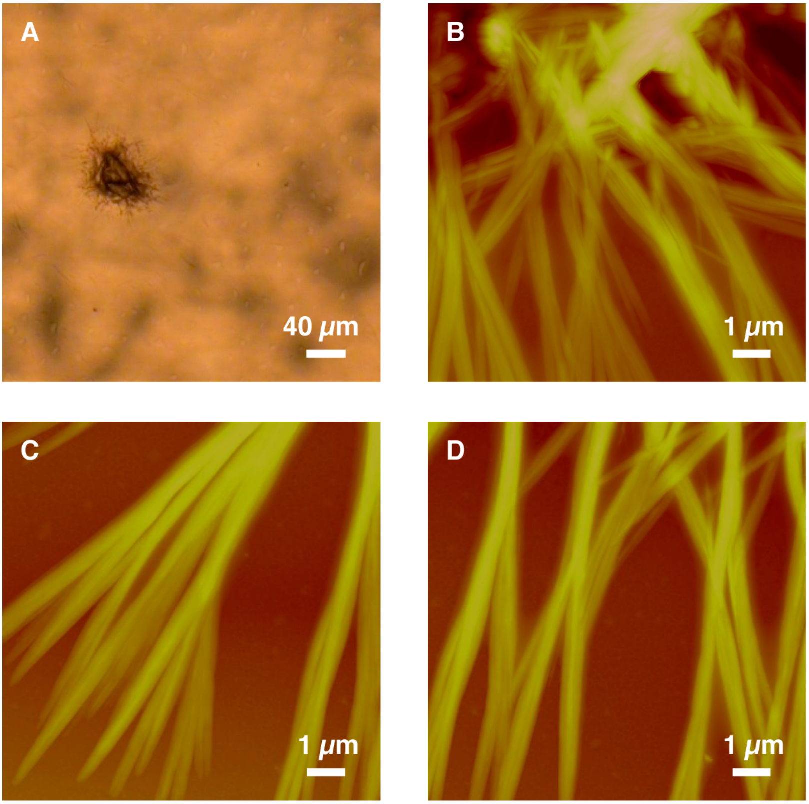

Figure 6.28: Optical (A) and AFM topography (B, C, D) images from samples made by dropcasting 50 μL of a $\sim 2\times10^{-5}$ M vinyl dendrimer solution on mica.

Figure 6.27C shows another group, i.e. a vinyl functional group which can potentially be used to link the dendrimers covalently. Samples were made by dropcasting a $\sim 2\times10^{-5}$ M solution on HOPG, mica, and silicon in a THF saturated tank. On both HOPG and mica, clusters of varying size were abundantly present. Upon investigation of the samples with the optical viewing system, an area was found on mica where fibre formation had occurred (figure 6.28). Similar as for fibres made from the dendrimer without additional groups to its periphery (i.e. D1), the fibres are composed of thinner fibres which are laterally interacting with each other and are several μm long.

On silicon (figure 6.29), large regions with thin layers were observed. The z-scale of figure 6.29B is barely 2 nm. When investigating the sample with the optical viewing system, an area with fibres was located (figure 6.29C) and AFM measurements were performed. Figures 6.29E and F reveal the 'individual' fibres which constitute the fibre network. Since layers seem to be formed easier than fibres for this system, the concentration was decreased and samples were made with a $\sim 2\times10^{-6}$ M vinyl dendrimer solution in THF (figure 6.30). This suppressed the layer formation and networks were observed with the optical viewing system (see inserts). AFM measurements show fibres which seem to be embedded in an amorphous matrix of aggregated vinyl dendrimer molecules. Figure 6.31A provides a high resolution zoom in on such an area revealing a network of fibres with an estimated width ranging around 6 nm.

AFM measurements were conducted and the stability of the fibres was investigated by trying to move an individual fibre with the AFM-tip (figure 6.31B and C). During scanning, the slow scanning axis was disabled at the location of the fibre. The drive amplitude of the tip was increased from 63 up to 315 mV leading to the disappearance of the fibre like structure in the image. This was followed by decreasing the drive amplitude back to its measuring value. The slow scan axis was enabled

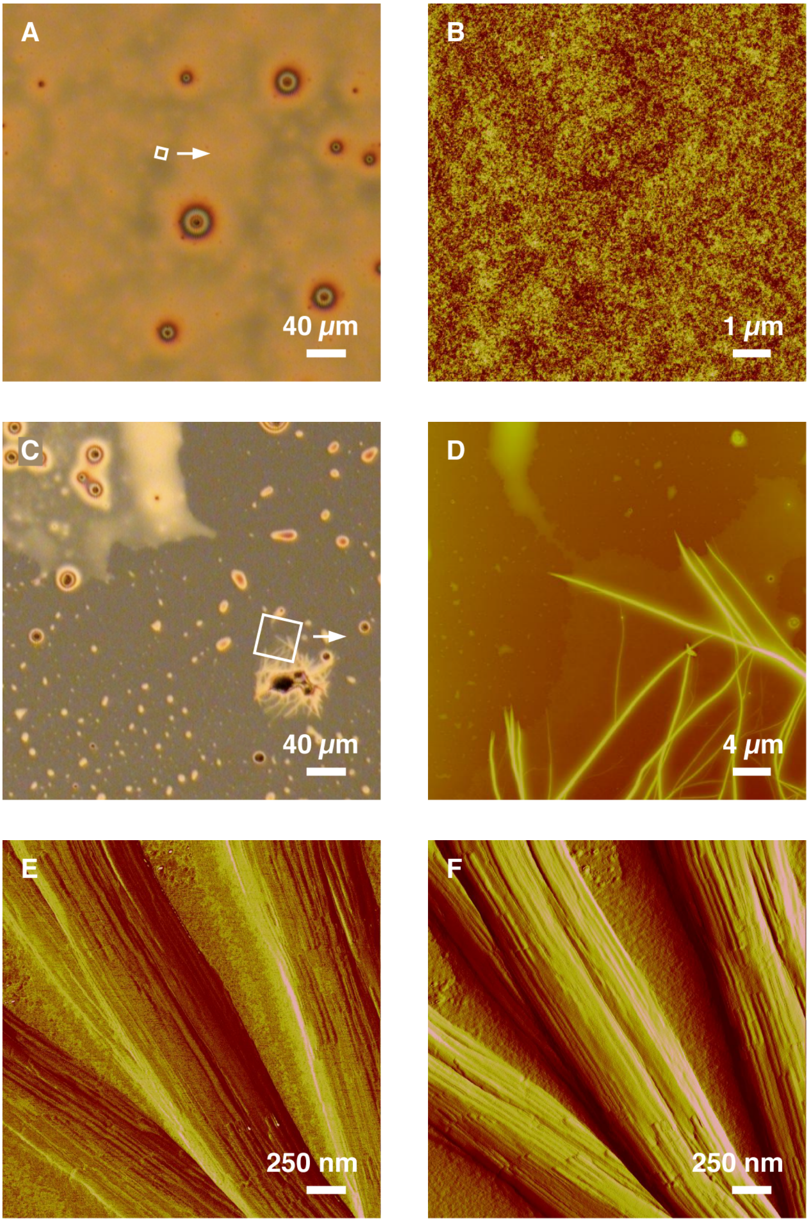

Figure 6.29: Optical images (A, C) and AFM topography (B, D), phase (E) and amplitude (F) images from samples made by dropcasting 50 μL of a $\sim 2\times10^{-5}$ M vinyl dendrimer solution on silicon.

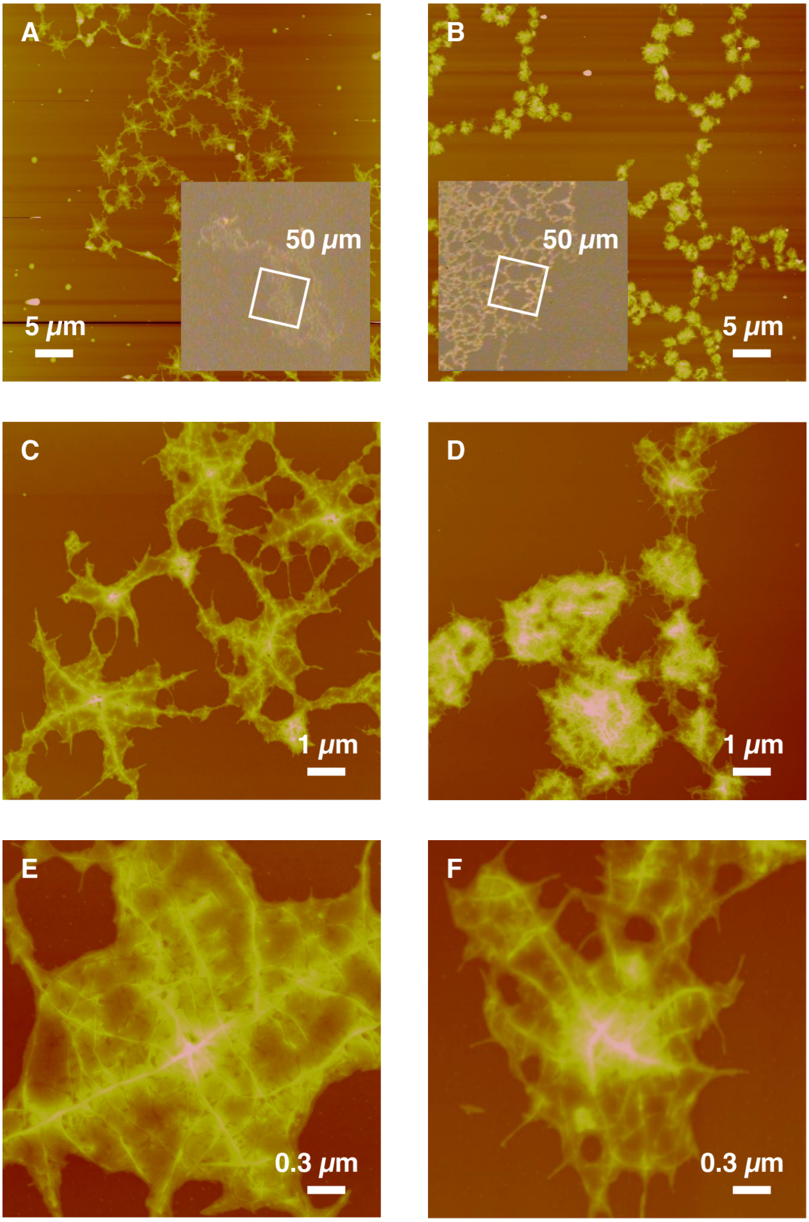

Figure 6.30: AFM topography images from samples made by dropcasting 50 μL of a $\sim 2\times10^{-6}$ M vinyl dendrimer solution on silicon. The inserts in A and B are optical images with a white square drawn on them to indicate the AFM area.

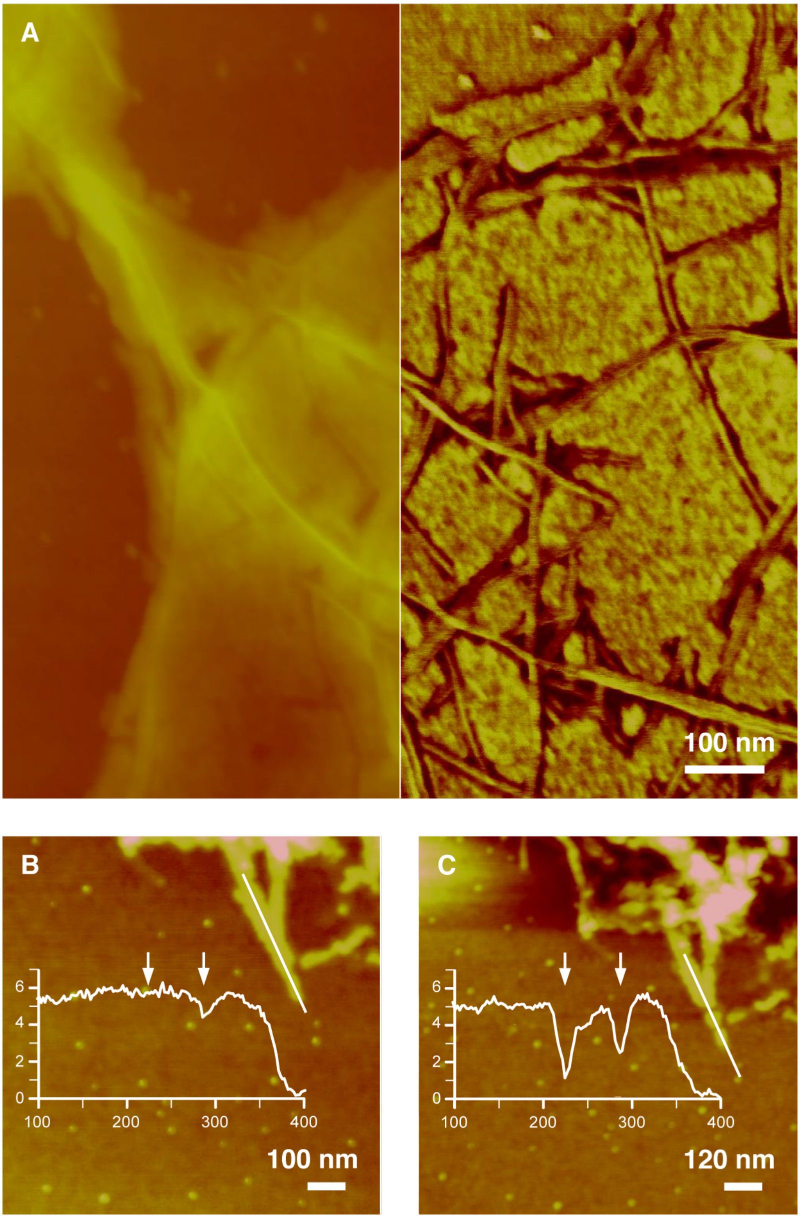

Figure 6.31: AFM topography (left side) and phase (right side) images (A) from samples made by dropcasting 50 μL of a $\sim 2\times10^{-6}$ M vinyl dendrimer solution on silicon and AFM topography images before (B) and after (C) force increase during scanning while disabling the slow scan axis. Cross section profiles along the fibre are depicted on top of the AFM images (height unit: nm).

and the scan area was slightly increased to study the effect of this force increase during scanning. It is clear that the fibre did not move, but was cut at two locations. The fact that the fibre was cut at two locations is attributed to the sudden force increase which could have led to some drift of the tip with respect to the sample surface.

Another approach to obtain stabilised fibres is the use of fluorine atoms at the periphery (figure 6.27D) which could be linked upon adding diamines after sample preparation. As these fluorine dendrimers do not form nanofibres like the second generation polyphenylene dendrimers (i.e. D1), this type of dendrimer can not be employed either to strengthen the polyphenylene nanofibres.

6.2.5 Discussion and Conclusions

Both the emergence and topological features of nanofibres made by second generation polyphenylene dendrimers D1 were found to be controlled by several parameters.

Upon dropcasting in a saturated environment, the substrate is initially coated with a uniform layer of the solution and the solvent evaporates slowly resulting in a supersaturated solution. Upon this increase of D1 concentration, aggregates can form in solution as was observed with light scattering experiments. Most probably the liquid layer on the substrate is very thin (nanometre region) at this stage of the sample preparation.

The fibre formation is likely to be directed by the fact that upon solvent evaporation, the liquid layer gets thinner in the z-direction, while no restrictions are present for the x-, nor y-direction.

The optical viewing system could visualise a random network of fibres before the solvent was completely evaporated as shown in the movie called ‘middle’ (see DVD). The nanofibres are lying on top of each other which supports the theory of fibre formation in supersaturated solutions just before complete solvent evaporation. Another observation that enforces this view is the broken fibres which were observed on both mica and HOPG. The breakage of fibres is most probably caused by strain during the deposition process in the late stage of the sample preparation.

In contrast to silicon, on mica and HOPG fibres are not randomly dispersed on the surface. The Fourier transform of large-scale AFM images of samples on HOPG highlights three axes along which the fibres are oriented. This is a direct consequence of the symmetry of the surface indicating once again that the crucial step for fibre formation takes place during the last moments of solvent evaporation as the surface plays an important role in directing the orientation of the nanofibres.

Dewetting effects can be of great importance as the surface of the substrate plays an important role during sample preparation. This was observed for the series of silicon substrates coated with a silane SAM. Two types of dewetting mechanisms may be acting in our system [de Gennes et al., 2004]. The liquid film may rupture by nucleation and growth of holes, which is favoured by a low surface tension of the topmost part of the substrate, i.e. the layer of the silane SAM. This mechanism is acting even for micrometre-thick films (albeit below a critical thickness), although the nucleation rate may be very slow for thick films. A second mechanism of dewetting may be operating as well, consisting of the amplification of capillary waves until the film ruptures, a process called spinodal dewetting. This second mechanism is dependent on the detailed balance of van der Waals forces between film and substrate, including the silane SAM layer and the layer of native silicon oxide. The air/film interface of films above a certain thickness (roughly two to three times the sum of the thickness of the SAM layer and of the native oxide layer) will essentially feel the van der Waals field of the bulk silicon, which stabilises the film. However, the air/film interface of films below this thickness will be affected by the silane and native oxide layers, which generally speaking tends to destabilise the film [Parsegian, 2006]. Film rupturing is thus probable to occur when the liquid film is thin enough, an effect which can be used to guide the self-assembly process of fibres, as will be demonstrated in chapter 7.

The fibre formation is a thermodynamically controlled process. Therefore, the 'optimised method of sample preparation' includes the use of a saturated environment at room temperature which avoids featureless deposits formation due to kinetical trapping and provides the molecules sufficient thermal mobility to acquire the most favoured interactions. Depending on the speed of solvent evaporation, which is under saturated environment mainly controlled by the temperature and humidity, the shape of the nanofibres differs slightly.

The nanofibres have a high temporal stability. Although D1 has a high thermal and chemical stability, the self-assembled fibres can not sustain chemical nor mechanical forces since these alter the forces which are responsible for fibre formation. Hence, one of the problems to be solved is the (mechanical) stabilisation of the nanofibres. Attempts were made to obtain fibres in which dendrimer molecules are covalently linked to each other by introducing functionalities which could covalently link the dendrimers in the nanofibres after self-assembly. Dendrimers with vinyl functional groups at the periphery were able to form nanofibres which are embedded in an amorphous matrix of aggregated dendrimer molecules. Although stability experiments could be carried out at a 'free' fibre end, the fibre formation needs to be fine-tuned before trying to stabilise the resulting fibres. Therefore, the stabilisation of the polyphenylene dendrimers remains an important challenge.

As stated before, the chemical structure of the building blocks in a self-assembling system is of great importance since it determines the forces between molecules and hence can change the self-assembly properties dramatically. This is clearly illustrated in the attemps to covalently stabilise the dendrimer nanofibres by attaching functional groups to their periphery. The presence of maleimide groups as well as the presence of fluorine atoms disturbed the fibre formation ability of the polyphenylene dendrimers.

That the π-π and van der Waals interaction among dendrimer branches are of crucial importance for the fibre formation, was also demonstrated by adding C_6F_6 to the solvent (THF). This results in quadrupolar interactions between the electron-rich phenyl groups of the D1 dendrimer and the added electrondeficient aromatic rings (C_6F_6). The presence of different amounts of perfluoroaromatic units as free guest molecules produces complex changes in the self-assembled surface morphology which can be explained in terms of the changes in the intermolecular interactions and the surface affinity. The morphology of the self-assembled aggregates is dictated by complex nucleation and dewetting processes depending on the amount and distribution of the perfluoroaromatics within the system. At low (5%) and intermediate (10%, 20%) amounts of C_6F_6 in the solvent mixtures, C_6F_6 'shields' the functional group of the dendrimer, inhibiting their specific interactions with neighbours.

6.3 General Conclusions

In this chapter, several parameters were investigated which are important for 2D self-assembly at surfaces into dendrimer nanofibres. The procedure to obtain nanofibres by dropcasting a $\sim 10^{-5}$ M dendrimer solution in THF on piranha cleaned silicon in a THF saturated tank will be referred to as the 'optimised method of sample preparation' in chapter 7.

During sample preparation, which involves the evaporation of the solvent, the concentration of the dropcast solution increases. When a sufficiently high concentration is attained, the nucleation of fibre growth is likely to be initiated in solution at the liquid/solid interface. The fact that the fibres are sometimes observed to lie on top of each other indicates that the fibre formation is initiated before complete solvent evaporation. The main driving force of the dendrimer nanofibre formation is attributed to π-π interactions between the phenyl groups of neighbouring dendrimers.

The visualisation of a dendrimer layer after rinsing fibre-containing samples with milli-Q-water hints that fibres are formed on top of a dendrimer layer, although AFM is not able to reveal its presence on areas where the (relatively large) fibres are present.

Chapter 7

Guided Self-Assembly of Dendrimers

Polyphenylene dendrimer D1 self-assembles into nanofibres on various substrates upon dropcasting as seen in chapter 6. There are several parameters that have an effect on the fibre formation including the solvent, the dendrimer concentration, the substrate, ... In this chapter three different strategies were followed in order to obtain controlled deposition of D1 dendrimers on a substrate and thereby aligning the nanostructures which are formed upon self-assembly of the dendrimer.

In a first approach soft lithography was applied, while the second approach includes the use of patterned substrates (nanotemplates) and the third involves extremely high magnetic fields (15 T) to influence the location and the orientation of nanostructures. These approaches can be classified as direct (1) or indirect (2 and 3) guiding methods.

7.1 Direct Approach using Soft Lithography

7.1.1 Introduction

The deposition of molecules on a substrate can be controlled with soft lithography (see 1.4.2) which generates patterns on a micrometre scale by using an elastomeric stamp or mold that has a specific topographical pattern on its surface. Molecules are hereby physically constrained to specific locations on the substrate leading to the generation of ordered microstructures. The device that was used for our experiments is made of polydimethylsiloxane (PDMS) and has 1.2 μm high pillar features that have a diameter of 5 μm and are 3 μm apart from each other (see figure 7.1).

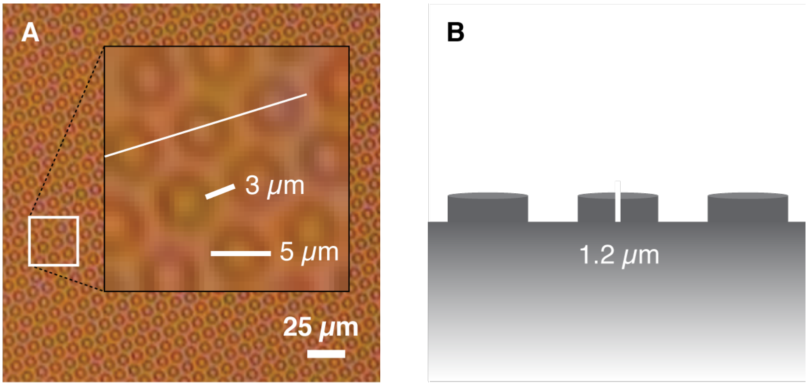

Figure 7.1: Optical image of the PDMS device (A) and schematic line profile (B) through the zoom in on A indicated with the line. The pillar features have a height of 1.2 μm, a diameter of 5 μm and are 3 μm apart from each other.

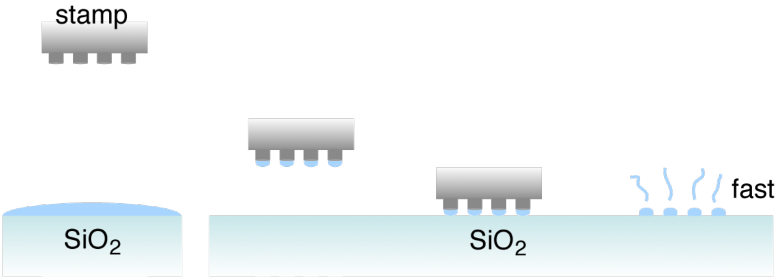

Figure 7.2: Scheme of the μCP approach.

Two different types of soft lithography were used: microcontact printing (μCP) and one based on microtransfer molding (μTM). In the first case the PDMS is used as a stamp, while in the latter case it is used as a mold.

7.1.2 PDMS as a Stamp

In the μCP approach (see figure 7.2), the relief pattern on the surface of the PDMS stamp is used to form patterns on the silicon surface by making contact.

The first step of μCP is to put ‘ink’, i.e. the dendrimer D1 solution, on top of the stamp. Therefore the stamp was brought in contact with a clean silicon surface on which solution of D1 was dropcast. After this indirect inking procedure, the stamp was placed on another clean silicon substrate in order to transfer the dendrimer molecules to the substrate in a THF saturated environment.

AFM images of this sample (figure 7.3) reveal the pattern of the PDMS stamp which is successfully transferred to the silicon substrate. A regular pattern of disk-like patches with a diameter of 5 μm and inter-patch distance of 3 μm is observed. Besides these patches which have a rather uniform background in the order of 10 to 25 nm in height, also smaller aggregates are observed in and in between these patches with random heights. This approach did not lead to the formation of nanofibres. The lack of fibre formation is probably caused by fast solvent evaporation upon indirect inking, kinetically trapping the dendrimers upon transfer to the substrate.

7.1.3 PDMS as a Mold

The second approach which uses soft lithography is based on (but slightly different from) μTM. In μTM a drop of liquid prepolymer is applied to

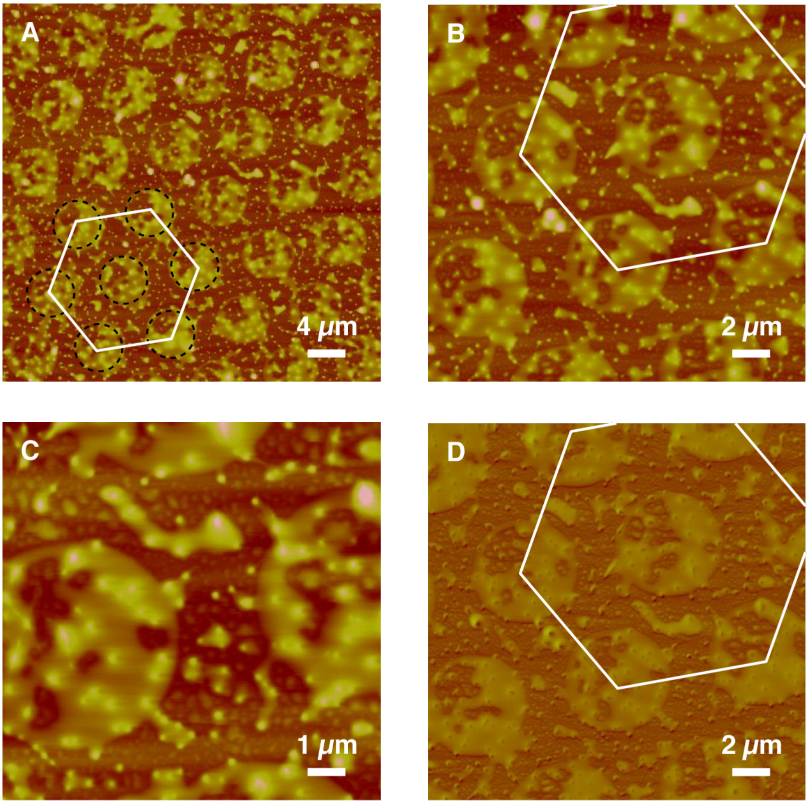

Figure 7.3: AFM topography (A, B, C) and phase (D) images from the sample made by μCP the dendrimer solution in THF on piranha cleaned silicon in a THF saturated tank by using a PDMS stamp which was inked indirectly. The black circles of 5 μm diameter separated from each other by 3 μm indicate regions with high dendrimer content.

the patterned surface of a PDMS mold and the excess liquid is removed. The filled mold is then placed in contact with the substrate and irratiated or heated. After the liquid precursor has cured to a solid, the mold is peeled away carefully to leave a patterned microstructure on the surface of the substrate.

In our case (see figure 7.4) a drop of dendrimer D1 solution (analog to the prepolymer) in THF was applied to the silicon substrate and

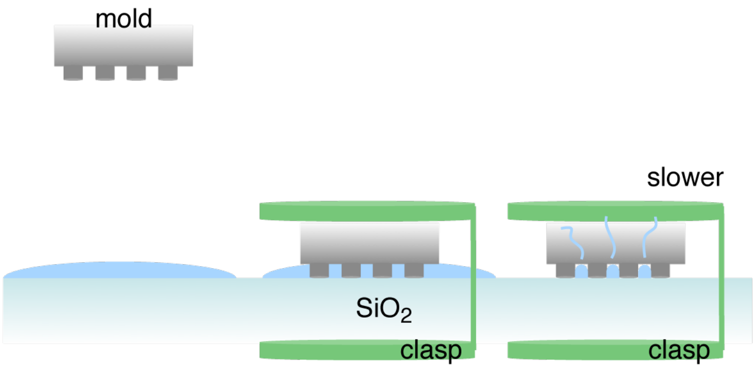

Figure 7.4: Scheme of the μTM based approach.

the mold was immediately pressed onto the silicon substrate (without first removing excess of solution). In order to inhibit movement during solvent evaporation the mold was fixed onto the silicon substrate leading to mechanical removal of excess solution by pushing the mold against the substrate. The solvent was left to dry in a THF saturated environment.

The inversed pattern of the mold is transferred successfully onto the silicon substrate (figure 7.5). At first sight, no nanofibres were formed, but large dendrimer aggregates which build up a honeycomb-like pattern instead. However, upon taking a closer look, one can see small fibres inside the pores. Figure 7.5 provides a zoom in on such a pore (F) and on the border of two pores (C and E) which reveals that nanofibres are formed underneath the large clusters. Topography profiles reveal heights ranging from a few nm up to a few tens of nm for the dendrimer fibres and a few tens of nm up to a few hundreds of nm for the clusters.

7.1.4 Discussion

In this section, soft lithographic approaches were applied as attempt to guide the formation of self-assembled dendrimer fibres. The basic

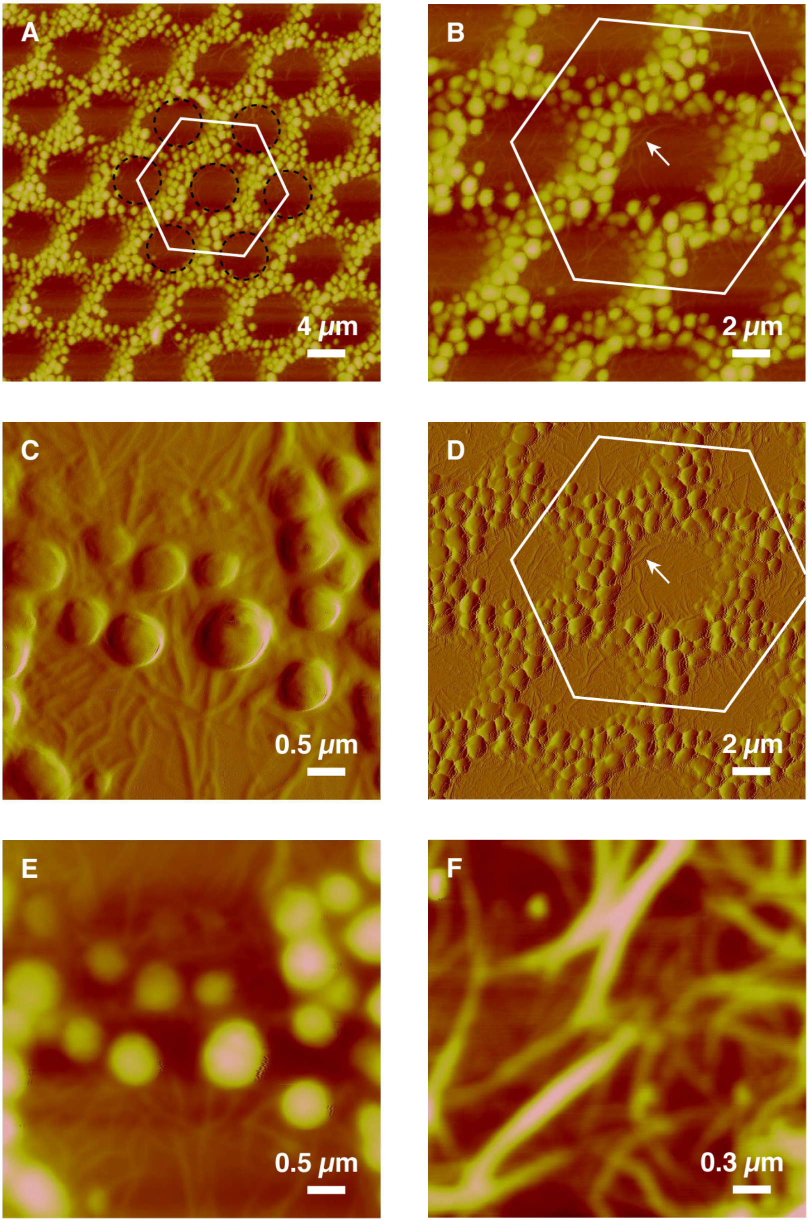

Figure 7.5: AFM topography (A, B, E, F) and amplitude (C, D) images of the sample made by putting a PDMS mold onto the dendrimer solution in THF on piranha cleaned silicon in a THF saturated tank. The black circles of 5 μm diameter separated from each other by 3 μm indicate regions with low dendrimer content.

idea is that the physical constraints caused by the stamp or mold which were used in the experiments would direct the deposition of the fibres to specific locations on the surface of the substrate.

When using the PDMS as a stamp in a μCP approach, a pattern of clusters could be observed which corresponds to the features on the stamp. However, this approach suffers some problems to guide self-assembled fibres made of dendrimer D1. This is to a great extent related to the mechanism of fibre formation. Due to manipulation with the stamps, most of the solvent is already evaporated before the pattern formation on the substrate can take place by making physical contact (figure 7.2). It is therefore not surprising that mainly (kinetically formed) clusters appear on the substrate when using μCP as guiding technique. The subtle balance of forces in the self-assembling system is disturbed by using this approach. Without any doubt, the solvent evaporation speed is a very crucial parameter that should be carefully controlled. Another problem is the deposition of material on locations where the stamp did not make physical contact. The origin of this lays in the fact that there is dendrimer solution in between the topographical features (figure 7.6A).

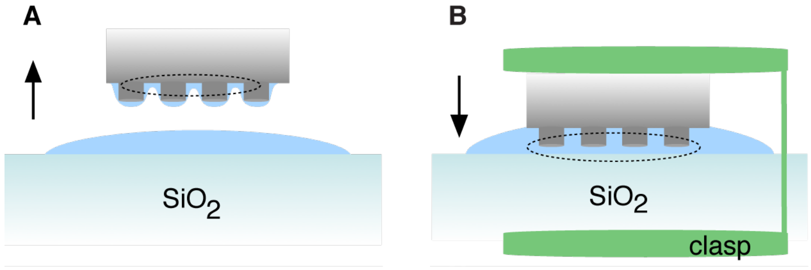

Figure 7.6: Schematic presentation of problems encountered when using soft lithography as guiding method for dendrimer fibres: indirect inking procedure (A) and mechanical removal of excess solution by clamping the mold on the substrate (B).

An approach based on μTM was chosen to solve this problem of cluster formation. The solvent is 'trapped' between the features of the mold itself and hence the solvent evaporation takes longer in this approach. This should give the dendrimers the opportunity to form the most favourable interactions possible, leading to the thermodynamic self-assembly into fibres. Nevertheless, in addition to fibres, clusters were also formed on the surface and deposition of molecules at 'forbidden' locations was observed with AFM. The physical contact between the mold and the substrate is not sufficient to remove dendrimer solution underneath the pillar features of the mold (figure 7.6B).

7.1.5 Conclusions

Features of the PDMS device could be successfully transferred into the formation of nanopatterns consisting of aggregated dendrimers. However, both μCP and the guiding technique based on μTM are unsuitable to control the deposition of dendrimers into ordered fibres on the substrate. Although the crucial step of dendrimer deposition on the sample was carried out in a saturated environment, problems connected to this approach (i.e. fast solvent evaporation, deposition underneath the mold features) made the soft lithographic approach not appropriate.

7.2 Indirect Approach using Nanotemplates

7.2.1 Introduction

The first indirect approach that was followed to guide the dendrimer deposition involves the dropcasting of dendrimer solution onto prepatterned substrates. In chapter 6 it is shown that dendrimer D1 forms fibres on silicon when the sample is made according to 'the optimised method of sample preparation'. This includes the use of a THF saturated environment to assure slow solvent evaporation, which is extremely crucial for the fibre formation since this is thermodynamically favoured. In the same chapter it is shown that the fibre formation does not occur if silicon is completely covered with a silane that forms a monolayer with a water contact angle around 110 °.

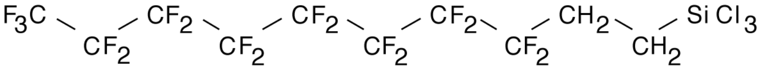

Figure 7.7: Chemical structure of the silane which was used to make the templates (1H,1H,2H,2H-perfluorodecyltrichlorosilane).

Therefore a perfluorodecyltrichlorosilane (see structure in figure 7.7) was used to form self-assembled monolayers on silicon via chemical vapour deposition[1]. On this fully covered substrate dendrimer D1 was dropcast according to the procedure described above ('the optimised method of sample preparation') to investigate whether dendrimer fibres could still be formed. This silane turned out to be the perfect candidate to modify silicon since samples made from this modified substrate showed no fibres (figure 7.8) as was expected from previous experiments with silicon substrates covered with silane (see section 6.2.1.5). Some clusters are visible with heights ranging from a few nm up to 25 nm. These clusters most probably result from the dewetting of the dendrimer/THF film into small droplets upon evaporation of the THF, resulting from the metastability in air of most organic fluid films on perfluorinated surfaces, below a critical thickness [de Gennes et al., 2004].

The principle of the fibre guiding method using nanotemplates contains several steps (see figure 7.9). (A) In a first step a piece of a silicon wafer is cleaned in a piranha solution followed by extensively rinsing with

---

[1] All the silanisation reactions were carried out in Prof. Jonas's group (by Cédric Buron).

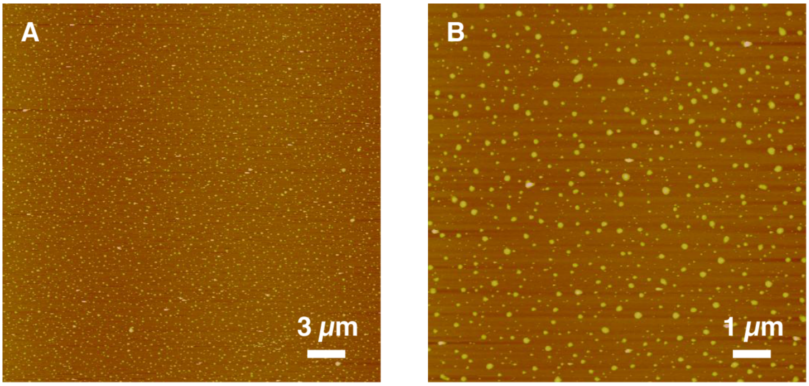

Figure 7.8: AFM topography images from samples made by dropcasting a 2.05×10^{-5} M dendrimer solution in THF on silane covered silicon in a THF saturated tank.

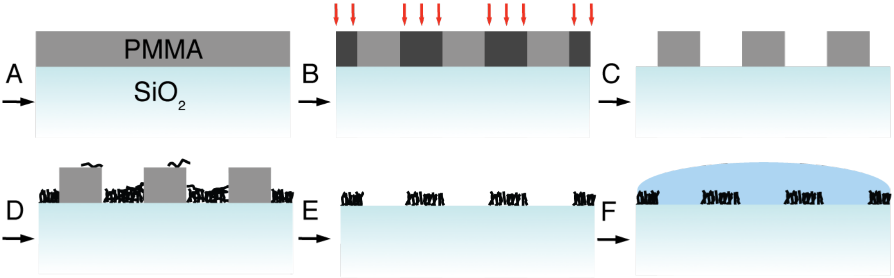

Figure 7.9: Principle of the 'nanofibre guiding method': standard silicon cleaning followed by spincoating of PMMA (A), e-beam lithography (B), development of exposed area (C), grafting of the perfluorosilane (D), cleaning with CH_2Cl_2 (E), deposition of the dendrimer solution according to the 'optimised method of sample preparation' (F), vide supra.

Milli-Q-water and drying the silicon by spincoating. Directly after cleaning, a poly(methyl methacrylate) (PMMA) film was spincoated on the wafer and annealed. (B) During a next step a nanolithographied PMMA mask was obtained using electron-beam lithography (EBL, see 1.4.1). (C) After resist development nanometre-sized regions of reactive silicon oxide were obtained. (D) The sample was introduced in a reactor where the silane was injected and left to react in the gas phase. Reaction only occurred through the mask with the PMMA free regions, while regions covered with PMMA were protected from silanisation, leading to the directed chemisorption of the silane on silicon. (E) In order to obtain binary nanopatterned surfaces composed of alternating silane and native silicon oxide regions, the remaining PMMA mask and ungrafted silane were removed with CH_2Cl_2. (F) The final step is the deposition of dendrimer D1 on these nanotemplates in a THF saturated tank according to 'the optimised method of sample preparation' as explained in chapter 6. In all the experiments a 2.05×10^{-5} M dendrimer solution in THF was used.

In the fibre guiding method, the areas of bare silicon were covered with PMMA and removed afterwards, and hence the pre-treatment of the substrate is different from that of 'the optimised method of sample preparation'. Samples were therefore made on silicon on which a PMMA film was spincoated, annealed and removed again with CH_2Cl_2 to investigate if this pre-treatment would have in influence on the fibre formation. Figure 7.10 shows optical and AFM images before and after dendrimer deposition[2]. Although small peaks of a few nm are observed before deposition of the dendrimer solution (the z-scale of the AFM image in figure 7.10A is 3 nm), the fibre formation was successful and thus the slightly different treatment of silicon causes no problems.

Two types of patterns were made: line patterns which are built up of

---

[2] Movie called 'pre-treatment' on DVD.

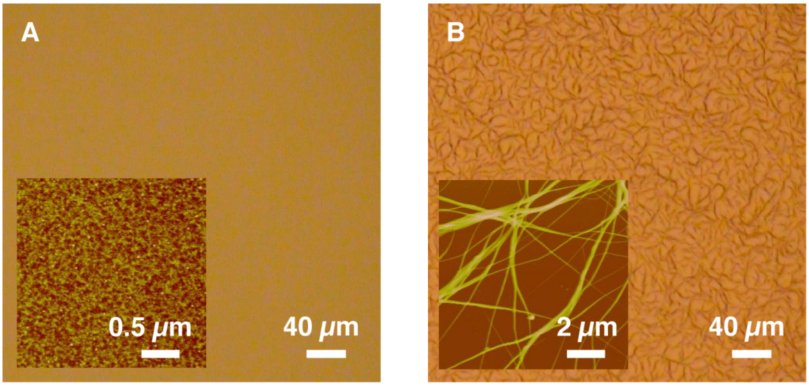

Figure 7.10: Optical images from samples before (A) and after (B) drop-casting a 2.05×10^{-5} M dendrimer D1 solution in THF on silicon treated as in the 'fibre guiding method' in a THF saturated tank. The inserts provide AFM topographical images of the sample.

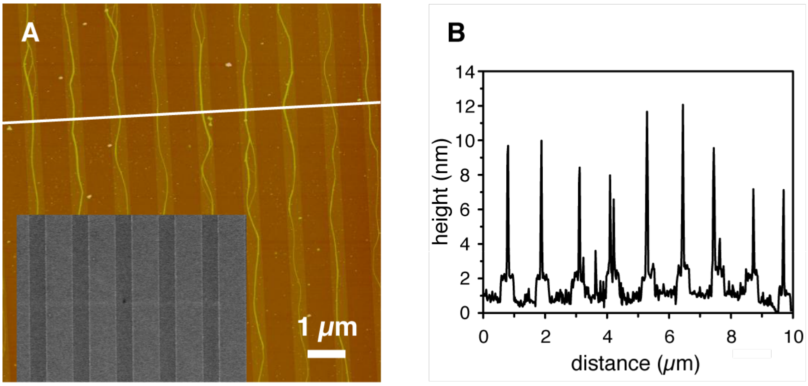

Figure 7.11: AFM topography image (A) from a sample made by drop-casting dendrimer D1 solution on the template. The insert shows the SEM image of the corresponding template: a binary patterned silicon substrate with silane lanes of 703±5 nm width which are separated by uncovered silicon areas of 405±5 nm width. Line profile (B) through the AFM image.

parallel ‘lanes’ of silane on silicon and block patterns which are built up of separated ‘blocks’ of silane on silicon. It is expected that the regions covered with silane will inhibit the nanofibre growth (as was the case for silicon completely covered with silane) and that self-assembly of the dendrimer will exclusivley take place in the silane-free regions.

7.2.2 Line Patterns

On the insert in figure 7.11A a scanning electron microscope (SEM, see 2.1) image[3] is shown of silicon covered with a series of parallel lanes consisting of deposited silane. The silane lanes are 703±5 nm wide and the distance between these lines, corresponding to the width of the uncovered silicon area, measures 405±5 nm.

The AFM image (figure 7.11) on a similar sample after dendrimer deposition shows successful fibre alignment. Besides nanofibres on the bare silicon regions, small clusters are observed which lie both on uncovered silicon as well as on the silane covered silicon areas. Most probably these dots are dendrimer aggregates. The line profile (figure 7.11B) reveals that the lanes of silanes which are deposited on top of the silicon appear to be lower than the silicon substrate. Most likely, the fibres grow on top of a bottom layer of aggregated dendrimers, causing an increased height for the (dendrimer covered) silicon regions compared to the silane covered silicon regions. This dendrimer layer could be imaged after rinsing a fibre-containing sample with milli-Q-water (see section 6.2.4).

Several templates such as shown in figure 7.11 were made in which the dimensions of the silane area, as well as the uncovered silicon area, were gradually changed to study the influence of the pattern dimensions on the fibre formation. In general, nanofibres made from D1 are not com-

---

[3] The SEM measurements were carried out in Prof. Jonas’s group (by Cédric Buron).

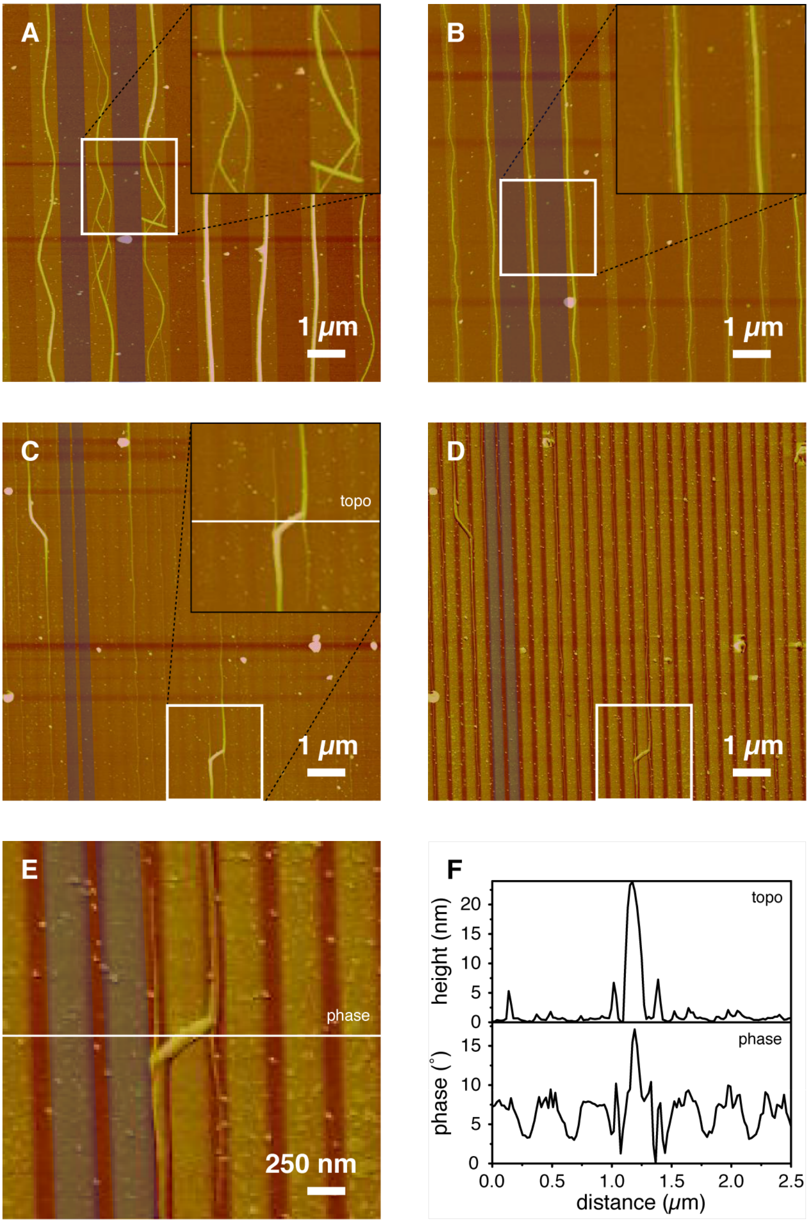

Figure 7.12: AFM topography (A, B, C) and phase (D, E) images from sample made by dropcasting dendrimer solution on a line patterned silicon substrate. Some silane lanes are highlighted. Width of the silane-free lanes is 672±5 nm (A), 286±5 nm (B), and 149±5 nm (C, D). Zoom in (E) of the area indicated in D. Line profiles (F) through topography and phase images.

pletely straight (see chapter 6). On the nanotemplates, fibres show many curves as long as the width of uncovered silicon lanes is large in comparison with the dendrimer nanofibre dimensions (figure 7.12A). Several fibres were observed that seem to open and close due to lateral interactions as shown on the insert. However, if the width of the silane-free lane decreases (figure 7.12B) the dendrimer fibres are almost perfectly aligned. However, there are limits to this alignment. If the width of the silane-free lanes gets too small (figure 7.12C and figure 7.13) fibres might 'jump' from one uncovered silicon lane to a neighbouring one. In figure 7.12D-E the corresponding phase images are shown, clearly highlighting the cross-talking between adjacent lanes.

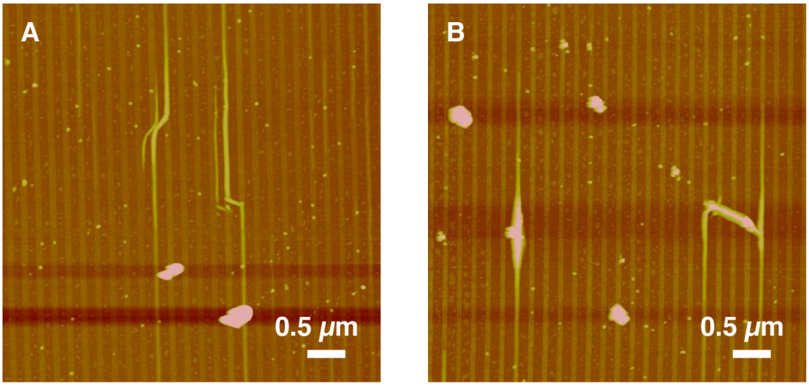

Figure 7.13: AFM topography images illustrating the 'jumping' effect. Sample made by dropcasting dendrimer solution on a line patterned silicon substrate. Width of the silane-free lanes is 83±5 nm (A) and 80±5 nm (B).

On the line patterns the dendrimer forms fibres with heights ranging from a few nm up to a few tens of nm and with widths at half height ranging from a few tens of nm up to a few hundreds of nm. The dendrimer fibres can be several μm long. Ignoring the outlayers, there is a slight tendency of the fibres to become thinner upon decreasing the silane-free lane width (see scatter graph in figure 7.14). From figure 7.12C, it is clear that further decreasing the width of the silane-free lanes (combined with decreasing the width of the silane lanes) is useless with respect to controlling the self-assembly since for small templates the fibres are not confined to a specific lane and thus the nanotemplates are unable to guide the fibre formation.

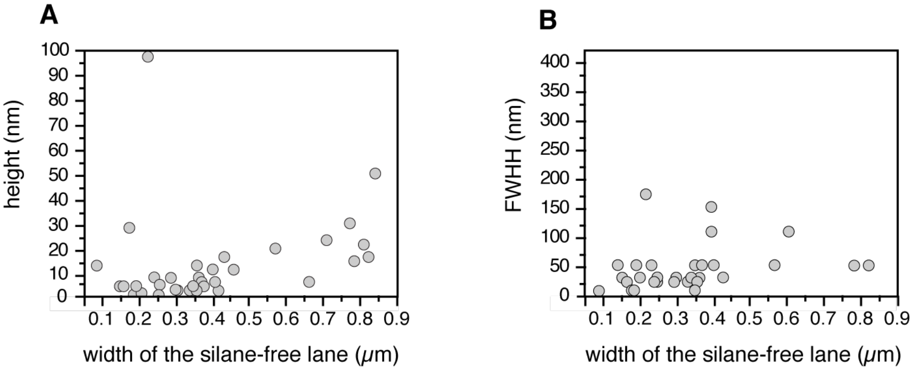

Figure 7.14: Scatter plots revealing the correlation between dimensions of the fibres (height (A) and FWHH (B)) and the dimensions of the binary line patterns (width of the silane-free lanes).

7.2.3 Block Patterns

Not only line patterns, but also block patterns were used to direct the self-assembly of the second generation polyphenylene dendrimer. In the set of experiments conducted with the binary block patterns (figure 7.15) the influence of different patterns on the fibre structure is investigated. Fibres are almost exclusively formed on uncovered silicon areas, with only a few exceptions that are shown.

For samples in which the areas of uncovered silicon were relatively large in comparison with the dendrimer nanofibre dimensions (figure 7.15A), the fibres are not yet limited in directionality and therefore ap-

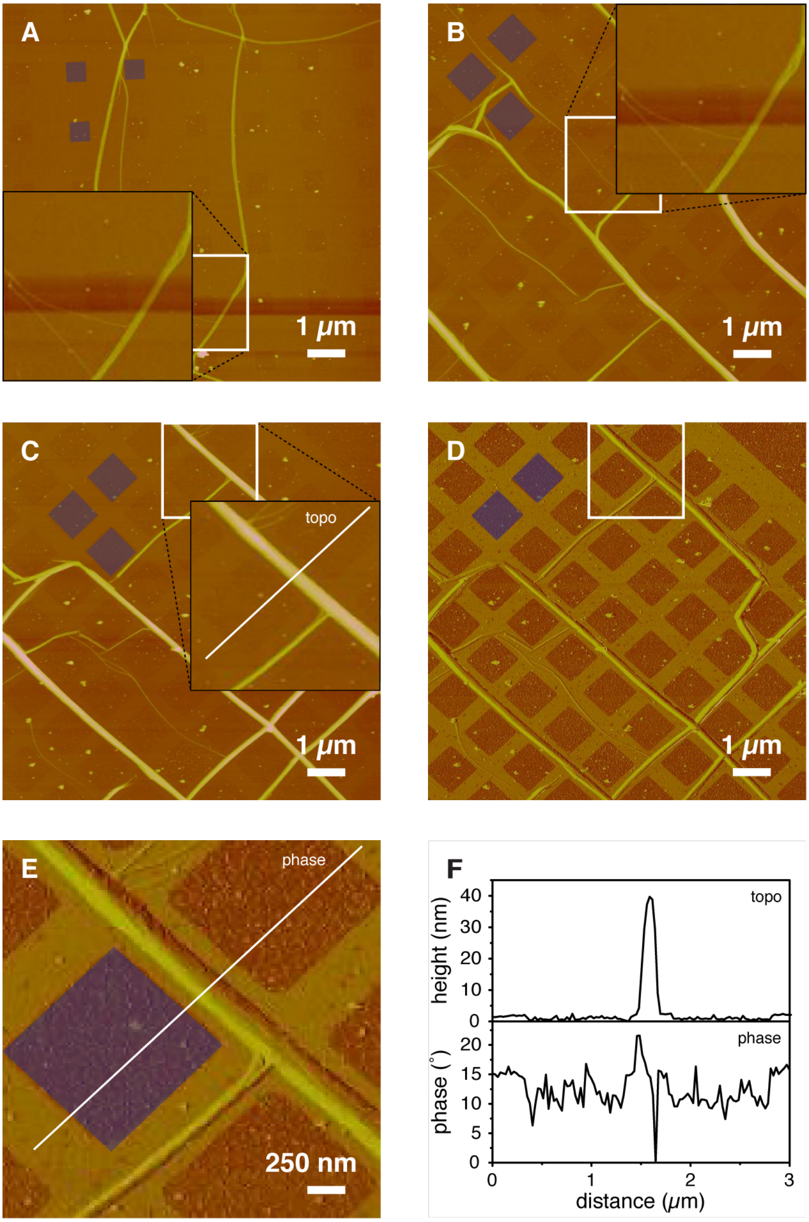

Figure 7.15: AFM topography (A, B, C) and phase (D, E) images from sample made by dropcasting dendrimer solution on a block patterned silicon substrate. Some silane blocks are highlighted. Width of the silane-free lanes is 940±5 nm (A), 512±5 nm (B), and 458±5 nm (C, D). Zoom in (E) of the area indicated in D. Line profiles (F) through topography and phase images.

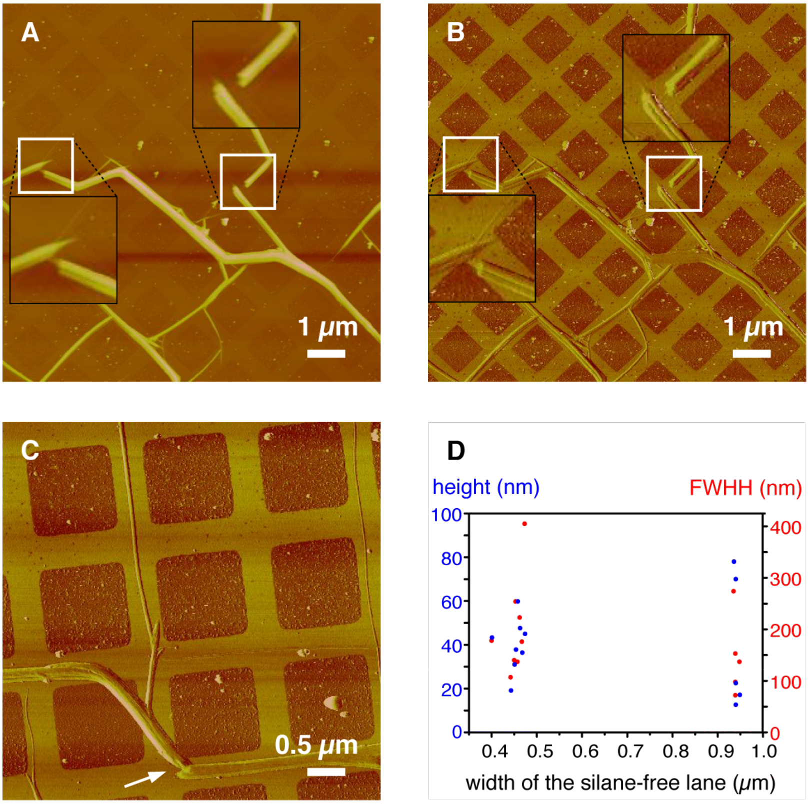

Figure 7.16: AFM topography (A) and phase (B, C) images from a sample made by dropcasting dendrimer solution on a block patterned silicon illustrating breakages in the nanofibres at cross points. Width of the silane-free lane is 451±5 nm (A, B) and 401±5 nm (C). Scatter plot (D) revealing the correlation between the dimensions of the fibres (height and FWHH) and the dimensions of the binary block patterns (width of the silane-free lanes).

pear curved. When investigating samples with smaller uncovered silicon regions (figure 7.15B) the dendrimer is forced to follow the orientation of the silane-free lanes and fibres are perfectly aligned according to the silane-free areas. Fibres tend to become straighter when areas of uncovered silicon become even smaller (figure 7.15C-E). Similar as for the line patterns, the line profile (figure 7.15F) suggests that the fibres lie on top of a dendrimer layer which is deposited on the bare silicon areas, causing the silane covered areas to be lower in topography.

In the case of block patterns, fibres do not 'jump' from one uncovered silicon lane to a neighbouring one as found for the line patterns, but tend to break (figure 7.16). This is probably due to the fact that the silane covered areas are too large for the fibres to bridge and seems to be caused by the stress imposed by forces controlling the alignment on the pattern. The statement that the fibre breaks is supported by the fact that, considering the entire AFM image, the dimension of the fibres is not homogeneous. The dimension of the two fibres at so-called 'breaking points' is comparable, which suggests that the two fibres were in fact one fibre until, at a certain stage in the sample preparation process, the strain on the fibre got too big and the fibre broke. At the broken edges small fibres can be observed which confirms the idea that all fibres are composed of smaller fibres which interact laterally to form fibres with larger dimensions. In figure 7.16C, the white arrow indicates the partial breakage of a fibre at a crossing point.

On the block patterns dendrimer D1 forms fibres with heights ranging from a few nm up to a few tens of nm and with widths at half height ranging from a few tens of nm up to a few hundreds of nm. The dendrimer fibres can be several μm long. There seems to be no real correlation between the dimensions of the fibres and the dimensions of the block pattern within the length scales probed (see scatter graph in figure 7.16D). It is clear that further decreasing the width of the silane-free lanes will not improve the degree of quality of the guided self-assembly since for small templates the fibres are broken.

Although the fibre guiding method was successful, a few exceptions were observed for the block patterns too. When samples with relatively large fibres were studied, the fibres were not always successfully aligned according to the designed binary block pattern. Large fibres cross the silane regions easily (figure 7.17A). Occasionally, the orientation of the fibres seems not to correlate with the pattern (figure 7.17B): the fibres are not on top of the silanes, but do not follow silane-free lanes either.

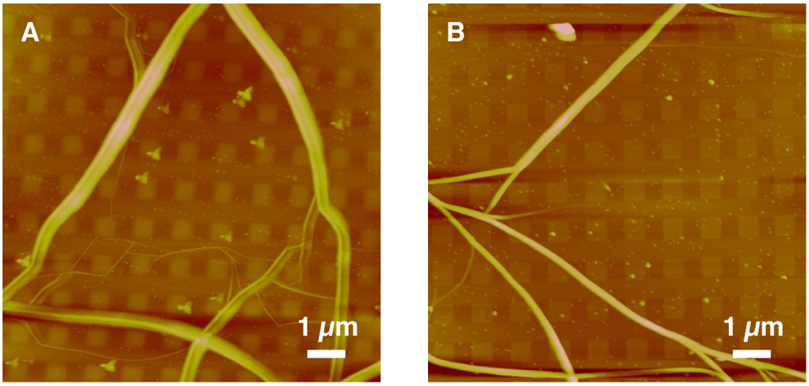

Figure 7.17: AFM topography images illustrating fibres that are not guided succesfully. Sample made by dropcasting dendrimer solution on a block patterned silicon substrate. Width of the silane-free lanes is (A) 474±5 nm and (B) 454±5 nm. The 'double' features in (A) are the result of a tip artefact.

7.2.4 Discussion

During sample preparation, and thus during the formation of the nanofibres several interactions take place: (1) solvent-mediated dendrimer-dendrimer interactions, (2) dendrimer-solvent interactions, (3) solvent-mediated dendrimer-substrate interactions, (4) solvent-substrate interactions, etc. Although all these interactions are imperative, there is a hierarchical interplay of the interactions during the fibre formation. The solvent film stability on the substrate determines preliminarily the areas where dendrimers can interact with the substrate. On areas where the film is stable the concentration of the dropcast solution increases upon solvent evaporation. When a sufficiently high concentration is attained, the nucleation of fibre growth is likely to be initiated in solution at the liquid/solid interface. At this point, fibres can be formed if the solvent-mediated dendrimer-dendrimer interactions (mainly π-π interactions between the phenyl groups of neighbouring dendrimers) and the solvent-mediated dendrimer-substrate interactions are in balance.

In the template approach, the stability of the dendrimer/THF solution on the patterned surfaces was used to control the nanofibre formation. Ignoring first the relatively minor disturbance created by the presence of the dendrimer molecule, the solution can be predicted to be stable on the bare silicon wafer. This is because bare silicon is covered by a $\sim$1.5 nm layer of hydroxylated native oxide, which may hydrogen-bond to THF. In addition, because the index of refraction of THF (1.405) lies in-between the one of native silicon oxide ($\sim$1.46) and the one of air (1), a molecularly thin layer of THF on bare silicon should be stable in air, as far as Van der Waals forces are concerned [de Gennes et al., 2004; Parsegian, 2006; Butt et al., 2003]. Thicker THF films will feel the effect of the underlying silicon substrate, which again tends to stabilise the films in air, since the index of refraction of Si (3.88) is larger than the one of THF. The conclusion is that the THF solution should wet the bare silicon surface in air. By contrast, perfluorinated materials have very low indices of refraction (below 1.4) and cannot interact specifically with THF, which implies that, on the perfluorinated layer in air, a molecularly-thin film of THF will not be stable. Thicker films will feel the beneficial stabilising field of Si, but will nevertheless be metastable below some micrometre-scale critical thickness [Parsegian, 2006].

Therefore, at some stage of the evaporation process, the THF solution dewets from the perfluorinated surfaces, leaving only small droplets behind the dewetting front, as is indeed observed. Dewetting of the solution from the perfluorinated lanes will result in an accumulation of solution on the wetted silicon lanes in the form of fluid ribbons, similarly to what was shown for polymer fluids on nanopatterned surfaces [Baralia et al., 2007]. In these fluid ribbons, the dendrimer molecules will slowly go through all their phase diagram upon evaporation of THF, having plenty of time to form nanofibres through π-π stacking interactions between neighbouring molecules. The process is by no way different from what arises on homogeneous Si surfaces, except for the confinement of the solution which favours the formation of aligned nanofibres. When the distance between neighbouring lanes is decreased, bridges of solution may form between two neighbouring silicon lanes, leading to cross-talking as observed experimentally.

7.2.5 Conclusions

The directed self-assembly of nanofibres composed of second generation polyphenylene dendrimers was carried out with success using prepatterned substrates. The restriction of fibre growth to a confined area was realised by using silane-patterned silicon templates leading to dendrimer self-assembly in fluid ribbons generated by templated dewetting. Additionally also the orientation and ordering of the fibres was affected. Fibres formed on bare silicon substrates showed no long-range order since they are formed with random orientation. In contrast, fibres grown in silane-free areas of silane-patterned silicon surfaces were relatively well-ordered: they are aligned parallel to the borders set by the silane patterns.

The procedure described in this section can be used to control the growth and orientation of nanosized objects. Since it combines self-assembly with top-down techniques, and because it is based on simple physico-chemical processes such as dewetting, this procedure is also applicable for other molecules which self-assemble upon solution drying, providing the correct self-assembly and dewetting conditions are met.

7.3 Indirect Approach using a High Magnetic Field

7.3.1 Introduction

This section describes the sample preparation of the self-assembling dendrimer nanofibres carried out in a high magnetic field[4] to gain insight in the internal structure of the fibres and to try to align these fibres with the direction of the applied field. In view of a comparative study, a second self-assembling system was studied in the high magnetic field which involves the macrocycle MC3. Its self-assembly behaviour is discussed in chapter 8 and the experiments in the magnetic field are given in chapter 9 where the two systems will be compared in section 9.2.

It is known that high magnetic fields can be applied to align molecules exhibiting anisotropic diamagnetism (see 1.4.5). The extra energy that a diamagnetic molecule obtains in a magnetic field is dependent on the diamagnetic susceptibility which is related to the molecular structure and can be minimised by re-orienting the molecules with respect to the field direction. For individual molecules the change in energy is small compared to the thermal energy which makes it improbable to magnetically align single molecules. But as explained in section 1.4.5, for materials that contain a sufficient amount of coupled molecules the magnetic field alignment can be significant if the magnetic energy is large enough to

---

[4] These experiments were carried out in the HFML (High Field Magnet Laboratory) in Nijmegen (together with Jeroen Gielen).

overcome the randomising thermal motion.

Dendrimer D1 consists of 64 phenyl groups which have most probably a random orientation with respect to each other. It is known that benzene molecules have a large diamagnetic anisotropy (-60×10^{-6} cm^3/mol) and hence will react to the applied field by orienting the plane of the molecules parallel to the field direction in order to minimise the acquired energy from the magnetic field [de Gennes and Prost, 1993]. Depending on the orientation of the phenyl groups inside the nanofibres, these groups could give the fibre the potential to obtain a sufficiently high anisotropy resulting in an alignment of the fibres. Since most probably the phenyl groups have random orientations inside the fibres (in order to acquire the best possible interaction with neighbour molecules), it is expected that the fibres will not align according to the field.

7.3.2 On a Substrate

The magnetic field experiments were carried out with a Bitter magnet mounted horizontally in order to induce a magnetic field with strength of 15 T parallel to the substrate. (Figure 7.18)

Similar to 'the optimised method of sample preparation' as described in chapter 6, a 2.05×10^{-5} M solution of dendrimer D1 was dropcast on a freshly cleaned piece of silicon wafer. During the experiment the temperature of the sample holder was kept constant at 22 °C with a thermostat and the sample holder contained a THF saturated atmosphere to ensure slow evaporation of the solvent during sample preparation. The samples were investigated with AFM (figure 7.19) and reveal dendrimer fibres that lie randomly on the substrate, entangled with each other. There was no alignment due to the magnetic field observed. Figure 7.19A and C are images recorded on highly concentrated regions, while images of lower concentrated regions are shown in figure 7.19B and D.

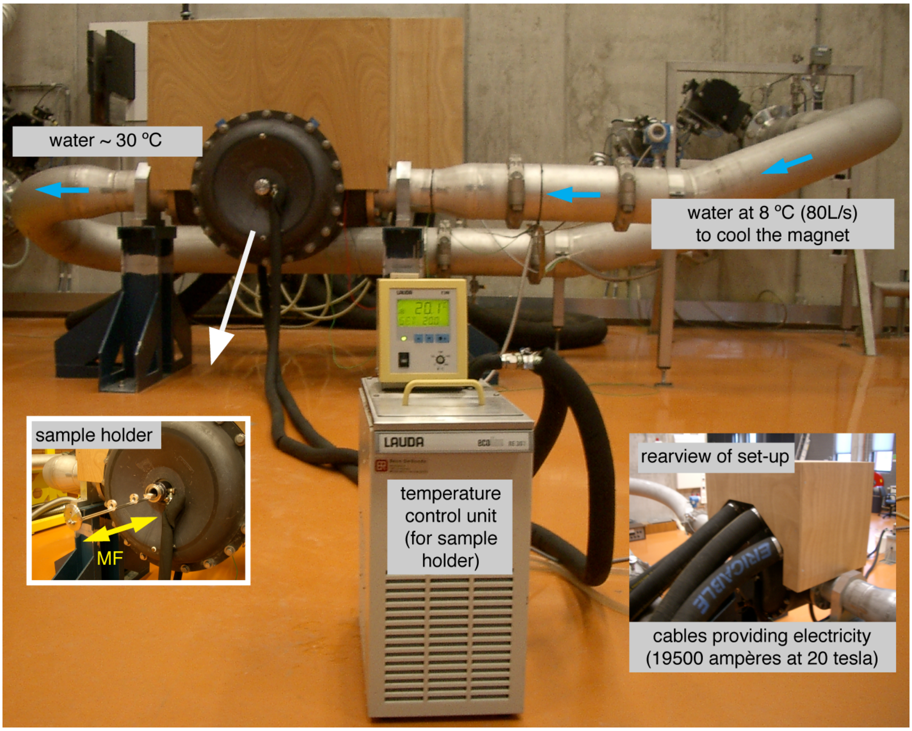

Figure 7.18: Picture of the set-up used for magnetic field experiments on a substrate. The direction of the magnetic field (MF) is indicated with the yellow arrow.

Two line profiles through the AFM image of the lower concentrated region are shown in figure 7.19E and F. The self-assembled fibres have heights ranging from several nm to a few tens of nm, widths at half height ranging from a few tens of nm to a few hundred nm, and dendrimer fibres can be several μm long. It should be pointed out that although these dimensions are in general comparable with the dimensions of fibres formed without a high magnetic field applied during sample preparation, two aspects are significantly different. The maximum height of the nanofibres is lower than generally observed without magnetic field. The smallest fibre that was observed was $\sim$5 nm high and had a width at half height of

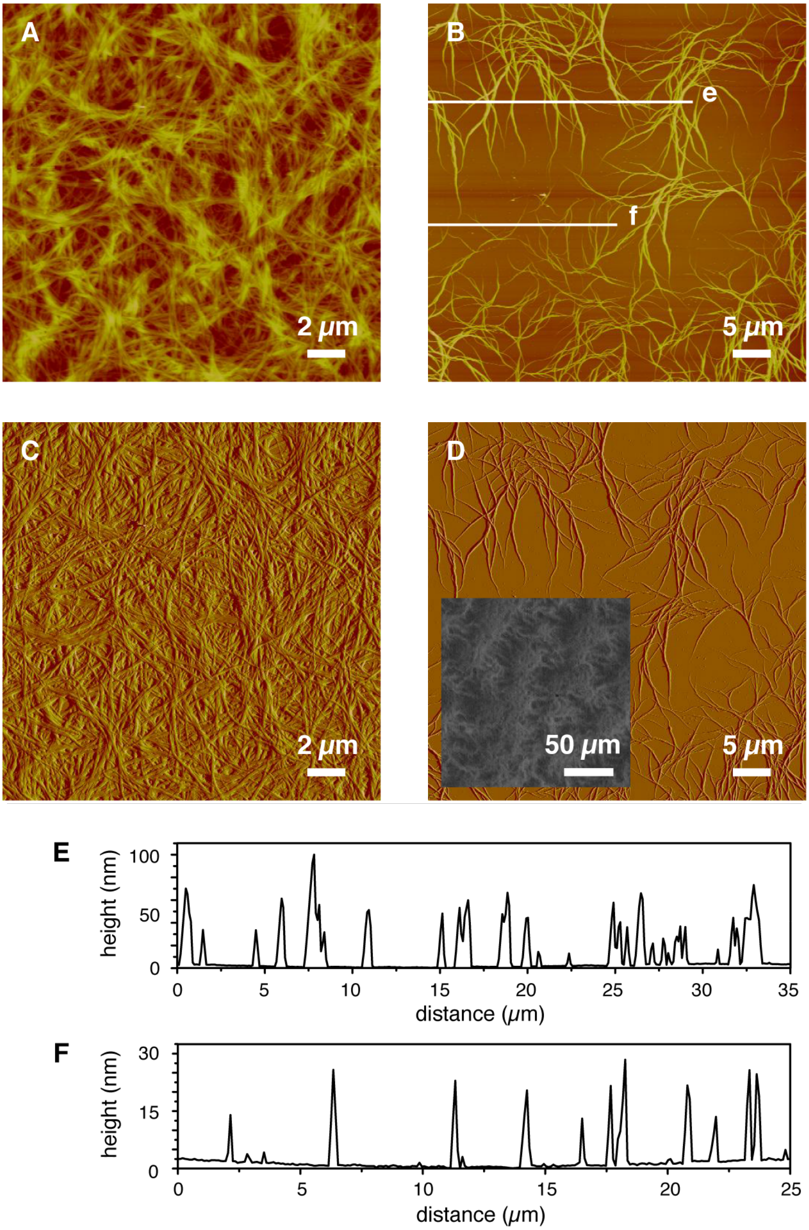

Figure 7.19: AFM topography (A, B) and corresponding amplitude (C, D) images from a sample made by dropcasting dendrimer solution on silicon while applying a high magnetic field (15 T). The lines on image B indicate the position of the line profiles shown in E and F. The insert on D is an optical image.

$\sim$30 nm. Although the fibres are still very long, much more 'fibre-ends' are observed as can be seen in figure 7.19B and D, indicating an effect of the magnetic field upon fibre formation.

As explained in chapter 6, almost all fibres are composed of smaller fibres which are entangled due to lateral interaction, leading to a broadening in fibre dimensions. This is also observed for fibres made in high magnetic field as revealed in figure 7.20.

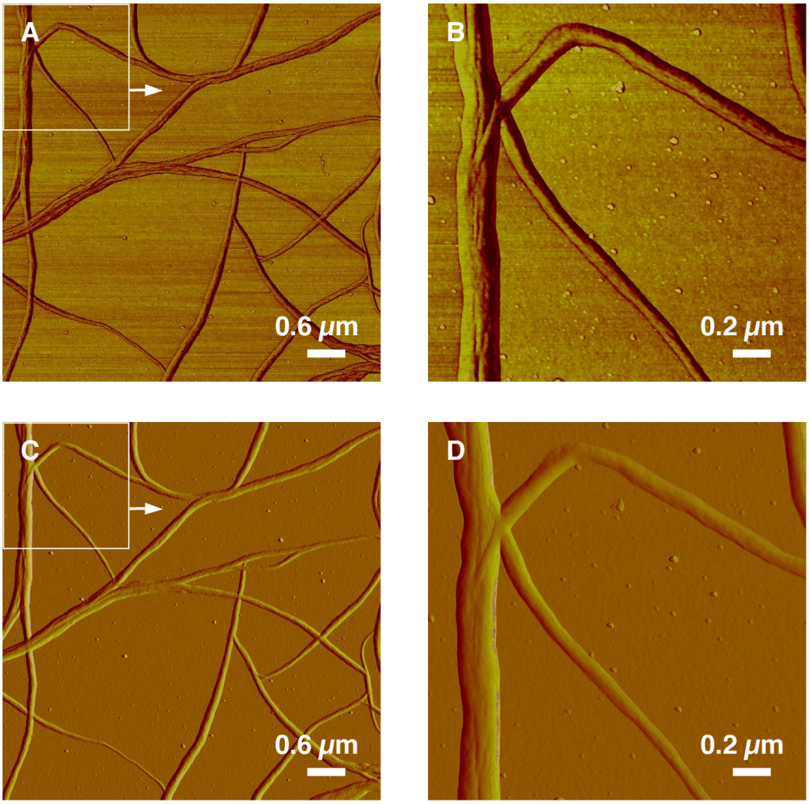

Figure 7.20: AFM phase (A, B) and amplitude (C, D) images from a sample made by dropcasting a $2.05{\times}10^{-5}$ M dendrimer solution in THF on silicon in THF saturated environment while applying a 15 T magnetic field.

7.3.3 Discussion

The aggregates of the rigid polyphenylene dendrimer D1 could not be aligned in the high magnetic field. It was expected that the applied field would have a negligible effect on the orientation of the fibre formation of the dendrimer, because dendrimer D1 has a rigid structure and therefore the phenyl groups probably cannot stack over large distances with the same orientation in the fibre structures. The resulting diamagnetic susceptibility of the molecules is too small to acquire orientation of the fibres by the magnetic field during their formation. The experiments in high magnetic field therefore support the idea that the phenyl groups do not have the same orientation inside the self-assembled fibres.

However, there was a weak interaction observed with the magnetic field. The orientation of the phenyl groups for minimum magnetic energy is different from the orientation of the phenyl groups for maximum interaction with neighbouring dendrimers and hence the magnetic force disfavours the self-assembling process. More 'fibre-ends' could be observed on samples made in the magnetic field. The maximum height of the nanofibres formed in a magnetic field is lower than generally observed without magnetic field indicating inhibition of lateral aggregation between 'individual' fibres due to the acquired magnetic energy.

7.3.4 Conclusions

As expected, the sample preparation in a high magnetic field does not lead to guidance of the self-assembled dendrimer fibres which gives us some valuable information about the internal structure of the fibres. The dendrimers interact with each other via the phenyl groups, but as the dendrimer has a rigid structure, these phenyl groups can not be all oriented in the same direction. They face random directions and thereby the interaction with the high magnetic field was not sufficient enough the guide the self-assembly process. This technique could however be useful to exclude (or at least strongly reduce) the lateral aggregation between ‘individual fibres’.

7.4 General Conclusions

In this chapter, several methods were followed in order to guide the self-assembly of nanofibres with dendrimer D1 as building blocks.

The soft lithographic approach (7.1) was based on putting physical constraints to the deposition of materials. Although patterns could be successfully transferred resulting in nanopatterns consisting of the aggregated dendrimers, the approach was not adequate for this complex system that requires special conditions such as saturated environment to ensure slow solvent evaporation. These conditions could not be met and therefore soft lithography could not be used to guide the self-assembly process of the nanofibres.

Chemical constraints were used in the nanotemplate approach (7.2) where binary nanopatterned surfaces composed of alternating perfluorosilane and native silicon oxide regions directed the solution of dendrimers onto specific locations of the sample surface and additionally oriented the formed nanofibres. Therefore, this method is perfectly suitable for guiding self-assembling fibres during their development.

In the last part, a high magnetic field which leads to bulk, contact free, non-destructive forces was applied to the system (7.3). This homogeneous force was able to strongly reduce the lateral interaction between small fibres, but could not align the nanofibres into a specific direction. However, these experiments provide us valuable information about the orientation of the phenyl groups in the fibres which is random.

Chapter 8

Self-Assembly of Macrocycles

The organisation of several shape-persistent macrocycles based on a phenyl-ethynyl-butadienyl backbone is evaluated in this chapter [Ziegler et al., 2005; Cheng et al., 2007] which is divided according to the structure of the backbone of the macrocycles (depicted in figure 4.7). On these backbones, a variety of side groups can be attached with different orientations in order to assess their influence upon the aggregation behaviour.

The self-assembling properties of these macrocycles are investigated on a substrate in both dry and wet conditions with AFM and STM, respectively. For the AFM experiments, macrocycle solutions were dropcast on several freshly cleaned substrates under ambient conditions and the solution was left to dry before measuring the sample at the solid/air interface. STM samples were prepared by dropcasting solutions in TCB on HOPG. Since TCB is a solvent with a low vapour pressure, the solvent evaporates slowly during the sample preparation and measurements were carried out at the solid/liquid interface while the solvent was still present. Light scattering was used to study the aggregation behaviour in solution.

8.1 Oligo-Alkyl-Substituted Macrocycles

Macrocycle MC1 and macrocycle MC2 have a phenyl-ethynyl-butadienyl backbone structure (figure 4.7A).

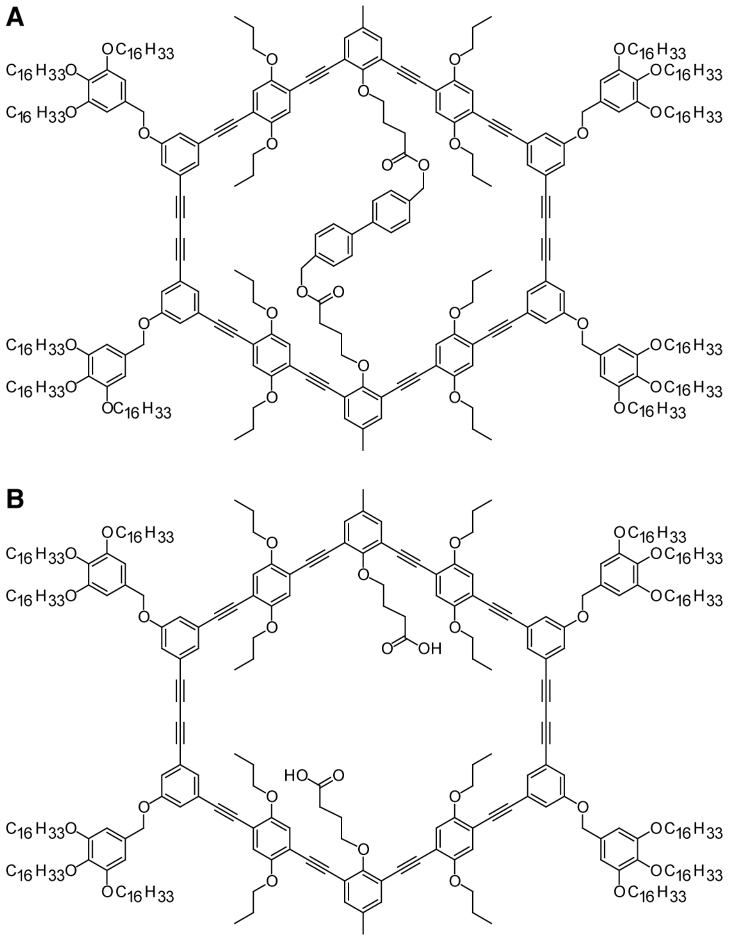

Figure 8.1: Chemical structure of oligo-alkyl-substituted macrocycles MC1 (A) and MC2 (B) with and without biphenyl bridge, respectively.

In both cases, the adaptable side groups which are attached at the line segments are propoxy groups that are free to change their orientation towards the centre of the ring or away from it. The extraannular oligo-alkyl groups contain twelve $C_{16}H_{33}$ chains in total. The macrocycles differ from each other by the intraannular groups attached to the vertices of the backbones. While for MC1 an intraannular bis(hydroxymethyl)biphenylene diester (to which will be referred to as the biphenyl bridge) fills the centre of the macrocycle, MC2 contains two intraannular carboxyl groups which are not linked to each other (figure 8.1).

8.1.1 Solution/Substrate Interface

STM reveals 2D layers of the macrocycles at the TCB/HOPG interface (figure 8.2) which are the result of physisorption on the substrate. The macrocycles order in rows and can easily be identified by their bright ring. Alkyl chains are fully extended and are interdigitated between macrocycle rows. The bright features inside the rings in figure 8.2A and B are most probably caused by the biphenyl bridge.

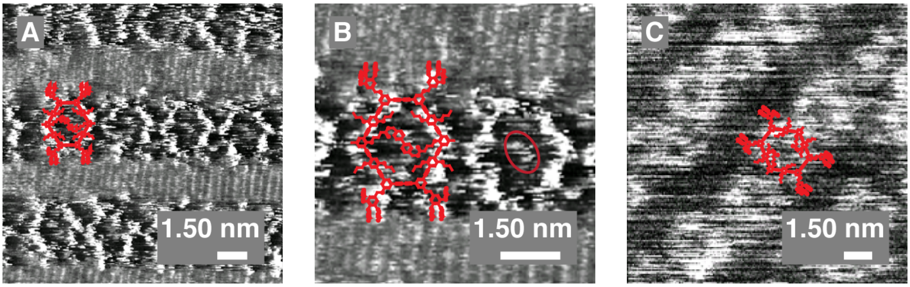

Figure 8.2: STM images of a monolayer of MC1 (A, B) and MC2 (C) formed at the TCB/HOPG interface. The molecular structures are superimposed on the images and in B the position of the biphenyl bridge is indicated.

8.1.2 Air/Substrate Interface

Upon dropcasting MC1 on silicon (figure 8.3A), the macrocycle forms relatively large clusters with variable dimensions with an average height of ∼19 nm. In addition, incomplete layer formation took place with an average height of ∼7.4 nm.

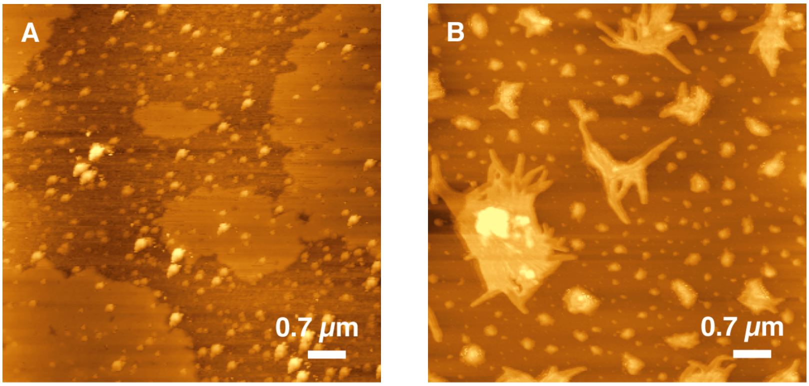

Figure 8.3: AFM images of MC1 adsorbed from a 1.17×10^{-4} M solution in TCB on silicon (A) and mica (B).

On mica (figure 8.3B), small clusters of MC1 with an average height of ∼9.7 nm are observed. Dendritic-like structures rather than layers are formed with an average height of ∼8.1 nm near the tail ends.

Clusters are rarely observed on HOPG (figure 8.4A-D). Incomplete layers with an average thickness of ∼3.0 nm and micrometre long fibres with an average height of ∼4.1 nm (measured with respect to the surrounding layer) are observed. Fibres which do not appear to lie on top of a surrounding layer have a mean height of ∼6.6 nm. Histograms are shown in figure 8.5.

A clear concentration dependence was observed on HOPG (figure 8.4). At low concentrations some clusters and incomplete layer formation are observed and fibres are absent. The thickness of the layers upon deposi-

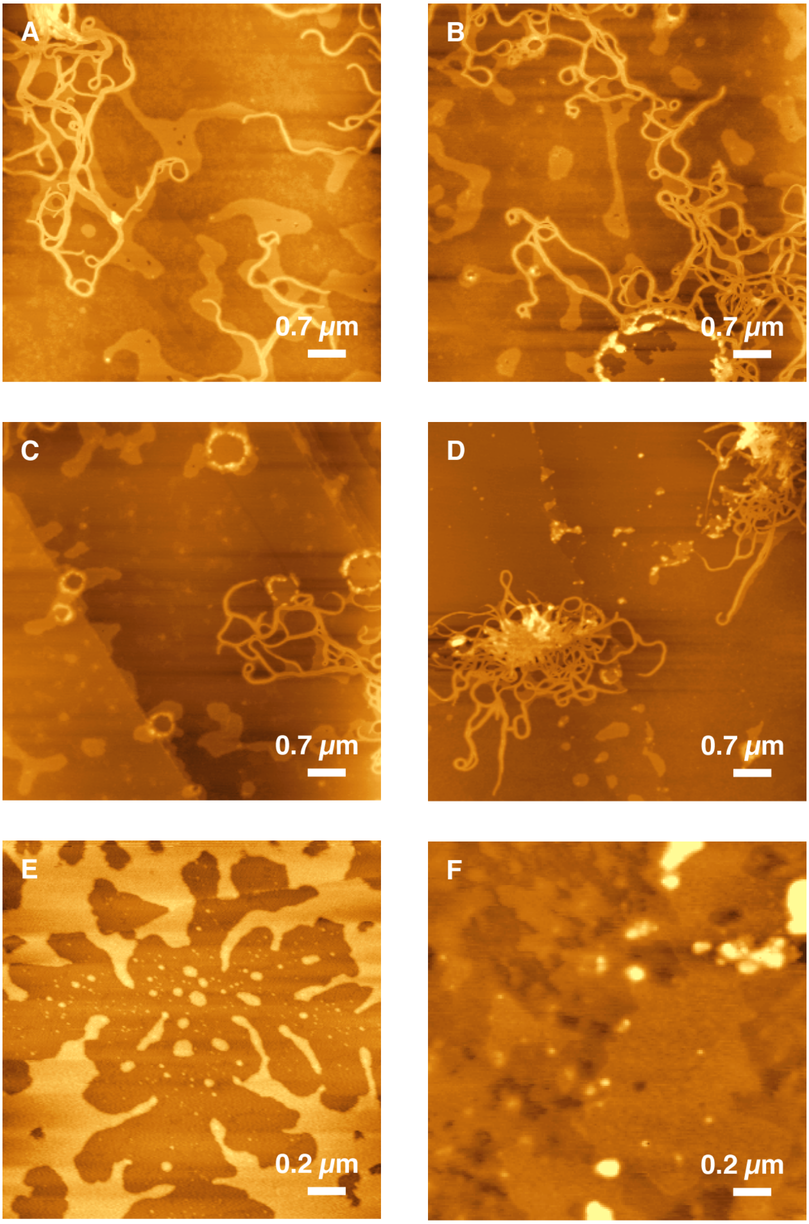

Figure 8.4: AFM images of MC1 adsorbed from a 1.17×10^{-4} M (A-D), 1.12×10^{-5} M (E) and 1.13×10^{-6} M (F) solution in TCB on HOPG.

tion of a 1.12×10^{-5} M solution (figure 8.4E) is ~3.2 nm and the average height of the tentacles is ~2.9 nm. The height of the clusters is about 3 nm too. For 1.13×10^{-6} M (figure 8.4F), the height between successive layers is only ~1.6 nm.

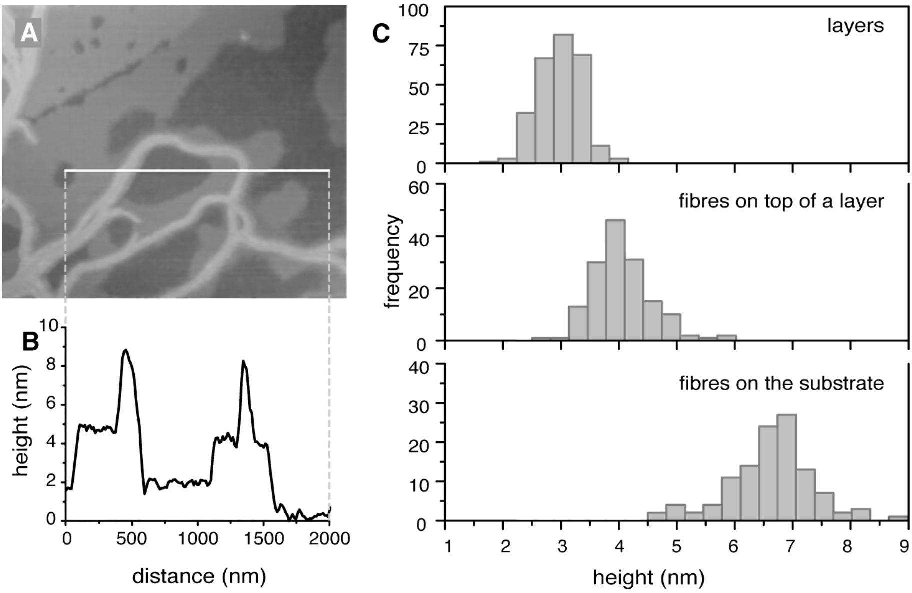

Figure 8.5: AFM image (A) of MC1 adsorbed from a 1.17×10^{-4} M solution in TCB on HOPG and corresponding line profile (B). Histograms (C) of the observed features: mean height of layers (3.0±0.4 nm), fibres on top of a layer (4.1±0.5 nm), and of fibres on the substrate (6.6±0.7 nm).

To investigate the influence of the biphenyl bridge on the self-assembly behaviour, an analogue of MC1 without the biphenyl bridge was also studied with AFM. Since HOPG turned out to be the best substrate to obtain fibres for MC1, this substrate was used to deposit MC2 under similar conditions. At low concentration (9.17×10^{-7} M) some clusters and very small layer regions are formed, but no 1D structures are observed (figure 8.6A). AFM images reveal fibrillar structures in the presence of clusters for concentrations of 1.06×10^{-4} M in TCB (figure 8.6B-C). At higher concentrations (1.00×10^{-3} M) whisker structures were observed (figure 8.6D).

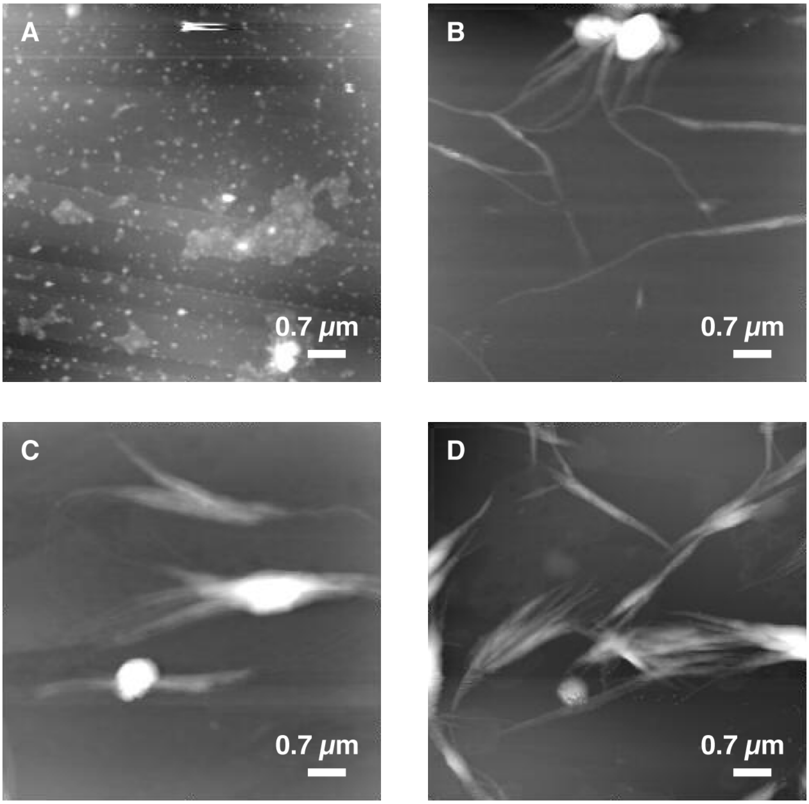

Figure 8.6: AFM images of MC2 adsorbed from a 9.17×10^{-7} M (A), 1.06×10^{-4} M (B, C) and 1.00×10^{-3} M (D) solution in TCB on HOPG.

8.1.3 Discussion and Conclusions

Although difficult to quantify, the degree of ordering at the TCB/HOPG interface was found to be highest for the macrocycle containing the biphenyl bridge (MC1). This was also observed for the analogue macrocycles with $C_{12}H_{25}$ chains instead of the $C_{16}H_{33}$ chains [Ziegler et al., 2005]. An explanation for this could be a stronger adsorption of the macrocycle lacking the biphenyl bridge (MC2) onto the graphite, and therefore leading to 'kinetic trapping'. Modeling involving molecular mechanics and molecular dynamics simulations[1] show that the molecules adopt a non-planar conformation in the absence of the solid support whereas planarisation takes place when they are adsorbed on the HOPG surface. This is supported in the STM images by the observation of bright features inside the MC1-rings indicating the position of the intraannular biphenyl bridge in the same plane as the aromatic backbone of the macrocycles on HOPG.

STM imaging has shown that macrocycles can form a 2D monomolecular thick layer on graphite where the conjugated backbone is lying parallel to the surface. Therefore, we argue that the MC1 layer formation as observed on graphite by AFM reflects the ordering of that same layer. The layer observed with AFM is probably not monomolecular, as the height of the layer is around 3 nm.

The fibres are slightly higher than the monolayer which suggests a different orientation of the second layer where molecules might be tilted. The anisotropic growth indicates that the macrocycles might form a columnar-like phase.

The sum of the thickness of the layers plus the thickness of the fibres on top of those layers measures ∼7.1 nm. This value is comparable to the mean height of fibres that do not appear to lie on top of a surrounding layer, suggesting that fibre formation only occurs on top of a layer. This might also explain the limited amount of fibres found on mica and silicon as these substrates lack layer formation. The width of the fibres is several tens of nm. In other words, the fibre formation can also be described as anisotropic terrace growth on top of a first layer.

---

[1] Molecular mechanics and molecular dynamics simulations were carried out in Prof. Lazzaroni's group (by Mathieu Surin).

In contrast to MC1 which forms exclusively layers and fibres, MC2 gives rise to whiskers. As the sole difference is the presence of the biphenyl group, it can be concluded that this group favours macrocycle fibril formation on graphite upon dropcasting followed by slow solvent evaporation.

8.2 Coil-Ring-Coil Macrocycles

Similar to MC1 and MC2, MC3 has a phenyl-ethynyl-butadienyl backbone structure (figure 4.7A) but differs in the nature of functional groups attached to the ring.

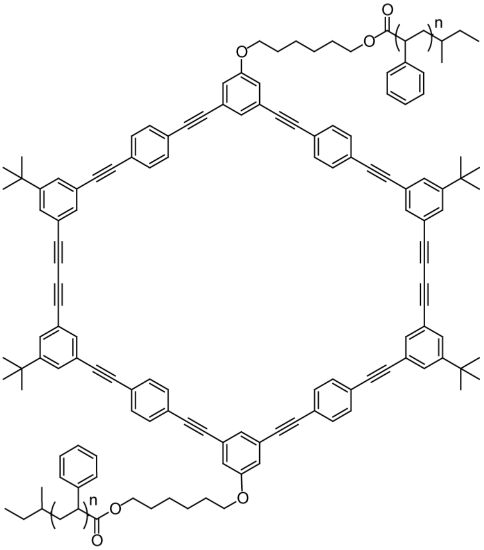

Figure 8.7: Chemical structure of the coil-ring-coil macrocycle MC3 (n≈22).

The shape-persistent macrocycle MC3 (figure 8.7) bears no intraannular nor adaptable side groups and has four extraannular *t*-butyl groups and two large flexible polystyrene chains attached to the vertices of the backbone in order to enhance the solubility of the molecule. The aggregation behaviour of this coil-ring-coil structure was studied in solution with light scattering techniques and at the air/solid interface with AFM.

8.2.1 In Solution

Both static and dynamic light scattering[2] were carried out to study the aggregation behaviour of MC3 in solution (method and experimental details are described in chapter 11).

The shape of the static light scattering graph (figure 8.8A), depicting the scattering intensity in function of the scattering vector, reveals the presence of cylindrical aggregates. Dynamic light scattering experiments were carried out and the diffusion coefficient (D) was plotted against the square of the scattering vector (q^2) as shown in figure 8.8B. By extrapolation to scattering vector zero degree, the translational diffusion coefficient (D_t) was found to be $\sim 1.5\times10^{-12} m^2/s$ and the length of the cylindrical aggregates was determined via equation 8.1 [Tirado et al., 1984].

$$\frac{3\pi\eta_0 L D_t}{k_B T} = ln\,(p+\nu) \tag{8.1}$$

$$\nu = 0.312 + 0.565/p - 0.100/p^2 \tag{8.2}$$

$$p = L/d \tag{8.3}$$

Parameters ν and p are related to the shape of the aggregates as expressed in equation 8.2 and 8.3, where L and d are the length and diameter of the aggregates, respectively. For a translational diffusion coefficient of $(1.5\pm0.2)\times10^{-12} m^2/s$, cylindrical aggregates with a length

---

[2] The light scattering was carried out in the HFML (High Field Magnet Laboratory) in Nijmegen (by Jeroen Gielen).

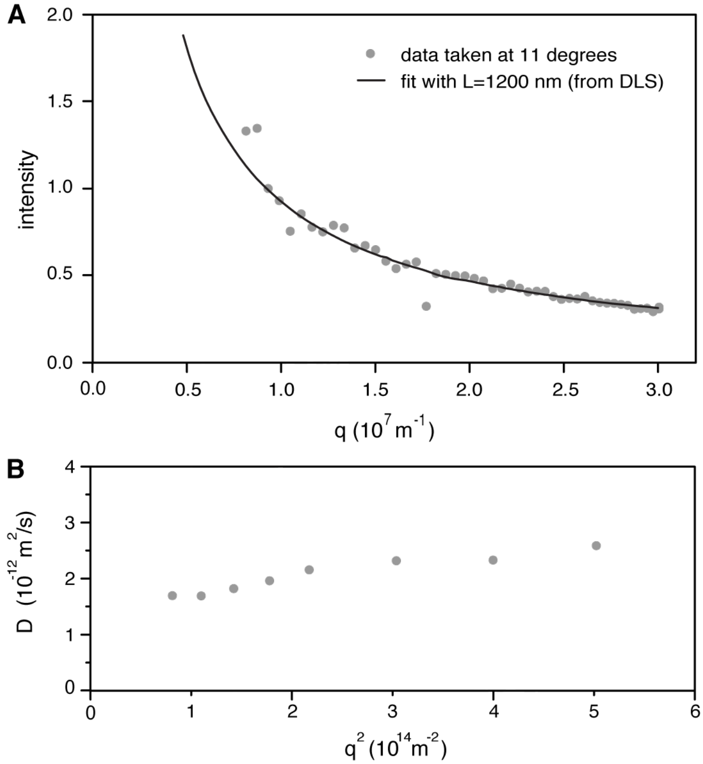

Figure 8.8: Scattering intensity of a ~10^{-4} M macrocycle solution as a function of the scattering vector by static light scattering of MC3 in C_6H_{12} at ~11 °C (A) and diffusion coefficients of the aggregates as a function of the scattering vector by dynamic light scattering experiments of MC3 in C_6H_{12} at ~11 °C (B).

of 1200 ± 200 nm were found by assuming the diameter of the cylindrical aggregates is around 10 nm.

The data points of the static light experiments are fitted with a model for cylindrical particles with a length of 1200 nm as was calculated from the dynamic light scattering experiments (figure 8.8B). The results correspond well with the values from the dynamic light scattering and therefore it can be concluded that the macrocycle aggregates probably have a cylindric shape and lengths of about 1200 nm at ~11 °C in C_6H_{12} solutions of $\sim 10^{-4}$ M.

8.2.2 On a Substrate

When dropcasting a MC3 solution in C_6H_{12} onto a freshly cleaved mica substrate in ambient conditions, self-assembled structures of the macrocycle are deposited on the substrate, as disclosed by AFM.

During deposition of a highly concentrated solution ($\sim 10^{-3}$ M), the solution occurs rather viscous which suggests network formation of the molecules (as was confirmed by the light scattering data, vide supra). AFM shows that this network is transferred to the substrate upon evaporation of the solvent: a dense packed network of material that is randomly aligned with respect to the mica substrate is visible (figure 8.9A, C, E). Also for a less concentrated solution ($\sim 10^{-4}$ M) a similar network is formed (figure 8.9B, D, F). The molecules assemble into 1D objects which are entangled, forming a closely packed network with locally ordered parallel aligned fibres (lateral interaction of fibres).

If the solution is even more diluted ($\sim 10^{-5}$ M), individual fibres with random orientation are visible in the AFM images (figure 8.10A, C, E). In the background, a layer with holes is still present. AFM images of samples made from the most diluted solution ($\sim 10^{-6}$ M) are shown in figure 8.10B, D, F. The individual fibres and background are very similar to the structures formed from the $\sim 10^{-5}$ M solution, and less fibres are observed.

8.2.3 Discussion and Conclusions

It is clear that on the mica substrate the fibres are overlapping each other, since on spots where the fibres cross, the height is roughly twice as high (figure 8.11A). The fibres seem to be very flexible making it

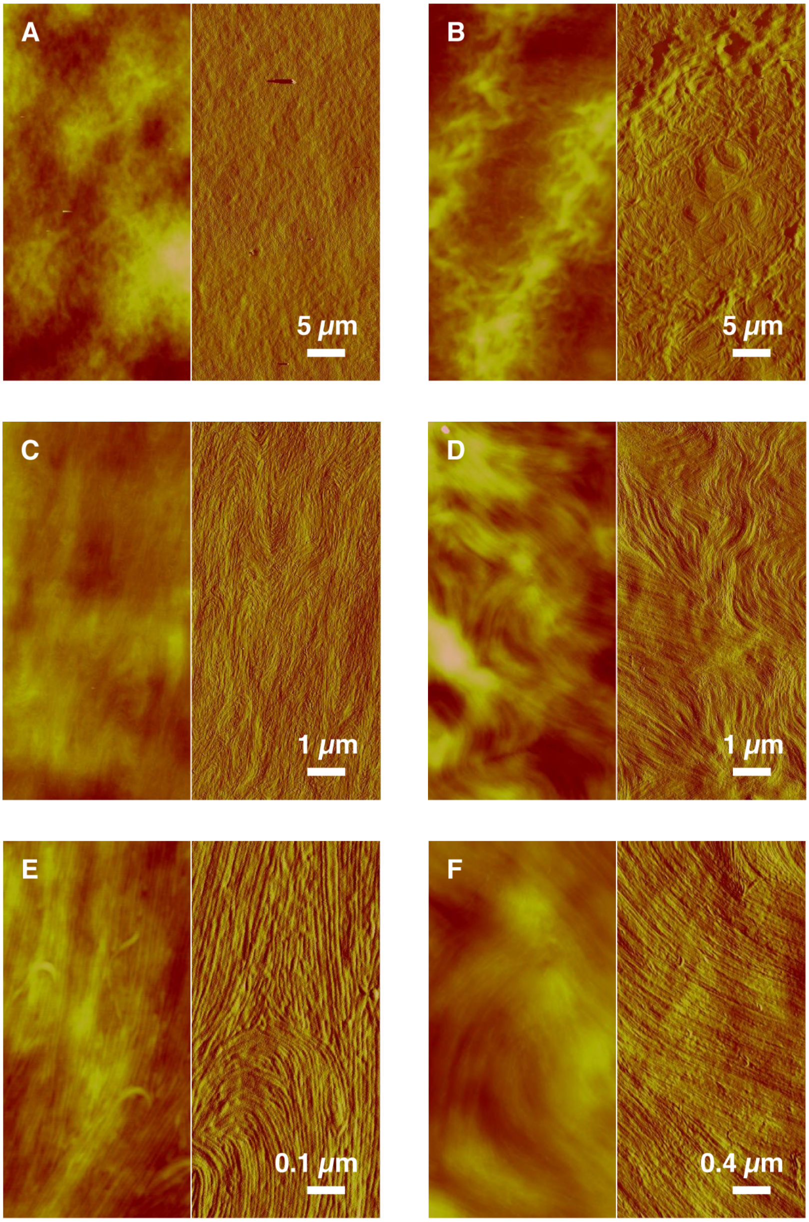

Figure 8.9: AFM topography (left half) and amplitude (right half) images of a $\sim 10^{-3}$ M (A, C, E) and $\sim 10^{-4}$ M (B, D, F) solution of MC3 in C_6H_{12} dropcast on mica.

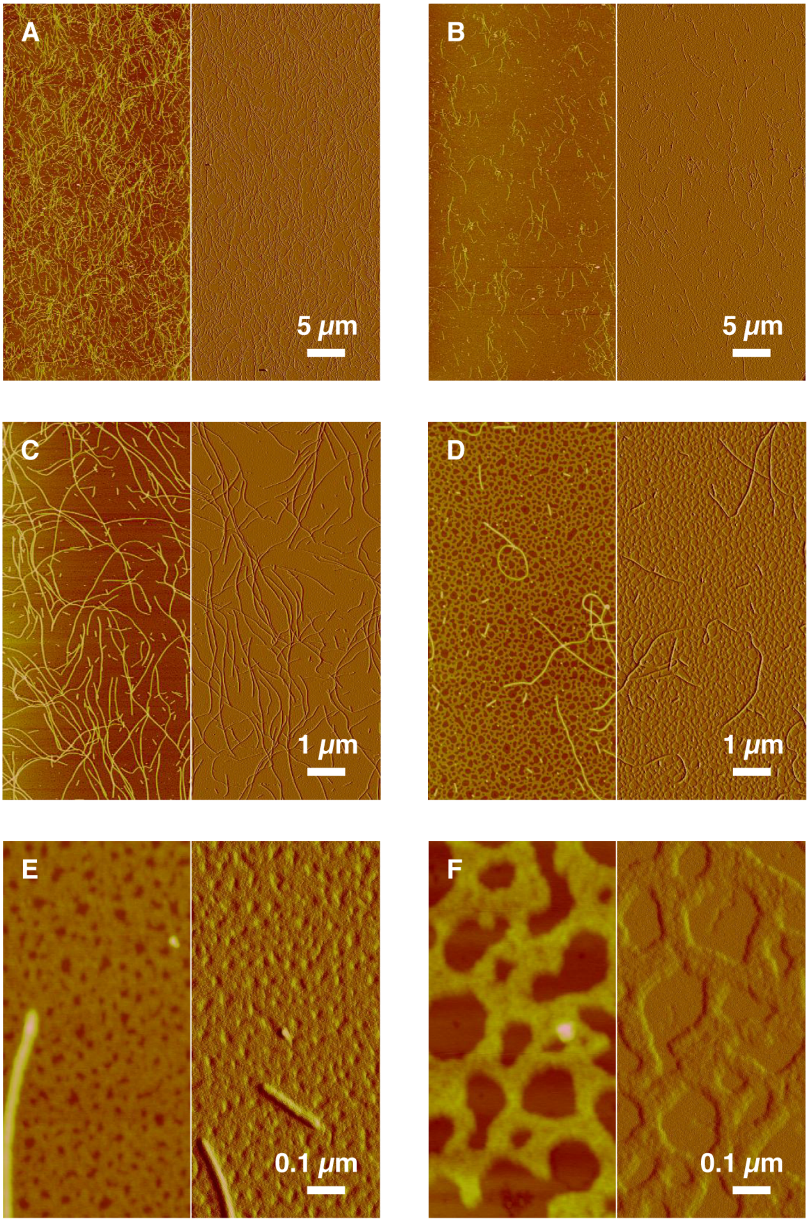

Figure 8.10: AFM topography (left half) and amplitude (right half) images of a ~10^{-5} M (A, C, E) and ~10^{-6} M (B, D, F) solution of MC3 in C_6H_{12} dropcast on mica.

difficult to determine which one lies on top.

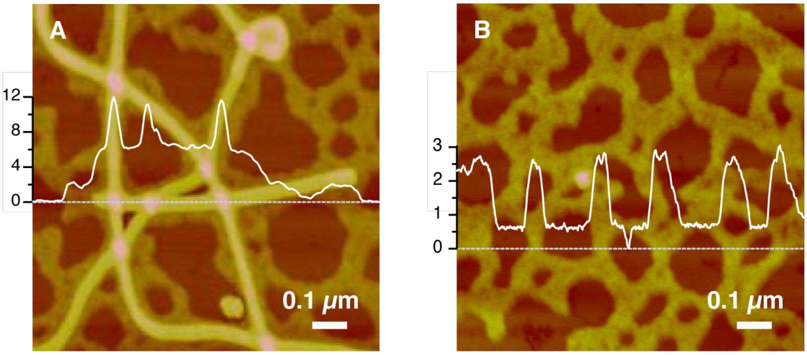

Figure 8.11: AFM images revealing the overlapping of fibres (A) and the background layer (B). Cross section profiles are depicted on top of the images (height unit: nm).

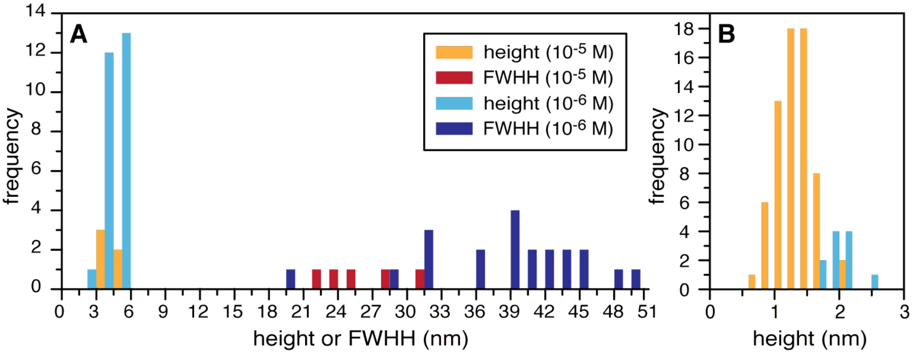

Figure 8.12: Histogram of the height and FWHH of the macrocycle fibres (A) and histogram of the height of the background layer (B).

The macrocycle fibres are always lying on top of an incomplete layer (as was also the case for the fibres made of MC1 which has the same backbone structure). The background on which the fibres are deposited is not bare mica, but a layer of macrocycle molecules (with holes in) deposited on top of mica. The holes in the unfinished layer are not uniform in

Table 8.1: Dimensions of the macrocycle fibres and background layer.

mean value	$\sim10^{-5}$ M	$\sim10^{-6}$ M
height of the macrocycle fibres	4.2±0.8 nm	4.5±0.8 nm
full width at half height	25±3 nm	37±8 nm
height of the background layer	1.3±0.3 nm	2.0±0.2 nm

dimension and are probably formed due to dewetting phenomena. Upon dilution of the dropcast solution the holes become larger. Histograms of the dimensions of the fibres and the background layer are depicted in figure 8.12 and mean values are shown in table 8.1.

For samples made from the $\sim10^{-5}$ M solution, small steps of about ~0.5 nm on top of the layer are observed (while noise is much less). This value could be correlated with the height of the macrocycle. Small wells in the holes of the incomplete background layer reveal similar dimensions: ~0.60 nm and ~0.58 nm, indicating that this is probable not bare mica either but yet another layer of molecules on which the incomplete layer was formed. The hypothesis of multilayer formation is enforced by the values for the height of the (uppermost) background layer. For samples made from a $\sim10^{-6}$ M concentration this layer is larger than compared to the background layer of samples made from a $\sim10^{-5}$ M. Therefore more material, and thus more layers, must be deposited under the upper layer of the latter since the amount of macrocycles deposited is ten times more.

8.3 Dibenzonaphthacene Rings

Shape-persistent macrocycle MC4 and macrocycle MC5 have a backbone structure containing polycyclic aromatic hydrocarbons (figure 8.13). The substitution of a benzene-derived corner piece in the macrocycle expands the size of the ring and rigidifies the backbone. The influence of extraannular side groups with different steric hinder and chemical composition was studied by comparing the aggregation behaviour of MC4 (which has four triisopropylsilyl side groups, TIPS) with MC5 (containing twelve $C_{16}H_{33}$ chains in total).

8.3.1 Solution/Substrate Interface

STM reveals that both macrocycles organise in 2D layers at the TCB/ HOPG interface (figure 8.14). Only short-range order could be observed.

8.3.2 Air/Substrate Interface

AFM was carried out at the air/substrate interface after complete solvent evaporation. Both compounds have been deposited on silicon, mica, and HOPG using TCB as solvent. Figure 8.15 shows the AFM images and cross section profiles of the nanostructures formed from MC4 on different substrates (see also table 8.2).

On HOPG (figure 8.15A and B), MC4 forms ordered islands. The height profile along the line marked in the AFM image indicates a height of 3 nm for these nanostructures. On silicon (figure 8.15C and D), several incomplete layers are formed on top of each other and the cross section reveals steps of about 3.5 nm. Clusters are also observed on top of the layers. In the case of mica, various structures are observed. On some areas on the substrate, MC4 assembled to an incomplete network with a height of about 3 nm, as shown by the cross section (figure 8.15E). While on other sites of the sample, a rough surface was formed (figure 8.15F).

In contrast to MC4, MC5 forms almost exclusively micrometre long fibres on both HOPG (figure 8.16A and B) and silicon (figure 8.16C and D). The height profile along the line marked in the AFM image indicates a fibre height of 4-7 nm and 7-11 nm, respectively. MC5 forms

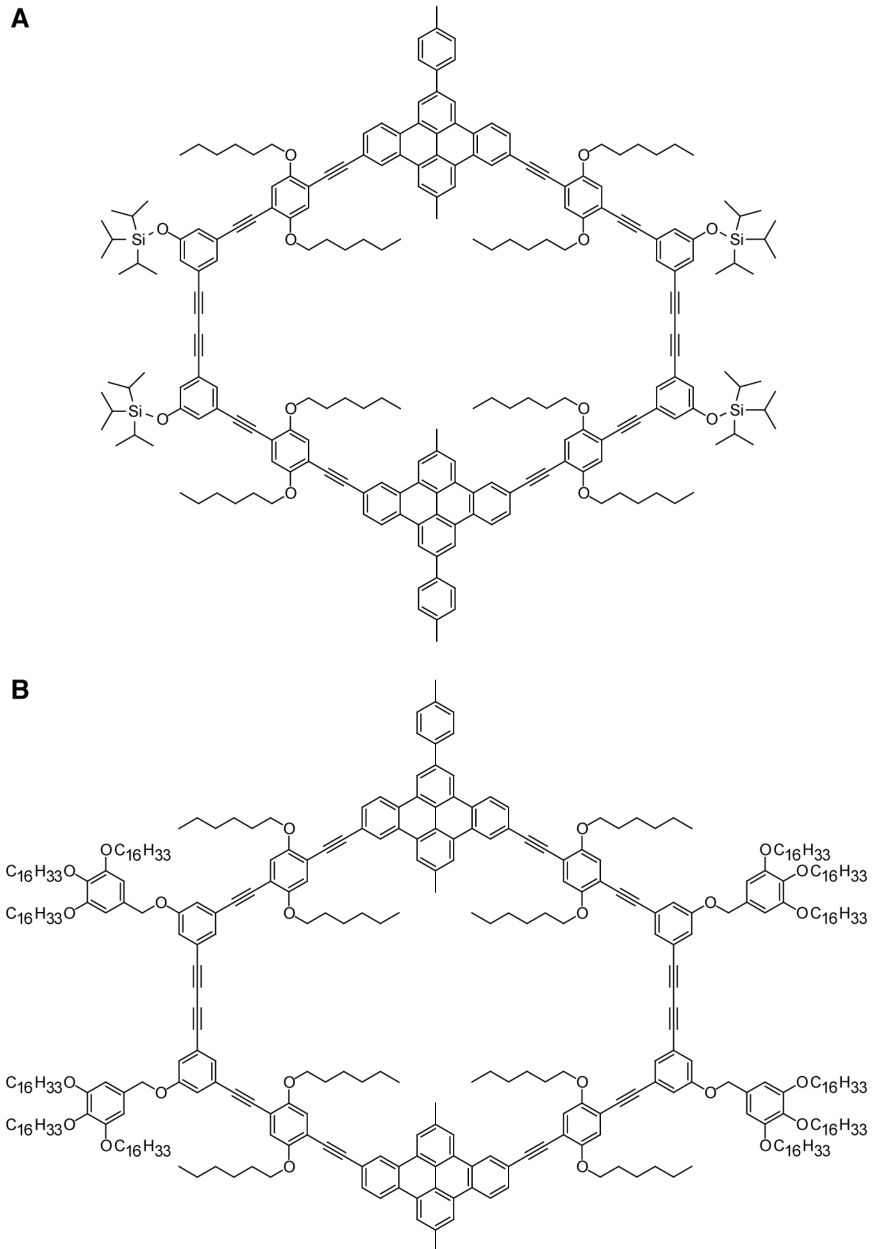

Figure 8.13: Chemical structure of the dibenzonaphthacene rings MC4 (A) and MC5 (B) with triisopropylsilyl (TIPS) and oligo-alkyl ($C_{16}H_{33}$) side groups, respectively.

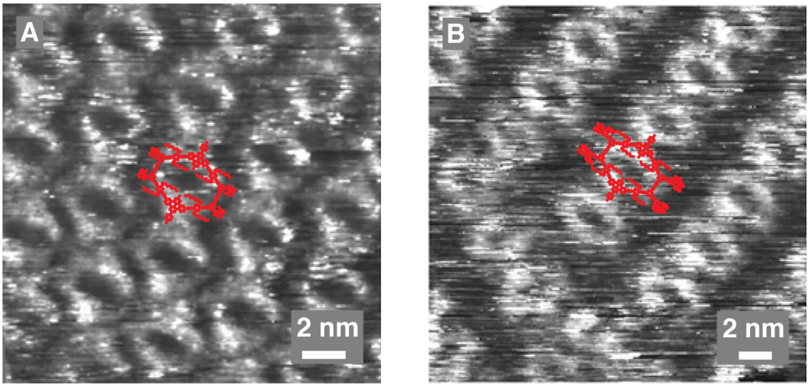

Figure 8.14: STM images of a locally ordered area of a monolayer of MC4 (A) and MC5 (B) formed at the TCB/HOPG interface. The molecular structures are superimposed on the images.

Table 8.2: Different nanostructures observed on various surfaces.

	MC4	MC5
HOPG	- ordered islands (height ∼3 nm)	- μm long fibres (height 4-7 nm)
silicon	- incomplete multilayers (height ∼3.5 nm) - clusters on top of layers	- μm long fibres (height 7-11 nm)
mica	- incomplete network (height ∼3 nm) - rough surface	- small worm-like structures (height 6-9 nm) - on top of an incomplete layer (∼1 nm high)

small worm-like structures on mica (figure 8.16E and F) with a height in the range of 6-9 nm lying on top of a 1-nm-high incomplete layer (see ‘plateaus’ in figure 8.16F).

8.3.3 Discussion and Conclusions

STM reveals that both MC4 and MC5 organise in 2D layers upon adsorption from TCB solution onto the HOPG surface.

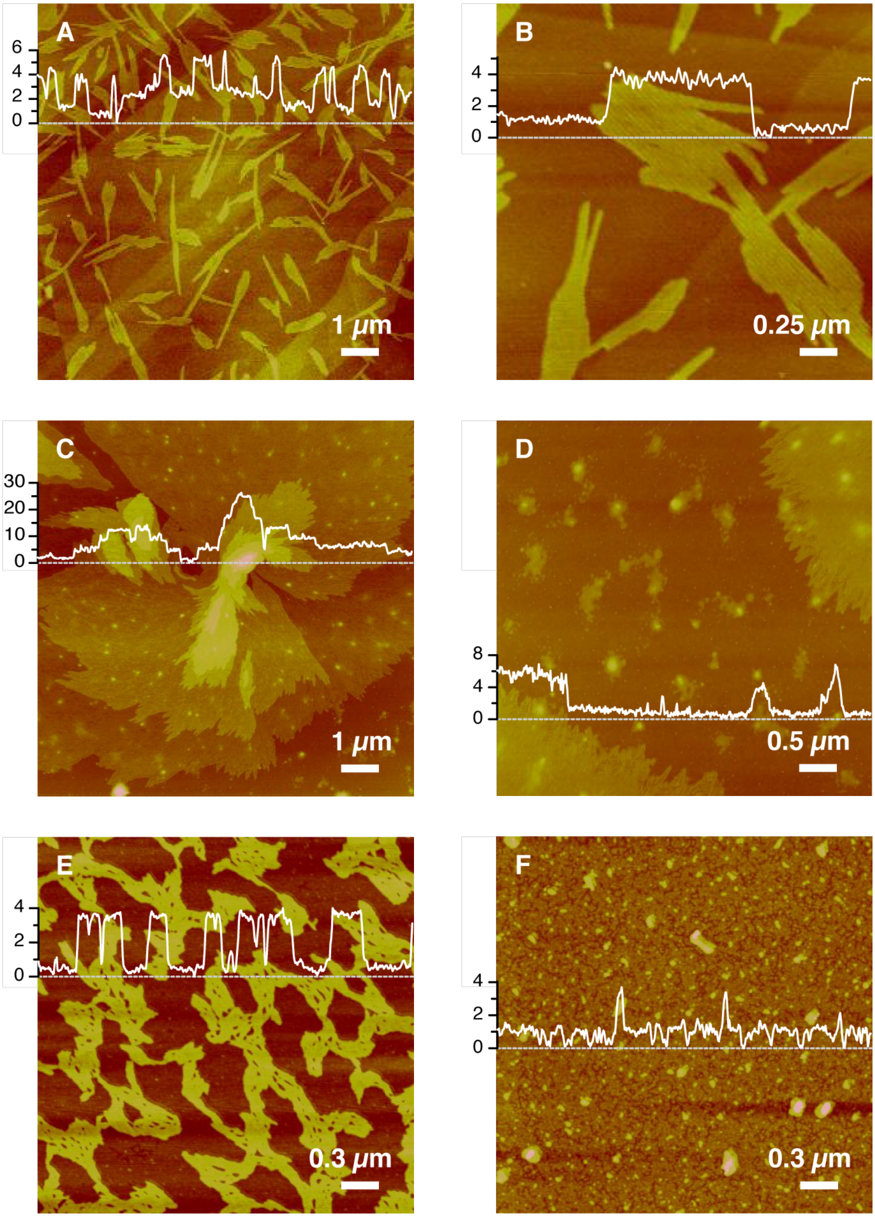

Figure 8.15: AFM topography images from samples made by dropcasting a ~10^{-4} M MC4 solution (TCB) on HOPG (A, B), silicon (C, D), and mica (E, F). Cross section profiles are indicated on each image (height unit: nm).

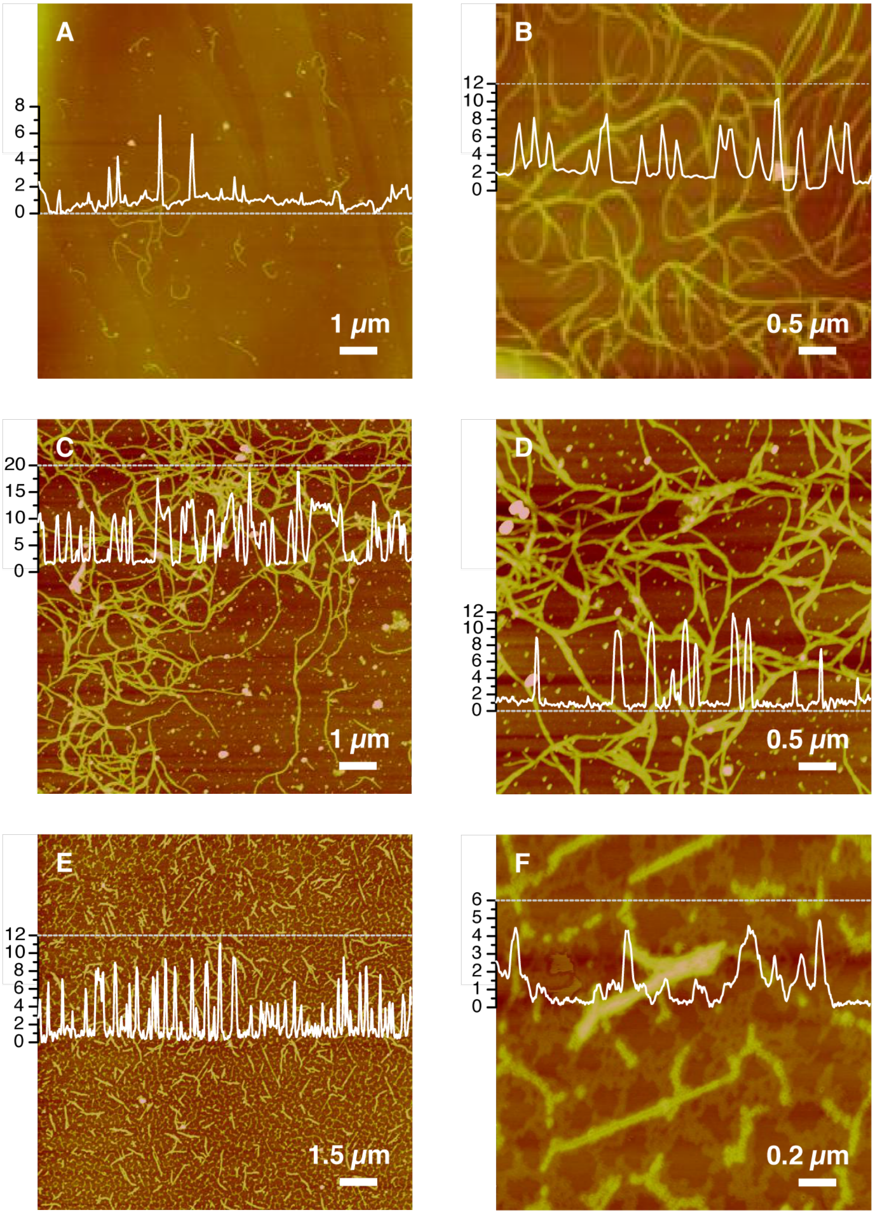

Figure 8.16: AFM topography images from samples made by dropcasting a ~10^{-4} M MC5 solution (TCB) on HOPG (A, B), silicon (C, D), and mica (E, F). Cross section profiles are indicated on each image (height unit: nm).

AFM was carried out at the air/substrate interface and reveals the formation of ordered nanostructures after slow TCB evaporation (table 8.2). The self-assembly of both compounds upon dropcasting from TCB depends on the substrate. On silicon and HOPG, MC4 forms well-ordered layers, while MC5 favours the formation of micrometre long fibres. Mica disturbs the intermolecular interactions and, as a result, the self-assembly process, leading to smaller and less well-defined nanostructures for both MC4 and MC5.

Both compounds differ only in the nature of the substituents: MC4 carries four TIPS groups, while MC5 is decorated with twelve $C_{16}H_{33}$ chains. The reason for their different behaviour must be related to the nature of the substituents. Despite the fact that the TIPS groups are quite bulky, the rigidity of the macrocycle limits the overall conformational flexibility of the molecule, and therefore these molecules are not hindered in forming well-ordered 2D patterns. In the case of alkyl substitution, 1D anisotropic growth is favoured.

Moreover, the spread in the height profile of the fibres of MC5 suggests the formation of multilayered structures that can in part be explained by the flexibility of the alkyl chains. The width of the fibres ranges from a few tens to several tens of nanometres, which substantially exceeds the dimensions of the molecules.

8.4 General Conclusions

Shape-persistent macrocycles can adsorb on the HOPG substrate via Van der Waals interactions involving the phenyl groups in the rigid backbone and alkyl chains. This physisorption makes it possible to visualise macrocycles by STM at the solution/substrate interface given that the interaction is strong enough. Since the distance between the STM-tip and the substrate is a few angstrom, only those macrocycles which are lying ‘flat’ on the substrate can be visualised.

AFM was employed to observe larger structures formed upon drop-casting and evaporation of the solvent. Measurements at the air/substrate interface led to the observation of different structures which allow to study the influence of side groups and substrate on the self-assembly process. If was found that the biphenyl bridge in MC1 and the alkyl chains in MC5 plays an important role in the formation of fibres. Both MC1 and MC3 were found to form fibres positioned on top of a (incomplete) layer. This layer most probable consists of macrocycles with a face-to-face orientation, while macrocycles inside the fibres are likely to be edge-on oriented. This hypothesis is enforced by the experiments with MC3 in a high magnetic field (see chapter 9). Although MC5 forms fibres on HOPG and silicon while no layers were observed, it is not sure whether fibres are formed directly on the ‘bare’ substrates. It could be that a small complete layer which is difficult to detect with AFM covers the substrate.

These results reveal the importance of the intra- and extraannular substitution of the macrocycles in creating patterned surfaces and nanoscale objects.

Chapter 9

Guided Self-Assembly of Macrocycles

In this chapter the effect of extremely high magnetic fields (20 T) on the self-assembled coil-ring-coil macrocycle (MC3) fibres in solution and on surfaces is described. Therefore, sample preparation was carried out inside a magnet. Since light scattering experiments (see chapter 8) indicate the existence of cylindrical aggregates in solution, magnetic fields were applied to the macrocycle in solution and birefringence experiments were done to reveal the alignment of the macrocycle fibres. As the self-assembled nanofibres can be transferred from solution onto the mica surface by dropcasting, a magnetic field was applied during this sample preparation and the existence of any preferred orientation on the mica substrate was investigated with AFM. As mentioned in section 7.3, this system will be compared to the self-assembled polyphenylene dendrimer fibres (D1 system) to study the differences of these two systems in response to a high magnetic field.

9.1 Indirect Approach using a High Magnetic Field

9.1.1 Introduction

One of the important conditions to obtain alignment of self-assembled structures in response to the magnetic field is that the magnetic anisotropy of the molecules should be sufficiently large. Furthermore, the relative orientation of the anisotropic groups in the aggregated structures has a strong impact on the alignment process.

MC3 contains 10 phenyl groups in the rigid backbone and 44 phenyl groups in its two flexible side chains. Benzene molecules have a large diamagnetic anisotropy (-60×10^{-6} cm^3/mol) and hence will react to the applied field by orienting the plane of the molecules parallel to the field direction in order to minimise the acquired energy from the magnetic field [de Gennes and Prost, 1993]. Depending on the orientation of the phenyl groups inside the nanofibres, they could give rise to a sufficiently high anisotropy resulting in an alignment of the fibres.

Most probably the macrocycles are stacked in a face-to-face way and hence a large number of phenyl groups will have the same orientation with respect to the fibre axis. Therefore, it is expected that the MC3 fibres will align according to the field in contrast to the D1 fibres (see chapter 7).

9.1.2 In Solution

In a first approach, a cuvette containing a macrocycle solution was put in the strong magnetic field[1] of 20 tesla.

If the magnetic field is able to align the fibres in solution, as is expected from theoretical considerations, a deviation from the random orientations of the macrocycle fibres results. This would cause double

---

[1] These experiments were carried out in the HFML (High Field Magnet Laboratory) in Nijmegen (by Jeroen Gielen).

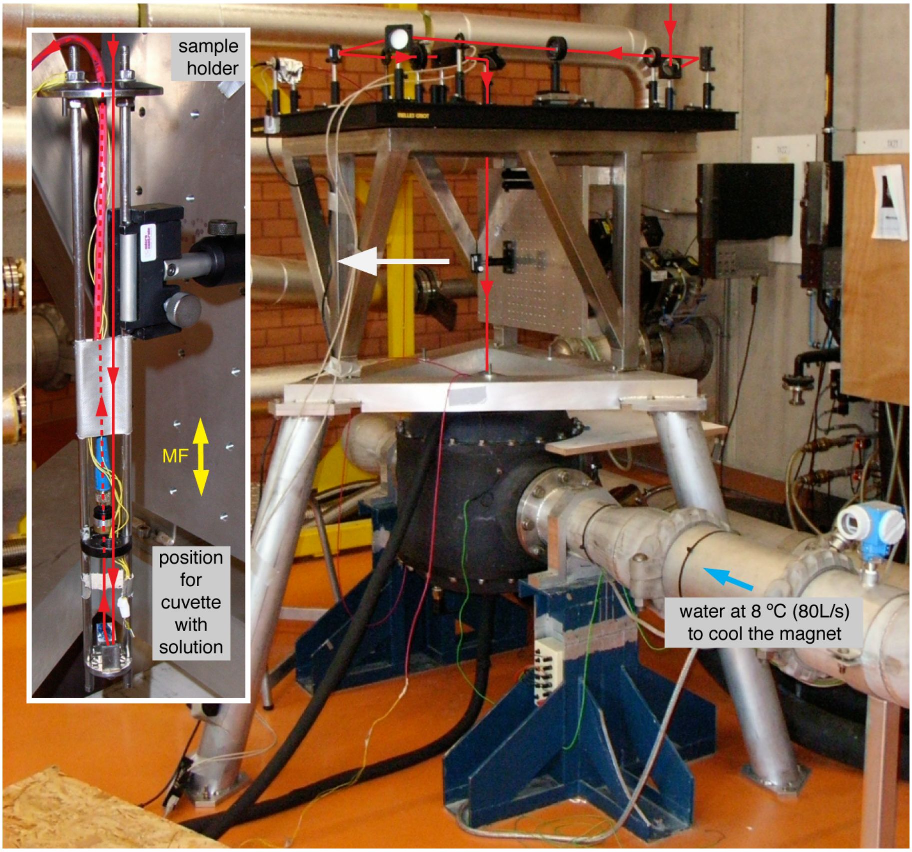

Figure 9.1: Picture of the set-up used for magnetic field experiments in solution. The direction of the magnetic field (MF) is indicated with the yellow arrow and the path of the laser beam is indicated in red.

refraction (birefringence, Δn) of light in the solution at right angles to the direction of light propagation, also referred to as the Cotton-Mouton effect. When polarised light enters the anisotropic solution containing oriented fibres, the light is refracted and divided into two separate components perpendicular to each other. If the polarised light waves pass through an analyzer, only those components of the light waves that are parallel to the polarisation direction of the analyzer pass through. The birefringence is measured parallel and perpendicular to the magnetic field direction. The difference in speed between the ordinary and extraordinary rays refracted in the solution causes a retardation (phase lag) of one ray with respect to the other which was measured during the experiment.

The magnetic field was swept from 0 to 20 T and back while keeping the temperature constant at 11 °C. Before the measurement, the sample had been at 11 °C for several days to make sure the aggregates were stable. Figure 9.2 shows the retardation in function of the applied magnetic field. When no field is applied (intercept with y-axis), no retardation was observed. However, upon applying a magnetic field (up to 20 T) retardation occurred indicating magnetically induced birefringence for the MC3 solution in a magnetic field.

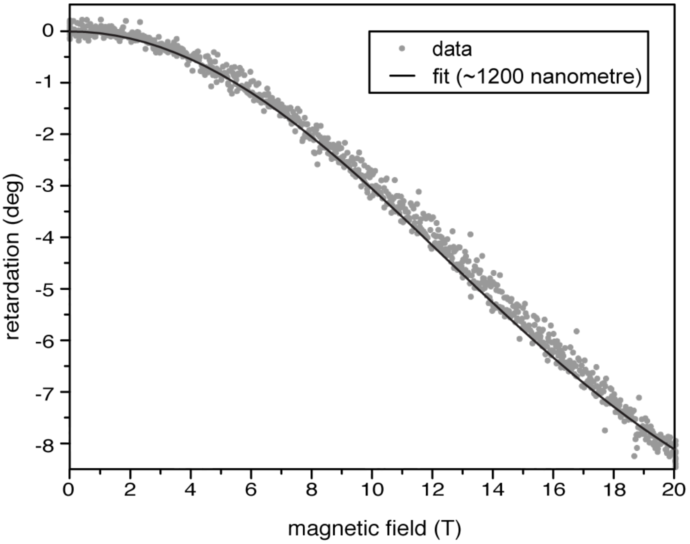

Figure 9.2: The phase lag between the ordinary and extraordinary rays refracted in the solution (retardation) in function of the magnetic field applied on the macrocycle solution at ∼11 °C reveals a magnetically induced birefringence.

As the retardation is proportional to the birefringence (equation 9.1), this latter can be used to theoretically fit the experimental data. The birefringence is given by equation 9.2 with n_{max} the largest measured birefringence. θ is the angle between the aggregate and the direction of the magnetic field (i.e. the z-axis), while ϕ is the angle between the aggregate and the x-axis.

$$retardation = \Delta n \left(\frac{360 \times thickness_{(cuvette)}}{\lambda} \right) \tag{9.1}$$

$$\Delta n \approx n_{max} \int \int \left(\cos^2 \theta - \sin^2 \theta \sin^2 \phi \right) f\left(\theta\right) \sin \theta d\theta \tag{9.2}$$

For cylindric-shaped molecules or aggregates, the distribution function ($f(\theta)$) is given by equation 9.3 with N the number of molecules in one aggregate, B the magnetic field, N_a Avogadro's number, k_B the Boltzmann's constant, T the temperature, χ_{xx} and χ_{zz} the molar susceptibility according to the x and z-axis, respectively and F_{norm} is the normalisation constant as expressed in equation 9.4.

$$f\left(\theta\right) = \frac{1}{F_{norm}} \exp \left(\frac{-\frac{N}{2} \left(\chi_{zz} - \chi_{xx}\right) B^2 \cos^2 \theta}{\mu_0 N_A k_B T} \right) \tag{9.3}$$

$$F_{norm} = \int \exp \left(\frac{-\frac{N}{2} \left(\chi_{zz} - \chi_{xx}\right) B^2 \cos^2 \theta}{\mu_0 N_A k_B T} \right) \sin \theta d\theta \tag{9.4}$$

The anisotropy in magnetic susceptibility for the macrocycle ($\chi_{zz} - \chi_{xx}$) is calculated by adding the magnetic susceptibility of the units the macrocycle consists of. The calculation is based on the number of phenyl groups, single bonds, and triple bonds present in the shape-persistent macrocycle backbone. The flexible side chains were not considered since there is no proof that these chains are stacked in the self-assembled structures and therefore it is difficult to predict their orientation inside the self-assembled fibres. A detailed derivation is given in chapter 11 and a theoretical value of about -$10^{-8} m^3/mol$ was calculated.

The expected behaviour of MC3 in solution in the magnetic field was fitted for aggregates with a length of 1200 nm and plotted on top of the measured birefringence of the solution in function of the applied magnetic field at ~11 °C (figure 9.2). The experimental data fit the theoretical plot very well.

The polar plot in figure 9.3 shows the orientation of the aggregates (θ) with a theoretical anisotropy in magnetic susceptibility of about $-10^{-8} m^3/mol$ in solution when placed in a high magnetic field of 20 T. The direction of the field is vertical and although aggregates have several orientations, a significant amount of them is expected to be aligned perpendicular to the magnetic field (i.e. at θ=90 and 270 degree).

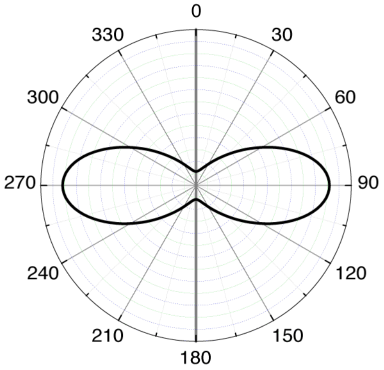

Figure 9.3: Polar plot of the theoretical orientation of the aggregates (θ) in solution. The direction of the magnetic field is according to the vertical axis.

9.1.3 On a Substrate

Immediately after dropcasting 25 μL of the macrocycle solution on the mica substrate, the sample was inserted in a Bitter magnet mounted horizontally in order to induce a magnetic field with strength of 20 T parallel to the substrate[2].

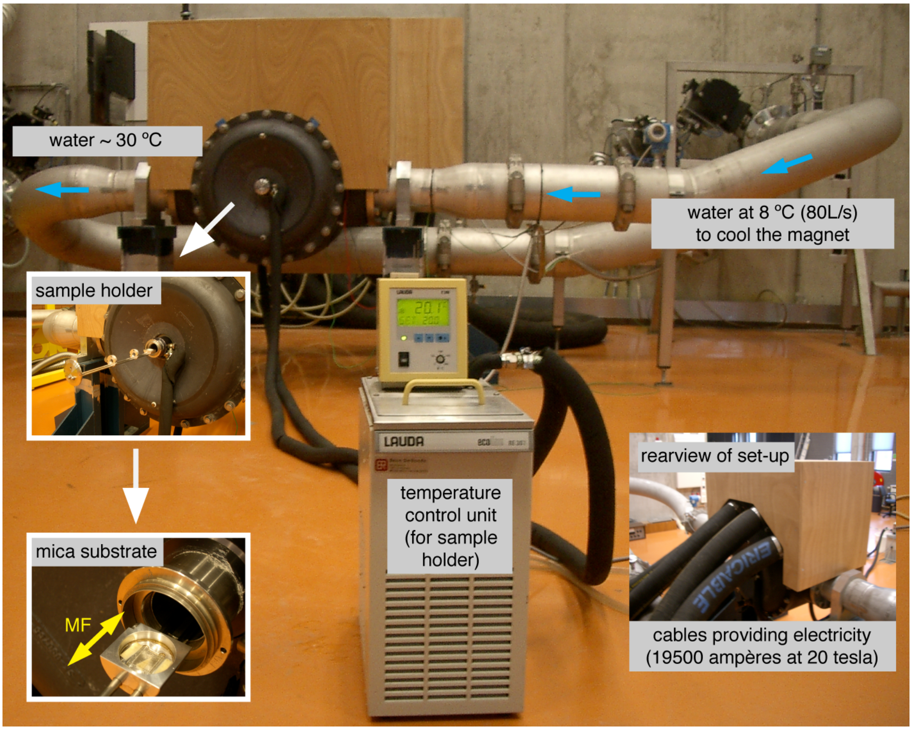

Figure 9.4: Picture of the set-up used for magnetic field experiments on a substrate. The direction of the magnetic field (MF) is indicated with the yellow arrow.

During the experiment the magnetic field was kept constant at 20 T and the temperature of the sample was maintained at 20 °C with a ther-

---

[2] These experiments were carried out in the HFML (High Field Magnet Laboratory) in Nijmegen (together with Jeroen Gielen).

mostat. After 10 minutes the solvent was evaporated and the samples were removed from the magnet and investigated with AFM.

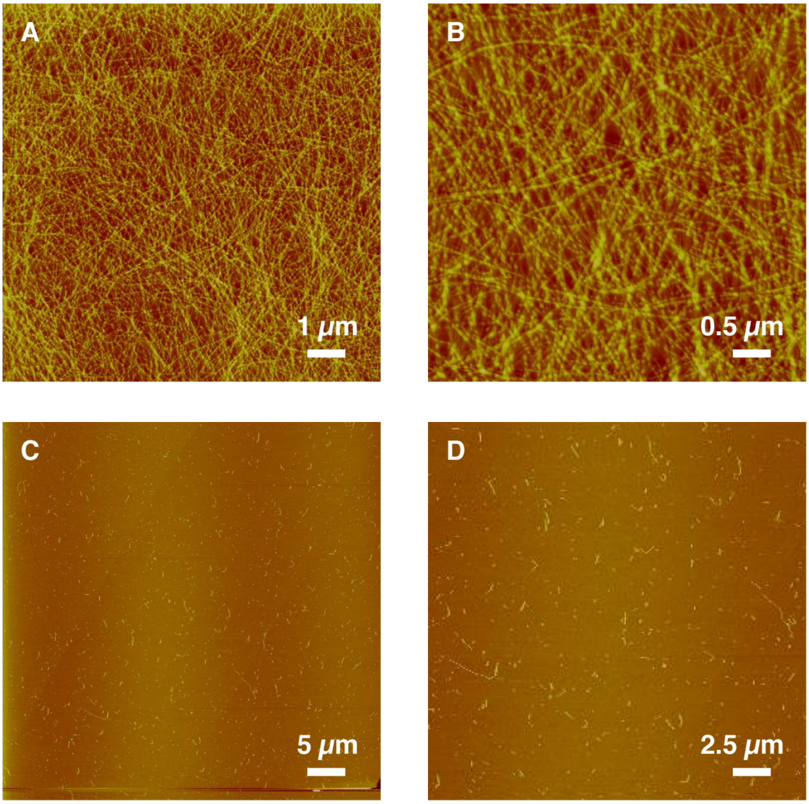

Figure 9.5: AFM topography images from a sample made by dropcasting 25 μL MC3 solution in C_6H_{12} with $\sim10^{-4}$ M (A, B) and $\sim10^{-5}$ M (C, D) on mica while applying a high magnetic field (20 T).

For both samples containing a dense network of fibres (figure 9.5A and B) and samples with short fibres (figure 9.5C and D), no alignment was observed. This can be explained by the solvent dynamics during sample evaporation. The evaporation of the solvent induces a solvent convection in the macrocycle solution which can cause randomisation of the aggregates present in the solution. Such effect was observed by optical microscopy for thiophene aggregates[3]. Despite the alignment of the aggregates in solution upon exposure of the magnetic field, the fibres appeared randomly oriented on the substrate after complete solvent evaporation.

9.1.4 Discussion and Conclusions

High magnetic fields (20 T) leading to bulk, contact free, non-destructive forces were used to successfully align the macrocycle aggregates in solution. This provided supplementary information about the internal structure of the fibres since the molecules should be self-assembled through π-π stacking in a face-to-face way in order to obtain a sufficiently high anisotropy necessary for significant interaction with the magnetic field and consequent alignment.

From the scattering experiments, it is obvious that the fibres observed on mica with AFM are already formed in solution before dropcasting. It was predicted from the magnetic experiments in solution that fibres should have the potential to align in a magnetic field during their transfer from solution to substrate. However, fibres did not align on the substrate, probably due to randomisation of the aggregates upon solvent evaporation.

9.2 General Conclusions

The self-assembled structures of the shape-persistent macrocycle MC3 can be aligned in solution in a high magnetic field (20 T) which confirmed that the molecules are self-assembled through π-π stacking in a face-to-face way.

---

[3] Private communication of Jeroen Gielen, HFML (High Field Magnet Laboratory) in Nijmegen.

If the macrocycle MC3 system is compared with the polyphenylene dendrimer D1 system (discussed in chapter 7), it is clear that although both types of fibres are formed by self-assembly, the orientation of the phenyl groups within the fibres must be different. Experiments in high magnetic fields indicate that the phenyl groups of the dendrimer system have a random orientation with respect to each other, while the phenyl groups of the macrocycle are ordered in a face-to-face fashion enabling alignment.

Chapter 10

Self-Assembly of PTM-C20

10.1 Introduction

In this chapter, the self-assembly properties of alkylated polychlorotriphenylmethyl derivatives on a substrate were investigated.

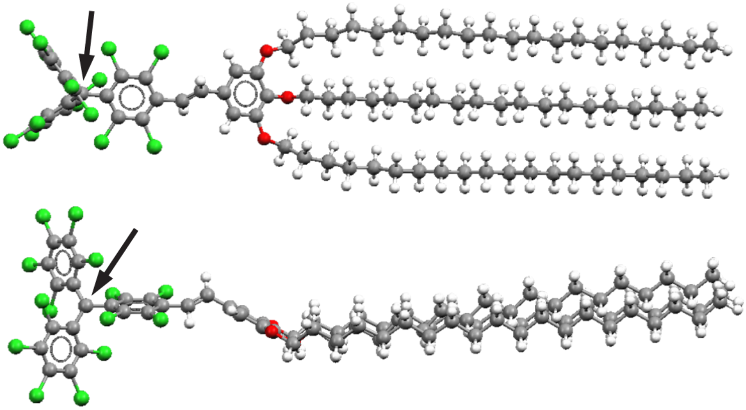

Figure 10.1: Two different views of the structure of PTM-C20-radical. The arrows indicate the central carbon atom containing the free electron.

The polychlorotriphenylmethyl derivative (PTM-C20-radical) contains a free electron located on the central carbon atom (indicated with arrows in figure 10.1) while the polychlorotriphenylmethane derivative (PTM-

C20-αH) carries a hydrogen atom at the central carbon atom. Both molecules have an additional benzene group attached via a vinylene bond in para position on one of the three central benzene groups. The additional benzene group has three large alkane chains ($C_{20}H_{41}$) connected to it. SPM techniques were used to evaluate the self-assembly behaviour of the PTM molecules. Spontaneous multilayer formation at the liquid/solid interface was probed by STM. Aggregate morphologies at the air/solid interface resulting from dropcasting were investigated with AFM. Magnetic force microscopy (MFM) and electrostatic force microscopy (EFM) were used to measure possible magnetic or (and) electrostatic responses of the assembled structures in order to try to distinguish the radical compound from the αH compound. In contrast to PTM-C20-αH, a paramagnetic response is expected for PTM-C20-radical due to the presence of a free electron [Ballester et al., 1971]. Magnetic susceptibility measurements with superconducting quantum interference devices (SQUID[1]) on similar derivatives (PTM-Fc, presence of a ferrocene group) revealed a difference for the radical and αH derivative[2].

10.2 The Radical and the α-Hydrogen Derivative

10.2.1 Scanning Tunnelling Microscopy

A drop of a solution of PTM-C20-radical in phenyloctane was put on the HOPG surface and STM experiments[3] were carried out at the phenyloctane/HOPG interface.

Figure 10.2 reveals disk-like structures which are ordered in rows. The distance between the disks in one row is around 0.77 nm. The centre-

---

[1] Superconducting quantum interference devices are very sensitive magnetometers used to measure extremely small magnetic fields, based on superconducting loops.

[2] Private communication of Núria Crivillers, Prof. Veciana's group in Barcelona.

[3] The STM experiments were carried out by Núria Crivillers and Shuhei Furukawa.

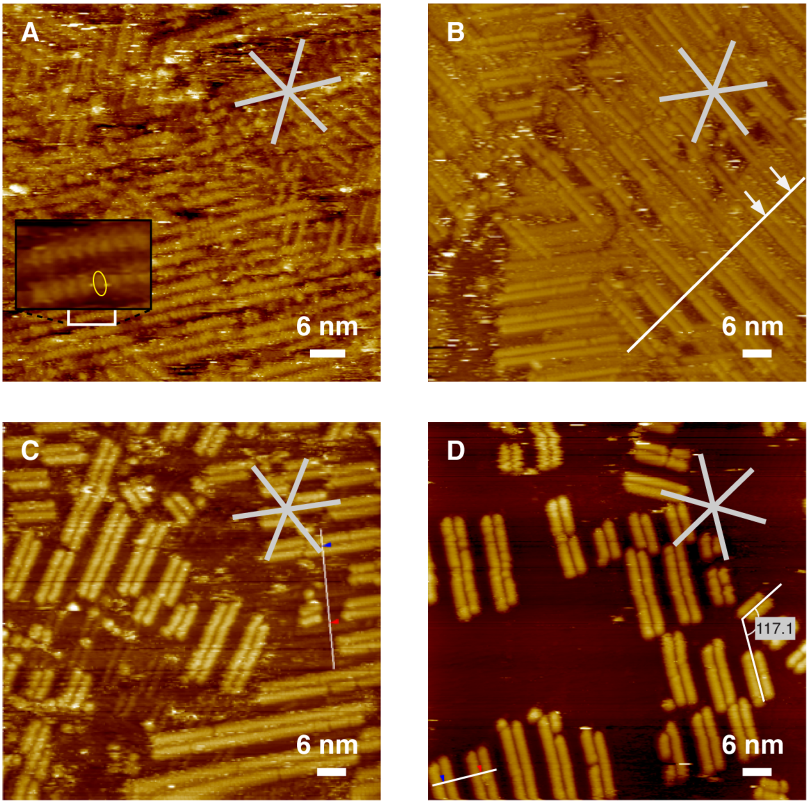

Figure 10.2: STM images of PTM-C20-radical molecules stacked in rows at the phenyloctane/HOPG interface. The rows are oriented according to the three directions as indicated on the images.

to-centre distance (indicated on figure 10.2B) between the dimer rows in which the radical parts are oriented in a head-to-head configuration measures 8 nm. These results are in lign with the length of a PTM molecules which is measured to be 4 nm (modelling with hyperchem).

The disks forming the bright rows are the conjugated parts of the molecules. One disk corresponds to one molecule. It is well known in STM imaging that conjugated moieties are more efficient in supporting the tunnelling process than alkyl chains which must be adsorbed in the darker areas. In this case, individual alkyl chains could not be resolved.

The stacked molecules are mainly oriented along the three directions as indicated on the STM images, revealing the influence of the substrate in directing the self-assembly of the PTM molecules.

10.2.2 Atomic Force Microscopy

30 μL of a 2.02×10^{-4} M solution of the PTM molecules dissolved in toluene was dropcast on HOPG and left to dry. Evaporation of toluene took typically a few minutes. The sample preparation and measurements were carried out in the 'dark' to avoid photochemical decomposition of the radical.

AFM images (figure 10.3) reveal that the radical derivative forms aggregated structures with heights of a few tens of nm up to more than 100 nm over the entire HOPG surface. It is clear that these large aggregates are composed of small ordered objects with a full width at half height of a few nm for the smallest objects. Figure 10.4 provides phase images on which individual rows are visible with a centre-to-centre distance around 8 nm, representing the same aggregated structures as the dimer rows observed in the STM images. Again, these objects are mainly oriented along three directions as is indicated on the upper right corner of the high resolution zoom in (figure 10.3C). This alignment is best observed in the phase images (right half of the AFM images). Islands of ordered aggregates are separated by an apparent amorphous film with only a few nm in roughness as can be seen in the upper line profile in figure 10.3C. The film thickness could not be determined. Experiments do not provide information whether the aggregate islands are on top of this layer or not.

The αH compound forms similar aggregates which have roughly the same height and are also composed of smaller nanostructures which are

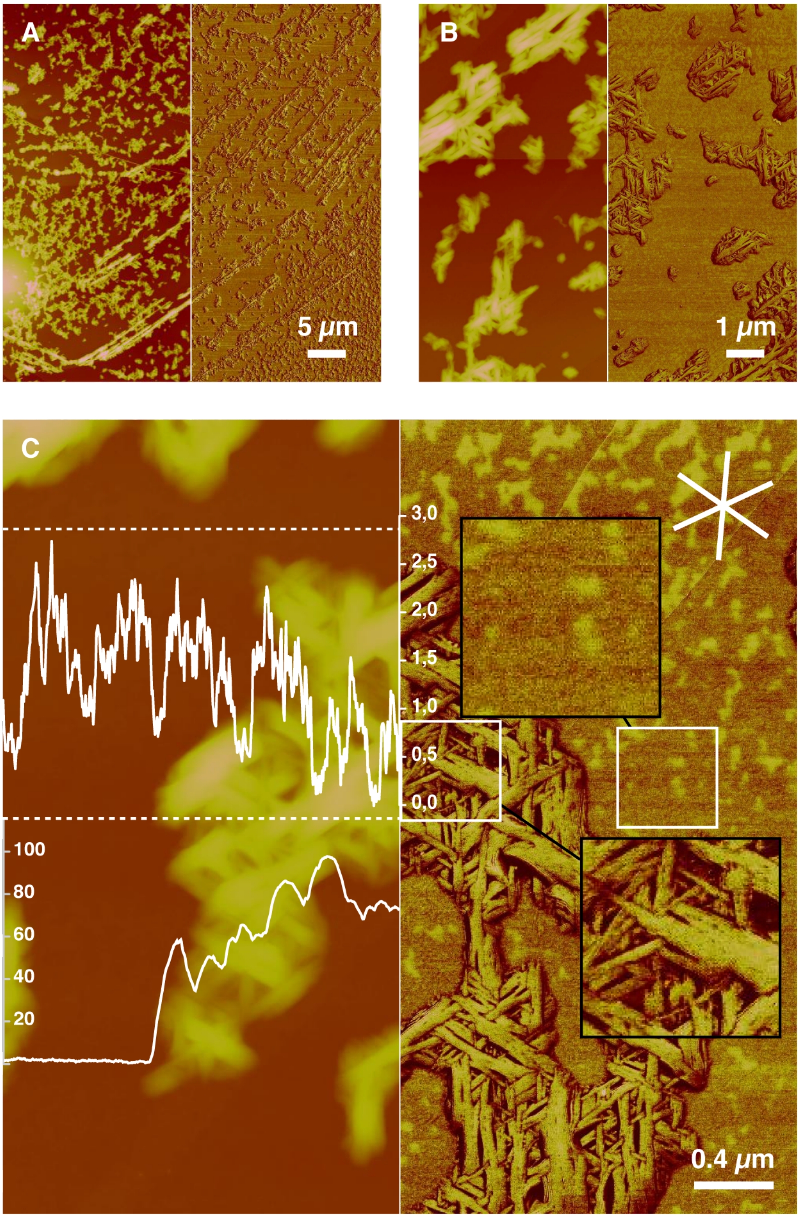

Figure 10.3: AFM topography (left half) and phase (right half) images from a sample made by dropcasting 30 μL of a 2.02×10^{-4} M solution of PTM-C20-radical in toluene on HOPG. Line profiles are depicted on top of the topography image (height unit: nm) and inserts on the phase image are two times enlarged, revealing the background layer and the preferred orientation of the nanostructures.

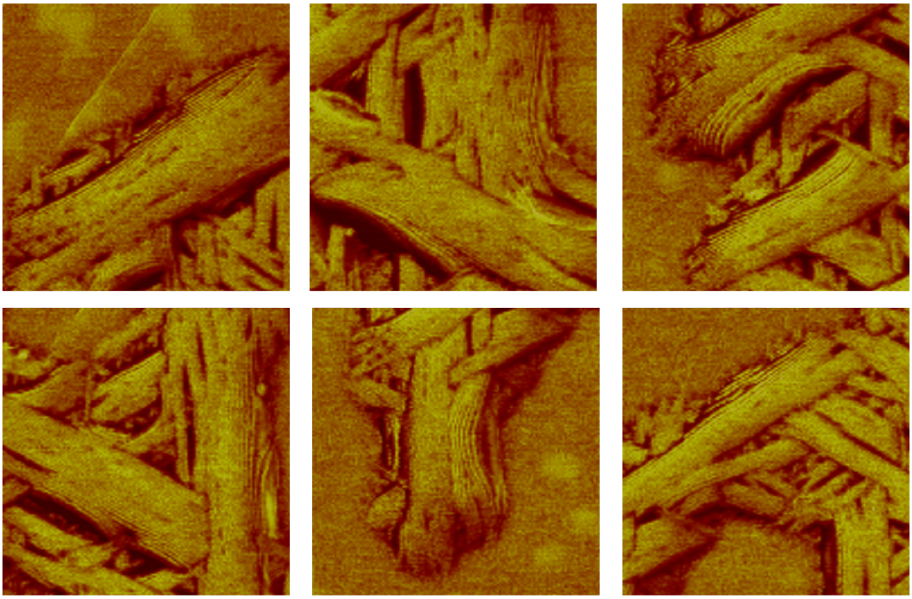

Figure 10.4: AFM phase images (500×500 nm) from a sample made by dropcasting 30 μL of a 2.02×10^{-4} M solution of PTM-C20-radical in toluene on HOPG revealing individual rows.

aligned along three directions on top of a very thin incomplete layer (figure 10.5).

10.2.3 Electrostatic and Magnetic Force Microscopy

A universal scanning force microscope (SFM, ‘Autoprobe M5’ from Veeco instruments) was used to characterise the long-range (magnetic and electrostatic) force interactions between the SFM tip and the sample surface. Conductive tips coated with a ferromagnetic film were employed. The SFM used works in the ‘flying mode’, i.e. the z-coordinate is fixed during scanning of the sample.

For each sample, measurements were carried out at different tip-to-sample distances and the interactions between the tip and the sample

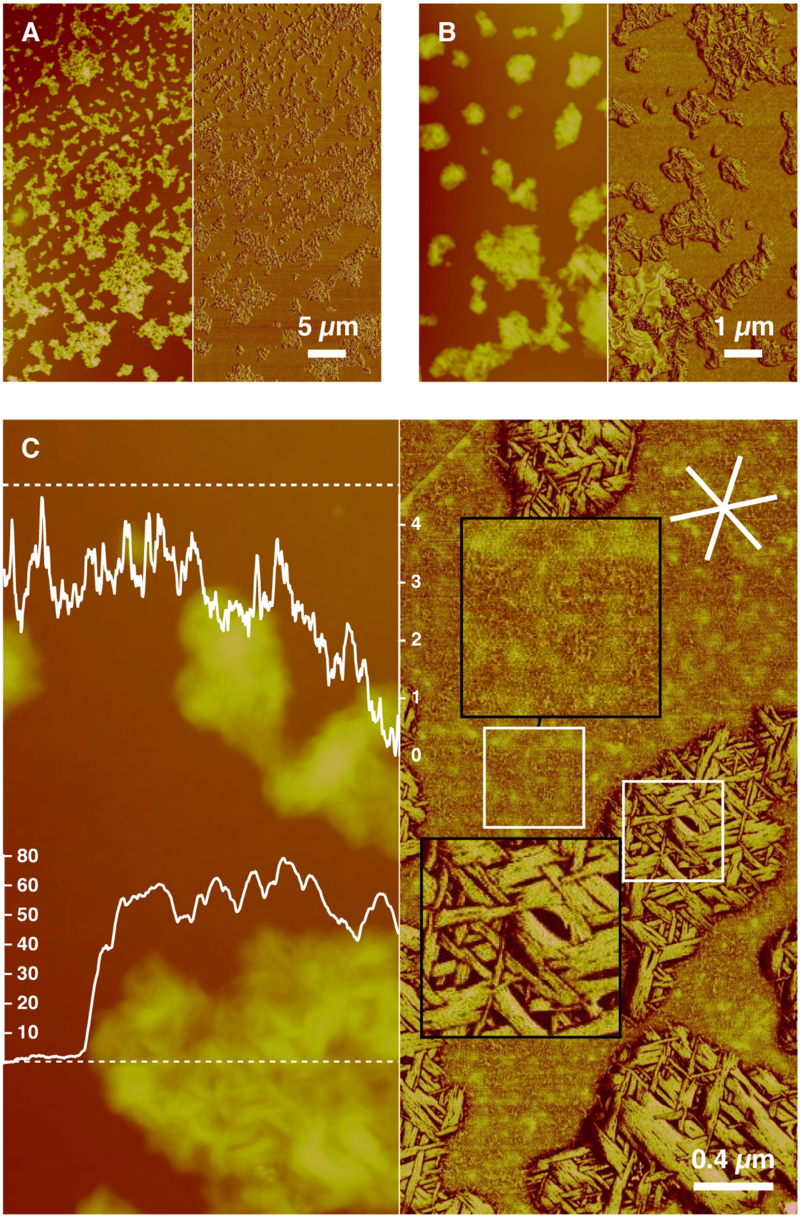

Figure 10.5: AFM topography (left half) and phase (right half) images from a sample made by dropcasting 30 μL of a 2.02×10^{-4} M solution of PTM-C20-αH in toluene on HOPG. Line profiles are depicted on top of the topography image (height unit: nm) and inserts on the phase image are two times enlarged, revealing the background layer and the preferred orientation of the nanostructures.

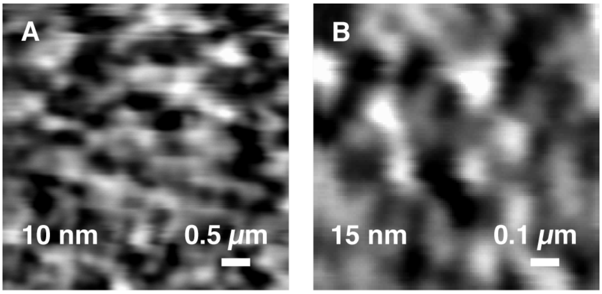

Figure 10.6: SFM images from a MFM test sample (FePt) with a tip-to-sample distance of 10 nm (A) and 15 nm (B).

were recorded[4]. At small distances, the interaction will be influenced by topography, but upon increasing distance, van der Waals interactions will disappear and long-range forces such as magnetic or electrostatic will dominate [Guggisberg et al., 2000].

First the performance of the set-up is evaluated from the results of the MFM measurements carried out on a ferromagnetic FePt film sample which contains small size (∼0.1 micron) magnetic domains with out of plane magnetisation (figure 10.6). A signal up to a relatively large tip-to-sample distance of 15 nm could be observed (figure 10.6B). The experimental minimum detectable force gradient was estimated as $\sim 10^{-4}$ N/m. This estimation was based on the expression for the thermodynamic limit of the force gradient detection by the AFM cantilever [Sarid, 1994], taking into account the measured parameters (the rigidity, the resonant frequency and the mechanical quality factor) of the cantilever used. The spatial resolution which was evaluated from the typical size of the observed features is ∼70 nm.

Figure 10.7 shows SFM images of the PTM samples. The images were obtained at different tip-to-sample distances and show that the signal

---

[4] These experiments were carried out in the physics department at the KULeuven (together with Alexander Volodin).

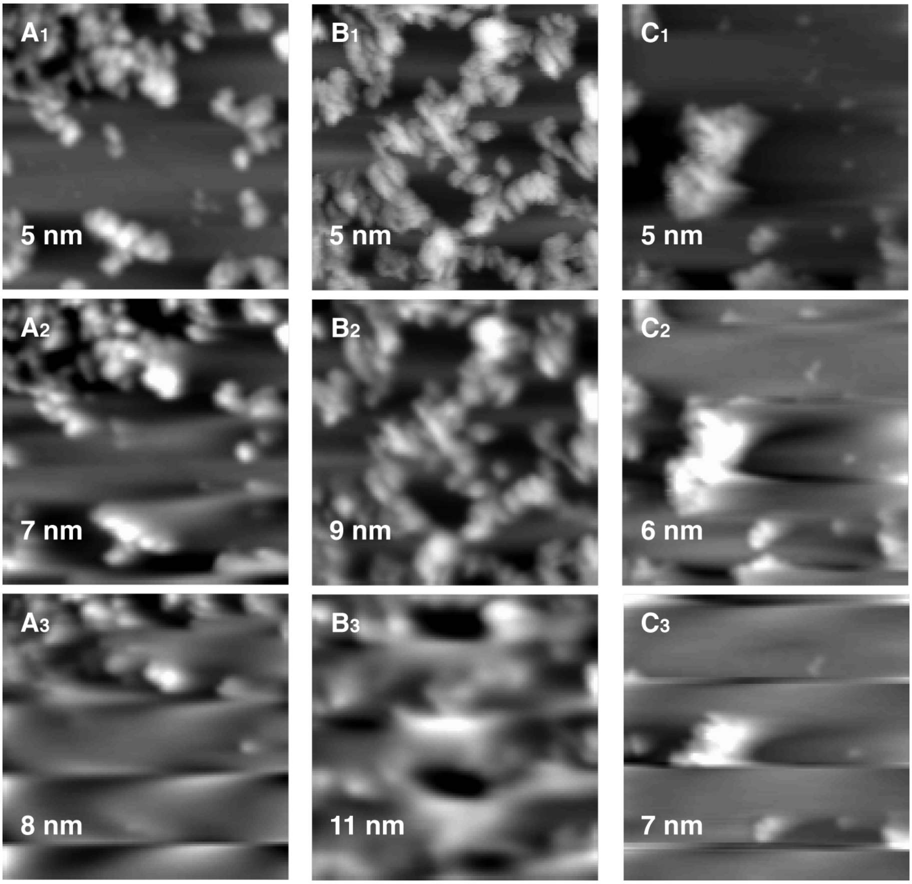

Figure 10.7: SFM images (5×5 μm) from a sample made by dropcasting 30 μL solution of PTM-C20-αH (A) and PTM-C20-radical (B, C) in toluene with 2.02×10^{-4} M. The measurements were carried out on isolated (A, B) and grounded HOPG substrates (C).

drops considerably at a distance of 8 nm for the PTM-C20-αH sample (first column: figure 10.7A_1, A_2, A_3). This reveals a relatively short range of interactions which are probably of the van der Waals type. For PTM-C20-radical (second column: figure 10.7B_1, B_2, B_3), some longer-range forces were observed as a significant signal is still detected at a tip-to-sample distance of 11 nm. The interaction is probably due to magnetic and/or electrostatic interaction.

To identify the nature of this long-range interaction, additional experiments were carried out on grounded samples[5] to minimise the electrostatic interaction which can be caused by electric charges of the molecular aggregates. This results in a significantly smaller range of interactions (third column: figure 10.7C_1, C_2, C_3) with respect to the isolated sample. The distance at which the signal drops considerably is around 7 nm, and thus the interaction is attributed to van der Waals forces. Therefore, the long-range forces detected for the isolated samples are most likely due to electrostatic interactions. These interactions may be caused by the surface charges of the aggregates which can appear, for example, due to the difference in the work functions of the aggregates and the substrate. An eventual very weak (paramagnetic) magnetic component could not be experimentally identified.

10.3 Conclusions

Both the radical and the α-hydrogen PTM-C20 derivative self-assemble in ordered structures on the HOPG surface, both at the solution/HOPG interface as well as after dropcasting and fast solvent evaporation. Both STM and AFM revealed ordering in rows. AFM showed large aggregated nanostructures which, as well as the rows observed with STM, are oriented along three directions. This is most probably related to the

---

[5] Samples were grounded by connecting them via a conductive wire to the earth.

symmetry of the HOPG substrate.

SFM experiments were performed at room temperature. Some long-range interactions were detected, which were only present in the case of PTM-C20-radical. However, further measurements with electrically grounded substrates show a similar range of interactions for the radical as for the isolated PTM-C20-αH. Therefore, it can be concluded that the long-range interactions observed in the first experiment were due to electrostatic interactions.

The sensitivity of the MFM technique is insufficient to distinguish the radical sample from the α-hydrogen derivative by the difference in the magnetic tip-to-sample interaction (on the level of $10^{-4}N/m$).

Chapter 11

Experimental Details

11.1 Products

- tetrahydrofuran (THF): Sigma-Aldrich (spectroscopic grade, 99.5+%, inhibitor free)

- 1,2,4-trichlorobenzene (TCB): Sigma-Aldrich (99%)

- polydimethylsiloxane (PDMS) stamps/molds: kindly provided by prof. J. Huskens from MESA+ (University of Twente)

- hydrogen peroxide (H_2O_2): Acros organics (p.a., 35 wt%) and Merck VWR (30%, for the binary pattern formation)

- sulphuric acid (H_2SO_4): Fisher Scientific (98%) and Merck VWR (98%, for the binary pattern formation)

- polymethylmethacrylate (PMMA): Polymer Laboratories (Mp: 141 500 g.mol-1, Mw/Mn: 1.01, Tg: 126C)

- perfluorosilane (CF_3-$(CF_2)_7$-$(CH_2)_2$-$SiCl_3$): Gelest (packed under anhydrous argon atmosphere)

- dichloromethane (CH_2Cl_2): Acros Organics (for the binary pattern formation)

- mica (muscovite): S.A. laborimpex (grade V-5)

- graphite (highly oriented pyrolytic graphite, HOPG): Advanced Ceramics, Inc., Cleveland (grade ZYB)

- silicon (100) wafers: Wacker and ACM (Applications Couches Minces, France, for the binary pattern formation)

11.2 Methods

Molecular modeling. Geometry optimisation of D1 was performed by a molecular mechanics method (Merck Molecular Force Field) using Spartan (Wave Function Inc., Irvine, CA).

Light scattering. A beam of laser light is focussed in the sample cell and particles in the scattering volume scatter light in all directions. Since the scattered light is the sum of the scattering by the individual aggregates present in the scattering volume, the scattered light undergoes either constructive or destructive interference. As the distance between the aggregates is constantly changing in time, the scattering intensity will fluctuate due to motion of the aggregates. Fluctuations in the scattering intensity are therefore related to the Brownian motion of the aggregates and provide information about the time scale of movement of the aggregates present in solution and hence can be correlated to the diffusion coefficient (D) of the aggregates. The scattered light was detected at several angles (θ) at which the detector is located with respect to the sample cell.

Measurements of the time averaged scattered intensity can be related to structural studied and are known as classical light scattering, a.k.a. static light scattering. Measurements of the time (or frequency) dependence of the scattered intensity constitute dynamic light scattering.

Dynamic light scattering (DLS) provides a spectral distribution of scattered intensity at different scattering angles. A time correlation function, also called auto correlation function, of a non-periodic property such as the intensity (I) trace recorded during a light scattering experiment is obtained by computing $I(t) \times I(t+\tau)$ and averaging the results over all starting times inside a defined period, with τ the delay time of the correlation function. For small τ, the aggregates did not move much from their initial state and the correlation is still high. After a long time (relative to the motion of the aggregates) and hence for large values of τ, the correlation between the intensity of scattering of the initial state with the final state elapses and the correlation exponentially decreases to zero. For monodisperse samples, the decay is a single exponential. The exponential decay is related to the motion of the aggregates and hence to the diffusion coefficient. To fit the decay (i.e. the auto correlation function), numerical methods are used based on calculations of assumed distributions.

For continuous polydispersed systems (solution of the second generation polyphenylene dendrimer D1, see chapter 6) the correlation function can be treat as the sum of single exponential decays with fractions $G(\Gamma)$ where Γ is the decay rate (equation 11.1).

$$g\left(t\right) = \int_{0}^{\infty} G\left(\Gamma\right) e^{-\Gamma t} d\Gamma \tag{11.1}$$

An inverse Laplace transform known as CONTIN (constrained regularisation method developed by Provencher [1982a,b]) was used to analyse the auto correlation function.

The obtained diffusion coefficients were used to calculate the hydrodynamic radius (R_h) based on the Stokes-Einstein relation (equation 11.2) with $k_B T$ the Boltzman factor and η the viscosity of the solvent (THF), assuming globular shaped aggregates.

$$D = \frac{k_B T}{6\pi\eta R_h} \tag{11.2}$$

The time variation of the scattered intensity of solution of the coil-ring-coil macrocycle MC3 (chapter 8) was examined by using a digital correlator to compute the auto-correlation function. This function was analysed with the cumulant method [Koppel, 1972] in order to extract the decay time which can be used to derive the diffusion constant D by using equation 11.3 with D_t and D_r the translational and rotational diffusion coefficient, respectively, and q the scattering vector [Aragon and Pecora, 1977]. The scattering vector (equation 11.4) is frequently used instead of the angle to plot scattering graphs since it includes the refractive index of the solvent $n_{solvent}$ and the wavelength of the laser beam λ (514 nm).

$$\frac{1}{\tau} = q^2 D_t + l\,(l+1)\,D_r \tag{11.3}$$

$$q = \frac{4\pi}{\lambda} \times n_{solvent} \times sin\frac{\theta}{2} \tag{11.4}$$

However, for small particles and for signals at a scattering angle of zero degree (and thus scattering vector of zero degree), the rotational diffusion coefficient can be neglected[1] and equation 11.5 can be applied for further calculations.

$$\frac{1}{\tau} = q^2 D \tag{11.5}$$

Plotting D versus q^2 (figure 11.1) may or may not show angular dependence depending on the anisotropy and polydispersity of the system. Monodisperse spherical aggregates will show no angular dependence and

---

[1] For a cylindric object, the scattering intensity at a scattering vector of zero degree (q=0) is the same for all the orientation angles (ϕ) and hence no rotational effect is included. Therefore, at a scattering vector of zero degree, the changes in scattering intensity originate from only translational diffusion.

thus no anisotropy, resulting in a horizontal line. Aggregates with a shape other than a sphere will show anisotropy and hence an angular dependence, as was observed for this system. The intercept (extrapolation to scattering vector zero degree) corresponds to the translational diffusion coefficient (D_t).

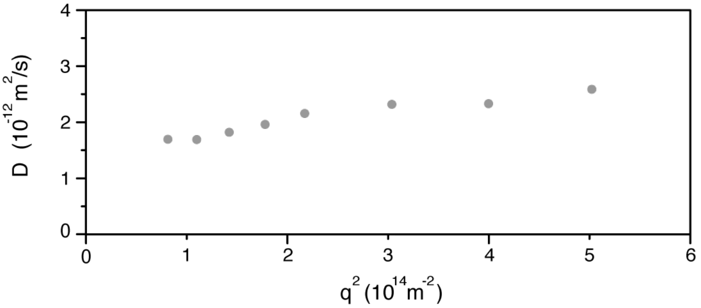

Figure 11.1: Diffusion coefficients of the aggregates as a function of the scattering vector by dynamic light scattering experiments of MC3 in C_6H_{12} at ~11 °C.

As static light scattering revealed cylindrical aggregates, equation 11.6 [Tirado et al., 1984] could be used to obtain additional information about the aggregates with η_0 the viscosity of the solvent and k_BT the Boltzman factor. Parameters ν and p are related to the shape of the aggregates as expressed in equation 11.7 and 11.8, where L and d are the length and diameter of the aggregates, respectively. Using equation 11.6, aggregates with a translational diffusion coefficient of $(1.5 \pm 0.2) \times 10^{-12}$m^2/s correspond to a p-value of 120. As the diameter of these aggregates was roughly estimated to be around 10 nm (from molecular considerations and AFM measurements), a length of 1200 ± 200 nm was calculated for the cylindrical aggregates via equation 11.8.

$$\frac{3\pi\eta_0 L D_t}{k_B T} = ln\,(p+\nu) \tag{11.6}$$

$$\nu = 0.312 + 0.565/p - 0.100/p^2 \tag{11.7}$$

$$p = L/d \tag{11.8}$$

Static light scattering (SLS) depicts the scattering intensity (I) in function of the angle (θ) at which it is measured. The shape of these graphs is dependent upon type and size of the aggregates. Therefore, models can be applied in order to investigate which aggregates are present in solution.

The data points obtained from a solution of the coil-ring-coil macrocycle MC3 (chapter 8) indicate the presence of cylindrical shaped aggregates and were fitted with a model (equation 11.9 [van de Hulst, 1981]) for aggregates with a length of 1200 nm, as was calculated from the dynamic light scattering experiments carried out on the same solution. Parameters a (=L/2) and b (=d/2) determine the shape of the aggregates, with L and d the length and diameter of the aggregates, respectively, while ϕ is the orientation angle of the cylindrical aggregate and J_1 is the first kind of the Bessel function.

$$I(\theta) \propto \int_0^{\frac{\pi}{2}} \left(\frac{\sin(qa\cos(\phi))}{qa\cos(\phi)} \frac{J_1(qb\sin(\phi))}{qb\sin(\phi)} \right)^2 \sin(\phi) d\phi \tag{11.9}$$

Preparation of samples for AFM. Before solution was dropcast on a substrate to completely cover the surface, substrates were pretreated as follows. Mica and HOPG were cleaved with scotch tape in order to remove the upper layers of the substrate. Silicon substrates were put in an ultrasonic bath for 10 min at room temperature in acetone and were then cleaned in a piranha solution (a 3:7 mixture of hydrogen peroxide and sulfuric acid) at 150 °C for about 20 min (or at 70 °C for about 30 min) to make sure all organic contaminants are removed and the substrate had become hydrophilic. Caution: Piranha solution is an extremely strong oxidising reagent. After this treatment, the substrate was thoroughly rinsed with ultra pure water (obtained by deionisation and purification using the milli-Q Reagent Grade Water System from Millipore) and blown dry with inert gas.

Binary pattern formation for guiding experiments of dendrimer D1. A solution of PMMA was prepared by dissolving the polymer in HPLC grade toluene (20g/L). To remove dust and undissolved polymer, the solution was filtered onto PTFE filters (Millipore, pore size 0.22 μm) and stored in a closed vessel. Silicon wafers were first cleaned in a piranha solution maintained at 70 °C for 25 min. The samples were then extensively washed with Milli-Q-water and dried by spincoating at 6000 rpm for 30s. Directly after cleaning, a PMMA film of about 95 nm thickness was spincoated on the wafers. The film was annealed at 170 °C for 12h. Nanolithographied masks were then obtained using a procedure based on electron beam lithography. After resist development to obtain nanoregions of reactive silicon oxide free of PMMA, the samples were introduced in a silanisation reactor. The perfluorinated silane was then injected and left to react in the gas phase for 24h. The reaction between the halide group of silane (-$SiCl_3$) and the silanol groups of the uncovered regions on the silicon substrate leads to a chemical linkage of silane to the surface. In order to obtain binary nanopatterned surfaces (alternating perfluorosilane and native silicon oxide regions), the remaining PMMA mask was removed in a CH_2Cl_2 soxhlet for 24h.

Preparation of samples for STM. Prior to imaging, all compounds under investigation were dissolved in TCB (macrocycles) or phenyloctane

(PTM derivatives) at a concentration of approximately 1 mg/g, and a drop of the solution was applied onto a freshly cleaved surface of HOPG.

Making movies with the optical viewing system. The movies were made at 20 frames per second where the actual time between two frames is 3 seconds. This means that every second of movie represents a one minute real time lapse. The screenshots were made using the following Applescript code:

```
repeat with shotcount from 1 to 3600
    do shell script "screencapture -tjpg screen"
    & (shotcount as string) & ".jpg"
    delay (3) -- delay three seconds
end repeat
```

These screenshots contained the whole desktop, while only the image of the frame grabbing software was needed. Using 'convert', part of ImageMagick, the image was cropped using the following bash script:

```
for i in ‘ls *.jpg‘ ;
do
    convert -quality 100 -crop 768x576+0+64 $i cropped/$i ;
done
```

When this was done, the movie was made using mencoder in the following command:

```
mencoder "mf://*.jpg" -mf fps=20 -ovc lavc -lavcopts \
    vcodec=msmpeg4v2:vbitrate=800 -o test.avi
```

Calculation of the contact angle during solvent evaporation of dendrimer D1 solution in THF on silicon. An estimation of the contact angle was obtained by calculating the height difference between two points in an optical image which was taken during solvent evaporation. The light beam of the optical viewing system is partially reflected at the air/solution interface, while the other part penetrates the film and is reflected at the film/substrate interface. The two reflected beams interfere constructively if equation 11.10 is followed.

$$2d = N\frac{\lambda}{n} \tag{11.10}$$

As d equals the thickness of the film, $2d$ represents the extra path length that the light beam which reflects at the film/substrate interface travels with respect to the beam which is reflected at the air/film interface. N is an integer and n is the index of refraction of the solution, which is approximately 1.5. As the calculation is based on the constructive interference of red light, the light beam has a wavelength (λ) of approximately 650 nm.

Figure 11.2 shows the optical image used for this calculation where the areas of constructive interference of red light are indicated with a white dotted line at the edge of the drying droplet. At each line, the film has a certain thickness d_2 or d_1 corresponding to equations 11.12 and 11.11, respectively.

$$2d_2 = N\frac{\lambda_{red}}{n} \tag{11.11}$$

$$2d_1 = (N-1)\,\frac{\lambda_{red}}{n} \tag{11.12}$$

$$d_2 - d_1 = \frac{\lambda_{red}}{2n} \tag{11.13}$$

The difference in film thickness (d_2-d_1) was calculated from equation 11.13 and a value around $2{\times}10^{-7}$ m was obtained. Since Δx ($3{\times}10^{-5}$ m)

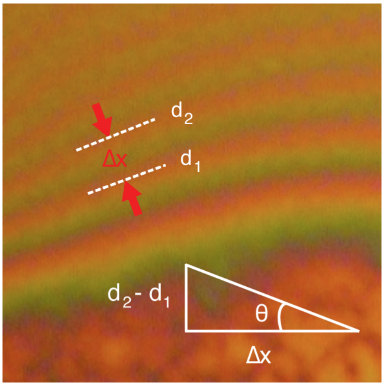

Figure 11.2: Optical image of the edge of a drying droplet of dendrimer D1 solution in THF on silicon.

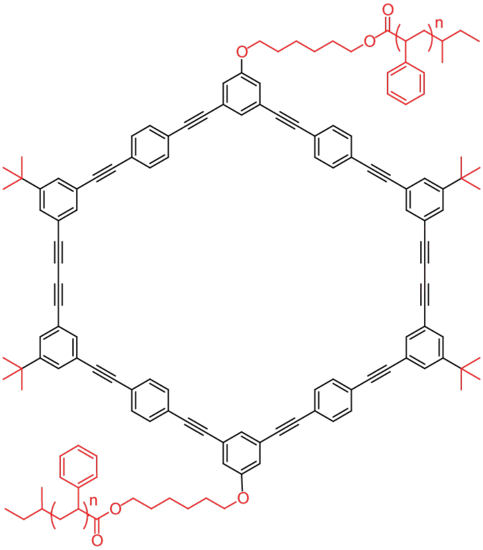

Figure 11.3: Chemical structure of the coil-ring-coil macrocycle MC3 (n≈22). The units which are omitted in the calculation are coloured red.

is known from the optical image, the contact angle θ was calculated via equation 11.14 resulting in a contact angle (θ) around 0.4 degree, which is extremely small.

$$\theta = \arctan\frac{d_2 - d_1}{\Delta x} \tag{11.14}$$

Calculation of the anisotropy in magnetic susceptibility for macrocycle MC3. The anisotropy in magnetic susceptibility for the macrocycle is calculated by adding the magnetic susceptibility of the units the macrocycle consists of [Maret and Dransfeld, 1985].

The shape-persistent macrocycle backbone of MC3 (figure 11.3) contains 10 phenyl groups, 12 triple bonds, and 28 single bonds. The two flexible side chains and the four bulky t-butyl groups were not considered in this calculation. There is no proof that the chains are stacked in the self-assembled structures and therefore it is difficult to predict their orientation inside the self-assembled fibres.

The shape of the backbone is considered to be a square. This simplifies adding of the magnetic susceptibility (vectors) by assuming that 6 triple and 14 single bonds are oriented in the x-direction, while an equal amount of them is oriented in the y-direction. This approximation is valid since the ring is more or less round and would therefore result in a similar vectorial sum. By adding the values, χ_{zz} and χ_{xx} (the magnetic susceptibility of MC3 perpendicular to and in the plane of the macrocycle backbone, respectively) can be obtained and a value of $\approx -1\times10^{-8} m^3/mol$ was calculated for the anisotropy in magnetic susceptibility of MC3 via equation 11.15.

$$\Delta\chi = \chi_{zz} - \chi_{xx} \tag{11.15}$$

11.3 Laboratory Apparatuses

STM. Discoverer STM (Topometrix, Inc., Santa Barbara, CA) along with an external pulse/function generator (model HP 8111 A) with negative sample bias. Tips were electrochemically etched from Pt/Ir wire (80%/20%, diameter 0.2 mm) in 2 N KOH/ 6N NaCN solution in water. The STM images were acquired in the constant height mode.

AFM. Multimode SPM system with a Nanoscope IV controller (Veeco Instruments, Inc., Santa Barbara, CA). A calibration silicon grating was used to calibrate the piezo scanner. The commercial rectangular silicon cantilevers from Veeco (115-135 μm long, 30-40 μm wide, 3.5-4.5 μm thick) have a nominal spring constant in the range of 20-80 N/m and a resonance frequency of 260-303 KHz. The dimension of the structures was obtained using the analysis program NanoScope 6.13R1 from Digital Instruments/Veeco and Fourier transformations were done using the analysis program SPIP.

Optical viewing system. The OVS can be used to build a set-up which can record optical images as well as make real time optical movies. The set-up includes a computer with an analog frame grabber device (Terratec Cinergy HybridT USB XS) and uses frame grabbing software (Elgato EyeTV).

Light scattering. The set-up for the light scattering measurements of the second generation polyphenylene dendrimer D1 (chapter 6) is constructed by the correlator ALV 5000, the goniometer SPE 81 and a He-Neon-Laser with the wavelength 633 nm.

The light scattering measurements of the coil-ring-coil macrocycle MC3 (chapter 8) were performed with a computerised homemade goniometer, using a step size of 2 degrees in the angular range of 25 to 120 degrees, corresponding to the scattering wave vectors of 8 to 30 $\mu\mathrm{m}^{-1}$. The wavelength of the incident light was 514 nm, produced by a argon ion laser (Spectra Physics, Stabilite 2017). The scattered intensity was measured using a single mode optical fibre with a collimating lens in combination with an ALV/SO-SIPD single photon detector, using a 5 s integration time per angle. A temperature controller was used to stabilise the temperature within 0.1 °C during the measurements.

Birefringence measurements in a high magnetic field. The alignment of the coil-ring-coil macrocycle MC3 aggregates in solution was measured in a set-up similar as described by Maret and Dransfeld [1985], using linear birefringence in a vertically mounted Bitter magnet up to 20 T. A He-Ne laser (1mW output, Melles Griot) with a wavelength of 632.8 nm was used as a light source, while the polarisation was modulated with a photo-elastic modulator (PEM-90, Hinds Instruments). The light transmitted through the sample was detected by a photodetector (Thorlabs, PDA55), two lock-in amplifiers (SR380, Stanford Research Systems) were used to recover the phase shift induced by the alignment of the aggregates.

Conclusions and Perspectives

Three types of well-defined molecular structures were studied: ‘globular’ shaped dendrimers (chapter 3), ‘torus’ shaped macrocycles (chapter 4), and polychlorotriphenylmethyl derivatives (chapter 5).

The self-assembly behaviour of these organic molecules on a surface was studied with scanning probe microscopes. Several parameters were investigated to examine their impact on the 2D self-assembly at surfaces into nanofibres.

The procedure to obtain nanofibres by dropcasting a $\sim 10^{-5}$ M second generation polyphenylene dendrimer solution in THF on piranha cleaned silicon in a THF saturated tank was found to be the ‘optimised method of sample preparation’ as fibres were abundantly formed on the substrate’s surface (chapter 6). The nucleation of fibre growth is likely to be initiated in solution at the liquid/solid interface. Aggregates are formed on a substrate when a sufficiently high concentration is attained upon solvent evaporation during the sample preparation. Dynamic light scattering experiments in higher concentrated solutions (6×10^{-5} M to 2×10^{-4} M) confirmed the presence of badly defined aggregates. The fact that the fibres are sometimes observed to lie on top of each other indicates that the fibre formation is mediated by solvent evaporation. The main driving force of dendrimer nanofibre formation is attributed to π-π interactions between the phenyl groups of neighbouring dendrimers. Experiments in solvent mixtures and studies of similar dendrimers with functional groups at the periphery indicate the crucial role of the dendrimer branches which can interdigitate to optimise the π-π interactions between neighbouring dendrimers.

Shape-persistent macrocycles (chapter 8) can physisorb on the HOPG substrate enabling visualisation of single molecules by STM given that the interaction between the molecules and the substrate's surface is strong enough. Oligo-alkyl-substituted macrocycles with a phenyl-ethynyl-butadienyl backbone structure and macrocycles consisting of dibenzonaphthacene rings form layers at the TCB/HOPG interface. However, the distance between the STM-tip and the substrate is a few angstrom at the most and hence only those macrocycles which are lying 'flat' on the substrate can be imaged. Although STM is a good technique to evaluate the affinity of the molecules with the (HOPG) substrate with high resolution, AFM is best suited to study the self-assmbly process since it can visualise larger structures and is applicable on a wider scale (no conductivity limitations). Light scattering experiments were performed on the coil-ring-coil macrocycles revealing the formation of cylindrically shaped aggregates in solution which could successfully be deposited to a substrate as was observed with AFM. Large structures formed upon dropcasting of solutions of the oligo-alkyl-substituted macrocycles and macrocycles consisting of dibenzonaphthacene rings, followed by evaporation of the solvent were observed with AFM at the air/substrate interface. The influence of side groups and substrate on the self-assembly process was examined indicating the importance of the biphenyl bridge in the oligo-alkyl-substituted macrocycle and the importance of the alkyl chains in the macrocycle consisting out of a dibenzonaphthacene ring in the formation of fibres. Both the oligo-alkyl-substituted macrocycle with the biphenyl bridge and the coil-ring-coil macrocycle were found to form fibres positioned on top of an (incomplete) layer. This layer most probably consists of macrocycles with a face-on orientation (cfr. STM experiments), while macrocycles inside the fibres are likely to be edge-on oriented. This hypothesis is enforced by the experiments with the coil-ring-coil macrocycle in a high magnetic field (vide infra). Although the macrocycle consisting out of a dibenzonaphthacene ring with alkyl chains attached to it, forms fibres on HOPG and silicon while no layers were observed, it is not sure whether fibres are formed directly on the 'bare' substrates. It could be that a small complete layer covers the substrate which is difficult to detect with AFM.

The polychlorotriphenylmethyl (radicular molecule) and polychlorotriphenylmethane derivatives evaluated in this work (chapter 10) self-assemble into dimer rows on the HOPG surface, both at the solution/HOPG interface as well as after dropcasting and fast solvent evaporation. STM and AFM revealed the rows are oriented along three directions, which is most probably related to the symmetry of the HOPG substrate. Attempts were carried out to distinguish the radical derivative from the α-hydrogen derivative by the difference in the magnetic tip-to-sample interaction. However, the long-range interactions observed with scanning force microscopy experiments at room temperature were due to electrostatic interactions and it can be concluded that the sensitivity of magnetic force microscopy is insufficient to discriminate the radical from the α-hydrogen derivative. This opens the possibility to study this system with magnetic resonance force microscope.

Techniques to exploit and manipulate the second generation polyphenylene dendrimer self-assembling system were evaluated in chapter 7. Soft lithography, based on putting physical constraints to the deposition of materials, was employed to successfully transfer patterns of the stamp/mold, resulting in nanopatterns consisting of the aggregated dendrimers. However, the special conditions such as a saturated environment to ensure slow solvent evaporation that are required for fibre formation could not be met and therefore the soft lithography approach was not adequate for guiding dendrimer nanofibres. The nanotemplate approach, based on chemical constraints, was able to guide the self-assembling fibres during their development. Binary nanopatterned surfaces composed of alternating perfluorosilane and native silicon oxide regions directed the solution of dendrimers onto specific locations of the sample surface and additionally oriented the formed nanofibres. The third approach, applying a high magnetic field leading to bulk, contact free, non-destructive forces during the sample preparation was able to reduce the lateral interaction between small fibres, but could not align the nanofibres into a specific direction. However, these experiments provide us valuable information about the orientation of the phenyl groups in the fibres that are found to have a random orientation with respect to each other.

The response to the magnetic field of the polyphenylene dendrimer system was compared with that of a coil-ring-coil macrocycle system (chapter 9). Both systems containing phenyl groups lead to nanofibres which are formed by self-assembly. In contrast to the dendrimer system, the magnetic field has an aligning effect on the macrocycle system and hence the orientation of the molecules within the fibres must be different. The self-assembled structures of the shape-persistent macrocycle can be aligned in solution in a high magnetic field (20 T) confirming that the molecules are self-assembled through π-π stacking in a face-on fashion, while the phenyl groups of the dendrimer system have a random orientation with respect to each other.

Implementing molecular self-assembly processes in a combined top-down/bottom-up approach could be a route towards creating nanostructures for the design of efficient functional devices in the nanoscale world. As these results indicate the potential and challenges of this approach, they open a path for further investigation of other self-assembling systems and combinations with other top-down techniques.

Bibliography

Aragon, S. R. and Pecora, R. Theory of dynamic light scattering from large anisotropic particles. *J. Chem. Phys.*, 66(6):2506–2516, 1977.

Autumn, K., Sitti, M., Liang, Y. C. A., Peattie, A. M., Hansen, W. R., Sponberg, S., Kenny, T. W., Fearing, R., Israelachvili, J. N., and Full, R. J. Evidence for van der waals adhesion in gecko setae. *Proc. Nat. Acad. Sci. U. S. A.*, 99(19):12252–12256, 2002.

Balakrishnan, K., Datar, A., Zhang, W., Yang, X. M., Naddo, T., Huang, J. L., Zuo, J. M., Yen, M., Moore, J. S., and Zang, L. Nanofibril self-assembly of an arylene ethynylene macrocycle. *J. Am. Chem. Soc.*, 128(20):6576–6577, 2006.

Ballester, M. Inert free-radicals (ifr) - a unique trivalent carbon species. *Acc. Chem. Res.*, 18(12):380–387, 1985.

Ballester, M., Riera, J., Castatier, J., Badfa, C., and J.M., M. Inert carbon free radicals. i. perchlorodiphenylmethyl and perchlorotriphenylmethyl radical series. *J. Am. Chem. Soc.*, 93(9):2215–2225, 1971.

Baralia, G. G., Filiâtre, C., Nysten, B., and Jonas, A. M. Nanodecoding by dewetting. *Advanced Materials*, 19(24):4453–4459, 2007.

Baralia, G. G., Pallandre, A., Nysten, B., and Jonas, A. M. Nanopatterned self-assembled monolayers. *Nanotechnology*, 17(4):1160–1165, 2006.

Barth, J. V., Weckesser, J., Cai, C. Z., Gunter, P., Burgi, L., Jeandupeux, O., and Kern, K. Building supramolecular nanostructures at surfaces by hydrogen bonding. *Angew. Chem.–Int. Ed.*, 39(7):1230–1234, 2000.

Bauer, R. E., Grimsdale, A. C., and Müllen, K. Functionalised polyphenylene dendrimers and their applications. *Top. Curr. Chem.*, 245:253–286, 2005.

Blasini, D. R., Flores-Torres, S., Smilgies, D. M., and Abruna, H. D. Stepwise self-assembly of ordered supramolecular assemblies based on coordination chemistry. *Langmuir*, 22(5):2082–2089, 2006.

Butt, H.-J., Graf, K., and Kappl, M. *Physics and Chemistry of Interfaces*. Wiley-VCH, 2003.

Cheng, X. H., Ver Heyen, A., Mamdouh, W., Uji-i, H., De Schryver, F., Höger, S., and De Feyter, S. Synthesis and adsorption of shape-persistent macrocycles containing polycyclic aromatic hydrocarbons in the rigid framework. *Langmuir*, 23(3):1281–1286, 2007.

Chou, S. Y., Krauss, P. R., and Renstrom, P. J. Imprint lithography with 25-nanometer resolution. *Science*, 272(5258):85–87, 1996.

Crespo-Biel, O., Dordi, B., Maury, P., Peter, M., Reinhoudt, D. N., and Huskens, J. Patterned, hybrid, multilayer nanostructures based on multivalent supramolecular interactions. *Chem. Mater.*, 18(10):2545–2551, 2006.

Crespo-Biel, O., Dordi, B., Reinhoudt, D. N., and Huskens, J. Supramolecular layer-by-layer assembly: Alternating adsorptions of guest- and host-functionalized molecules and particles using multivalent supramolecular interactions. *J. Am. Chem. Soc.*, 127(20):7594–7600, 2005.

Crivillers, N., Mas-Torrent, M., Perruchas, S., Roques, N., Vidal-Gancedo, J., Veciana, J., Rovira, C., Basabe-Desmonts, L., Ravoo, B. J., Crego-Calama, M., and Reinhoudt, D. N. Self-assembled monolayers of a multifunctional organic radical. *Angew. Chem.–Int. Ed.*, 46(13):2215–2219, 2007.

Cui, Y., Wei, Q. Q., Park, H. K., and Lieber, C. M. Nanowire nanosensors for highly sensitive and selective detection of biological and chemical species. *Science*, 293(5533):1289–1292, 2001.

de Gennes, P. G., Brochard-Wyart, F., and Quéré, D. *Capillarity and Wetting Phenomena - Drops, Bubbles, Pearls, Waves.* Springer, 2004.

de Gennes, P. G. and Prost, J. *The physics of Liquid Crystals.* Oxford University Press, 1993.

Degenhart, G. H., Dordi, B., Schonherr, H., and Vancso, G. J. Micro- and nanofabrication of robust reactive arrays based on the covalent coupling of dendrimers to activated monolayers. *Langmuir*, 20(15):6216–6224, 2004.

Dykes, G. M. Dendrimers: a review of their appeal and applications. *J. Chem. Technol. Biotechnol.*, 76(9):903–918, 2001.

El Ghzaouit, A., Gauffre, F., Caminade, A. M., Majoral, J. P., and Lannibois-Drean, H. Self-assembly of water-soluble dendrimers into thermoreversible hydrogels and macroscopic fibers. *Langmuir*, 20(21):9348–9353, 2004.

Finocchiaro, A., Failla, S., and Consiglio, G. Phosphorylated macrocycles: structures, complexing properties, and molecular recognition. *Russ. Chem. Bull.*, 54(6):1355–1372, 2005.

Fischer, M. and Höger, S. Synthesis of a shape-persistent macrocycle with intraannular carboxylic acid groups. *Tetrahedron*, 59(47):9441–9446, 2003a.

Fischer, M. and Höger, S. Synthesis of a shape-persistent macrocycle with intraannular sulfonate groups. *Eur. J. Org. Chem.*, (3):441–446, 2003b.

Franz, A., Bauer, W., and Hirsch, A. Complete self-assembly of discrete supramolecular dendrimers. *Angew. Chem.–Int. Ed.*, 44(10):1564–1567, 2005.

Fréchet, J. M. J. Dendrimers and supramolecular chemistry. *Proc. Nat. Acad. Sci. U. S. A.*, 99(8):4782–4787, 2002.

Ge, L., Sethi, S., Ci, L., Ajayan, P. M., and Dhinojwala, A. Carbon nanotube-based synthetic gecko tapes. *Proc. Nat. Acad. Sci. U. S. A.*, 104(26):10792–10795, 2007.

Ge, P. H., Fu, W., Herrmann, W. A., Herdtweck, E., Campana, C., Adams, R. D., and Bunz, U. H. F. Structural characterization of a cyclohexameric meta-phenyleneethynylene made by alkyne metathesis with in situ catalysts. *Angew. Chem.–Int. Ed.*, 39(20):3607–3610, 2000.

Gimeno, N. and Vilar, R. Anions as templates in coordination and supramolecular chemistry. *Coord. Chem. Rev.*, 250(23-24):3161–3189, 2006.

Goncalves, R. P. and Scheuring, S. Manipulating and imaging individual membrane proteins by afm. *Surf. Interface Anal.*, 38(11):1413–1418, 2006.

Grave, C., Lentz, D., Schafer, A., Samori, P., Rabe, J. P., Franke, P., and Schlüter, A. D. Shape-persistant macrocycles with terpyridine units: Synthesis, characterization, and structure in the crystal. *J. Am. Chem. Soc.*, 125(23):6907–6918, 2003.

Grave, C. and Schlüter, A. D. Shape-persistent, nano-sized macrocycles. *Eur. J. Org. Chem.*, (18):3075–3098, 2002.

Guggisberg, M., Bammerlin, M., Loppacher, C., Pfeiffer, O., Abdurixit, A., Barwich, V., Bennewitz, R., Baratoff, A., Meyer, E., and Guntherodt, H. J. Separation of interactions by noncontact force microscopy. *Phys. Rev. B: Condens. Matter*, 61(16):11151–11155, 2000.

Halim, M., Pillow, J. N. G., Samuel, I. D. W., and Burn, P. L. Conjugated dendrimers for light-emitting diodes: Effect of generation. *Adv. Mater.*, 11(5):371–374, 1999.

Hierlemann, A., Campbell, J. K., Baker, L. A., Crooks, R. M., and Ricco, A. J. Structural distortion of dendrimers on gold surfaces: A tapping-mode afm investigation. *J. Am. Chem. Soc.*, 120(21):5323–5324, 1998.

Hoeben, F. J. M., Jonkheijm, P., Meijer, E. W., and Schenning, A. P. H. J. About supramolecular assemblies of pi-conjugated systems. *Chem. Rev.*, 105(4):1491–1546, 2005.

Höger, S. Highly efficient methods for the preparation of shape-persistent macrocyclics. *J. Polym. Sci. Pol. Chem.*, 37(15):2685–2698, 1999.

Höger, S. Shape-persistent macrocycles: From molecules to materials. *Chem.–Eur. J.*, 10(6):1320–1329, 2004.

Höger, S., Bonrad, K., Mourran, A., Beginn, U., and Moller, M. Synthesis, aggregation, and adsorption phenomena of shape-persistent macrocycles with extraannular polyalkyl substituents. *J. Am. Chem. Soc.*, 123(24):5651–5659, 2001.

Höger, S., Enkelmann, V., Bonrad, K., and Tschierske, C. Alkyl-substituted shape-persistent macrocycles: The first discotic liquid crystal composed of a rigid periphery and a flexible core. *Angew. Chem.-Int. Ed.*, 39(13):2268–2270, 2000.

Höger, S. and Meckenstock, A. D. Template-directed synthesis of shape-persistent macrocyclic amphiphiles with convergently arranged functionalities. *Chem.-Eur. J.*, 5(6):1686–1691, 1999.

Höger, S., Morrison, D. L., and Enkelmann, V. Solvent triggering between conformational states in amphiphilic shape-persistent macrocycles. *J. Am. Chem. Soc.*, 124(23):6734–6736, 2002.

Hong, S. H., Zhu, J., and Mirkin, C. A. Multiple ink nanolithography: Toward a multiple-pen nano-plotter. *Science*, 286(5439):523–525, 1999.

Hu, J., Zhang, Y., Gao, H. B., Li, M. Q., and Hartmann, U. Artificial dna patterns by mechanical nanomanipulation. *Nano Lett.*, 2(1):55–57, 2002.

Huang, J. X., Kim, F., Tao, A. R., Connor, S., and Yang, P. D. Spontaneous formation of nanoparticle stripe patterns through dewetting. *Nat. Mater.*, 4(12):896–900, 2005.

Hunter, C. A. and Sanders, J. K. M. The nature of pi-pi interactions. *J. Am. Chem. Soc.*, 112(14):5525–5534, 1990.

Huo, F. W., Xu, H. P., Zhang, L., Fu, Y., Wang, Z. Q., and Zhang, X. Hydrogen-bonding based multilayer assemblies by self-deposition of dendrimer. *Chem. Commun.*, (7):874–875, 2003.

Huskens, J., Deij, M. A., and Reinhoudt, D. N. Attachment of molecules at a molecular printboard by multiple host-guest interactions. *Angew. Chem.–Int. Ed.*, 41(23):4467–4471, 2002.

Jung, K. H., Shin, H. K., Kim, C. K., and Kwon, Y. S. Characterization of self-assembled dendrimers on au(111) substrate by scanning probe microscopy. *Mater. Sci. Eng. C-Biomimetic Supramol. Syst.*, 24(1-2):177–180, 2004.

Jung, K. H., Shin, H. K., Kwon, Y. S., and Kim, C. Morphology properties of self-assembled dendrimer on au(111) using tapping mode atomic force microscopy. *Colloid Surf. A-Physicochem. Eng. Asp.*, 257-258:191–194, 2005.

Kim, T. I., Baek, J. U., Bai, C. Z., and Park, J. S. Synthesis of novel poly(amido ethylenimine) (pameim) dendrimer and its self-assembly with plasmid dna. *Bull. Korean Chem. Soc.*, 27(11):1894–1896, 2006.

Kimura, M., Ueki, H., Ohta, K., Hanabusa, K., Shirai, H., and Kobayashi, N. Nanoscopic fibrous assemblies made of metallophthalocyanine-terminated amphiphilic polymers. *Chem.–Eur. J.*, 10(20):4954–4959, 2004.

Kohli, N., Dvornic, P. R., Kaganove, S. N., Worden, R. M., and Lee, I. Nanostructured crosslinkable micropatterns by amphiphilic dendrimer stamping. *Macromol. Rapid Commun.*, 25(9):935–941, 2004.

Koppel, D. E. Analysis of macromolecular polydispersity in intensity correlation spectroscopy - method of cumulants. *J. of Chem. Phys.*, 57(11):4814, 1972.

Kumar, S. Self-organization of disc-like molecules: chemical aspects. *Chem. Soc. Rev.*, 35(1):83–109, 2006.

Laureyn, W. *PhD thesis: Physico-chemical study on the use of silanes for the realisation of oxide-based biosensor interfaces.* Katholieke Universiteit Leuven, 2002.

Lee, K. B., Park, S. J., Mirkin, C. A., Smith, J. C., and Mrksich, M. Protein nanoarrays generated by dip-pen nanolithography. *Science*, 295(5560):1702–1705, 2002.

Leguen, E., Chassepot, A., Decher, G., Schaaf, P., Voegel, J. C., and Jessel, N. Bioactive coatings based on polyelectrolyte multilayer architectures functionalized by embedded proteins, peptides or drugs. *Biomol. Eng.*, 24(1):33–41, 2007.

Lehn, J. M. Toward self-organization and complex matter. *Science*, 295(5564):2400–2403, 2002.

Leon, J. W., Kawa, M., and Fréchet, J. M. J. Isophthalate ester-terminated dendrimers: Versatile nanoscopic building blocks with readily modifiable surface functionalities. *J. Am. Chem. Soc.*, 118(37):8847–8859, 1996.

Li, F. I., Thaler, S. M., Leo, P. H., and Barnard, J. A. Dendrimer pattern formation in evaporating drops. *J. Phys. Chem. B*, 110(51):25838–25843, 2006a.

Li, Y., Qian, F., Xiang, J., and Lieber, C. M. Nanowire electronic and optoelectronic devices. *Mater. Today*, 9(10):18–27, 2006b.

Lin, C. H. and Tour, J. Hydrogen-bond-assisted pi-stacking of shape-persistent cyclophanes. *J. Org. Chem.*, 67(22):7761–7768, 2002.

Liu, D. J., De Feyter, S., Cotlet, M., Stefan, A., Wiesler, U. M., Herrmann, A., Grebel-Koehler, D., Qu, J. Q., Müllen, K., and

De Schryver, F. C. Fluorescence and intramolecular energy transfer in polyphenylene dendrimers. *Macromolecules*, 36(16):5918–5925, 2003a.

Liu, D. J., De Feyter, S., Cotlet, M., Wiesler, U. M., Weil, T., Herrmann, A., Müllen, K., and De Schryver, F. C. Fluorescent self-assembled polyphenylene dendrimer nanofibers. *Macromolecules*, 36(22):8489–8498, 2003b.

Loi, S., Wiesler, U. M., Butt, H. J., and Müllen, K. Formation of nanorods by self-assembly of alkyl-substituted polyphenylene dendrimers on graphite. *Chem. Commun.*, (13):1169–1170, 2000.

Luryi, S., Xu, J., and Zaslavsky, A. *Future Trends in Microelectronics: The Nano Millennium.* Wiley-IEEE Press, 2002.

Maret, G. and Dransfeld, K. Biomolecules and polymers in high steady magnetic-fields. *Top. Appl. Phys.*, 57:143–204, 1985.

Maspoch, D., Domingo, N., Ruiz-Molina, D., Wurst, K., Vaughan, G., Tejada, J., Rovira, C., and Veciana, J. A robust purely organic nanoporous magnet. *Angew. Chem.-Int. Ed.*, 43(14):1828–1832, 2004.

Maspoch, D., Ruiz-Molina, D., and Veciana, J. Old materials with new tricks: multifunctional open-framework materials. *Chem. Soc. Rev.*, 36(5):770–818, 2007.

Maury, P., Peter, M., Crespo-Biel, O., Ling, X. Y., Reinhoudt, D. N., and Huskens, J. Patterning the molecular printboard: patterning cyclodextrin monolayers on silicon oxide using nanoimprint lithography and its application in 3d multilayer nanostructuring. *Nanotechnology*, 18(4):044007, 2007.

McNaught, A. P. and Wilkinson, A., editors. *Compendium of Chemical Terminology - The Gold Book*. International Union of Pure and Applied Chemistry, 1997.

Mena-Osteritz, E. and Bauerle, P. Self-assembled hexagonal nanoarrays of novel macrocyclic oligothiophene-diacetylenes. *Adv. Mater.*, 13(4):243–246, 2001.

Moore, J. S. Shape-persistent molecular architectures of nanoscale dimension. *Acc. Chem. Res.*, 30(10):402–413, 1997.

Nakao, K., Nishimura, M., Tamachi, T., Kuwatani, Y., Miyasaka, H., Nishinaga, T., and Iyoda, M. Giant macrocycles composed of thiophene, acetylene, and ethylene building blocks. *J. Am. Chem. Soc.*, 128(51):16740–16747, 2006.

Newkome, G. R., YAO, Z. Q., BAKER, G. R., and GUPTA, V. K. Micelles .1. cascade molecules - a new approach to micelles - a [27]-arborol. *J. Org. Chem.*, 50(11):2003–2004, 1985.

Nguyen, T. Q., Martel, R., Avouris, P., Bushey, M. L., Brus, L., and Nuckolls, C. Molecular interactions in one-dimensional organic nanostructures. *J. Am. Chem. Soc.*, 126(16):5234–5242, 2004.

Nijhuis, C. A., Huskens, J., and Reinhoudt, D. N. Binding control and stoichiometry of ferrocenyl dendrimers at a molecular printboard. *J. Am. Chem. Soc.*, 126(39):12266–12267, 2004.

Onclin, S., Huskens, J., Ravoo, B. J., and Reinhoudt, D. N. Molecular boxes on a molecular printboard: Encapsulation of anionic dyes in immobilized dendrimers. *Small*, 1(8-9):852–857, 2005.

Pace, C. N., Shirley, B. A., McNutt, M., and Gajiwala, K. Forces contributing to the conformational stability of proteins. *Faseb J.*, 10(1):75–83, 1996.

Pallandre, A., Glinel, K., Jonas, A. M., and Nysten, B. Binary nanopatterned surfaces prepared from silane monolayers. *Nano Lett.*, 4(2):365–371, 2004.

Parsegian, V. A. *Van der Waals Forces - A Handbook for Biologists, Chemists, Engineers, and Physicists.* Cambridge University Press, 2006.

Pathak, S., Singh, A. K., McElhanon, J. R., and Dentinger, P. M. Dendrimer-activated surfaces for high density and high activity protein chip applications. *Langmuir*, 20(15):6075–6079, 2004.

Piner, R. D., Zhu, J., Xu, F., Hong, S. H., and Mirkin, C. A. "dip-pen" nanolithography. *Science*, 283(5402):661–663, 1999.

Provencher, S. W. A constrained regularization method for inverting data represented by linear algebraic or integral-equations. *Comput. Phys. Commun.*, 27(3):213–227, 1982a.

Provencher, S. W. Contin - a general-purpose constrained regularization program for inverting noizy linear algebraic and integral-equations. *Comput. Phys. Commun.*, 27(3):229–242, 1982b.

Rezende, C. A., Lee, L. T., and Galembeck, F. Liquid templating for nanoparticle organization into complex patterns. *Langmuir*, 23(5):2824–2828, 2007.

Rolandi, M., Suez, I., Dai, H. J., and Fréchet, J. M. J. Dendrimer monolayers as negative and positive tone resists for scanning probe lithography. *Nano Lett.*, 4(5):889–893, 2004.

Roques, N., Maspoch, D., Datcu, A., Wurst, K., Ruiz-Molina, D., Rovira, C., and Veciana, J. Self-assembly of carboxylic substituted ptm radicals: From weak ferromagnetic interactions to robust porous magnets. *Polyhedron*, 26(9-11):1934–1948, 2007.

Roques, N., Maspoch, D., Domingo, N., Ruiz-Molina, D., Wurst, K., Tejada, J., Rovira, C., and Veciana, J. Hydrogen-bonded self-assemblies in a polychlorotriphenylmethyl radical derivative substituted with six meta-carboxylic acid groups. *Chem. Commun.*, (38):4801–4803, 2005.

Rose, G. D., Fleming, P. J., Banavar, J. R., and Maritan, A. A backbone-based theory of protein folding. *Proc. Nat. Acad. Sci. U. S. A.*, 103(45):16623–16633, 2006.

Ross, C. Patterned magnetic recording media. *Ann. Rev. Mater. Res.*, 31:203–235, 2001.

Rozkiewicz, D. I., Ravoo, B. J., and Reinhoudt, D. N. Reversible covalent patterning of self-assembled monolayers on gold and silicon oxide surfaces. *Langmuir*, 21(14):6337–6343, 2005.

Salaita, K., Wang, Y. H., and Mirkin, C. A. Applications of dip-pen nanolithography. *Nat. Nanotechnol.*, 2(3):145–155, 2007.

Sarid, D. *Scanning Force Microscopy.* Oxford University Press, Oxford, 1994.

Schlupp, M., Weil, T., Berresheim, A. J., Wiesler, U. M., Bargon, J., and Mullen, K. Polyphenylene dendrimers as sensitive and selective sensor layers. *Angew. Chem.–Int. Ed.*, 40(21):4011–4015, 2001.

Shetty, A. S., Fischer, P. R., Stork, K. F., Bohn, P. W., and Moore, J. S. Assembly of amphiphilic phenylacetylene macrocycles at the air-water interface and on solid surfaces. *J. Am. Chem. Soc.*, 118(39):9409–9414, 1996.

Shirakawa, M., Fujita, N., and Shinkai, S. A stable single piece of unimolecularly pi-stacked porphyrin aggregate in a thixotropic low molecular weight gel: A one-dimensional molecular template for polydiacetylene wiring up to several tens of micrometers in length. *J. Am. Chem. Soc.*, 127(12):4164–4165, 2005.

Shklyarevskiy, I. O., Boamfa, M. I., Christianen, P. C. M., Touhari, F., van Kempen, H., Deroover, G., Callant, P., and Maan, J. C. Magnetic field induced alignment of cyanine dye j-aggregates. *J. Chem. Phys.*, 116(19):8407–8410, 2002.

Shklyarevskiy, I. O., Christianen, P. C. M., Maan, J. C., Schenning, A. P. H. J., Meijer, E. W., Henze, O., and Feast, W. J. Magnetic field alignment of liquid crystalline pentathiophene. *Mol. Cryst. Liquid Cryst.*, 410:551–556, 2004.

Shklyarevskiy, I. O., Jonkheijm, P., Christianen, P. C. M., Schenning, A. P. H. J., Del Guerzo, A., Desvergne, J. P., Meijer, E. W., and Maan, J. C. Magnetic alignment of self-assembled anthracene organogel fibers. *Langmuir*, 21(6):2108–2112, 2005.

Sporer, C., Ratera, I., Ruiz-Molina, D., Zhao, Y. X., Vidal-Gancedo, J., Wurst, K., Jaitner, P., Clays, K., Persoons, A., Rovira, C., and Veciana, J. A molecular multiproperty switching array based on the redox behavior of a ferrocenyl polychlorotriphenyhnethyl radical. *Angew. Chem.-Int. Ed.*, 43(39):5266–5268, 2004.

Sugimoto, Y., Pou, P., Abe, M., Jelinek, P., Perez, R., Morita, S., and Custance, O. Chemical identification of individual surface atoms by atomic force microscopy. *Nature*, 446(7131):64–67, 2007.

Tirado, M. M., Martinez, C. L., and Delatorre, J. G. Comparison of theories for the translational and rotational diffusion-coefficients of rodlike macromolecules - application to short dna fragments. *J. Chem. Phys.*, 81(4):2047–2052, 1984.

Tomalia, D. A., Baker, H., Dewald, J., Hall, M., Kallos, G., Martin, S., Roeck, J., Ryder, J., and Smith, P. A new class of polymers - starburst-dendritic macromolecules. *Polym. J.*, 17(1):117–132, 1985.

Tsukruk, V. V., Rinderspacher, F., and Bliznyuk, V. N. Self-assembled multilayer films from dendrimers. *Langmuir*, 13(8):2171–2176, 1997.

Tully, D. C. and Fréchet, J. M. J. Dendrimers at surfaces and interfaces: chemistry and applications. *Chem. Commun.*, (14):1229–1239, 2001.

van de Hulst, H. C. *Light scattering by small particles.* Dover Publications, Inc. New York, 1981.

van Hameren, R., Schon, P., van Buul, A. M., Hoogboom, J., Lazarenko, S. V., Gerritsen, J. W., Engelkamp, H., Christianen, P. C. M., Heus, H. A., Maan, J. C., Rasing, T., Speller, S., Rowan, A. E., Elemans, J. A. A. W., and Nolte, R. J. M. Macroscopic hierarchical surface patterning of porphyrin trimers via self-assembly and dewetting. *Science*, 314(5804):1433–1436, 2006.

Ver Heyen, A. *Master's Thesis: Manipulatie van nanodeeltjes met atomaire krachtmicroscopie.* Katholieke Universiteit Leuven, 2003.

von Sonntag, J., Knolle, W., Naumov, S., and Mehnert, R. Deprotonation and dimerization of maleimide in the triplet state: A laser flash photolysis study with optical and conductometric detection. *Chem.–Eur. J.*, 8(18):4199–4209, 2002.

Vosch, T., Antoku, Y., Hsiang, J. C., Richards, C. I., Gonzalez, J. I., and Dickson, R. M. Strongly emissive individual dna-encapsulated ag nanoclusters as single-molecule fluorophores. *Proc. Natl. Acad. Sci. U. S. A.*, 104(31):12616–12621, 2007.

Vyawahare, S., Craig, K. M., and Scherer, A. Patterning lines by capillary flows. *Nano Lett.*, 6(2):271–276, 2006.

Wang, J. F., Chen, J. Y., Jia, X. R., Cao, W. X., and Li, M. Q. Self-assembly ultrathin films based on dendrimers. *Chem. Commun.*, (6):511–512, 2000.

Wiesler, U. M., Berresheim, A. J., Morgenroth, F., Lieser, G., and Müllen, K. Divergent synthesis of polyphenylene dendrimers: The role of core and branching reagents upon size and shape. *Macromolecules*, 34(2):187–199, 2001.

Wiesler, U. M. and Müllen, K. Polyphenylene dendrimers via diels-alder reactions: the convergent approach. *Chem. Commun.*, (22):2293–2294, 1999.

Xia, Y. N. and Whitesides, G. M. Soft lithography. *Annu. Rev. Mater. Sci.*, 28:153–184, 1998.

Xu, S. and Liu, G. Y. Nanometer-scale fabrication by simultaneous nanoshaving and molecular self-assembly. *Langmuir*, 13(2):127–129, 1997.

Yamaguchi, Y. and Yoshida, Z. Shape-persistency and molecular function in heteromacrocycles: Creation of heteroarenecyclynes and arene - azaarenecyclynes. *Chem.–Eur. J.*, 9(22):5430–5440, 2003.

Yang, H. B., Hawkridge, A. M., Huang, S. P. D., Das, N., Bunge, S. D., Muddiman, D. C., and Stang, P. J. Coordination-driven self-assembly of metallodendrimers possessing well-defined and controllable cavities as cores. *J. Am. Chem. Soc.*, 129(7):2120–2129, 2007.

Yip, H. L., Zou, J. Y., Ma, H., Tian, Y. Q., Tucker, N. M., and Jen, A. K. Y. Patterning of robust self-assembled n-type hexaazatrinaphthylene-based nanorods and nanowires by microcontact printing. *J. Am. Chem. Soc.*, 128(40):13042–13043, 2006.

Zeng, C. G., Wang, B., Li, B., Wang, H. Q., and Hou, J. G. Self-assembly of one-dimensional molecular and atomic chains using striped alkanethiol structures as templates. *Appl. Phys. Lett.*, 79(11):1685–1687, 2001.

Zeng, F. W. and Zimmerman, S. C. Dendrimers in supramolecular chemistry: From molecular recognition to self-assembly. *Chem. Rev.*, 97(5):1681–1712, 1997.

Zhang, H., Grim, P. C. M., Foubert, P., Vosch, T., Vanoppen, P., Wiesler, U. M., Berresheim, A. J., Müllen, K., and De Schryver, F. C. Properties of single dendrimer molecules studied by atomic force microscopy. *Langmuir*, 16(23):9009–9014, 2000.

Zhang, H., Grim, P. C. M., Tiu, D. J., Vosch, T., De Feyter, S., Wiesler, U. M., Berresheim, A. J., Müllen, K., Van Haesendonck, C., Vandamme, N., and De Schryver, F. C. Probing carboxylic acid groups in replaced and mixed self-assembled monolayers by individual ionized dendrimer molecules: An atomic force microscopy study. *Langmuir*, 18(5):1801–1810, 2002a.

Zhang, H. M., Xie, Z. X., Mao, B. W., and Xu, X. Self-assembly of normal alkanes on the au(111) surfaces. *Chem.–Eur. J.*, 10(6):1415–1422, 2004a.

Zhang, J. S. and Moore, J. S. Aggregation of hexa(phenylacetylene) macrocycles in solution - a model system for studying pi-pi interactions. *J. Am. Chem. Soc.*, 114(24):9701–9702, 1992.

Zhang, M., Bullen, D., Chung, S. W., Hong, S., Ryu, K. S., Fan, Z. F., Mirkin, C. A., and Liu, C. A mems nanoplotter with high-density parallel dip-pen manolithography probe arrays. *Nanotechnology*, 13(2):212–217, 2002b.

Zhang, W., Kraft, S., and Moore, J. S. Highly active trialkoxymolybdenum(vi) alkylidyne catalysts synthesized by a reductive recycle strategy. *J. Am. Chem. Soc.*, 126(1):329–335, 2004b.

Zhang, W. and Moore, J. S. Shape-persistent macrocycles: Structures and synthetic approaches from arylene and ethynylene building blocks. *Angew. Chem.-Int. Ed.*, 45(27):4416–4439, 2006.

Zhang, W. and Moore, J. S. Alkyne metathesis: Catalysts and synthetic applications. *Adv. Synth. Catal.*, 349(1-2):93–120, 2007.

Zhao, D. H. and Moore, J. S. Shape-persistent arylene ethynylene macrocycles: syntheses and supramolecular chemistry. *Chem. Commun.*, (7):807–818, 2003.

Zhu, S. Z., Zhu, S. F., Jin, G. F., and Li, Z. T. Strong phenyl-perfluorophenyl pi-pi stacking and c-(hf)-f-...-c hydrogen bonding interactions in the crystals of the corresponding aromatic aldimines. *Tetrahedron Lett.*, 46(15):2713–2716, 2005.

Ziegler, A., Mamdouh, W., Ver Heyen, A., Surin, M., Uji, H., Abdel-Mottaleb, M. M. S., De Schryver, F. C., De Feyter, S., Lazzaroni, R., and Höger, S. Covalent template approach toward functionalized oligo-alkyl-substituted shape-persistent macrocycles: Synthesis and properties of rings with a loop. *Chem. Mater.*, 17(23):5670–5683, 2005.

Zimmerman, S. C., Zeng, F. W., Reichert, D. E. C., and Kolotuchin, S. V. Self-assembling dendrimers. *Science*, 271(5252):1095–1098, 1996.

Publications

'From 2D to 3D crystallization: a combined STM and AFM study on the assembly of a spoked molecular wheel on graphite'
Shengbin Lei, Dennis Mössinger, Mathieu Surin, Jens Hornung, **An Ver Heyen**, Roberto Lazzaroni, Sigurd Höger, and Steven De Feyter
In preparation

'Self-assembly of macrocycles and their response to a high-magnetic field'
An Ver Heyen, Jeroen Gielen, Sigurd Höger, Peter C. M. Christianen, and Steven De Feyter
In preparation

'Guiding self-assembly of a second generation polyphenylene dendrimer into well defined patterns'
An Ver Heyen, Cédric C. Buron, Qin Tianshi, Roland Bauer, Alain M. Jonas, Klaus Müllen, Frans C. De Schryver, and Steven De Feyter
In preparation

'Pentafluorophenyl decorated polyphenylene dendrimers synthesis and self-assembly'
Roland Bauer, Di Liu, **An Ver Heyen**, Frans C. De Schryver, Steven De Feyter, and Klaus Müllen
Macromolecules 40(14):4753-4761, 2007

‘Synthesis and adsorption of shape-persistent macrocycles containing polycyclic aromatic hydrocarbons in the rigid framework’
Xiaohong Cheng, **An Ver Heyen**, Wael Mamdouh, Hiroshi Uji-i, Frans C. De Schryver, Sigurd Höger, and Steven De Feyter
Langmuir 23(3):1281-1286, 2007

‘Solid-state assemblies and optical properties of conjugated oligomers combining fluorene and thiophene units’
Mathieu Surin, Prashant Sonar, Andrew C. Grimsdale, Klaus Müllen, Steven De Feyter, Satoshi Habuchi, Stefano Sarzi, Els Braeken, **An Ver Heyen**, Mark Van der Auweraer, Frans C. De Schryver, Massimiliano Cavallini, Jean-Fran cois Moulin, Fabio Biscarini, Cristina Femoni, Roberto Lazzaroni, and Philippe Leclère
J. Mater. Chem. 17(8):728-735, 2007

‘Covalent template approach toward functionalized oligo-alkyl-substituted shape-persistent macrocycles: synthesis and properties of rings with a Loop’
Andreas Ziegler, Wael Mamdouh, **An Ver Heyen**, Mathieu Surin, Hiroshi Uji-i, Mohammed M. S. Abdel-Mottaleb, Frans C. De Schryver, Steven De Feyter, Roberto Lazzaroni, and Sigurd Höger
Chem. Mater. 17(23):5670-5683, 2005

Presentations

'Guided fibre formation of a polyphenylene dendrimer'
Poster presentation at the Leuven Nano-Conference - LNC'07, June 5-6, 2007, Leuven, Belgium

'Unravelling and guiding the fibre formation of a polyphenylene dendrimer'
Oral presentation at KULeuven, May 25, 2007, Leuven, Belgium

'Self-assembly of dendrimers and macrocycles on the nanometre scale'
Poster presentation at the International Conference on Nanoscience and Technology: NANO9 meets STM'06 (ICN+T 2006), July 30-August 4, 2006, Basel, Switzerland

'Study of nanofibres with atomic force microscopy'
Oral presentation at spring school 'Chiral Expression and Transfer at the Nanoscale' in combination with the Netherlands Supramolecular Community Meeting, April 5-7, 2006, Nijmegen, Netherlands

'Self-assembly of dendrimers and macrocycles into fibrillar structures'
Poster presentation at IAP-meeting, March 11-12, 2005, Leuven, Belgium

'Study of molecular self-assembly on the nanometre scale with atomic force microscopy'
Oral presentation at KULeuven, January 21, 2005, Leuven, Belgium

‘Manipulation of matter on the nanometre scale, with atomic force microscopy’
Poster presentation on Nanotech day, April 23, 2004, Leuven, Belgium

‘Manipulatie van materie op nanometerschaal met atomaire krachtmicroscopie’
Poster presentation at VJC7, April 16, 2004, Gent, Belgium

Biography

An Ver Heyen was born on 28 October 1978 in Geel, Belgium. After finishing her secondary education at the Rozenberg in Mol where she studied Latin and Sciences (Latijn-Wetenschappen), she went straight on to pursue a university education in Leuven. She received a Bachelor's degree in Chemistry (Kandidaat in de Scheikunde) and a Master's degree in Chemistry (Licentiaat in de Scheikunde) from the Katholieke Universiteit Leuven in Belgium. She graduated cum laude on 5 July 2003. Her Master's thesis, titled 'Manipulatie van nanodeeltjes met atomaire krachtmicroscopie', was supervised by Prof. F. C. De Schryver and Dr. S. De Feyter. She started working as a doctoral student in the Molecular and Nanomaterials research group of the Chemistry Department of the Katholieke Universiteit Leuven in October 2003, under supervision of Prof. Em. F. C. De Schryver and Prof. S. De Feyter, funded by the Katholieke Universiteit Leuven. She completed her Ph.D. thesis, titled 'Unravelling and guiding the molecular self-assembly on surfaces', in February 2008.